

Some pages of this thesis may have been removed for copyright restrictions.

If you have discovered material in Aston Research Explorer which is unlawful e.g. breaches copyright, (either yours or that of a third party) or any other law, including but not limited to those relating to patent, trademark, confidentiality, data protection, obscenity, defamation, libel, then please read our [Takedown policy](#) and contact the service immediately (openaccess@aston.ac.uk)

TO MY MOTHER

'Along the road of life I have a friend divine
who walks with me and gently leads the way;
He gives me joy and makes the darkest night to shine.'

THE MECHANICS OF DRAWING WIRE AT ELEVATED TEMPERATURES

by

NGIAP HIANG LOH

Submitted in fulfilment of the requirements

for the degree of

DOCTOR OF PHILOSOPHY

Faculty of Engineering

Department of Production Technology and Production Management

The University of Aston in Birmingham

June, 1983

Supervisor: Professor D H Sansome

THE UNIVERSITY OF ASTON IN BIRMINGHAM
Department of Production Technology and Production Management

THE MECHANICS OF DRAWING WIRE AT ELEVATED TEMPERATURES

Submitted in fulfilment of the requirements
for the degree of Doctor of Philosophy

Author: NGIAP HIANG LOH

Year: 1983

Summary

Although elevated temperature drawing of wire has been an industrial process for a number of years it has not been investigated systematically and many facets of the process have not been understood. Consequently a continuous in-line heat treatment draw process was developed. The technique of drawing mild steel, medium carbon steel and M2 'high speed' steel wires up to 700°C and about 45% area of reduction was established.

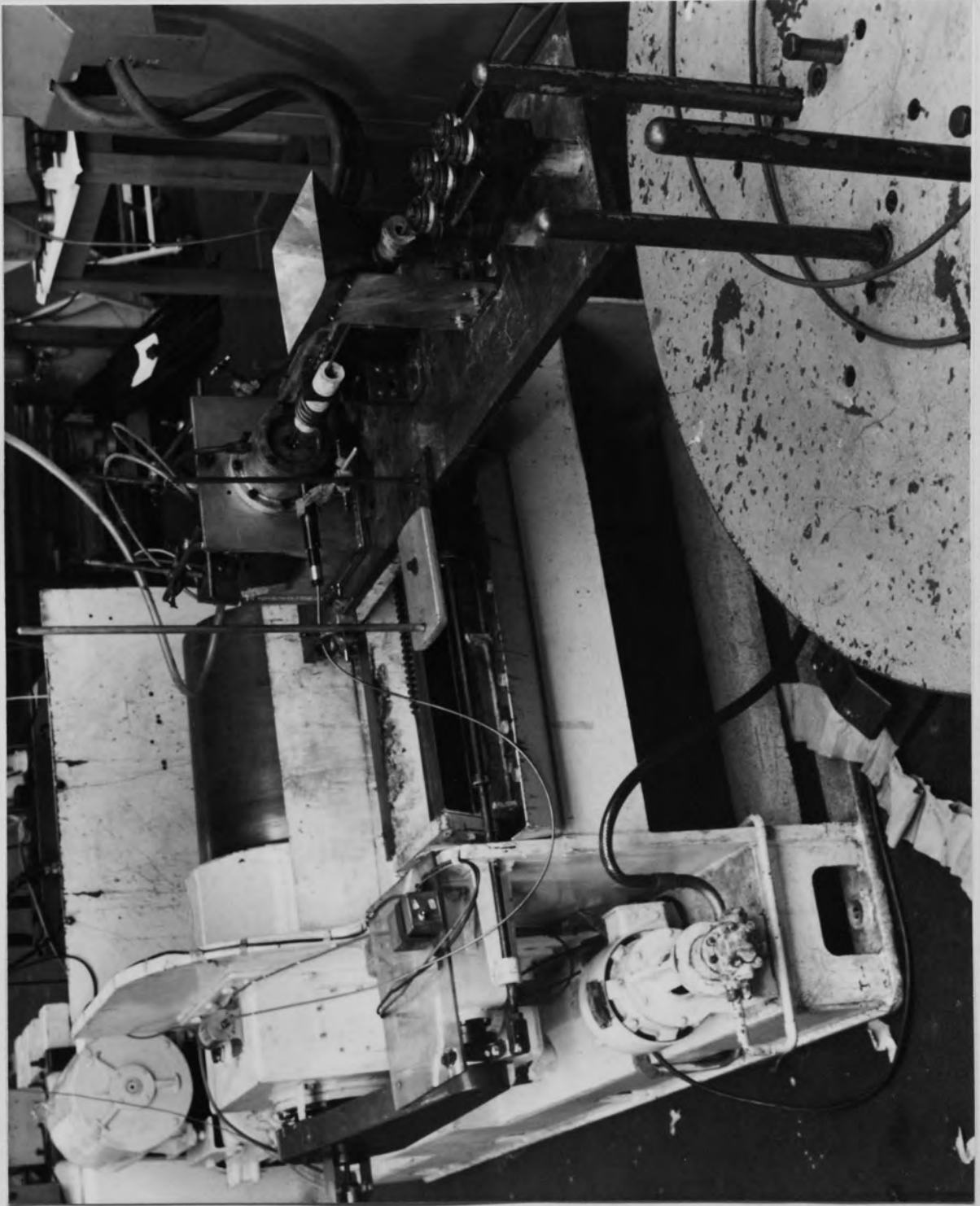
The mechanics of wire drawing at elevated temperatures has been studied in depth theoretically and practically. An upper bound solution was derived and solved numerically, to establish the draw stress and other data, for a range of variables.

The stress, strain, strain rate and temperature were related mathematically by the power law and the velocity-modified temperature respectively. This enabled the flow stress distribution in the deformation zone to be calculated, after taking into consideration the temperature rise due to deformation and frictional work. Based on the flow stress distribution, a mean flow stress was calculated and used in the upper bound solution. Adiabatic conditions were assumed to prevail. A special computer program was written to plot the strain, strain rate, temperature and flow stress distributions.

The effects of draw temperature, area of reduction and lubricant were investigated experimentally. For a constant draw speed of 20 ft min⁻¹, the strain-ageing region was found in the approximate temperature range of 200°C - 400°C. In general, the experimental draw stresses required at elevated temperatures were lower than those developed in cold drawing.

The experimental and theoretical results for medium carbon steel were in satisfactory agreement, except for draw temperatures of 600°C and above. The results of mild steel and M2 'high speed' steel could not be verified theoretically due to a lack of suitable stress-strain data but such evidence as is available leads to the conclusion that the theory is in agreement with the experimental results.

Key words: Elevated temperature drawing
Wire drawing
Upper bound solution
Forming temperature distribution
High temperature lubricants



Frontispiece

C O N T E N T S

	<u>Page No</u>
List of Figures	x i
List of Tables	x v
List of Photographs	x vi
Nomenclature	xvii

CHAPTER ONE

INTRODUCTION AND LITERATURE REVIEW

1.1	Introduction.	1
1.2	Effects of strain rate and temperature on the flow stress of metals at elevated temperatures.	4
1.3	Cold, warm and hot working.	8
1.4	Formulae to relate stress, strain, strain rate and temperature at elevated temperatures.	9
1.4.1	Stress-strain relationships.	10
1.4.2	Combined effect of temperature and strain rate.	10
1.4.2.1	Zener and Holloman relationship.	10
1.4.2.2	Velocity-modified temperature.	12
1.4.3	Formulae used in the theoretical analysis.	16
1.5	Temperature distribution in the deformation zone.	18
1.5.1	Calculating the temperature and flow stress distributions for the theoretical analysis.	23

	<u>Page No</u>
1.6 Friction.	24
1.6.1 Coulomb friction μ .	24
1.6.2 Constant friction factor m .	25
1.6.3 Determination of μ and m by experiments.	25
1.6.3.1 Split die method.	26
1.6.3.2 Oscillating die method.	26
1.6.3.3 Die rotation method.	27
1.6.3.4 Indirect method.	27
1.7 Upper-bound solutions of axisymmetric forming problems through conical dies.	29
1.7.1 A brief outline of the upper-bound solution developed for the drawing of wires at elevated temperatures.	34
1.8 Other forming processes at elevated temperatures.	35
1.8.1 Hot tube drawing.	35
1.8.2 Hot rolling.	36
1.8.3 Hot extrusion.	38

CHAPTER TWO

THEORETICAL ANALYSIS OF THE DRAWING OF WIRE AT ELEVATED TEMPERATURES

2.1 Introduction.	43
2.2 The upper-bound solution for the drawing of wire at elevated temperatures.	44
2.2.1 The flow model.	44

		<u>Page No</u>
2.2.2	The shear surfaces.	46
2.2.3	The velocity field.	46
2.2.3.1	Derivation of the velocity field.	46
2.2.4	The strain rate components.	51
2.2.4.1	Equivalent strain rate.	53
2.2.5	Equivalent mean strain.	53
2.2.6	Establishing the temperature and flow stress distributions in the deformation zone.	54
2.2.6.1	Relationship between stress, strain, strain rate and temperature.	55
2.2.6.2	Temperature rise due to deformation work.	58
2.2.6.3	Temperature rise due to frictional work.	59
2.2.6.4	Procedure for calculating the temperature and flow stress distributions in the deformation zone.	60
2.2.7	The internal power of deformation per unit volume.	61
2.2.7.1	The total internal power of deformation.	64
2.2.8	Power losses in shearing at the inlet and outlet shear surface.	66
2.2.9	Power losses in friction between the die and wire interface.	68
2.3	The compilations of the computer programs.	70
2.3.1	Introduction.	70
2.3.2	Sub-program 'Constant'.	70

	<u>Page No</u>
2.3.3 Sub-program 'Curve'.	72
2.3.4 The computer program 'Draw'.	73
2.3.4.1 The co-ordinate system employed in the computer program.	73
2.3.4.2 The computer program layout.	74
2.3.5 The computer program 'Contour'.	74

CHAPTER THREE

EXPERIMENTAL EQUIPMENT AND DRAW PROCESS

3.1	Experimental equipment.	80
3.1.1	The bull-block.	80
3.1.2	The induction heater.	80
3.2	Draw process materials.	82
3.2.1	Drawing dies.	82
3.2.1.1	Chromium carbide dies.	82
3.2.1.2	Die design.	82
3.2.1.3	'Syalon' dies.	87
3.2.2	Test materials.	88
3.2.2.1	Mild steel EN2B.	88
3.2.2.2	Medium carbon steel EN8D.	89
3.2.2.3	M2 'high speed' steel.	89
3.2.3	Lubricants.	91

3.2.3.1	Hot rolling oil RH12.	91
3.2.3.2	Dag 2961.	91
3.2.3.3	Dag 2543.	92

CHAPTER FOUR

DESIGN AND MANUFACTURE OF NON-MEASURING EQUIPMENT

4.1	Introduction.	93
4.2	Non-measuring equipment.	95
4.2.1	Lubricator assembly.	96
4.2.2	Induction heating assembly.	98
4.2.2.1	Flexible extension.	99
4.2.2.2	Induction coil.	99
4.2.2.3	Support for the induction coil and the ceramic tube.	102
4.2.3	Die-holder assembly.	104

CHAPTER FIVE

DESIGN, INSTRUMENTATION AND CALIBRATION OF MEASURING EQUIPMENT

5.1	Introduction.	107
5.2	The loadcell.	108

	<u>Page No</u>
5.2.1 Design of the loadcell.	108
5.2.2 Instrumentation of the loadcell.	110
5.2.3 Calibrating the loadcell.	110
5.3 The torquemeter.	116
5.3.1 Design of the torquemeter.	116
5.3.2 Instrumentation of the torquemeter.	116
5.3.3 Static calibration of the torquemeter.	118
5.4 The tachometer.	122
5.4.1 Instrumentation of the tachometer.	122
5.4.2 Calibrating the tachometer.	126
5.5 The infra-red thermal monitor.	128
5.5.1 Introduction.	128
5.5.2 Instrumentation of the thermal monitor.	128
5.5.3 Calibration of the thermal monitor.	129
5.5.4 Emissivity calibration.	133
5.5.4.1 The resistance heating unit.	133
5.5.4.2 Procedure for the emissivity calibration.	135

CHAPTER SIX

STRESS-STRAIN DATA

6.1 Compression testing of materials.	139
6.1.1 Introduction.	139

	<u>Page No</u>
6.1.2 The cam plastometer.	140
6.1.3 Preparation of specimens and test procedure.	142
6.2 Stress-strain data used in the theoretical analysis.	144
6.2.1 Introduction.	144
6.2.2 Mild steel EN2B.	144
6.2.3 Medium carbon steel EN8D	147
6.2.4 M2 'high speed' steel.	152

CHAPTER SEVEN

EXPERIMENTAL PROCEDURE AND TECHNIQUE

7.1	Introduction.	154
7.2	Preliminary preparations.	155
7.3	The drawing technique.	157

CHAPTER EIGHT

OBSERVATIONS AND DISCUSSION OF RESULTS

8.1	Introduction.	160
8.2	Observations.	160
8.3	Discussion of the experimental results.	162

	<u>Page No</u>
8.4 Discussion of the theoretical results.	165
8.5 Contour plottings.	174
8.6 Graphical results and contour plots	179

CHAPTER NINE

<u>CONCLUSIONS</u>	232
--------------------	-----

CHAPTER TEN

<u>SUGGESTIONS FOR FURTHER WORK</u>	236
-------------------------------------	-----

CHAPTER ELEVEN

APPENDICES

A1	Acknowledgements.	241
A2	Supporting papers.	242
A3	Supplementary proofs.	258
A4	Theoretical results.	265
A5	Experimental results.	281
A6	Computer programs.	286
A7	Mechanical drawings.	297
A8	List of references.	308

LIST OF FIGURES

		Page No
Figure No	Title	
1.1	Effect of strain rate required to compress aluminium to 40% reduction at various temperatures. After Alder (14).	5
1.2	Ultimate stress of mild steel at various temperatures and strain rates. After Manjoine (18).	5
1.3	True stress as a function of the true strain ϵ and velocity-modified temperature T_m for SAE 1020 steel. After MacGregor (29).	14
1.4	True stress as a function of true strain ϵ and velocity-modified temperature T_m for annealed brass. After MacGregor (29).	14
1.5	Stress against velocity-modified temperature T_m for a strain of 0.1. After MacGregor (30).	15
1.6	True stress against temperature. After Nakayama (32).	15
1.7	Relationships between B , n and T_m . After Oxley (34).	17
1.8	Temperature distribution in drawing steel wire from 0.2 to 0.16 in with a speed of 196.8 ft min^{-1} , and coefficient of friction of 0.05. After Siebel (7).	20
1.9	The triangular velocity field. After Avitzur (59).	31
1.10	Schematic representation of the interaction of strain, strain rate, and temperature on extrusion. After Hirst (68).	40

<u>Figure No</u>	<u>Title</u>	
2.1	The flow model.	45
2.2	A view along ρ - θ plane for the shear surfaces.	47
2.3	Diagrammatic relationship between the various angles.	48
2.4	Dimensioning the deformation zone for computation purposes.	56
2.5	The flow chart of the computer program 'DRAW'.	76
2.6	The modified computer results.	79
3.1	Drawing dies.	84
3.2	Profile of chromium carbide die No 5 after polishing (10x magnifications).	86
4.1	Schematic diagram of equipment set-up.	94
4.2	Lubricator assembly.	97
4.3	Induction coil.	101
4.4	Assembly of the ceramic support.	103
4.5	Die-holder assembly.	105
5.1	Alignment of the strain gauges and the circuit diagram of the loadcell.	109
5.2 - 5.6	Calibration graphs of the loadcell.	111
5.7	Alignment of the strain gauges and the circuit diagram of the torque-meter.	117
5.9	Calibration graph of the torque-meter.	121
5.10	Circular disc.	123

<u>Figure No</u>	<u>Title</u>	
5.12	Circuit diagram of the tachometer.	125
5.13	Calibration graph of draw speed against tachometer output and galvanometer deflection.	127
5.14	Circuit diagram of the infra-red thermal monitor.	130
5.15 - 5.16	Calibration graphs of the infra-red thermal monitor.	131
5.17	Circuit diagram of the resistance heating unit.	134
5.18	The wire sample.	136
6.1	Die assembly.	141
6.2	True stress-strain data for 0.16%C steel. After Oyane (33).	145
6.3	Graph of log stress against log strain for the 0.16%C steel of figure 6.2. After Hastings (80).	145
6.4	Flow stress as a function of the strain (ϵ) and velocity-modified temperature T_m for Oyane's data, 0.16% plain carbon steel.	146
6.5	Effects of strain rate and temperature on the lower yield stress of a 0.12% plain carbon steel. After Campbell (81).	148
6.6	Relationship between B, n and T_m for Oyane's data, 0.16% plain carbon steel.	149
6.7	Effect of temperature on the stresses for pure iron and various carbon steels. After Oyane (33).	151
6.8	Stress ratio of 0.39%C and 0.16%C steels against velocity-modified temperature T_m .	151

		<u>Page No</u>
<u>Figure No</u>	<u>Title</u>	
6.9	Relationships between B, n and velocity-modified temperature T_m for Samanta's data (83).	153
8.1 - 8.41	Graphical results.	179
8.42 - 8.53	Contour plots.	220
A7.1	Base plate.	297
A7.2	Snugger.	298
A7.3	Flexible extension.	299
A7.4	Lower coil clamp.	300
A7.5	Upper coil clamp.	301
A7.6	Ceramic holder.	302
A7.7	Coil support.	303
A7.8	Plate.	304
A7.9	Die-holder.	305
A7.10	Die-holder cover.	306
A7.11	Die support.	307

LIST OF TABLES

		<u>Page No</u>
<u>Table No</u>	<u>Title</u>	
3.1	Measurements of the chromium carbide die profiles after polishing.	85
3.2	Chemical compositions of mild steel, medium carbon steel and M2 'high speed' steel.	90
5.1	Emissivity values for mild steel, medium carbon steel and M2 'high speed' steel.	138
A4	Theoretical results.	265
A5	Experimental results.	281

LIST OF PHOTOGRAPHS

		<u>Page No</u>
<u>Photograph No</u>	<u>Title</u>	
	Frontispiece.	ii
5.8	Torquemeter calibration.	120
5.11	Mounting of tachometer.	124

N O M E N C L A T U R E

General symbols (Upper case)

A	=	area of reduction
B	=	constant
N_{ϕ}	=	number of equally spaced arc divisions
N_{θ}	=	number of equally spaced angular divisions
P_d	=	total internal power of deformation
P_f	=	total power of friction
P_1	=	total power of shearing at inlet surface Γ_1
P_2	=	total power of shearing at outlet surface Γ_2
Q	=	conversion factor between mechanical and thermal energies
R_1	=	radius of undrawn wire
R_2	=	radius of drawn wire
S	=	surface area
S_t	=	surface area subjected to body traction
T	=	drawing temperature
T_N	=	new temperature after considering temperature rise
T_m	=	velocity-modified temperature
V_1	=	inlet linear velocity
V_2	=	outlet linear velocity
V_a	=	volume of element at the die-wire interface
Y	=	yield stress of material
Y_d	=	mean yield stress
Y_m	=	mean yield stress of a flow line
Y_f	=	mean yield stress for calculating the total power of friction

General symbols (lower case)

c	=	exponential constant
d	=	density of wire
k	=	yield stress in shear
K	=	constant used in velocity-modified temperature equation
m	=	constant friction factor
n	=	strain-hardening index
sp	=	specific heat of wire

Greek Symbols

u_{ρ}	=	radial velocity in deformation zone at radius ρ from apex
u_1	=	radial velocity in deformation zone at shear surface Γ_1
u_2	=	radial velocity in deformation zone at shear surface Γ_2
α	=	die semi-angle
β	=	inclination of the shear plane to the draw-axis (measured in clockwise direction)
ρ	=	radial distance from the virtual apex to any point in the deformation zone
ρ_1, ρ_2	=	radial distance from the shear surfaces Γ_1 and Γ_2 respectively
ρ_0	=	radial distance from the virtual apex to the intersection point of the die and wire at entry
η	=	angle between the shear plane and a line perpendicular to the radius ρ
τ	=	shear stress
$\sigma_{(I, J)}$	=	new flow stress of a point (I, J) in the deformation zone after taking into account the temperature rise
$\sigma_0(I, J)$	=	original flow stress of a point (I, J) in the deformation zone before taking into account the temperature rise

σ	= stress tensor
σ'	= stress deviator tensor
σ_m	= hydrostatic stress tensor
$\dot{\epsilon}_0$	= standard strain rate used in the velocity-modified temperature T_m
$\dot{\epsilon}$	= strain rate
$\dot{\bar{\epsilon}}$	= equivalent strain rate
$\dot{\epsilon}_{ij}$	= strain rate component
$\bar{\epsilon}_{(I, J)}$	= equivalent strain at a point (I, J)
$\Delta \bar{\epsilon}_{(I, J)}$	= equivalent strain increment between 2 points, ie (I-1, J) and (I, J)
$\bar{\epsilon}_T$	= equivalent strain from shear surface Γ_1 to Γ_2
ϵ	= strain
Δv_1	= velocity discontinuity at shear surface Γ_1
Δv_2	= velocity discontinuity at shear surface Γ_2
Δv_f	= velocity discontinuity at conical surface die
$\Delta T_{(I, J)}$	= temperature rise due to deformation work when the particle travels from (I-1, J) to (I, J)
$\Delta \theta_{(I, J)}$	= temperature rise due to frictional work when the particle travels from (I-1, J) to (I, J)
Δt	= time travel
θ	= inclination of radial line and the draw axis

Subscripts

1, 2 = refer to entry and exit surfaces of wire respectively

CHAPTER ONE

INTRODUCTION AND LITERATURE REVIEW

I. INTRODUCTION AND LITERATURE REVIEW

1.1 INTRODUCTION

Drawing in its simplest form, consists of "pulling material" through a die under pre-determined conditions. There is evidence that wire was cold drawn through dies successfully before 1350 BC during ancient Egyptian civilizations (1,2). It is fascinating to note that the material used had been strips of gold, formed into fine wire by drawing through dies used for decorating garments.

Today, the drawing process is of fundamental importance to mankind with the well established branches of wire, rod, tube and strip drawing.

The rapid rate of industrial development or markets compel an expansion in the varieties of metal wires produced. With each technological advancement, either materials of better quality are required - and frequently these are more difficult to form into the required shapes - or the costs of manufacture increase and it is necessary to adopt new procedures to remain competitive. One of the ways to achieve an article of better quality at lower cost is to introduce a more efficient production process and the replacement of the cold draw process by drawing at elevated temperatures falls into this category. An elevated temperature is a temperature above the normal ambient temperature.

Elevated temperature wire drawing has not been widely employed for several reasons: it is difficult to change traditional methods and practices, the flow of information has been restricted and many of the techniques are considered to be confidential. However, there are powerful advantages associated with elevated temperature drawing.

It is known that generally the resistance to deformation decreases as the working temperature increases and this enables difficult-to-cold-draw materials to be drawn more easily. Also, in appropriate circumstances, with elevated temperature drawing, the manufacturing costs of the wire can be greatly reduced by the elimination of intermediate annealing, pickling and associated operations, consequently production times can be shortened.

A very comprehensive literature review on the warm drawing of wire was carried out by Loh and Sansome⁽³⁾ and it is shown that elevated temperature wire drawing is practised in various countries to an increasing extent and is employed mainly for drawing materials which are difficult to cold-draw. It is also used in conjunction with appropriate heat treatments to yield products of the required tensile strength and mechanical properties. The La Salle Steel Company⁽⁴⁾ in America claimed to produce steel bar with a hardness of 30 Rockwell C, tensile strength of 62.5 tonf in⁻² and a yield strength of 55.8 tonf in⁻² by selecting bars of the desired composition and drawing at the required temperature and reduction of area.

The earliest history of warm or hot wire drawing is uncertain but it is known that as early as 1932 Francis⁽⁵⁾ studied the behaviour of wire drawing lubricants at elevated temperatures. Since then various researchers and companies have employed this technique using lead bath heating, resistance heating, induction heating and salt bath heating. Various materials such as beryllium, high speed steel, stainless steel, high alloy steels, titanium alloys and high chromium steel are drawn at elevated temperatures. The commonly used lubricants are graphite and molybdenum disulphide. The die material generally used is tungsten carbide.

Though the art of cold drawing dated before 1350 BC, no serious thought was given to the mechanics of cold drawing until about 1900. The earliest papers on wire drawing are generally qualitative and empirical in nature. In 1927, Sachs⁽⁶⁾ used the 'slab' method to give a logical analysis of the drawing process. After the proposal of Sachs' equation, the theoretical development of cold drawing grew very rapidly and various methods of analysis were used to improve theory and advance knowledge of the process. Research workers Siebel⁽⁷⁾, Korber and Eichinger⁽⁸⁾, Davis and Dokos⁽⁹⁾ and MacLellan⁽¹⁰⁾ refined and improved the drawing theory. With the development of plasticity theory, upper bound solutions were formulated by Avitzur⁽¹¹⁾, Kobayashi⁽¹²⁾ and others. In brief, extensive investigations in the cold drawing of metals have already been undertaken by various researchers, and a comprehensive account of the theories can be found in the standard textbook by Thomsen⁽¹³⁾. Generally, the theories of cold wire drawing assumed a flow stress which is independent of strain rate and temperature.

1.2 EFFECTS OF STRAIN RATE AND TEMPERATURE ON THE FLOW STRESS OF METALS AT ELEVATED TEMPERATURES

Most of the theories of cold metal working operations assume that the work material is deformed with constant flow stress which is independent of temperature and strain rate. This could be tolerated for cold deformation but at elevated temperatures, the flow stress of the material is sensitive to temperature and strain rate.

The strain rate of a metal is proportional to the working speed and the temperature rise due to deformation and frictional work increases as the speed increases. Speed and temperature may have a positive or negative effect on the friction between the material and the die. Thus besides affecting the draw stress, the surface finish of the drawn wire will be affected too.

Alder and Philipp⁽¹⁴⁾ studied the effects of strain rate and temperature on the resistance of metals by subjecting them to compression testings on the cam plastometer. The effects of strain rate and temperature on aluminium with a 40 per cent reduction are shown in figure 1.1. As the strain rate increases the resistance to deformation increases. As the temperature increases the resistance to deformation decreases. Similar effects were also observed by Cook⁽¹⁵⁾ in the compression testings of various steels at temperatures of 900°C - 1200°C and a strain rate range of 1.5 s⁻¹ to 100 s⁻¹.

Doraivelu⁽¹⁶⁾ studied the effects of temperature on the flow stress of 1.5% C, 11.2% Cr steel at a strain rate of 10 s⁻¹. He found that there were two temperature ranges where the flow stress increased as the temperature increased due to the strain-ageing effect and phase transformation; they were 150°C-200°C and 800°C-900°C

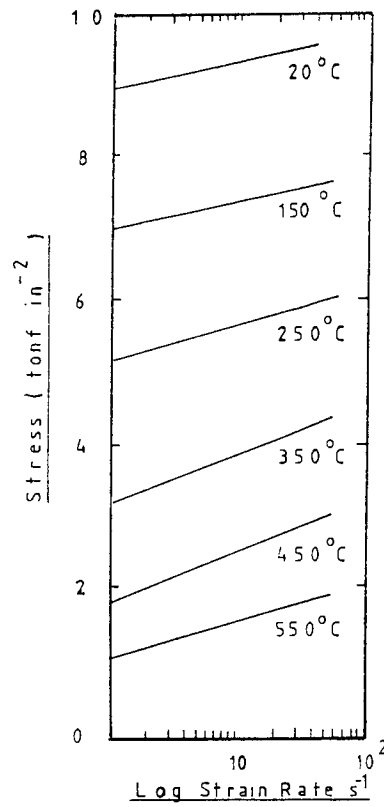


Figure 1.1: Effect of strain rate required to compress aluminium to 40% reduction at various temperatures. After Alder (14)

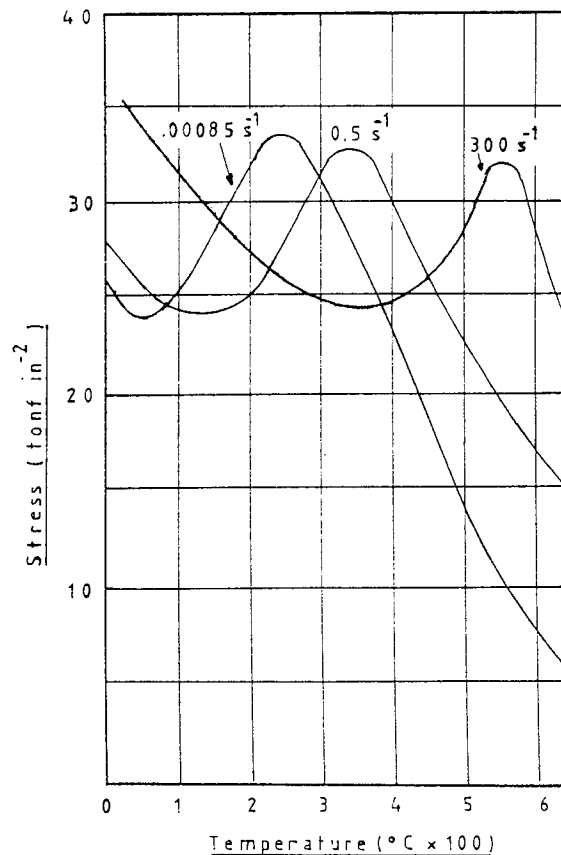


Figure 1.2: Ultimate stress of mild steel at various temperatures and strain rates. After Manjoine (18)

respectively. Suzuki⁽¹⁷⁾ also recognised the effects of strain-ageing and phase transformation on the flow stress of mild steel, but his compression data did not show the effects, due to the wider temperature interval employed in his tests.

Manjoine⁽¹⁸⁾ performed tension tests at elevated temperatures up to 600°C and also found that a strain-ageing region occurs in mild steel, and that this range extended from about 50°C to 250°C when a slow strain rate of 0.00085 s⁻¹ was applied. When the strain rate was raised to 300 s⁻¹, the strain-ageing region moved to higher temperatures, in the range of about 350°C-550°C. The results are shown in figure 1.2.

From the studies of the various investigators mentioned above two things are clear. Firstly, the effects of strain rate and temperature on the flow stress of a metal at elevated temperatures cannot be neglected⁽⁸⁹⁾. Secondly, the work of Manjoine showed that for a particular strain, it cannot always be generalised that as the strain rate increases the flow stress increases, and as the temperature increases the flow stress decreases, since the combined effects of strain rate and temperature must be considered together.

It is appreciated, also, that the flow stress may be dependent on macroscopic-microscopic metallurgical effects such as the non-uniform transverse distribution of grain size and recrystallisation, but it was felt that these effects would be small by comparison with the changes in yield stress arising from the temperature and strain rate characteristics of a metal.

As mentioned earlier, the mechanics of cold wire drawing investigated by the various researchers all neglect the effects of strain rate and temperature on the flow stress, and it is believed that

similarly no attention has been paid to these effects in studies on the mechanics of wire drawing at elevated temperatures. Consequently, it was in the light of the numerous potential advantages of elevated temperature wire drawing and the lack of practical and theoretical knowledge that this research programme was undertaken.

Unlike well-established cold drawing practices, elevated temperature wire drawing posed laboratory problems. Since not much light has been thrown on this subject, the art of drawing wire has had to be developed in the laboratory before the mechanics could be studied. Thus the first objective of the research was to develop a continuous in-line softening heat treatment draw process and to establish the art of wire drawing at elevated temperatures.

The next objective was the theoretical development of an upper bound solution to predict the draw stresses at elevated temperatures. The computer programme developed enables the temperature and flow stress distributions to be predicted so considerably enhancing the understanding of the deformation process.

Due to the non-existence of papers on the specific problems concerned with the mechanics of wire drawing at elevated temperatures other elevated temperature deformation processes are reviewed.

1.3 COLD, WARM AND HOT WORKING

One definition of hot working is generally accepted universally as "working at a temperature above the recrystallisation temperature of the metal". According to Ford and Alexander⁽¹⁹⁾, metals are said to be cold-worked if they become permanently harder during the working process. Thus, as pointed out by Ford and Alexander, steel is essentially cold worked at 500-600°C. Mamalis⁽²⁰⁾ has reported that the term "warm working" refers to working a metal at a temperature above the normal ambient temperature but below the recrystallisation temperature; this is a generally accepted metallurgical categorisation.

The recrystallisation temperature of a metal is also dependent on the speed and degree of deformation, thus in certain circumstances it may be difficult to distinguish hot working from warm working. In view of an emergence of definitions of "cold", "warm" and "hot" working with the passage of time and the difficulty in differentiating them with precision, the author has adopted in the literature review that follows, the term used by investigators at the time they wrote their respective papers.

1.4 FORMULAE TO RELATE STRESS, STRAIN, STRAIN RATE AND TEMPERATURE AT ELEVATED TEMPERATURES

It has long been recognised that the flow stress of a metal at elevated temperatures is dependent on the strain rate and temperature.

These effects could be studied and true stress-strain curves of metals at elevated temperatures and various strain rates could be published.

The effects of the strain rate and temperature on the flow stress is discussed in section 1.2 and will not be discussed here.

When stress-strain behaviour is examined over a range of strain rates and temperatures it is cumbersome to report the results as a complete series of stress-strain curves. Further, the data are suitable for conditions that prevail in the test, that is, at a particular temperature, strain rate and strain. It is improbable that experimental data will be available for the exact deformation conditions prevailing in the process. Thus attempts have been made by many investigators to fit mathematical equations to the stress-strain curves at different temperatures and strain rates to permit the properties prevailing in the process to be predicted. While the limitation of algebraic equations describing the stress-strain behaviour must be recognised, it is advantageous to apply them to experimental data so that constants can be evaluated from which the flow stress at any strain can be subsequently computed. This is particularly useful if these equations can be combined with those for strain rate and temperature.

A great amount of work has already been done in trying to correlate stress-strain curves by mathematical relationships, thus only the more common formulae and those of relevance to this work will be reviewed.

1.4.1 Stress-strain Relationships

Two of the common equations used to express the stress (σ) - strain (ϵ) relationship at elevated temperatures are:

a) Power law

$$\sigma = B\epsilon^n$$

b) Semi-logarithmic law

$$\sigma = A + B \ln \epsilon$$

where A, B and n are constants dependent on strain rate and temperature. n is commonly termed as the strain-hardening index.

Hodierne⁽²¹⁾ fitted the stress-strain data of mild steel at temperatures from 30°C to 700°C and a strain rate of 10 s⁻¹ to 10³ s⁻¹ to the power law. As reported by Rao⁽²²⁾, Grothe⁽²³⁾ and Doraivelu⁽²⁴⁾ also fitted their data using the power law for low carbon steels and 18-4-1 alloy steel for a wide range of temperatures and strain rates.

Samanta⁽²⁵⁾ found that the semi-logarithmic law fits the stress-strain data of tool steel at hot working temperatures reasonably well.

1.4.2 Combined Effect of Temperature and Strain Rate

1.4.2.1 Zener and Holloman Relationship

Zener and Holloman⁽²⁶⁾ proposed that the flow stress of a material is a function of the strain rate and temperature and is

expressed as

$$\sigma = f \left[\dot{\epsilon} \exp \frac{Q}{RT} \right]$$

where $\dot{\epsilon}$ = strain rate

Q = activation energy of the metal

R = universal gas constant

T = absolute temperature

The above equation was originally employed by Zener and Hollomon for steel and aluminium over a large temperature range and small strain rate range. Based on this, values of activation energy which are independent of temperature have been obtained for a number of pure metals and simple alloys which are deformed at temperatures greater than half the homologous temperature. However, this has been found to be invalid at lower temperatures and for more complex alloys in which precipitation processes can occur within the temperature range of interest.

Since then the formula has been modified by various researchers like Jonas⁽²⁷⁾, Sellars and Tegart⁽²⁸⁾. The commonly used equation for hot deformation is that by Sellars and Tegart and the equation is expressed as

$$\dot{\epsilon} = A(\sinh \alpha \sigma)^{n'} \exp \left(\frac{-Q}{RT} \right)$$

where A , α and n' are constants which are independent of temperature and stress.

1.4.2.2 Velocity - modified Temperature

In 1946, MacGregor and Fisher⁽²⁹⁾ conducted slow speed tension tests (true strain rate in the range of $5 \times 10^{-5} \text{ s}^{-1}$ to $500 \times 10^{-5} \text{ s}^{-1}$) on annealed SAE 1020 steel, SAE 1045 steel and brass in the temperature range $70^{\circ}\text{C} - 665^{\circ}\text{C}$. A "velocity-modified temperature" parameter was proposed by them. Instead of expressing the flow stress as a function of three variables, namely, temperature, strain and strain rate, they proposed the temperature and strain rate to be combined in a single equation termed the "velocity-modified temperature T_m ". This leaves the flow stress as a function of T_m and strain. The expression given is,

$$T_m = T(1 - \kappa \ln \frac{\dot{\epsilon}}{\dot{\epsilon}_0})$$

where T = testing temperature in degrees absolute

$\dot{\epsilon}_0$ = a base strain rate

$\dot{\epsilon}$ = true strain rate

κ = material constant

This form gives the expected qualitative result that an increase in strain rate is equivalent to a decrease in temperature. This concept was examined by MacGregor and Fisher by comparison with the tension data and found to give satisfactory correlation.

The constant $\dot{\epsilon}_0$ is arbitrarily selected and in their experiment was taken as $100 \times 10^{-5} \text{ s}^{-1}$. The constant κ was selected - presumably by trial and error - such that when the stress is plotted against T_m for the various values of strain, smooth curves result. The curves of true stress versus velocity-

modified temperature for annealed SAE 1020 steel and brass are shown in figures 1.3 and 1.4.

Then in 1946, MacGregor and Fisher⁽³⁰⁾ verified the same theory with new data for strain rates up to 0.5 s^{-1} and found that the expression can still be applied. Manjoine's data for mild steel was plotted by MacGregor and Fisher and this is shown in figure 1.5. The points fall on a smooth curve.

More recently Inoue⁽³¹⁾, as reported by Nakayama⁽³²⁾, has applied the velocity modified temperature concept to tension data of several steels at temperatures ranging from 830°C to 1230°C and at strain rates of 0.8 to 75 s^{-1} . Inoue found satisfactory correlation by the use of the velocity-modified temperature T_m . Nakayama, using MacGregor's data for SAE 1020 plotted the stress-temperature curve for strain rate values of 10^3 and 10^4 s^{-1} as shown in figure 1.6. Manjoine⁽¹⁸⁾ has shown that as the strain rate increases, the "strain-ageing" region tends to move to the higher temperatures and Oyane's⁽³³⁾ data indicated that for mild steel at a strain rate of 430 s^{-1} , a peak stress occurs at about 600°C . Both the observations are found in figure 1.6, thus giving greater support to the reliability of the concept of the velocity-modified temperature.

Oxley⁽³⁴⁾ went further to simplify the use of the concept in metal cutting by assuming that the true stress-true strain curve for a particular combination of temperature and strain rate can be represented by the power relationship:

$$\sigma = B\epsilon^n$$

where B and n are dependent on T_m . It was discovered that he had used $\log \frac{\dot{\epsilon}}{\dot{\epsilon}_0}$ instead of $\ln \frac{\dot{\epsilon}}{\dot{\epsilon}_0}$ in the velocity-modified

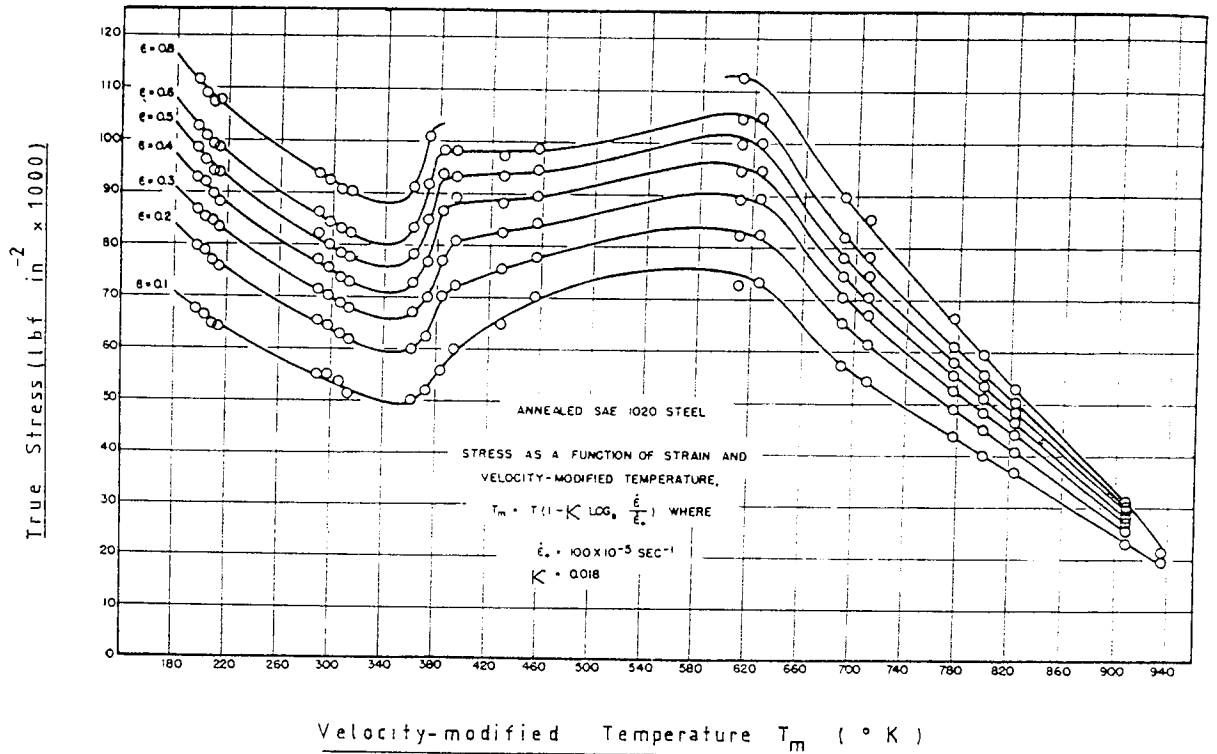


Figure 1.3: True stress as a function of the true strain ϵ and velocity-modified temperature T_m for SAE 1020 steel. After MacGregor (29)

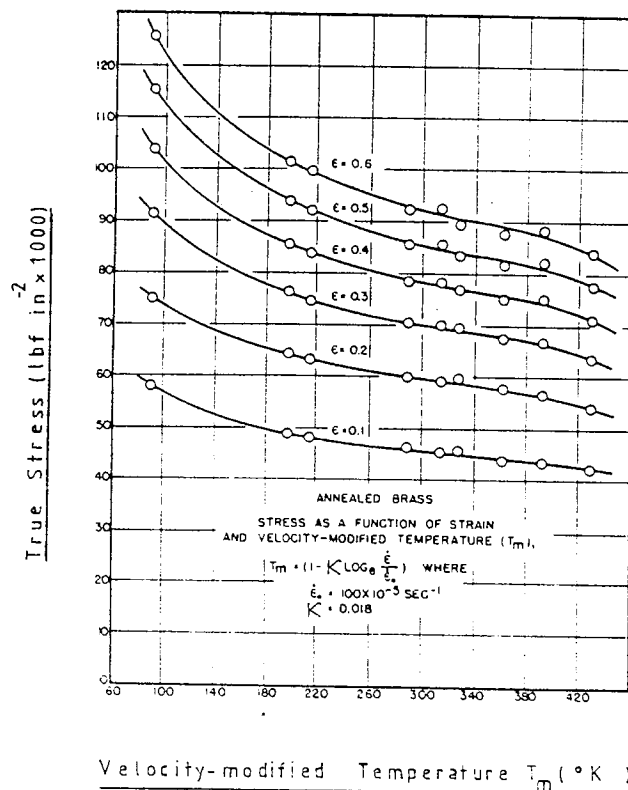


Figure 1.4: True stress as a function of true strain ϵ and velocity-modified temperature T_m for annealed brass. After MacGregor (29)

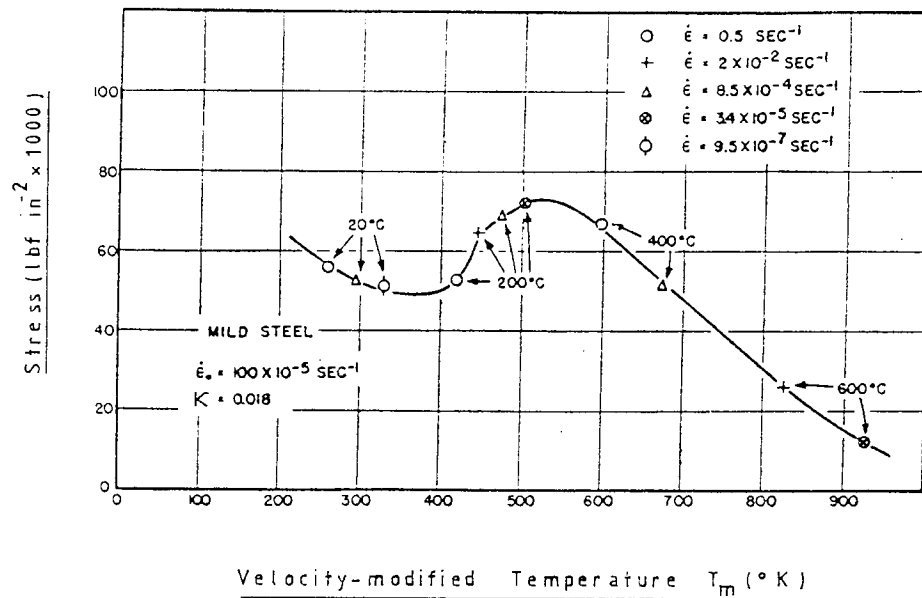


Figure 1.5: Stress against velocity-modified temperature T_m for a strain of 0.1. After MacGregor (30)

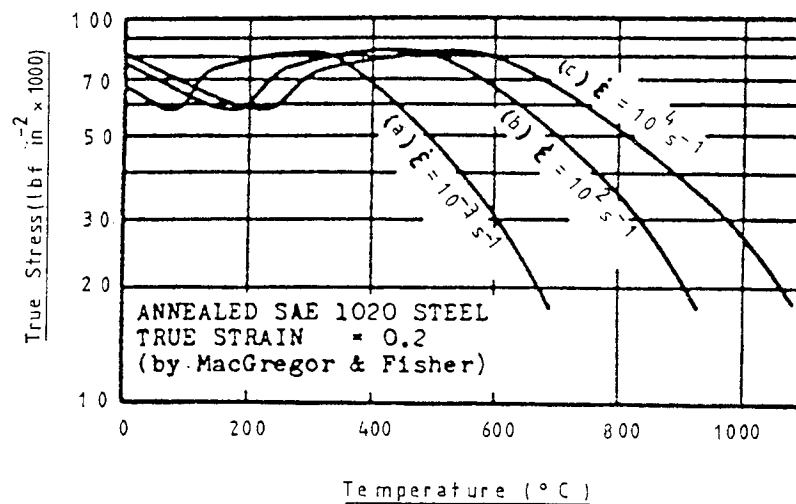


Figure 1.6: True stress against temperature. After Nakayama (32)

temperature equation. A typical plot of the relationship is shown in figure 1.7. Thus by representing the curves mathematically, the stress at any strain can be calculated, as B and n can be found.

1.4.3 Formulae Used in the Theoretical Analysis

The stress-strain data used in the theoretical analysis were found to fit the power relationship. Also, graphs of flow stress against the velocity-modified temperature yield reasonably smooth curves. Thus the author used the technique established by Oxley to calculate the various stresses at different strains, temperatures and strain rates. This allows the effects of strain, strain rate and temperature of any point in the deformation zone to be considered. Consequently, the theory does not have to depend on the use of a mean temperature and strain rate but rather to take into consideration the effects of the variations of strain rate and temperature in the deformation zone. Besides being able to predict the temperature distribution, the flow-stress distribution can also be predicted.

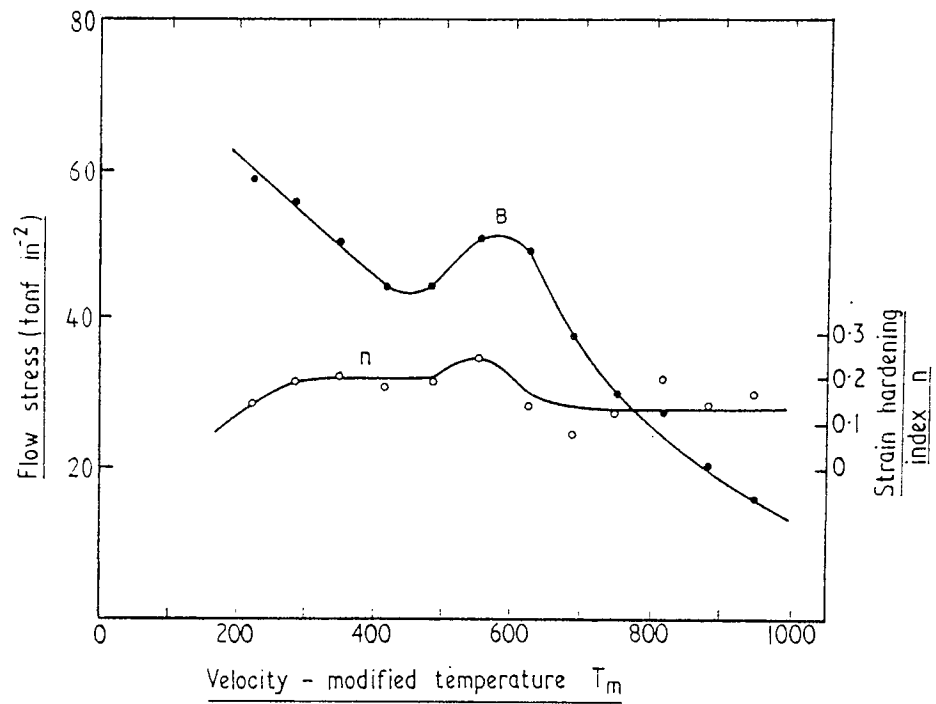


Figure 1.7: Relationships between B, n and T_m .
After Oxley (34)

1.5 TEMPERATURE DISTRIBUTION IN THE DEFORMATION ZONE

During deformation the work done in the material and by friction at the die-workpiece interface is dissipated as heat which is manifested as a rise in temperature. 'High' temperatures can bring about undesirable metallurgical changes such as "hot shortness" in extrusion, poorer lubricant performance, aggravating die wear, and can result in poor drawn wire surface quality. Since the speed of drawing used in industry is rather high, the heat is often evolved within a millisecond or less, thus high temperatures and steep temperature gradients can be expected near the surface of the wire. Large differences of temperature between the core and surface of the wire are the cause of residual stresses which may be undesirable in subsequent use. The frictional conditions at the die-wire interface will also be affected in a complex manner.

It is difficult to measure the temperature distribution in the deformation zone, although Ranger⁽³⁵⁾ has measured the temperature distribution at the die-wire interface. Thus a theoretical approach to establish the temperature distribution in the deformation zone would be advantageous.

Siebel and Kobitsch⁽³⁶⁾ were probably the first to calculate the distribution of temperature within the deforming wire during the wire drawing process. An analytical approach was used with the following assumptions being made:

- a) homogenous plastic deformation, constant yield stress,
and a die pressure equal to the yield stress,
- b) the temperature increase due to friction is parabolic

in or near the tool-material interface,

- c) there is no heat flow in axial direction, and
- d) only 20 per cent of the friction heat flows into the die while the rest remains in the material.

The temperature distribution calculated for the cold drawing of wire with an area of reduction of 36 per cent at a speed of 196.8 ft min⁻¹ is shown in figure 1.8. It is clear that a wide temperature gradient exists at the die-wire interface and the highest temperature rise is about 175°C assuming a coefficient of friction of 0.05.

Perhaps the most unique contribution is that by Bishop⁽³⁷⁾ who in 1955 used a numerical method to estimate the temperature field in plane strain extrusion of an ideal plastic material. He neglected friction and used a 90° die which allows square meshes to be used for the numerical analysis. The necessary velocity and strain rate distributions were derived from a simple slipline field. The complex problem of heat generation, conduction and transportation was separated into two parts due to difficulties in storing all the data in the difference equation. Thus the heat generation and transportation were regarded as occurring instantaneously, followed by a time interval in which conduction takes place. The process was repeated until a steady-state temperature distribution was reached. This method has the disadvantage that the mathematics involved are rather complicated and as claimed by Tay⁽³⁸⁾, the heat generation, conduction and transportation can be handled simultaneously by modern computers with a large memory core.

The slip-line field solution proposed by Alexander⁽³⁹⁾ for hot-rolling was adapted by Johnson and Kudo⁽⁴⁰⁾ for use as an upper bound

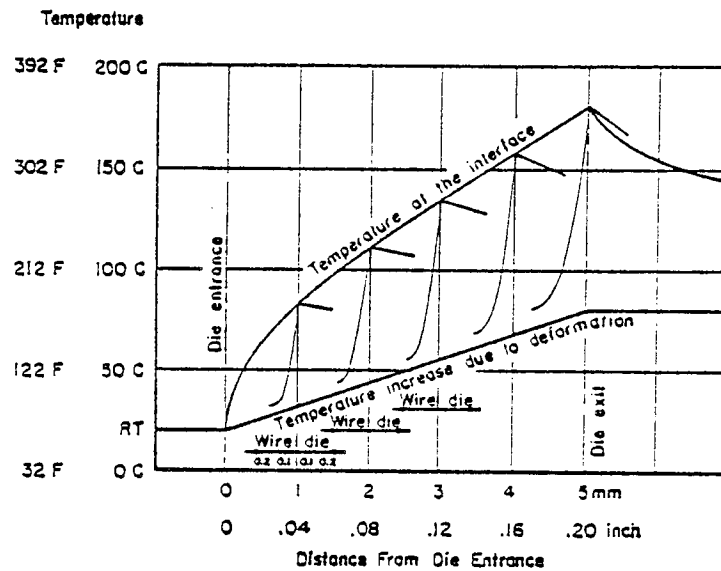


Figure 1.8: Temperature distribution in drawing steel wire from 0.2 in to 0.16 in with a speed of $196.8 \text{ ft min}^{-1}$, and coefficient of friction of 0.05. After Siebel (7)

to evaluate the temperature distribution through the roll-gap. The whole operation was assumed to be adiabatic.

Altan⁽⁴¹⁾ calculated the temperature rise for cold wire drawing by assuming that deformation takes place under the die defined by an entry boundary and an exit boundary, and that a volume element moves by following the flow line in the deformation zone. The type of boundaries assumed were not stated and from the diagram given, it was inferred that spherical boundaries were assumed and the flow was towards the apex of the die. The temperature rise due to deformation work ΔT and frictional work $\Delta \theta$ in a time interval Δt is given by,

$$\Delta T = \frac{\bar{\sigma} \dot{\epsilon} \Delta t}{J C \rho}$$

$$\Delta \theta = \frac{\mu \bar{\sigma} V S \Delta t}{J C_a \rho_a V_a}$$

where $\bar{\sigma}$ = flow stress of the drawn wire

$\dot{\epsilon}$ = effective strain rate

J = conversion factor between mechanical and thermal energies

C = specific heat of the material

ρ = specific weight of the material

β = per cent deformation energy transformed into heat

V = velocity at the interface

S = surface area at the interface

V_a = volume element

C_a; ρ_a = average specific heat and specific weight at the interface

Heat conduction was taken into consideration according to the technique derived by Bishop.

Altan simulated the same drawing condition as Siebel and Kobitzsch (see figure 1.8) and found that the temperatures in the wire and die showed good agreement, though the maximum interface temperature at the exit calculated by Altan is lower than that of Siebel and Kobitzsch by about 18°C .

In another paper by Altan and Kobayashi⁽⁴²⁾ the same approach was applied to cold and hot extrusion of metals through conical dies. The technique was extended to predict the temperature of the billet before extrusion taking into account the cooling of the billet in air and the transfer of heat to the container. The study was very comprehensive and the effects of the various parameters on the temperature distributions were investigated. The effects could be summarized as follows:

- a) the mechanical and thermal properties of the metal affects the magnitude of the heat generated,
- b) the temperatures developed increase as the following variables increase in magnitude:
 - i) coefficient of friction,
 - ii) extrusion ratio,
 - iii) strain rate and
 - iv) die angle

With the development of the powerful finite element technique various investigators⁽⁴³⁻⁴⁵⁾ have used it to establish the temperature distribution for continuous dieless drawing, hot hydrostatic extrusion and cold wire drawing. The heat generation and heat conduction could

be taken into account simultaneously.

1.5.1 Calculating the Temperature and Flow Stress Distributions
for the Theoretical Analysis

The author also calculated the temperature rise due to deformation and frictional work for points in the deformation zone and simplified the calculations by assuming adiabatic deformation. All the work done was assumed to degenerate to heat. Also, mathematical relationships between stress, strain, strain rate and temperature are assumed (see section 1.4.3), therefore the flow stress distribution in the deformation zone, taking into consideration the local temperature rise, can be established. The upper bound solution developed for predicting the draw stress takes into consideration the variations of the flow stress in the deformation zone.

1.6 FRICTION

Although a considerable amount of work has been done to understand the mechanism of friction, it is an area where there still exist some uncertainties because of the complexity of the surface conditions prevailing under metal working situations. Friction is an important parameter in any metal forming process, as it affects the forming loads, the surface temperature and the life of the tools. There are several theories formulated to define the friction phenomenon. The following discussion will be limited to Coulomb's Law and the constant friction factor.

1.6.1 Coulomb Friction u

If the tangential stress τ at any point on the surface (between two bodies in contact) is proportional to the normal pressure 'p', between them, and opposite to the direction of motion, then this state of friction is described by the Coulomb friction law:

$$u = \frac{\tau}{p}$$

Although the coefficient of friction in many metal deformation processes may not be a constant, u is often taken as a constant for a given die and material, for simplicity. Also, it is said to be independent of the velocity for the same reasons.

1.6.2 Constant friction factor m

Sometimes, it is convenient to express friction as a fraction of shear yield stress when one of the two bodies in contact is fully plastic. Hence,

$$\tau = mk$$

where m = friction factor

k = yield stress in shear.

For von Mises materials,

$$\tau = m \frac{Y}{\sqrt{3}}$$

where Y = yield stress of material.

Von Mises materials are materials which do not undergo elastic deformation, do not strain harden and obey von Mises' stress-strain rate law.

The friction factor m is taken as a constant for a given die and material, and is also independent of both the die pressure and the velocity. It was postulated that m varies between 0 and 1 for frictionless case and maximum possible friction.

This concept of friction is preferred by some investigators because the computations of friction losses are considerably simplified⁽⁴⁶⁾.

1.6.3 Determination of u and m by Experiments

The weakest feature in any theoretical approach is in making some reasonable substitution for u or m . In this section, the various techniques employed in cold drawing to establish the coefficient of

friction μ and constant friction factor m are discussed.

1.6.3.1 Split Die Method

The problem of determining the coefficient of friction μ for cold drawing persisted until in 1952, when MacLellan⁽⁴⁷⁾ used the split die technique to ascertain the mean die pressure in his experiments in wire drawing. The die was in two halves and the forces, tending to separate the two halves were measured concurrently with the draw force. The coefficient of friction μ between the die and the wire was assumed constant and an expression was proposed to estimate its value using the draw force, die-splitting force and the die semi-angle, all of which could be obtained from experiments.

Later, the split die method was improved by Yang⁽⁴⁸⁾ then modified by Major⁽⁴⁹⁾ who simplified the procedure. However, calibration of the die has remained a problem.

1.6.3.2 Oscillating Die Method

In 1965, Moore and Wallace⁽⁵⁰⁾ developed a torsionally oscillating die to determine the coefficient of friction in their tube sinking experiments. With this technique it was found that the calibration of the equipment used in the experiment was considerably simpler than that required by the split die method. In oscillating the die, inertia problems arose and it was deemed necessary to rotate the die continuously to eliminate these problems.

1.6.3.3 Die Rotation Method

It has been known for quite a long time that by rotating the die, it is possible to draw with a lower value of draw load. In 1931, Greenwood and Thomson⁽⁵¹⁾, and Linicus and Sachs⁽⁵²⁾, all used the rotating die method to determine the coefficient of friction between the wire and die in wire drawing experiments. Later, this technique was investigated further by Rothman and Sansome⁽⁵³⁾ with experiments in drawing rods through a rotating die. A theory was proposed by these authors to explain the reduction in draw load when the die was rotated and hence the difference used to calculate the coefficient of friction between the rod and the die. It was noted that this method of calculating the coefficient of friction is not accurate at high rotational speed. This is probably due to the rise in temperature which affects the viscosity of the lubricant film and hence the μ . Hofsten and Linstrand⁽⁵⁴⁾ have reported temperature increases of approximately 25% as compared with a stationary die.

1.6.3.4 Indirect Method

In 1968, an indirect technique to determine the coefficient of friction μ and constant friction factor m for cold drawing was proposed by Evans and Avitzur⁽⁵⁵⁾. Using the upper bound technique, they derived an equation for the draw stress which takes into account μ or m . The draw stress equation was then differentiated with respect to the die semi-angle α and the derivative equated to zero to give the optimum die-angle.

By determining the draw stresses experimentally with different die-angles and reductions in area, the optimum die angle can be found. If all the known parameters are substituted into the equation, the only unknown is u or m (depending on the equation used). The advantage of this method is its simplicity of equipment used - only a load cell and a set of dies are required. No calibration of the die is required and splitting of the die is unnecessary.

Although the importance of knowing the coefficient of friction u or the constant friction factor m in establishing the frictional conditions at the die-wire interface is appreciated, no attempt was made in this research to determine u or m . For convenience, the concept of constant friction factor m was used in the theoretical analysis. Since the values of m have not been determined experimentally, families of curves of draw stresses against draw temperatures for various values of m were plotted. The results are shown in Chapter Eight.

1.7 UPPER-BOUND SOLUTIONS OF AXISYMMETRIC FORMING PROBLEMS THROUGH CONICAL DIES

Perhaps, the most commonly used upper-bound theorem for axisymmetric forming problems through conical dies is that by Prager and Hodge⁽⁵⁶⁾. The theorem which is for von Mises 'perfect' plastic material states that, "Among all kinematically admissible strain rate fields, the actual one minimises the power." Drucker⁽⁵⁷⁾ extended this theorem to include the velocity discontinuities. Thus, the following expression is a minimum for the actual velocity:

$$J^* = \frac{2}{\sqrt{3}} Y \int_V \sqrt{\frac{1}{2} \dot{\epsilon}_{ij} \dot{\epsilon}_{ij}} dV + \int_{S_T} \tau |\Delta v| dS - \int_{S_t} T_i v_i dS$$

where J^* = externally supplied power

$\dot{\epsilon}_{ij}$ = strain rate

V = volume of deformation

τ = resistance to shear

S = surface subjected to shear

Δv = velocity discontinuity

T_i = pre-determined body traction

Y = flow stress

v_i = velocity at entry and exit surfaces having T_i

A kinematically admissible velocity field is defined as the velocity field where the normal component of the postulated velocity field of the deforming material equals that of the tool, over the surface of contact, when it satisfies the relaxed continuity and prescribed boundary velocity requirements, provided the velocity of the die is predetermined. A strain rate field derived from a kinematically

admissible velocity field is kinematically admissible.

The actual externally supplied J^* is never higher than the value predicted by using the expression given earlier. In the case of wire drawing, the externally supplied power is provided by the front draw pull. The first term computes the power of internal deformation, over the volume of deformation. The second term expresses the shear power over the surface of velocity discontinuities including the boundary between the tool and the material. The last term includes the power supplied by predetermined body tractions. The back stress applied in wire drawing, or back and front tension in rolling, can be taken as an example for traction.

When metal moves in and out of the plastic zone in the die, it is sheared to change the direction of flow and this constitutes the redundant work in a deformation process. Theoretical analysis of the redundant work, therefore, depends on the shape of the boundaries chosen. There are, of course, an infinite number of boundaries which can be chosen. In the absence of knowledge of the exact boundary existing in nature, it is necessary to determine the upper bound solutions for various different shapes and then to obtain the lowest upper bound.

The use of Prager and Hodge upper bound theorem using spherical boundaries is available in detail in the book of Avitzur⁽⁵⁸⁾ and thus it is not repeated here.

Avitzur⁽⁵⁹⁾ used a triangular velocity field to predict the draw stress for flow through converging dies. The surfaces of velocity discontinuity Γ_1 and Γ_2 are conical surfaces as shown in figure 1.9 and they meet at the axis of symmetry. The position of their intersection point along the axis of symmetry is temporarily assumed

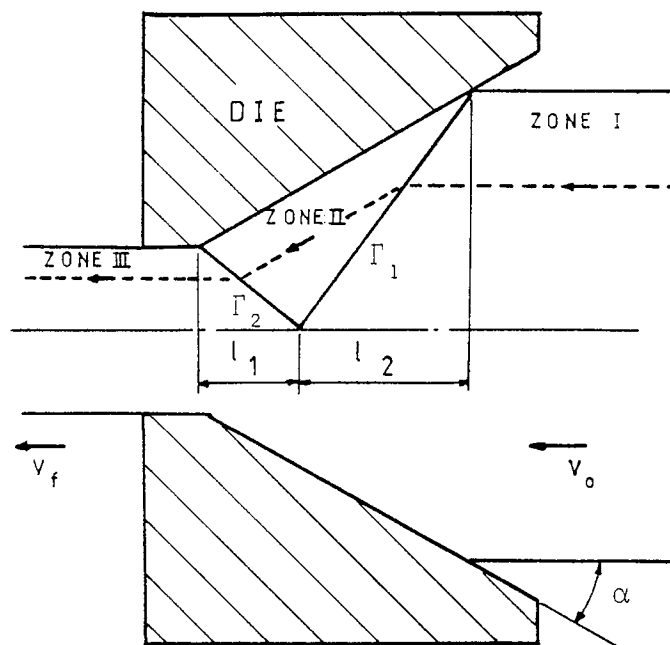


Figure 1.9: The triangular velocity field.
After Avitzur (59)

arbitrarily and the power of deformation, computed using Prager and Hodge's upper bound theorem, is minimised with respect to the intersection point, which is governed by l_2 . Zones I and III are rigid bodies moving at an axial velocity of V_0 and V_f respectively. Changes in direction occur at the surfaces Γ_1 and Γ_2 so that the velocity in zone II is parallel to the surface of the die. The derivation for the draw stress is complex and the solution is bulkier than that for spherical field with a complex iteration procedure for one of the parameters. Thus, the equation will not be presented here.

Avitzur compared the solutions obtained by the spherical and triangular velocity fields. He found that the solution predicted by the triangular velocity field is higher than that of the spherical velocity field. For both of the velocity fields as the die semi-angle increases up to about 7° the relative drawing stress decreases and then it increases with continuing increase in the die semi-angle. This is because smaller die angles are associated with long contact between the workpiece and the die and thus with high friction losses. The optimum die angle is therefore 14° .

Osakada⁽⁶⁰⁾ derived an equation for the extrusion pressure in axisymmetric extrusion by assuming elliptical boundaries and flow is towards the virtual apex of the die. The upper bound value of the extrusion pressure p calculated is given by:

$$\begin{aligned} \frac{P}{Y} = & \frac{2 \ln R}{\sin^2 \alpha} \int_0^\alpha \sin \theta (g^2 \cos \theta + g g' \sin \theta) \times \sqrt{1 + \frac{1}{12} \left(\frac{3 g g' \cos \theta + (g'^2 + g g'' - g^2) \sin \theta}{g^2 \cos \theta + g g' \sin \theta} \right)^2} d\theta \\ & + \frac{4}{\sqrt{3}} \frac{1}{\sin^2 \alpha} \int_0^\alpha \sin^2 \theta (g^2 + g'^2) d\theta \\ & + \frac{1}{\sqrt{3}} \frac{m \ln R}{\sin \alpha} [\cos \alpha + g'(\alpha) \sin \alpha] \end{aligned}$$

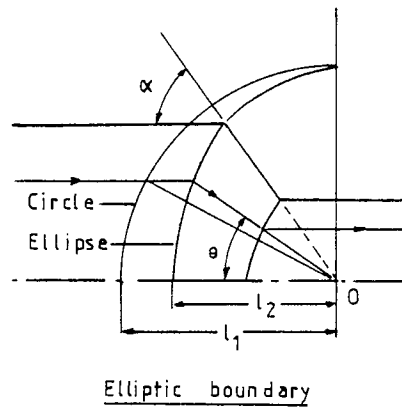
where
$$g = \sqrt{\frac{\cos^2 \alpha + \rho^2 \sin^2 \alpha}{\cos^2 \theta + \rho^2 \sin^2 \theta}}$$

$$g' = \frac{dg}{d\theta}$$

$$g'' = \frac{dg'}{d\theta}$$

$R =$ extrusion ratio

The upper bound value is minimised with respect to ρ defined by $\frac{l_2}{l_1}$ where l_2 and l_1 are as shown below.



1.7.1 A Brief Outline of the Upper Bound Solution

Developed for the Drawing of Wires at Elevated Temperatures

The concept of Prager and Hodge's upper bound solution on the power J^* was used by the author to obtain the upper bound solution for the drawing of wires at elevated temperatures. In an attempt to obtain the lowest upper bound, the shape of the inlet plastic boundary was assumed to be exponential in shape following the relationship:

$$\rho = \rho_0 \exp c(\theta - \alpha)$$

where,

ρ = radial distance from a point on the inlet boundary
to the virtual apex of the die

ρ_0 = radial distance from the intersection point of the
die and inlet boundary to the virtual apex of the die

c = a constant which is varied to obtain the lowest upper
bound

θ = angle made by a point on the boundary with the axis of
symmetry

α = die semi-angle

Flow towards the virtual apex of the die was assumed and the upper bound is minimised with respect to c . Chapter 2 gives a detailed analysis of the theoretical solution.

1.8 OTHER FORMING PROCESSES AT ELEVATED TEMPERATURES

1.8.1 Hot Tube Drawing

It appears that little work has been done on the drawing of tubes at elevated temperatures, but a patent⁽⁶¹⁾ on the warm drawing of tubes which are difficult to cold work was granted in 1971. As early as 1944, Sachs⁽⁶²⁾ put forward a theory using the equilibrium approach for the hot drawing of thin-walled tubing through a stationary die. The assumptions made were: the material was rigid plastic, there was no tube sinking (ie. it is a close pass draw), and the tube was thin walled (thus plane strain condition can be assumed). Realising the dependence of the flow stress on temperature and strain rate, Sachs assumed that the flow stress σ depends primarily upon the strain rate and was related by the equation

$$\sigma = a \dot{\epsilon}^b$$

where a and b are constants and temperature dependent. He expressed the strain rate in terms of its radial position in the deformation zone by the formula:

$$\dot{\epsilon} = \frac{V_o h_o}{h^2} (\tan \alpha - \tan \beta)$$

where V_o = velocity on entry to die

α = die semi-angle

β = mandrel semi-angle

h_o = thickness of tube on entry to die

h = thickness of tube

The theory developed predicted the die pressure distribution for mild steel at a draw temperature of 650°C. The die semi-angle was 2°

and a parallel mandrel was assumed. The validity of the theory was not supported by any experimental results.

Since then, it appears that there have not been any further developments in this area.

1.8.2 Hot Rolling

Early developments in the theory of rolling were directed towards the calculation of rolling load and torque.

Ekelund⁽⁶³⁾ developed an equation for the roll load in hot-rolling of strip, taking account of the influence of strain rate on the mean yield stress. The remainder of the formula is the same as for cold-rolling, though the numerical value of the coefficient of friction will be higher. The equation derived takes the form,

$$\frac{p}{w} = \left(\sigma + \frac{2V\eta\sqrt{\Delta h/R}}{h_a + h_b} \right) \sqrt{R\Delta h} \left(1 + \frac{1.6u\sqrt{R\Delta h} - 1.2\Delta h}{h_a + h_b} \right) \text{ ----(a)}$$

where

p	=	deforming load
w	=	width of strip
σ	=	static yield stress
V	=	velocity of rolling
η	=	viscosity of the hot material
Δh	=	reduction in strip thickness
R	=	roll radius
h _a	=	strip thickness after rolling
h _b	=	strip thickness before rolling
u	=	coefficient of friction

He carried the empirical approach a stage further and gave formulae for the "viscosity" of the hot steel, the coefficient of friction , and even the "static" yield stress , the latter in terms of percentage composition of constituent elements. The formulae proposed were:

$$\eta = 0.01(19,910 - 1.42T)$$

$$\mu = 0.84 - 0.0004T \quad (\text{for billet temperature } T \\ \text{in excess of } 700^{\circ}\text{C})$$

$$\sigma = 100 (1.4 + C + Mn + 0.3 Cr)$$

The general form of the equation (a) is useful, though it is usually desirable to determine the mean yield stress directly for the temperature and strain rate conditions.

Then in 1943, Orowan⁽⁶⁴⁾ put forward a general theory on roll-pressure distribution based on the equilibrium method to cover both hot and cold rolling, taking into account slipping and sticking friction. The equations put forward were too complex for general use in industry.

Utilising earlier work of Orowan, Sims⁽⁶⁵⁾ developed equations for rolling load and torque. The analytical integrations of the roll pressure is made possible by the use of small-angle approximations for trigonometrical functions, and it is assumed that conditions of sticking friction apply.

With the invention of the cam plastometer by Orowan⁽⁶⁶⁾ in 1950, the generation of true stress-strain curves of metals at elevated temperatures and constant strain rate was made possible. This enabled Cook and McCrum⁽⁶⁷⁾ to prepare curves of roll force and torque for a wide range of rolling conditions and steels. The curves were prepared based on the theoretical analysis of Sims. Mean values of the yield

stresses for the load and torque were used to compensate for the changes in yield stress of the material being rolled due to work hardening and thermal softening in the roll gap.

Cook and McCrum claimed that the loads and torques calculated using the data generated by the cam plastomer and Sims' formulae agree reasonably with measurements made during the hot rolling of steel in a laboratory mill.

With the introduction of plasticity theory, Alexander⁽³⁹⁾ constructed a slip-line field solution for the hot rolling of strip. He assumed sticking friction over the whole arc of contact. The derivation is complex and difficult. Again, like the previous researchers, the solutions can take no account of yield stress variations due to strain rate changes in the roll gap.

1.8.3 Hot Extrusion

Hirst and Ursell⁽⁶⁸⁾, basing their work on the formula derived by Johnson⁽⁶⁹⁾ from slip-line field considerations proposed the equation for hot extrusion of aluminium alloy as:

$$\frac{P}{Y} = (0.47 + 1.2 \log_e R) \exp \frac{4uL}{D}$$

where

Y = flow stress corresponding to a particular
temperature, strain and strain rate

R = extrusion ratio

L = billet length

D = billet diameter

To facilitate the application of their theory to the problem of hot lubricated extrusion, they introduced a useful diagram of interacting the variables, strain, strain rate and temperature as shown in figure 1.10. The left-hand side of the diagram shows the limitations on the extrusion ratio R set by the available capacity of the press. As the temperature increases, so that maximum extrusion ratio achievable increases owing to a decrease in yield stress of the material. The right-hand side of the diagram defines the thermal limitations due to temperature rise in deforming the metal.

Theoretically developed curves for an aluminium alloy were established and compared with experimental results. They state that the choice of suitable values for the yield stress is somewhat arbitrary, and selected cam plastometer results obtained at a strain rate of 30 s^{-1} , thereby obtaining good agreement with experiment. The author disagrees with their method of establishing the flow stress.

Farag and Sellars⁽⁷⁰⁾ extended the upper-bound solution derived by Kudo⁽⁷¹⁾ for cold extrusion to determine the pressures for axisymmetric extrusion of aluminium at a temperature range of 230°C - 500°C , ram speeds of 0.5 - 55 ft min^{-1} and extrusion ratios of 4.75 - 3.6 . They determined the flow stress of the billet material by hot torsion testing at 350°C - 500°C and strain rates of 2×10^{-3} to 4 s^{-1} . The flow stress of the material was considered to be a function of the Zener-Hollomon parameter Z as discussed in section 1.4.2.1

The Zener-Hollomon parameter was modified to take into account adiabatic temperature rise. Thus the modified Zener-Hollomon parameter Z_{mod} can be expressed as,

$$Z_{\text{mod}} \cong \frac{4 D_o^2 V \tan \alpha}{(D_o d)^{3/2}} \exp \frac{Q}{2R} \left(\frac{1}{T_o} + \frac{1}{T_f} \right)$$

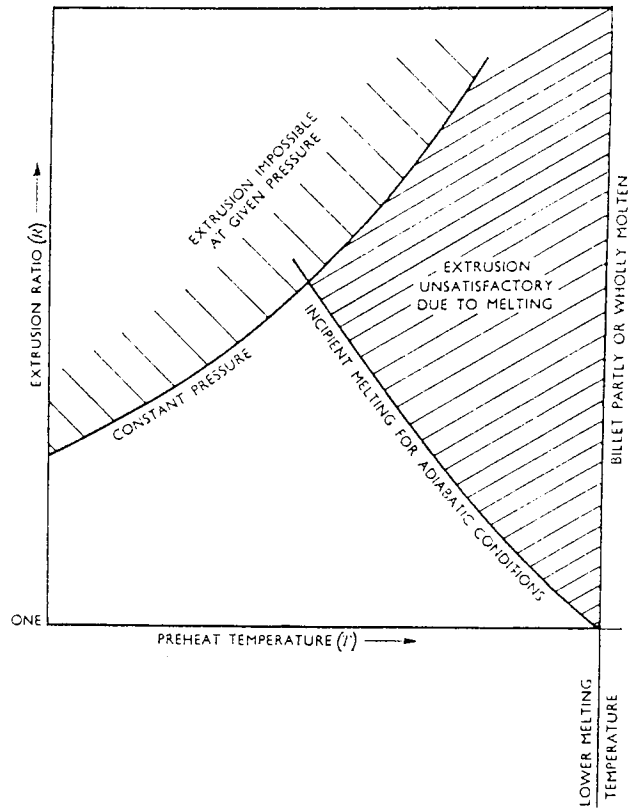


Figure 1.10: Schematic representation of the interaction of strain, strain rate and temperature on extrusion. After Hirst (68)

where V = ram speed
 T_o = billet temperature
 T_f = emergent bar temperature obtained by
considering the work done in extrusion

The flow stress corresponding to Z_{mod} can be found from a plot of Z against σ which is a straight line. Values of the mean flow stress are then substituted into Kudo's upper bound equations to determine the extrusion pressure.

The equations for the round and smooth dies used by Kudo are:

$$\frac{P}{Y} = 1.06 + 1.55 \ln R \quad (\text{rough die})$$
$$\frac{P}{Y} = 0.88 + 1.30 \ln R \quad (\text{smooth die})$$

The experimental points fall between values predicted by the above equations.

In 1974, Childs⁽⁷²⁾ investigated the metal flow of mild steel in hot extrusion. A split billet of mild steel was heated to 1170°C and partially extruded through a 90° die. The strain rate and strain distributions which occurred in the flow zone have been calculated from measurements of the distortion of grids inscribed on the split surface. Again, the steady state flow stress is assumed to be a function of the Zener-Hollomon parameter Z (discussed in 1.4.2.1).

The mathematical representation above enables the temperature and flow stress distribution to be calculated. Adiabatic heating was assumed and frictional heat was neglected.

The equivalent strain rate was calculated from the general formula

$$\dot{\epsilon} = \sqrt{\frac{2}{3} \dot{\epsilon}_{ij} \dot{\epsilon}_{ij}}$$

and the internal energy dissipation rate was found by numerical integration of the product of σ and $\dot{\epsilon}$. By equating the energy to the rate of external work, the average pressure on the ram was found.

The ram pressure measured experimentally was higher than the predicted. This is obvious as the pressure calculated by Childs is actually a lower bound value.

CHAPTER TWO

THEORETICAL ANALYSIS OF THE DRAWING OF WIRE AT ELEVATED TEMPERATURES

II. THEORETICAL ANALYSIS OF THE DRAWING OF WIRE AT ELEVATED TEMPERATURES

2.1 INTRODUCTION

This chapter presents the theoretical analysis of the drawing of wire at elevated temperatures. A form of upper bound solution was derived in the analysis of the process having as its main objective: a study of the process variables which is compared with the experimental results.

A form of minimum upper bound solution, based on the energy approach was derived which gave the least work done in deformation. The solution essentially comprised: firstly, an assumed inlet shear surface of which the distance between a point on the shear surface and the virtual apex of the die follows an exponential relationship which can be varied; secondly, the deformation zone was divided into small elemental areas and the temperature rise at each point due to deformation and frictional work at the die-wire interface was calculated. The new flow stress at each point was evaluated by assuming mathematical relationships between the stress, strain, temperature and strain rate. Thirdly, the power to overcome friction, shearing at inlet and exit surfaces and deformation work were calculated based on the flow stress distribution mentioned earlier. Finally, the overall power of work was minimised by varying the shape of the inlet shear surface.

The upper bound solutions had to be solved numerically with the aid of specially written computer programs which are discussed in section 2.3.

2.2 THE UPPER BOUND SOLUTION FOR THE DRAWING OF WIRE AT ELEVATED TEMPERATURES

The upper bound theorem formulated by Prager and Hodge⁽⁵⁶⁾ for rigid perfectly plastic solids states that: "Among all the kinematically admissible strain rate fields, the actual one minimises the power." Drucker⁽⁵⁷⁾ extended this theorem to include the velocity discontinuities. Thus, the expression

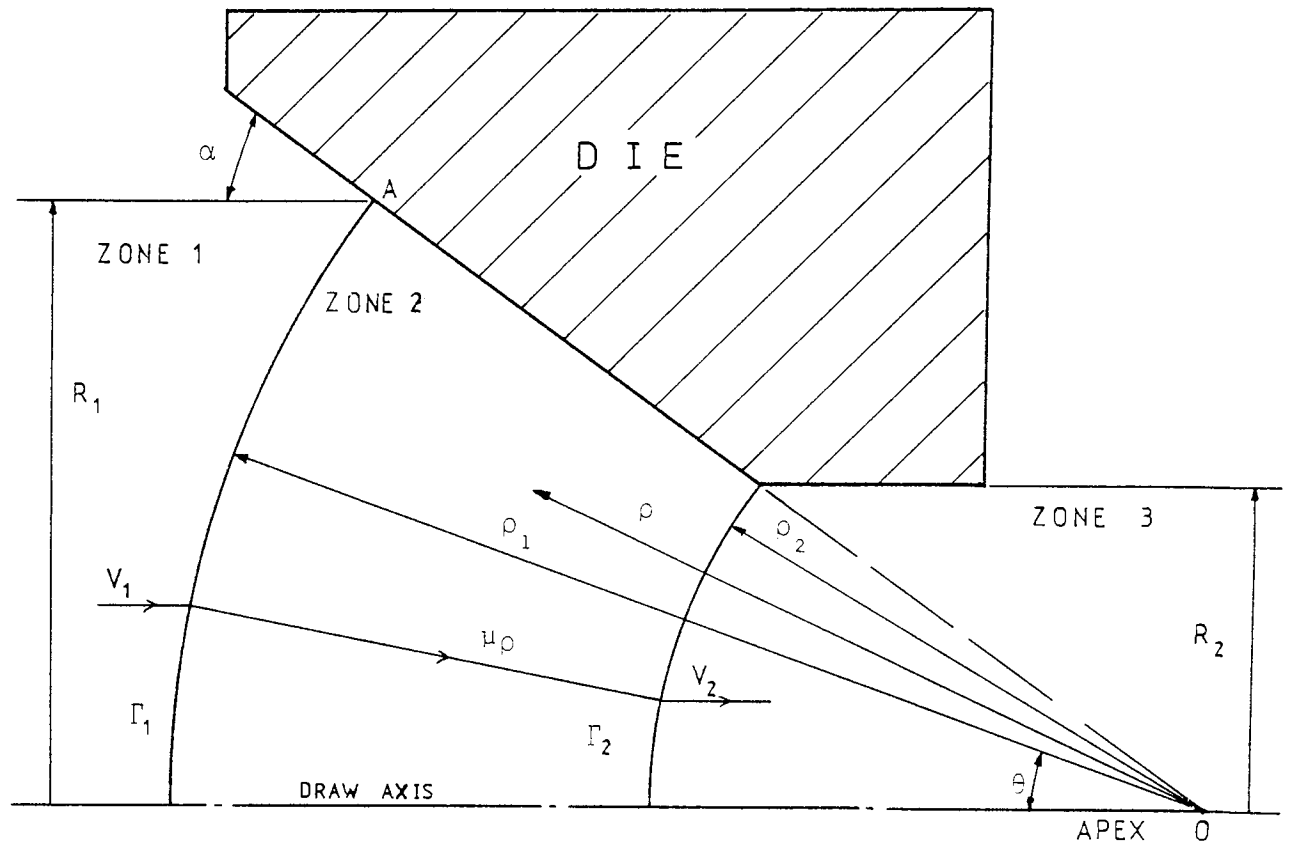
$$J^* = \frac{2}{\sqrt{3}} Y \int_V \sqrt{\frac{1}{2} \dot{\epsilon}_{ij} \dot{\epsilon}_{ij}} dV + \int_{S_F} \tau |\Delta v| dS - \int_{S_t} \tau_i v_i dS$$

is a minimum for the actual velocity. The actual externally supplied power, J^* , is never higher than that computed by the above equation.

The above expression combines three different power quantities. The first term represents the internal power of deformation within the volume of the deforming body. The second term expresses the shear power at surfaces of velocity discontinuities including the frictional boundaries. The last term includes the power supplied by predetermined body tractions. These tractions are for example, the back tension applied in a metal forming process, but, for this theoretical analysis, the back tension was assumed to be negligible.

2.2.1 The Flow Model

The postulated velocity field model is shown diagrammatically in figure 2.1. The inlet and outlet shear surfaces Γ_1 and Γ_2 respectively were assumed to be exponential in shape. It was assumed that under a steady flow, a particle enters the inlet shear surface Γ_1



$$\rho_O = OA$$

Figure 2.1: The flow model

with a uniform linear velocity V_1 , parallel to the draw axis. The plastic deformation occurs only in zone 2.

2.2.2 The Shear Surfaces

The inlet shear surface Γ_1 was assumed to be exponential in shape and ρ_1 follows the equation:

$$\rho_1 = \rho_o \exp(c(\theta - \alpha)) \quad \text{-----}(1)$$

where c is a variable used to minimise the draw stress.

Due to volume constancy, the shape of Γ_2 and Γ_1 are geometrically similar, therefore,

$$\rho_2 = \rho_o \sqrt{1 - A} \exp(c(\theta - \alpha)) \quad \text{-----}(2)$$

where A is the area of reduction.

2.2.3 The Velocity Field

The velocity field in the deformation zone was assumed to be directed towards the virtual apex O of the drawing die. Using spherical co-ordinates, the velocities in the deformation zone in the ρ , θ and ϕ directions are μ_ρ , μ_θ and μ_ϕ respectively.

2.2.3.1 Derivation of the Velocity Field

To satisfy the continuity of flow at the inlet shear surface Γ_1 , the normal velocity component on each side of the inlet shear surface must be equal. Therefore, with reference to figure 2.2a, the velocity at shear surface Γ_1 is

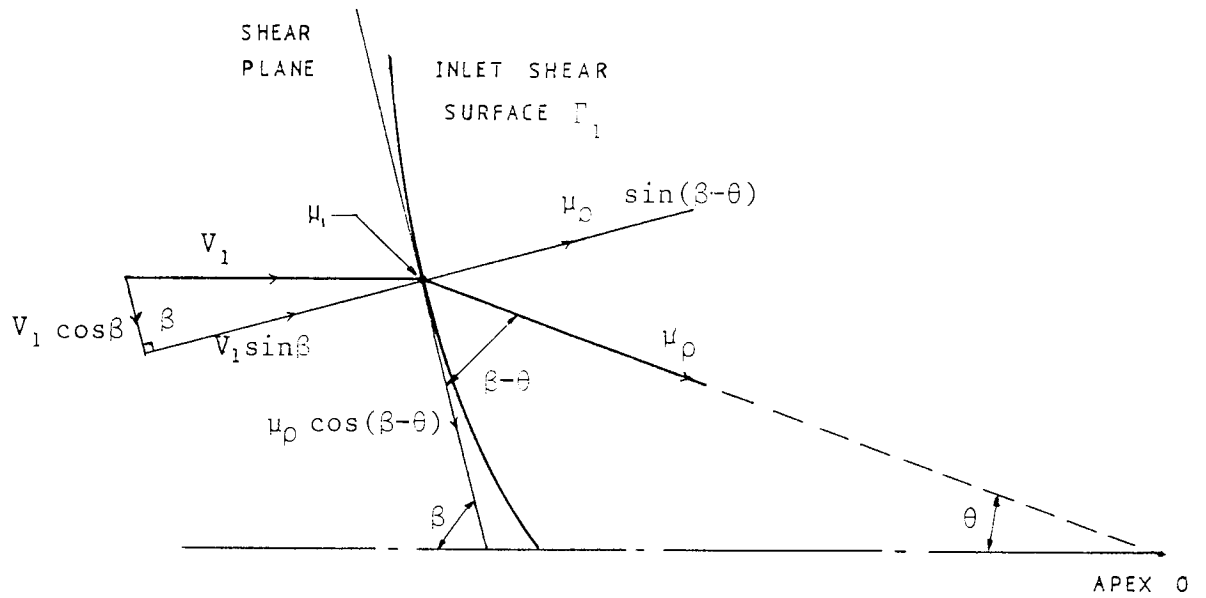


Figure 2.2(a): A view along ρ - θ plane for the inlet shear surface Γ_1

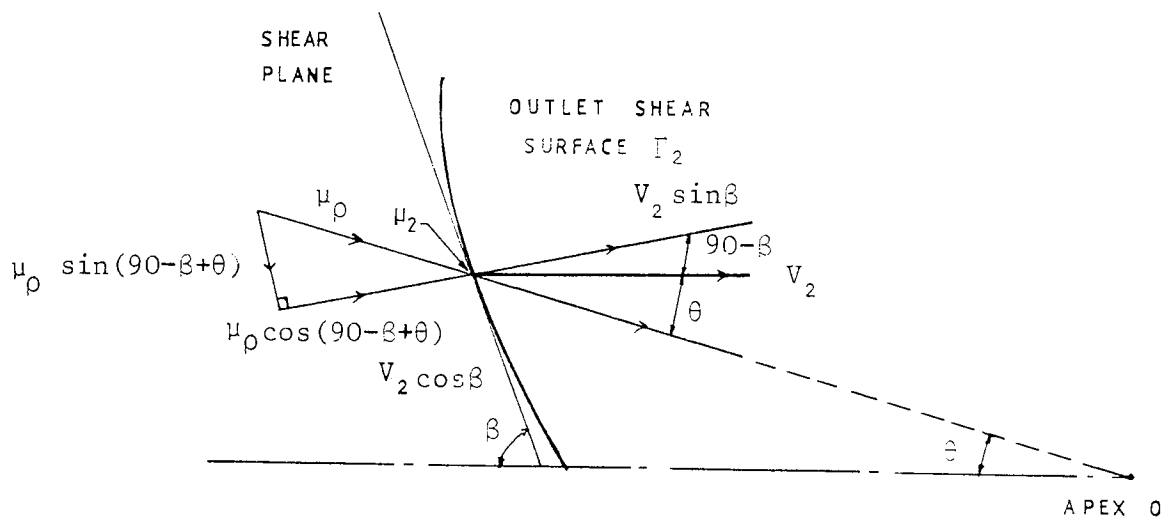


Figure 2.2(b): A view along ρ - θ plane for the outlet shear surface Γ_2

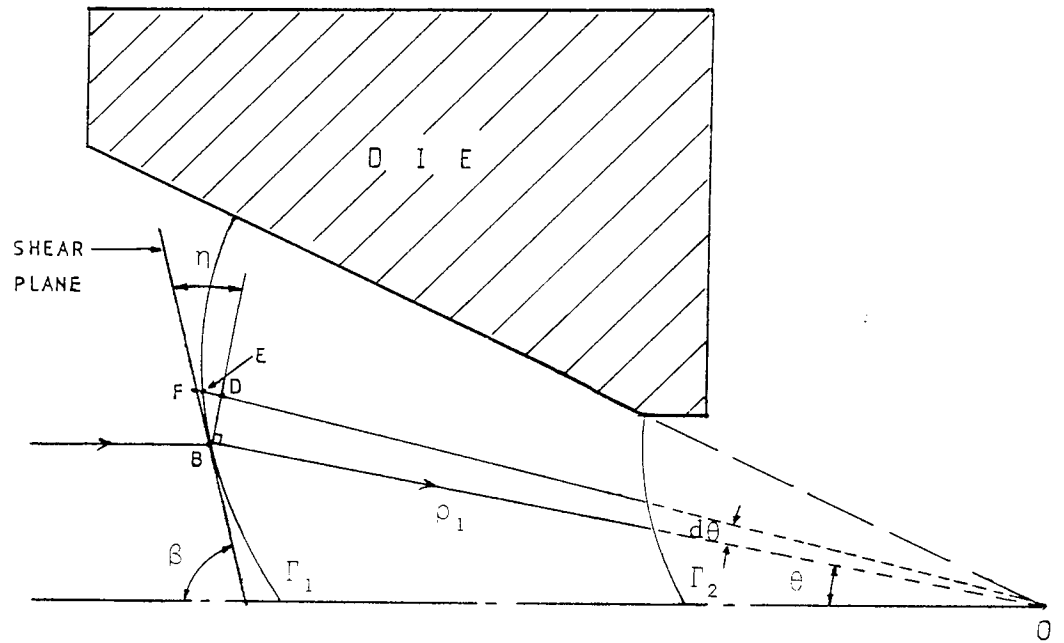


Figure 2.3: Diagrammatic relationship between the various angles

$$\mu_1 \sin(\beta - \theta) = V_1 \sin \beta$$

$$\mu_1 = \frac{V_1 \sin \beta}{\sin(\beta - \theta)} \quad \text{-----}(3)$$

From figure 2.3,

$$\tan(d\theta) = \frac{BD}{\rho_1}$$

Since $d\theta$ is very small, therefore it is justified to assume that:

$$\tan(d\theta) = d\theta$$

$$OB = OD$$

$$BD = \rho_1 d\theta$$

$$\angle FDB = 90^\circ$$

$$\tan \eta \approx \frac{ED}{BD}$$

$$= \frac{d\rho_1}{\rho_1 d\theta}$$

$$= \frac{1}{\rho_1} \cdot \frac{d\rho_1}{d\theta}$$

$$= \frac{1}{\rho_1} \cdot \frac{d\rho_o \exp(c(\theta - \alpha))}{d\theta}$$

$$= c \frac{\rho_o}{\rho_1} \exp(c(\theta - \alpha)) \quad \text{-----}(4)$$

From equation (1),

$$\rho_1 = \rho_o \exp(c(\theta - \alpha))$$

$$\text{Therefore, } \tan \eta = c \quad \text{-----}(5)$$

The relationships of the various angles can be established

from figure 2.3 as follows:

$$\eta = 90 - (\beta - \theta) \quad \text{-----}(6)$$

$$\beta = 90 - \eta + \theta \quad \text{-----}(6a)$$

$$\begin{aligned} \therefore \sin \beta &= \sin(90 - (\eta - \theta)) \\ &= \cos \eta \cos \theta + \sin \eta \sin \theta \end{aligned} \quad \text{-----}(7)$$

$$\begin{aligned} \text{and } \sin(\beta - \theta) &= \sin(90 - \eta) \\ &= \cos \eta \end{aligned}$$

Thus, equation (3) can be expressed as

$$\mu_1 = V_1(\cos \theta + c \sin \theta) \quad \text{-----}(8)$$

This is the radial velocity of an element of distance ρ_1 from the virtual apex O, ie. a point on shear surface Γ_1 to the apex O.

Therefore, the velocity of the element at radial distance ρ (see figure 2.1) within the deformation zone can be calculated from the volume constancy requirement giving:

$$\begin{aligned} \mu_\rho &= \left(\frac{\rho_1}{\rho}\right)^2 \mu_1 \\ &= V_1 \left(\frac{\rho_1}{\rho}\right)^2 (\cos \theta + c \sin \theta) \end{aligned}$$

From equation (1),

$$\rho_1 = \rho_o \exp(c(\theta - \alpha))$$

$$\text{Therefore, } \mu_\rho = V_1 \left(\frac{\rho_o}{\rho}\right)^2 \exp(2c(\theta - \alpha))(\cos \theta + c \sin \theta) \quad \text{-----}(9)$$

Similarly, maintaining continuity at the outlet shear surface

Γ_2 and with reference to figure 2.2b,

$$V_2 \sin \beta = \mu_2 \cos(90^\circ - \beta + \theta) \quad \text{-----}(10)$$

From equation (3) and maintaining volume constancy, that is,

$$\mu_1 \rho_1^2 = \mu_2 \rho_2^2,$$

$$V_2 = V_1 \left(\frac{\rho_1}{\rho_2} \right)^2 \frac{\sin \beta}{\sin(\beta - \theta)}$$

$$V_2 = V_1 \left(\frac{\rho_1}{\rho_2} \right)^2$$

The above equation satisfies the volume constancy requirement.

2.2.4 The Strain Rate Components

The strain rate components can be expressed in terms of the derived velocity component μ_ρ as μ_θ and μ_ϕ and are both zero in value.

The strain rates expressed as a function of the velocity components are given by:

$$\dot{\epsilon}_\rho = \frac{\delta \mu_\rho}{\delta \rho} \quad \text{-----}(11)$$

$$\dot{\epsilon}_\theta = \frac{1}{\rho} \cdot \frac{\delta \mu_\theta}{\delta \theta} + \frac{\mu_\rho}{\rho} \quad \text{-----}(12)$$

$$\dot{\epsilon}_\phi = \frac{1}{\rho \sin \theta} \cdot \frac{\delta \mu_\phi}{\delta \phi} + \frac{\mu_\rho}{\rho} + \frac{\mu_\theta}{\rho} \cot \theta \quad \text{-----}(13)$$

$$\dot{\gamma}_{\rho\theta} = \frac{1}{2} \left| \frac{\delta \mu_\theta}{\delta \rho} - \frac{\mu_\theta}{\rho} + \frac{1}{\rho} \frac{\delta \mu_\rho}{\delta \theta} \right| \quad \text{-----}(14)$$

$$\dot{\gamma}_{\theta\phi} = \frac{1}{2} \left| \frac{1}{\rho \sin \theta} - \frac{\delta \mu_{\theta}}{\delta \phi} + \frac{1}{\rho} \frac{\delta \mu_{\phi}}{\delta \theta} - \frac{\cot \theta}{\rho} \mu_{\phi} \right| \quad \text{-----(15)}$$

$$\dot{\gamma}_{\phi\rho} = \frac{1}{2} \left| \frac{\delta \mu_{\phi}}{\delta \rho} - \frac{\mu_{\phi}}{\rho} + \frac{1}{\rho \sin \theta} \frac{\delta \mu_{\rho}}{\delta \phi} \right| \quad \text{-----(16)}$$

Hence the strain rates can be obtained by the appropriate substitution of the various derivatives of the velocity component μ_{ρ} in the above equations. The proofs of the following derivatives are shown in the appendix, A3.1.

$$\dot{\epsilon}_{\rho} = -2V_1 \frac{\rho_0^2}{\rho^3} \exp(2c(\theta - \alpha))(\cos \theta + c \sin \theta) \quad \text{-----(17)}$$

$$\dot{\epsilon}_{\theta} = V_1 \frac{\rho_0^2}{\rho^3} \exp(2c(\theta - \alpha))(\cos \theta + c \sin \theta) \quad \text{-----(18)}$$

$$\dot{\epsilon}_{\phi} = V_1 \frac{\rho_0^2}{\rho^3} \exp(2c(\theta - \alpha))(\cos \theta + c \sin \theta) \quad \text{-----(19)}$$

$$\begin{aligned} \dot{\gamma}_{\rho\theta} = \frac{1}{2} V_1 \frac{\rho_0^2}{\rho^3} [& 3c \exp(2c(\theta - \alpha)) \cos \theta + \\ & (2c^2 \exp(2c(\theta - \alpha)) - \exp(2c(\theta - \alpha))) \\ & \times \sin \theta] \quad \text{-----(20)} \end{aligned}$$

$$\dot{\gamma}_{\theta\phi} = 0 \quad \text{-----(21)}$$

$$\dot{\gamma}_{\phi\rho} = 0 \quad \text{-----(22)}$$

The incompressibility equation is given by:

$$\dot{\epsilon}_{\rho} + \dot{\epsilon}_{\theta} + \dot{\epsilon}_{\phi} = 0$$

stituting the respective values from equations (17) - (22) into the above equation gives zero value. Thus, the velocity fields derived

satisfy the incompressibility condition.

2.2.4.1 Equivalent Strain Rate

The equivalent strain rate $\frac{\dot{\epsilon}}{\epsilon}$ is expressed as:

$$\frac{\dot{\epsilon}}{\epsilon} = \sqrt{\frac{2}{3} (\dot{\epsilon}_{\rho\rho}^2 + \dot{\epsilon}_{\theta\theta}^2 + \dot{\epsilon}_{\phi\phi}^2 + 2(\dot{\gamma}_{\rho\theta}^2 + \dot{\gamma}_{\theta\phi}^2 + \dot{\gamma}_{\theta\rho}^2))}$$

Substituting equations (17) - (22) into the above equation gives:

$$\frac{\dot{\epsilon}}{\epsilon} = 2V_1 \frac{\rho_o^2}{\rho^3} \exp(2c(\theta - \alpha)) \left[(\cos \theta + c \sin \theta)^2 + \frac{1}{12} (3c \cos \theta + (2c^2 - 1) \sin \theta)^2 \right]^{\frac{1}{2}} \quad \text{-----(23)}$$

The full derivation is given in the appendix A3.2

2.2.5 Equivalent Mean Strain

To calculate the temperature rise due to deformation at each point in the deformation zone, the equivalent strain at that point has to be known together with other parameters.

For a particular flow line in the deformation zone, the radial velocity is given by equation (9) as:

$$u_\rho = V_1 \left(\frac{\rho_o}{\rho} \right)^2 \exp 2c(\theta - \alpha) (\cos \theta + c \sin \theta)$$

For a particle to move a small radial distance $d\rho$, the time dt taken is given by:

$$dt = \frac{d\rho}{\mu_p} \quad \text{-----}(24)$$

the equivalent mean strain $\bar{\epsilon} = \int_0^t \dot{\epsilon} dt$

Substituting equations (23) and (24) into the above gives:

$$\begin{aligned} \bar{\epsilon} &= \int_{\rho_1}^{\rho} 2V_1 \frac{\rho_o^2}{\rho^3} \exp 2c(\theta - \alpha) \left[(\cos \theta + c \sin \theta)^2 \right. \\ &\quad \left. + \frac{1}{12} (3c \cos \theta + (2c^2 - 1) \sin \theta)^2 \right] \frac{1}{2} \\ &\quad \times \frac{d\rho}{V_1 \frac{\rho_o^2}{\rho^3} \exp 2c(\theta - \alpha) (\cos \theta + c \sin \theta)} \\ &= \int_{\rho_1}^{\rho} \frac{2}{\rho} \left[1 + \frac{1}{12} \left(\frac{3c \cos \theta + (2c^2 - 1) \sin \theta}{(\cos \theta + c \sin \theta)} \right)^2 \right] \frac{1}{2} d\rho \\ \text{Therefore, } \bar{\epsilon} &= 2 \ln \frac{\rho_1}{\rho} \left[1 + \frac{1}{12} \left(\frac{3c \cos \theta + (2c^2 - 1) \sin \theta}{\cos \theta + c \sin \theta} \right)^2 \right] \frac{1}{2} \quad \text{-----}(25) \end{aligned}$$

2.6 Establishing the Temperature and Flow stress

Distributions in the Deformation Zone

It was assumed that adiabatic conditions prevail and that both plastic and frictional work degenerate into heat; redundant work is partly taken into account.

To evaluate the temperature rise due to plastic and frictional work, the necessary velocity, equivalent strain and equivalent strain rate at that point in the deformation zone must be known. The new flow stress at that point, taking into account the appropriate temperature rise, was evaluated also by assuming mathematical relationships between

the flow stress, equivalent strain, equivalent strain rate and the new temperature.

For the purpose of computing, the deformation zone was divided into $N_\rho + 1$ arcs, whose shapes are geometrically similar to the inlet and outlet shear surfaces. For a particular flow line, the distance $(\rho_1 - \rho_2)$ were divided into N_ρ equally spaced divisions. Similarly, the die semi-angle was divided into N_θ equally spaced angles. Thus, the whole deformation zone can be identified by co-ordinates (I, J) as shown in figure 2.4; any points on the inlet and outlet shear surfaces can be identified as $(1, J)$ to $(N_\rho + 1, J)$. Similarly, any point on the conical part can be represented as $(I, 1)$ where I varies along the conical part.

2.2.6.1 Relationship Between Stress, Strain, Strain Rate and Temperature

For the materials investigated, it was assumed that the true stress-strain curve obeyed the power relationship:

$$\sigma = B\bar{\epsilon}^n \quad \text{-----}(26)$$

for a particular temperature and strain rate.

Thus, given a set of stress-strain curves for the material covering the whole range of temperatures and strain rates, the value of B and n for a particular temperature and strain rate can be found by plotting $\log \sigma$ against $\log \epsilon$.

In order to apply the B and n values obtained from the true stress-strain curves to a range of temperatures and strain rates, it was assumed that the opposing effects of temperature and strain rate were related to a single parameter known as the velocity-

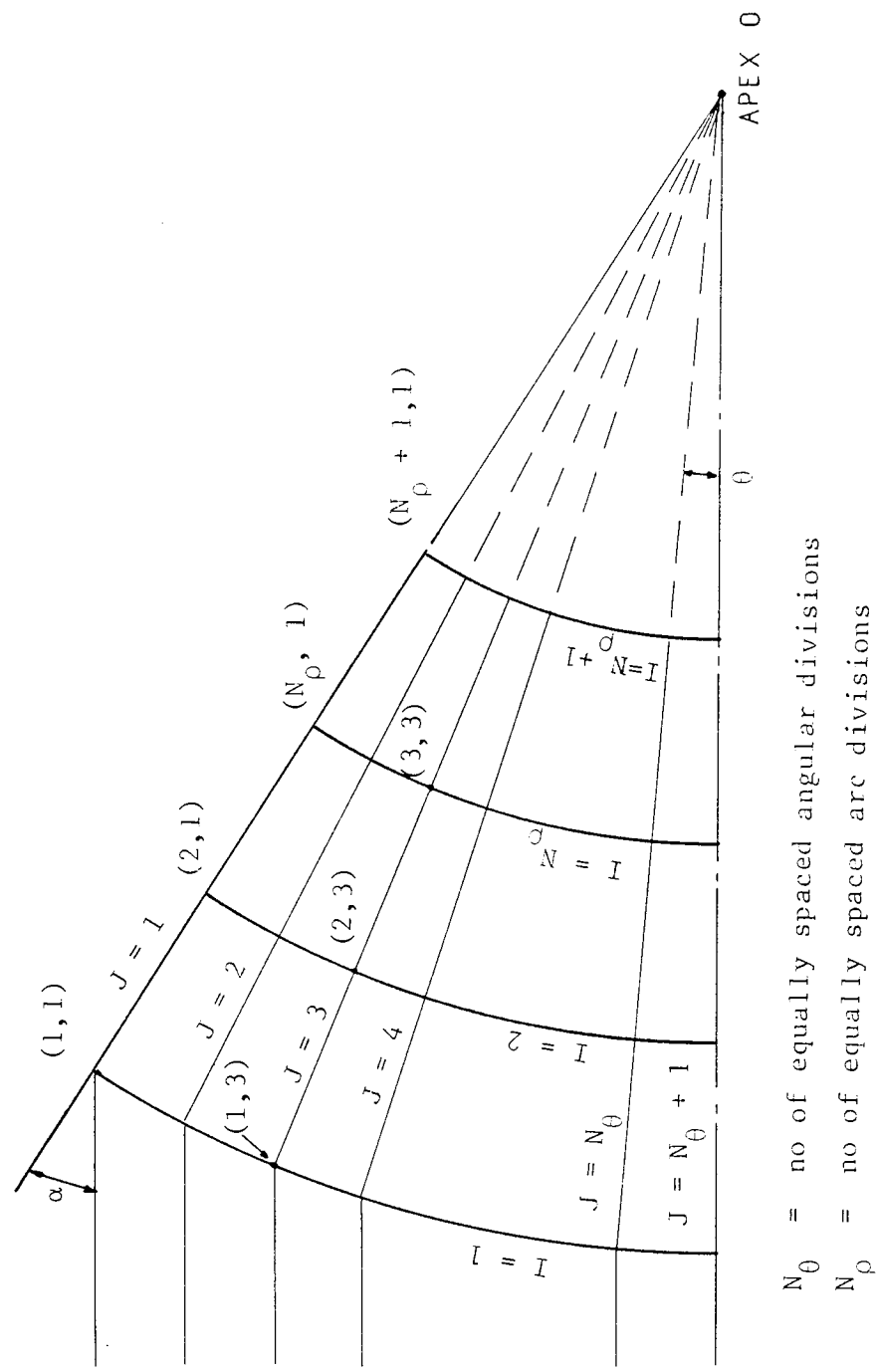


Figure 2.4: Dimensioning the deformation zone for computation purposes

modified temperature (see section 1.4.2.2), and expressed as:

$$T_m = T(1 - \kappa \ln \frac{\dot{\epsilon}}{\dot{\epsilon}_0})$$

The above formula was modified to take into consideration the temperature rise ΔT that arises in the compression tests. Thus, T_m is expressed as:

$$T_m = (T + \Delta T)(1 - \kappa \ln \frac{\dot{\epsilon}}{\dot{\epsilon}_0}) \quad \text{-----}(27)$$

Before using equation (27), a suitable value of κ was found by trial and error, using the computer sub-program 'CONSTANT', which is discussed in section 2.3.2.

Having established κ , the value of T_m can be calculated for various temperatures and strain rates. Since the respective values of B and n are known, graphs of B and n against T_m were plotted. The relationships between B and T_m , and n and T_m , are expressed mathematically by polynomials with the assistance of the computer program 'CURVE' (see section 2.3.3). Thus, for a particular value of T_m , the values of B and n can be evaluated. Consequently, the flow stress pertaining to a particular equivalent strain can be calculated by equation (26).

The stress-strain data used in the theoretical analysis can be found in Chapter 6. The following graphs are also included in that chapter:

- a) $\log \sigma$ against $\log \epsilon$ to determine B and n
- b) curves of σ against T_m for various strains
- c) constant B against T_m

d) strain-hardening index n against T_m .

Graphs (b) - (d) were plotted after having found a suitable value of κ for the T_m equation.

2.2.6.2 Temperature Rise Due to Deformation Work

In the deformation zone (ie. zone 2) work is done when a particle travels from point to point along the flow streamlines eg. (I,J) to (I + 1,J) and this work will be dissipated as heat. Since the process is assumed to be adiabatic and that all work is converted into heat, the temperature rise due to deformation work at (I + 1,J) is expressed in section 1.5 and can be written as:

$$\Delta T_{(I+1,J)} = \frac{\sigma \Delta \bar{\epsilon}_{(I+1,J)}}{Q \cdot s_p \cdot d} \quad \text{-----}(28)$$

where,

$$\Delta \bar{\epsilon}_{(I+1,J)} = \text{equivalent mean strain between the points (I,J) and (I + 1,J)}$$

$$\sigma = \frac{1}{2} \left(\sigma_o_{(I+1,J)} + \sigma_{(I,J)} \right)$$

$$\sigma_o_{(I+1,J)} = \text{flow stress at the point (I + 1,J) without taking into consideration the temperature rise due to deformation and frictional work}$$

$\sigma_{(I,J)}$ = new flow stress at the point (I,J)
taking into consideration the temperature
rise due to deformation and frictional
work

(The method of calculating ΔT is explained in section 2.2.6.4)

2.2.6.3 Temperature Rise Due to Frictional Work

The temperature rise at a point due to friction at the die-wire interface (ie. $J = 1$) is expressed in section 1.5 and can be written as:

$$\Delta\theta_{(I+1,J)} = \frac{m \sigma \mu_p S \Delta t}{\sqrt{3} Q_{sp} d V_a} \quad \text{-----}(29)$$

$$\text{where } \sigma = \frac{1}{2} \left(\sigma_o_{(I+1,J)} + \sigma_{(I,J)} \right)$$

(The method of calculating $\Delta\theta$ is explained in section 2.2.6.4.)

For computation purposes, $\Delta\theta$ can be expressed as:

$$\Delta\theta_{(I+1,1)} = \frac{3 m \sigma \sin\alpha}{2\sqrt{3} Q_{sp} d} \cdot \frac{1}{\cos\theta(2) - \cos\theta(1)} \cdot \frac{(\rho_{(I,1)} - \rho_{(I+1,1)})(\rho_{(I,1)}^2 - \rho_{(I+1,1)}^2)}{\rho_{(I,1)}^3 - \rho_{(I+1,1)}^3} \quad \text{-----}(30)$$

(The full derivation is shown in appendix, A3.3.)

The specific heat sp and density d of the material are assumed to be independent of temperature.

2.2.6.4 Procedure for Calculating the Temperature and
Flow Stress Distributions in the Deformation Zone

The initial temperature of a point in the deformation zone was assumed to be that of the drawing temperature, denoted by T . For a particular flow line, eg. at point (2,1), the equivalent mean strain, equivalent strain rate and temperature (ie. T in this case) are known, therefore, the flow stress at (2,1) can be calculated and represented by $\sigma_{(2,1)}$. When the particle travels from (1,1) to (2,1), the temperature rise is given by equations (28) and (30). Thus, the new temperature at (2,1) is given by:

$$T_{N(2,1)} = T + \Delta\theta_{(2,1)} + \Delta T_{(2,1)}$$

Since the temperature at the inlet shear surface is assumed to be that of the drawing temperature, therefore,

$$T = T_{(1,J)}$$

Thus, T_N can be expressed generally as:

$$T_{N(I+1,J)} = T_{(I,J)} + \Delta\theta_{(I+1,J)} + \Delta T_{(I+1,J)}$$

Taking the temperature rise into consideration the new flow stress $\sigma_{(2,1)}$ at point (2,1) can be calculated as before, but the temperature is now $T_{N(2,1)}$ instead of T .

As the particle travels to the next point (3,1), the equivalent mean strain $\bar{\epsilon}_{(3,1)}$, equivalent strain rate $\dot{\bar{\epsilon}}_{(3,1)}$

and the temperature, which is now $T_{N(2,1)}$, are known, the flow stress $\sigma_{o(3,1)}$ can be calculated. The additional work done per unit volume due to an equivalent strain increment $\Delta \bar{\epsilon}_{(3,1)}$ (ie. $\bar{\epsilon}_{(3,1)} - \bar{\epsilon}_{(2,1)}$) is given by the area under the stress-strain curve for the strain increment considered; thus:

$$\sigma \Delta \bar{\epsilon}_{(3,1)}$$

where σ is taken as the mean between $\sigma_{o(3,1)}$ and $\sigma_{(2,1)}$, defined as $\frac{1}{2} (\sigma_{o(3,1)} + \sigma_{(2,1)})$. Therefore, the temperature rise in travelling from (2,1) to (3,1) is given by equation (28). The same technique was applied at the die-wire interface in calculating the temperature rise due to frictional work. The whole procedure was repeated for each J line. Consequently, the new temperature T_N and the new flow stress $\sigma_{(I,J)}$ distributions in the deformation zone are known.

2.2.7 The Internal Power of Deformation Per Unit Volume

The internal power required to deform a unit volume of material can be expressed in terms of the derived strain rate components.

The rate of internal work per unit volume is given by:

$$\dot{W}_i = \sigma_\rho \dot{\epsilon}_\rho + \sigma_\theta \dot{\epsilon}_\theta + \sigma_\phi \dot{\epsilon}_\phi + 2(\tau_{\rho\theta} \dot{\gamma}_{\rho\theta} + \tau_{\theta\phi} \dot{\gamma}_{\theta\phi} + \tau_{\phi\rho} \dot{\gamma}_{\phi\rho})$$

$$\equiv \sigma_{ij} \dot{\epsilon}_{ij}$$

----- (31)

But the stress tensor is formed by a stress deviator tensor, σ' , and the hydrostatic stress tensor, σ_m .

Therefore:

$$\sigma = \sigma' + \sigma_m \quad \text{-----}(32)$$

Expressing the equation (31) in terms of the corresponding deviator tensors, gives:

$$\begin{aligned} \therefore \dot{W}_i &= (\sigma'_\rho + \sigma_m) \dot{\epsilon}_\rho + (\sigma'_\theta + \sigma_m) \dot{\epsilon}_\theta + (\sigma'_\phi + \sigma_m) \dot{\epsilon}_\phi \\ &\quad + 2(\tau_{\rho\theta} \dot{\gamma}_{\rho\theta} + \tau_{\theta\phi} \dot{\gamma}_{\theta\phi} + \tau_{\phi\rho} \dot{\gamma}_{\phi\rho}) \\ &= \sigma'_\rho \dot{\epsilon}_\rho + \sigma'_\theta \dot{\epsilon}_\theta + \sigma'_\phi \dot{\epsilon}_\phi + (\dot{\epsilon}_\rho + \dot{\epsilon}_\theta + \dot{\epsilon}_\phi) \sigma_m \\ &\quad + 2(\tau_{\rho\theta} \dot{\gamma}_{\rho\theta} + \tau_{\theta\phi} \dot{\gamma}_{\theta\phi} + \tau_{\phi\rho} \dot{\gamma}_{\phi\rho}) \\ &\equiv \sigma'_{ij} \dot{\epsilon}_{ij} + \sigma_m \dot{\epsilon}_i \end{aligned} \quad \text{-----}(33)$$

Assuming constancy of volume, then:

$$(\dot{\epsilon}_\rho + \dot{\epsilon}_\theta + \dot{\epsilon}_\phi) = 0$$

Hence, equation (33) becomes:

$$\begin{aligned} \dot{W}_i &= \sigma'_\rho \dot{\epsilon}_\rho + \sigma'_\theta \dot{\epsilon}_\theta + \sigma'_\phi \dot{\epsilon}_\phi + 2(\tau_{\rho\theta} \dot{\gamma}_{\rho\theta} + \tau_{\theta\phi} \dot{\gamma}_{\theta\phi} + \tau_{\phi\rho} \dot{\gamma}_{\phi\rho}) \\ &= \sigma'_{ij} \dot{\epsilon}_{ij} \end{aligned} \quad \text{-----}(34)$$

For each strain rate component $\dot{\epsilon}_{ij}$, substituting its value from the von Mises stress-strain rate law (58), viz:

$$\dot{\epsilon}_{ij} = \frac{\pm \sqrt{\frac{1}{2} \dot{\epsilon}_{ij} \dot{\epsilon}_{ij}}}{k} \sigma'_{ij} \quad \text{-----}(35)$$

Substituting equation (35) for the corresponding strain rate tensors of equation (34), gives:

$$\begin{aligned} \dot{W}_i &= \frac{\pm \sqrt{\frac{1}{2} \dot{\epsilon}_{ij} \dot{\epsilon}_{ij}}}{k} \left| \sigma_{\rho}^{\prime 2} + \sigma_{\theta}^{\prime 2} + \sigma_{\phi}^{\prime 2} + 2(\tau_{\rho\theta}^2 + \tau_{\theta\phi}^2 + \tau_{\phi\rho}^2) \right| \\ &= \frac{\pm \sqrt{\frac{1}{2} \dot{\epsilon}_{ij} \dot{\epsilon}_{ij}}}{k} \sigma'_{ij} \sigma'_{ij} \quad \text{-----}(36) \end{aligned}$$

Since von Mises suggested the second invariant of the stress deviator J_2 , as the criterion for the yield of the material and therefore, at yield:

$$\begin{aligned} J_2 &= \frac{1}{2} (\sigma_{\rho}^{\prime 2} + \sigma_{\theta}^{\prime 2} + \sigma_{\phi}^{\prime 2}) + \tau_{\rho\theta}^2 + \tau_{\theta\phi}^2 + \tau_{\phi\rho}^2 \\ &= \frac{1}{2} \sigma'_{ij} \sigma'_{ij} = k^2 \quad \text{-----}(37) \end{aligned}$$

Substituting equation (37) in equation (36) gives:

$$\begin{aligned} \dot{W}_i &= \frac{\pm \sqrt{\frac{1}{2} \dot{\epsilon}_{ij} \dot{\epsilon}_{ij}}}{k} \cdot 2k^2 \\ \dot{W}_i &= \frac{2Y_d}{\sqrt{3}} \sqrt{\frac{1}{2} \dot{\epsilon}_{ij} \dot{\epsilon}_{ij}} \\ \dot{W}_i &= \frac{Y_d}{\sqrt{3}} \sqrt{2[\dot{\epsilon}_{\rho}^2 + \dot{\epsilon}_{\theta}^2 + \dot{\epsilon}_{\phi}^2] + 2[\dot{\gamma}_{\rho\theta}^2 + \dot{\gamma}_{\theta\phi}^2 + \dot{\gamma}_{\phi\rho}^2]} \quad \text{-----}(38) \end{aligned}$$

Equation (38) expresses the internal power of deformation per unit volume of material in terms of the derived strain rate components.

2.2.7.1 The Total Internal Power of Deformation

The total internal power of deformation P_d is obtained by integrating the equation over the entire volume of the deformation zone. Therefore,

$$P_d = \int_V \dot{W}_i dV$$

Substituting equation (38) into the above gives:

$$\begin{aligned} P_d &= \frac{Y_d}{\sqrt{3}} \int_V \sqrt{2[(\dot{\epsilon}_\rho^2 + \dot{\epsilon}_\theta^2 + \dot{\epsilon}_\phi^2) + 2(\dot{\gamma}_{\rho\theta}^2 + \dot{\gamma}_{\theta\phi}^2 + \dot{\gamma}_{\phi\rho}^2)]} dV \\ &= Y_d \int_V \dot{\epsilon} dV \end{aligned} \quad \text{-----(39)}$$

$$dV = \rho^2 \sin\theta d\theta d\phi d\rho \quad \text{-----(40)}$$

Substituting equations (23) and (40) into equation (39) gives:

$$\begin{aligned} P_d &= 2V_1 Y_d \frac{\rho_o^2}{\rho} \int_0^{2\pi} \int_{\rho_2}^{\rho_1} \int_0^\alpha \sin\theta \exp(2c(\theta-\alpha)) F d\theta d\phi d\rho \\ \text{where,} \quad F &= \left[(\cos\theta + c\sin\theta)^2 + \frac{1}{12} (3c\cos\theta + (2c^2-1)\sin\theta)^2 \right]^{\frac{1}{2}} \\ P_d &= 4\pi V_1 Y_d \rho_o^2 \ln\left(\frac{\rho_1}{\rho_2}\right) \int_0^\alpha \sin\theta \exp(2c(\theta-\alpha)) F d\theta \end{aligned} \quad \text{-----(41)}$$

Due to the difficulty in integrating the above equation

analytically, numerical integration was used.

2.2.7.2 Calculation of Mean Yield Stress Y_d

For a particular flow line, the flow stress $\sigma_{(I,J)}$ and equivalent strain $\bar{\epsilon}_{(I,J)}$ of the point (I,J) are known. Therefore $\sigma_{(I,J)}$ can be plotted against $\bar{\epsilon}_{(I,J)}$ and then integrated numerically to find the area under the curve. Thus the mean yield stress $Y_m(J)$ for that particular flow line is given by:

$$Y_m(J) = \frac{\int_{\bar{\epsilon}_{(1,J)}}^{\bar{\epsilon}_{T(J)}} \sigma_{(I,J)} d\bar{\epsilon}_{(I,J)}}{\bar{\epsilon}_{T(J)} - \bar{\epsilon}_{(1,J)}} \quad \text{-----}(42)$$

where $\bar{\epsilon}_{T(J)}$ = equivalent strain at shear surface Γ_2

$\bar{\epsilon}_{(1,J)}$ = equivalent strain at shear surface Γ_1
which is zero

The yield stress Y_d used in equation (41) is given by:

$$Y_d = \frac{\int_{\bar{\epsilon}_{T(J)}}^{\bar{\epsilon}_{T(1)}} Y_m(J) d\bar{\epsilon}_{T(J)}}{\bar{\epsilon}_{T(1)} - \bar{\epsilon}_{T(J)}} \quad \text{-----}(43)$$

As it is not feasible to represent mathematical relationships between the flow stress and equivalent strain, therefore, equations (42) and (43) were integrated numerically.

2.2.8 Power Losses in Shearing at the Inlet and Outlet Shear Surfaces

It was assumed that the shearing of material occurs on both the inlet and exit shear surfaces causing velocity discontinuities of the material. Such velocity discontinuities at the inlet and the exit shear surfaces were obtained from the resultant tangential components of velocities (along the shear surface) on one side relative to the other.

The velocity discontinuities for the shear surfaces Γ_1 and Γ_2 are Δv_1 and Δv_2 respectively and their derivation is shown in the appendix, A3.4.

The power losses in shearing at the shear surface are given by:

$$P = \int_S \tau |\Delta v_1| dS \quad \text{-----(44)}$$

where,

$$dS = \frac{2\pi r dr}{\sin \beta}$$

$$r = \rho_1 \sin \theta$$

$$= \rho_0 \exp(c (\theta - \alpha)) \sin \theta$$

$$\frac{dr}{d\theta} = \rho_0 \exp(c (\theta - \alpha)) \cos \theta + c \rho_0 \exp(c (\theta - \alpha)) \sin \theta$$

$$dr = \rho_0 \exp(c (\theta - \alpha)) [\cos \theta + c \sin \theta]$$

From equations (1) and (7):

$$\rho_1 = \rho_0 \exp(c (\theta - \alpha))$$

$$\sin \beta = \cos \eta \cos \theta + \sin \eta \sin \theta$$

Therefore,

$$dS = 2\pi \rho_o^2 \exp(2c(\theta-\alpha)) \frac{\sin\theta(1+c \tan\theta)}{\cos\eta + \sin\eta \tan\theta} d\theta \quad \text{-----}(45)$$

Substituting the various parameters into equation (44), the power loss due to shearing at the inlet shear surface Γ_1 is given by,

$$\begin{aligned} P_1 &= \int_0^\alpha \tau |V_1 [\sin\theta(1+c^2)] \cos(\eta)| \frac{2\pi \rho_o^2 \exp(2c(\theta-\alpha)) \sin\theta(1+c \tan\theta)}{\cos\eta + \sin\eta \tan\theta} d\theta \\ &= 2\pi \tau \rho_o^2 V_1 \int_0^\alpha \exp(2c(\theta-\alpha)) \sin^2\theta(1+c^2) \left(\frac{(1+c \tan\theta) \cos\eta}{\cos\eta + \sin\eta \tan\theta} \right) d\theta \\ &= 2\pi \tau \rho_o^2 V_1 \int_0^\alpha \exp(2c(\theta-\alpha)) \sin^2\theta(1+c^2) \left(\frac{1+c \tan\theta}{1+\tan\eta \tan\theta} \right) d\theta \end{aligned}$$

Since the von Mises yield criterion was assumed, $\tau = \frac{Y_d}{\sqrt{3}}$.

Substituting equation (5) and $\tau = \frac{Y_d}{\sqrt{3}}$ into P_1 gives:

$$P_1 = \frac{2\pi Y_d}{\sqrt{3}} \rho_o^2 V_1 \int_0^\alpha \exp(2c(\theta-\alpha)) \sin^2\theta(1+c^2) d\theta \quad \text{-----}(46)$$

Similarly, the power loss due to shearing at the exit shear surface is given by:

$$P_2 = 2\pi \frac{Y_d}{\sqrt{3}} \rho_o^2 V_1 \int_0^\alpha \exp(2c(\theta-\alpha)) \sin^2\theta(1+c^2) d\theta \quad \text{-----}(47)$$



2.2.9 Power Losses in Friction Between the Die and Wire Interface

In practice, slipping friction occurs between the die and the workpiece, consequently, work is done against these friction losses.

The velocity discontinuity Δv_f at the die-wire interface is the velocity at the interface and is defined by equation (9) where θ is now equal to the die semi-angle α .

$$\begin{aligned}\Delta v_f &= V_1 \left(\frac{\rho_o}{\rho} \right)^2 \exp(2c(\theta - \alpha)) (\cos \theta + c \sin \theta) \\ &= V_1 \left(\frac{\rho_o}{\rho} \right)^2 (\cos \alpha + c \sin \alpha)\end{aligned}$$

An element on the conical surface, $ds_f = 2\pi \rho \sin \alpha d\rho$.

At the die-wire interface, where the wire first meets the die,

$$\beta = 90 + \alpha$$

$$\eta = 0$$

And since $c = \tan \eta$, therefore,

$$\Delta v_f = V_1 \left(\frac{\rho_o}{\rho} \right)^2 \cos \alpha \quad \text{-----}(48)$$

Assuming constant friction factor, the shear stress of the material τ is given by:

$$\tau = \frac{mY_f}{\sqrt{3}}$$

It is postulated that m takes values from 0 to 1, ie. zero for the frictionless case and unity for sticking friction. The yield stress

Y_f is the mean yield stress at the die-wire interface and from section 2.2.7.2, it is represented by $Y_m(1)$.

The power losses at the die-wire interface are defined by:

$$P_f = \int_{\rho_2}^{\rho_1} \tau \left| \Delta v_f \right| ds_f \quad \text{-----}(49)$$

Substituting the respective values into equation (49) gives:

$$\begin{aligned} P_f &= \int_{\rho_2}^{\rho_1} \frac{mY_f}{\sqrt{3}} \left| V_1 \left(\frac{\rho_o}{\rho} \right)^2 \cos \alpha \right| 2\pi\rho \sin\alpha d\rho \\ &= \frac{2\pi}{\sqrt{3}} mY_f V_1 \rho_o^2 \ln\left(\frac{\rho_1}{\rho_2} \right) \cos \alpha \sin \alpha \quad \text{-----}(50) \end{aligned}$$

ρ_1 and ρ_2 are also represented by $\rho_{(1,1)}$ and $\rho_{(N_\rho + 1,1)}$ respectively.

Y_f was eventually replaced by Y_d (see section 2.2.7.2) in equation (50). The reasons for using Y_d to calculate the frictional power are explained in Chapter Eight.

2.3 THE COMPILATIONS OF THE COMPUTER PROGRAMS

2.3.1 Introduction

The main computer program 'DRAW' and two sub-programs 'CONSTANT' and 'CURVE', all written in Fortran77, were especially developed to solve the upper bound solution stated in the preceding sections. The necessity for the computer programs arose from:

- a) the numerical solutions used in the theoretical analysis, producing equations which cannot be solved using general analytical methods
- b) the need to determine by trial and error the numerical value of the constant κ which is used in the T_m equation. Manual graph plotting would be time consuming
- c) the need to represent mathematical relationships between B and T_m , and n and T_m .

A special program 'CONTOUR' was written to plot the strain, strain rate, temperature and flow stress distributions.

2.3.2 Sub-Program 'CONSTANT'

The sub-program 'CONSTANT' was written to select the appropriate value of κ used in the T_m equation. It is basically a graph plotting program based on the Ginograf routine available on the ICL 1904S computers.

The following data were fed into the program:

- a) test temperatures, strain rates, flow stresses and corresponding strains, all of which were extracted from the stress-strain curves.
- b) constant B and strain-hardening index n which were found from the plot of $\log \sigma$ against $\log \epsilon$.

For a particular value of κ , the program performs two main operations:

- a) it computes the values of T_m taking into consideration the temperature rise in the compression tests
- b) it plots curves of flow stress against T_m for various values of strains.

The curves were all plotted on one graph which enabled the shape of the curves to be easily compared.

Assuming that all work degenerates into heat and that adiabatic conditions prevail, the temperature rise due to deformation work is given by:

$$\Delta T = \int_{\epsilon_1}^{\epsilon_2} \frac{\sigma d\epsilon}{Q_{sp} d}$$

Since the stress-strain curves were assumed to obey the power relationship, the substitution could be made giving:

$$\Delta T = \int_{\epsilon_1}^{\epsilon_2} \frac{B \epsilon^n}{Q_{sp} d} d\epsilon$$

The graphs of $\log \sigma$ against $\log \epsilon$ were generally linear in the strain range of 0.2 to 0.4 (see Chapter Six), therefore a mid-value of 0.3 was used as the upper integration limit. The lower integration limit was 0. The velocity-modified temperature equation thus becomes:

$$T_m = (T + \Delta T) \left(1 - \kappa \ln \frac{\dot{\epsilon}}{\epsilon_0} \right)$$

where T and ΔT are expressed in degrees absolute.

After computing T_m , the computer plots the curves of flow stress against T_m for various values of strains.

The computations and graph plotting were repeated for different values of κ by using a do-loop in the computer program. The various graphs were studied visually, and the value of κ which gave curves of similar shape for the various strains, was chosen to be used in the T_m equation.

2.3.3 Sub-program 'CURVE'

After establishing the value of κ to be used in the T_m equation, a graph of B against T_m was plotted manually. The curve of B against T_m was divided into suitable sections for curve fitting, as it is generally inadvisable to fit a general curve through all the points - especially if the curve has peaks and troughs.

The program 'CURVE' determines least squares polynomial approximations of degrees 0,1,2,... M for the set of data points (the minimum number of data points is $M + 1$). Each polynomial is

represented in the Chebyshev series form. This form of representing a polynomial was preferred to the power series form since it leads to greater accuracy. Special attention was paid to the selection of data points so that they represented the actual shape of the curve under consideration.

The corresponding values of T_m and B were fed into the program. For each degree of polynomial, the program printed the residual, and the values of B and T_m calculated from the polynomial. Generally, the smaller the residual, the better is the curve fit; however this may not always be the case, and so to ensure the selection of the curve of 'best fit', the printed values of B and T_m were compared with the graph of B and T_m and the most appropriate one chosen.

The same procedure was repeated for representing the strain-hardening index n and T_m by polynomials.

The mathematical relationships between B and T_m , and n and T_m , were fed into the main computer program 'DRAW'.

2.3.4 The Computer Program 'DRAW'

2.3.4.1 The Co-ordinate System Employed in the Computer Program

A co-ordinate system, referred in terms of a two-dimensional array, was employed in the program. This two-dimensional array system was defined on the basis of the number of intersection points between the circular band and radial lines shown in figure 2.4 of section 2.2.6.

2.3.4.2 The Computer Program Layout

A detailed flow chart of the computer program is shown in figure 2.5. The program was written to solve the upper bound solution for the draw stresses, and also to predict the temperature and flow stress distributions in the deformation zone.

The deformation zone was divided into twenty arc divisions ($N_\rho = 20$) and twenty angular divisions ($N_\theta = 20$). The program computes the upper bound solutions for a given area of reduction, draw speed, constant friction factor, wire diameter and a range of draw temperatures. For a given draw condition, the various powers mentioned in the preceding sections, the temperature and flow stress distributions and the draw stress, were computed for a particular value of c . The value of c was varied using a do-loop in the computer program. The range of c used was from -0.2 to 0.2 in steps of 0.02. The minimum draw stress was established by comparing the draw stress developed for each value of c .

A modified printout of a set of the results (ie. without the temperature and flow stress distributions) is shown in figure 2.6.

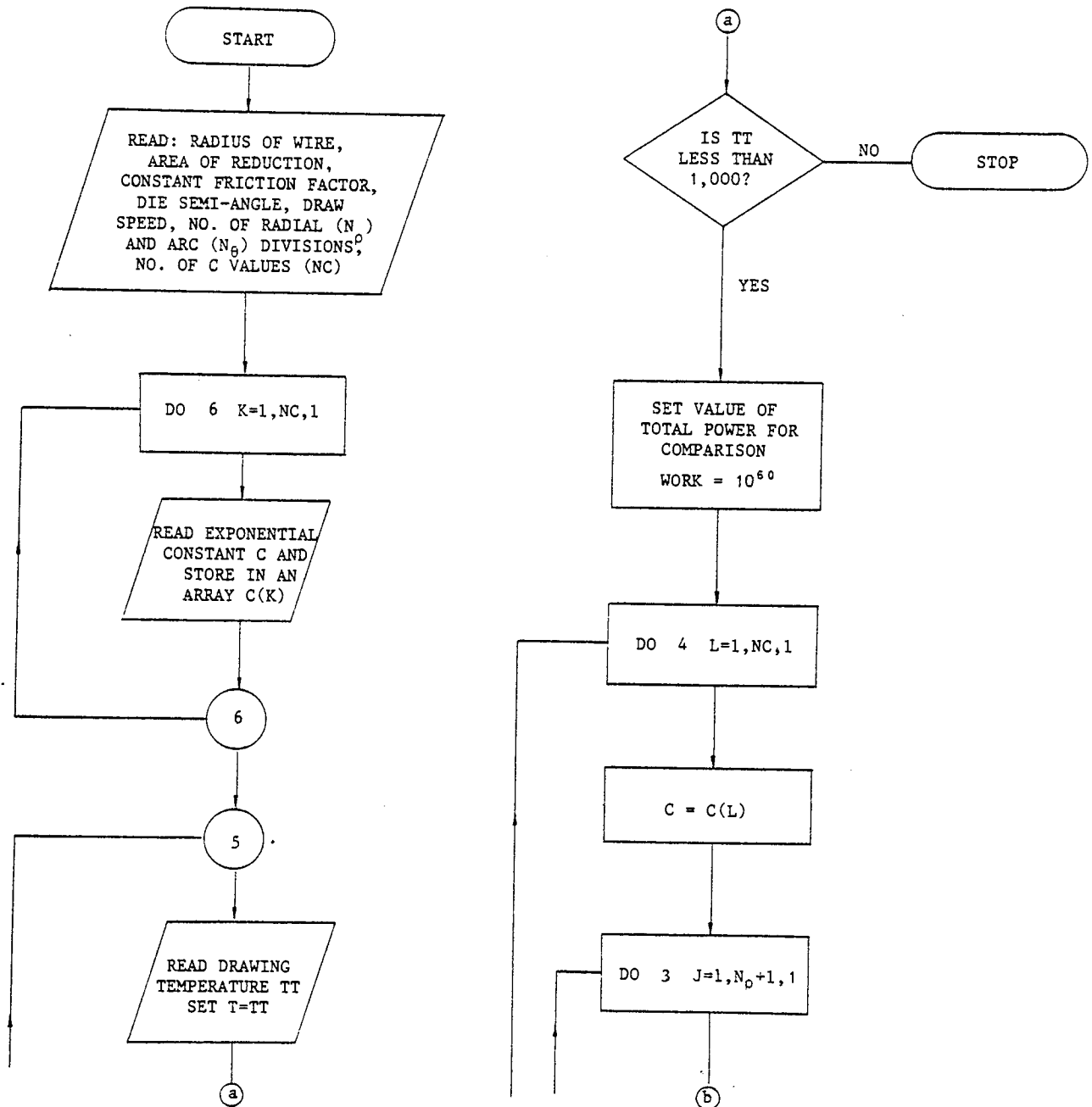
2.3.5 The Computer Program 'CONTOUR'

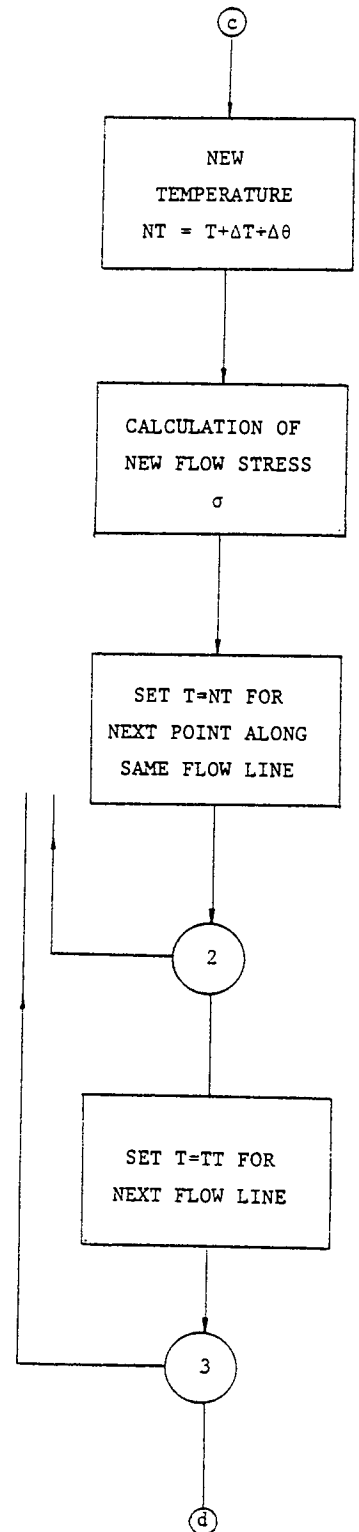
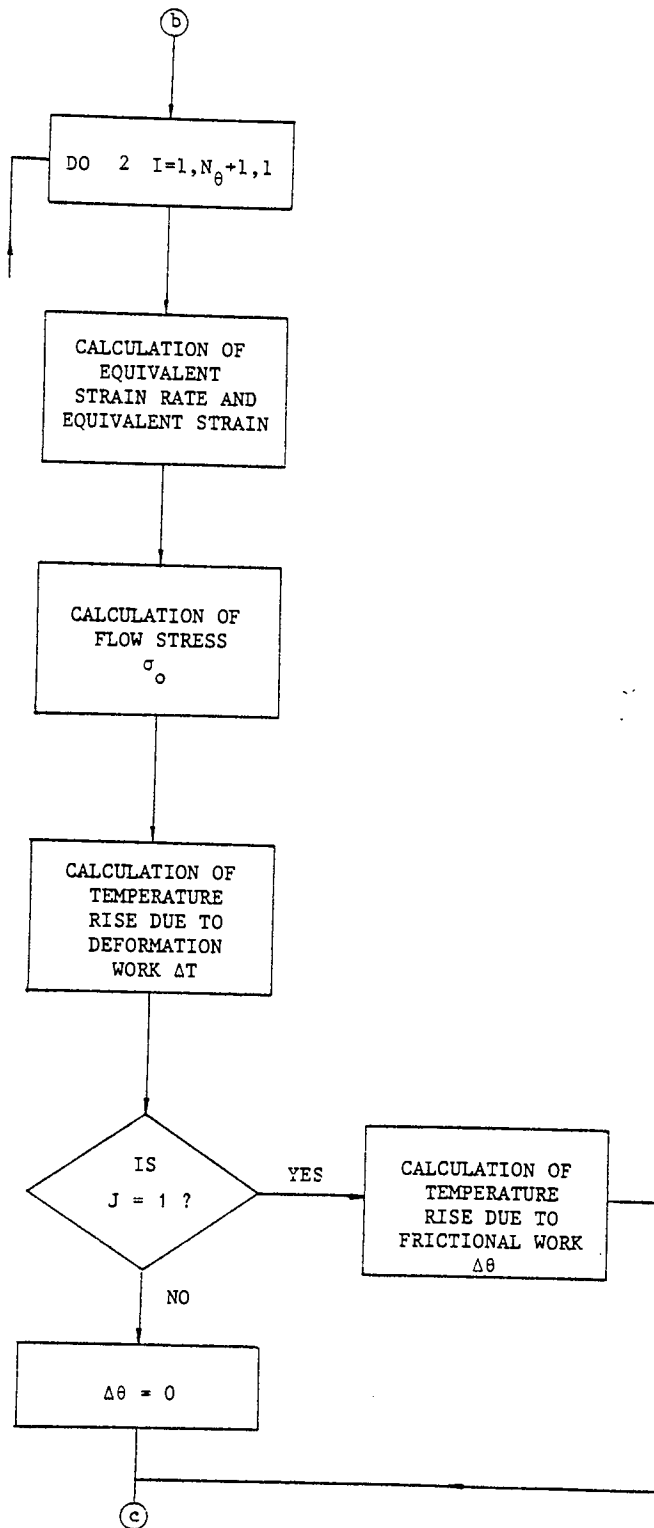
The computer program 'CONTOUR' was also written in Fortran77 and uses the Ginosurf routines which are available on the ICL computers. The Ginosurf routine provides facilities for producing contour maps. The program was used to plot the strain, strain rate, temperature and flow stress distributions in the deformation zone.

Three variables were fed into the computer: the X-Y co-ordinate points and the corresponding values of Z, the contour of which is plotted. From the data given, an interpolation of the Z values is carried out by standard routines available in the computer. The contour map is produced from the interpolated values according to the contour levels specified.

The main disadvantage of the Ginosurf routine is its inability to smooth the interpolated points before drawing the contour, thus producing irregular curves.

Figure 2.5: The flow chart of the computer program 'DRAW'





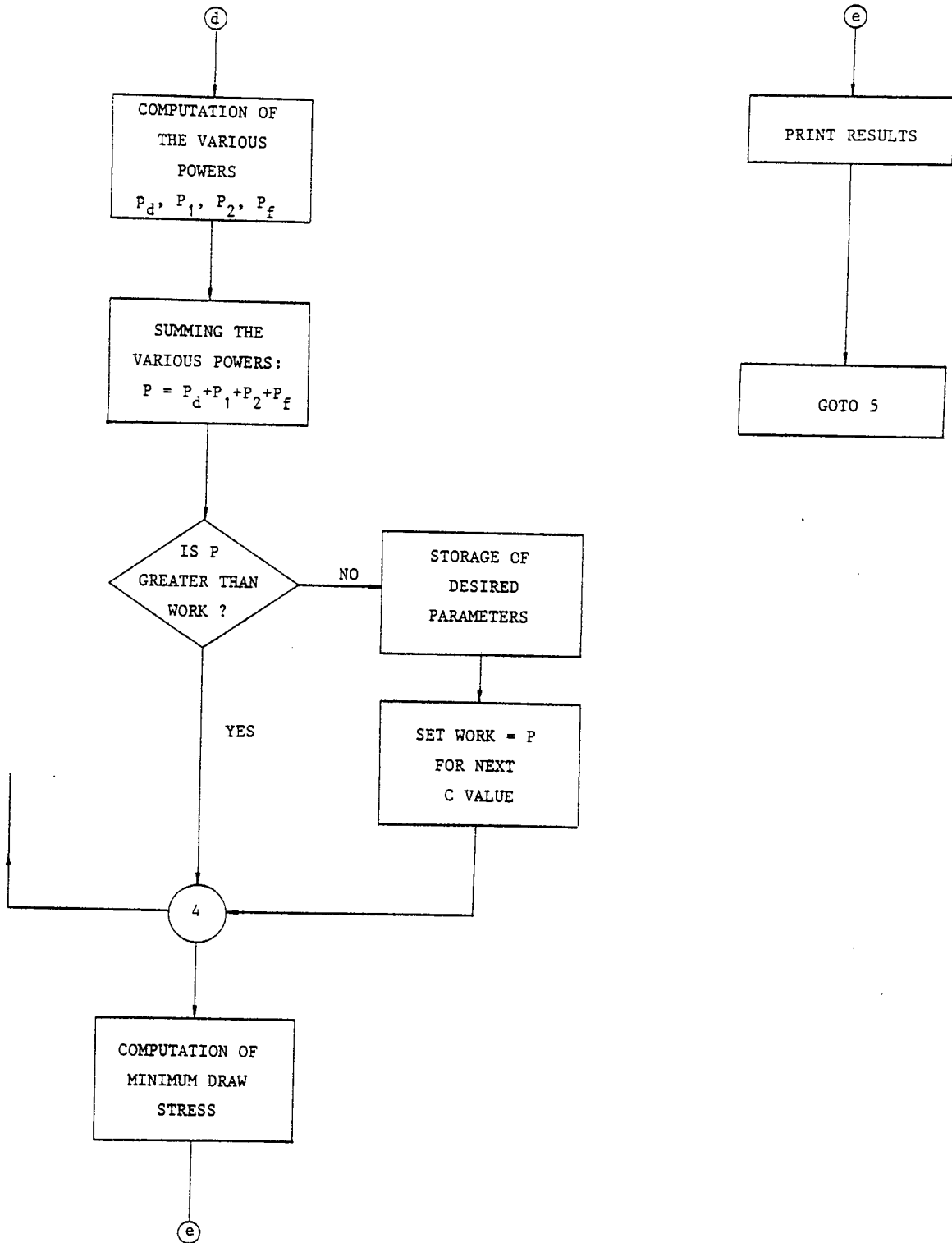


Figure 2.6: The modified computer results

MEAN STRAIN-RATE BY ATKINS FORMULA 9.697530
MATERIAL:MEDIUM CARBON STEEL
DRAWING TEMPERATURE IN DEGREES CENTRIGRADE 100.0000
AREA OF REDUCTION 35.00000 PERCENT
DIE SEMI-ANGLE IN DEGREES 9.000000
ORIGINAL RADIUS OF WIRE IN INS. 1.180000E-01
FINAL RADIUS OF WIRE IN INS 9.513464E-02
SPEED OF DRAWING IN FT. PER MIN 20.00000
CONSTANT FRICTION FACTOR M 1.000000E-01
EXPONENTIAL CONSTANT C 1.600000E-01
POWER OF DEFORMATION PD IN FT LB PER SEC. 340.0018
POWER OF FRICTION IN FT LB PER SEC 122.7543
POWER OF SHEARING AT INLET IN FT LB PER SEC 48.05554
POWER OF SHEARING AT OUTLET IN FT LB PER SEC 48.05554
TOTAL POWER OF DRAWING FT LB PER SEC 558.8672
MEAN YIELD STRESS CYD IN TONF PER SQ. IN 36.84350
MEAN YIELD STRESS AT INLET IN TONF PER SQ. IN 36.84350
MEAN YIELD STRESS AT OUTLET TONF PER SQ. IN 36.84350
MEAN YIELD STRESS AT CONICAL SURFACE TONF PER SQ. IN 37.78305
MINIMUM DRAW STRESS IN TONF PER SQ. IN 26.32425

MATERIAL:MEDIUM CARBON STEEL
DRAWING TEMPERATURE IN DEGREES CENTRIGRADE 200.0000
AREA OF REDUCTION 35.00000 PERCENT
DIE SEMI-ANGLE IN DEGREES 9.000000
ORIGINAL RADIUS OF WIRE IN INS. 1.180000E-01
FINAL RADIUS OF WIRE IN INS 9.513464E-02
SPEED OF DRAWING IN FT. PER MIN 20.00000
CONSTANT FRICTION FACTOR M 1.000000E-01
EXPONENTIAL CONSTANT C 2.000000E-01
POWER OF DEFORMATION PD IN FT LB PER SEC. 341.0745
POWER OF FRICTION IN FT LB PER SEC 123.7311
POWER OF SHEARING AT INLET IN FT LB PER SEC 48.96502
POWER OF SHEARING AT OUTLET IN FT LB PER SEC 48.96502
TOTAL POWER OF DRAWING FT LB PER SEC 562.7356
MEAN YIELD STRESS CYD IN TONF PER SQ. IN 37.13668
MEAN YIELD STRESS AT INLET IN TONF PER SQ. IN 37.13668
MEAN YIELD STRESS AT OUTLET TONF PER SQ. IN 37.13668
MEAN YIELD STRESS AT CONICAL SURFACE TONF PER SQ. IN 36.35354
MINIMUM DRAW STRESS IN TONF PER SQ. IN 26.50646

CHAPTER THREE

EXPERIMENTAL EQUIPMENT AND DRAW PROCESS MATERIALS

III. EXPERIMENTAL EQUIPMENT AND DRAW PROCESS MATERIALS

3.1 EXPERIMENTAL EQUIPMENT

3.1.1 The Bull Block

The drawing machine used was a horizontal bull block which was used by Winsper(73) and Dawson(74) for ultrasonic drawing. It consisted of a fabricated steel frame on which was mounted an 18 in diameter drum having an 18 in long working surface. The drum, which was carried on a carbon ^{steel} shaft, was mounted horizontally and supported in heavy duty roller bearings and driven through a totally enclosed wormgear. The base of the frame formed a reservoir for the lubrication of the gears. The bull-block was provided with a traversing table which was mounted on guides and was driven by a lead screw to give 0.75 in traverse per revolution of the drum.

The drum shaft was driven through a variable speed Carter gear and a four speed gear box by a 15 hp squirrel cage induction motor. The bull-block was designed for drawing speeds of 120, 240, 360 and 480 ft min⁻¹ which are selected by means of the gear box. The drum speed is infinitely variable from 1.3 ft min⁻¹ up to 480 ft min⁻¹. The bull-block operates at constant horsepower and therefore with increasing draw speed the die pull available decreases proportionally.

3.1.2 Induction Heater

A 500 kHz high frequency induction heater was used to heat the wire before entry to the die. The induction heater is rated at 15 kW

continuous output with an intermittent maximum output of 25 kW. For control of the power during the heating cycle, an on-load current control has been fitted; this control allows adjustment of the power through a ratio of approximately 10:1.

There are various other methods of heating the wires for elevated temperature drawing and these have been discussed by Loh and Sansome (3). The reasons for choosing induction heating and this particular heater were:

- (a) an induction heater was available
- (b) it does not occupy a large area like the lead bath
- (c) it does not emit noxious and toxic fumes as does a lead bath
- (d) the risk of overheating with induction heating is less than with resistance heating, which also has a tendency to damage the surface of the wire.

3.2 DRAW PROCESS MATERIALS

3.2.1 Drawing Dies

3.2.1.1 Chromium Carbide Dies

Chromium carbide dies were recommended by an established die manufacturer for this particular research. This was preferred to tungsten carbide as it is supposed to maintain its strength up to about 800°C.

In the preliminary trials, the dies were used to draw mild steel wires. The lubricants used were hot rolling oil RH12 and Dag 2961. Different methods of spraying the oil onto the wire were investigated but pick-up on the dies was a frequent occurrence. The dies were polished to remove any welded metals. Crack lines were observed on the die cone; this was due to the thermal stresses created when the heated wire was in contact with the die.

3.2.1.2 Die Design

To reduce the number of parameters to be studied in this research, the design of the die was made uniform for all the dies made. Ten dies were designed for a wire diameter of 6 mm with areas of reduction between 15 to 60 per cent, in increments of 5 per cent. The studies of Wistreich⁽⁷⁵⁾ showed that the optimum die angle varies with the area of reduction. Since the range of area of reduction used was rather wide and in order to reduce the

number of parameters to be studied in this research, a die semi-angle of 9° was used. This value was selected as, according to the findings of Wistreich, it is the optimum die semi-angle for a 45 per cent area of reduction and this is approximately the mid-range value of the ten dies. The die relief angle was 15° .

As the intersection point of the conical section and the radius arc might not blend smoothly, the die profile was designed such that the wire would not meet the die at that intersection point. This was achieved by making the diameter at the intersection point to be 8 mm which is greater than the diameter of the undrawn wire. A small land having a length of 0.2 times the diameter of the drawn wire was made to maintain dimensional stability. The die design is shown in figure 3.1.

Before the dies were used, plastic replicas of the profiles were made to ascertain the shape of the die. As the die diameter is rather small and with tapers at both ends, it is very difficult to make an impression of the whole profile. Consequently, plastic replicas extending from the conical section to the land were made. Before the replicas were made, the dies were thoroughly cleaned and degreased by Inhibisol. The exit end of the die was sealed with plasticine. Releasing agent was smeared on the die with a fine brush. Viscous liquid plastic was prepared to the proportion of one volume of powder to one volume of the liquid. The mixture was stirred for a few seconds and then poured immediately but steadily into the die, thus avoiding pipe holes. The plastic was allowed to set for about an hour. When the replicas had set, they were ejected from the dies. The die profile was measured on a Nikon profile projector having ten times magnification.

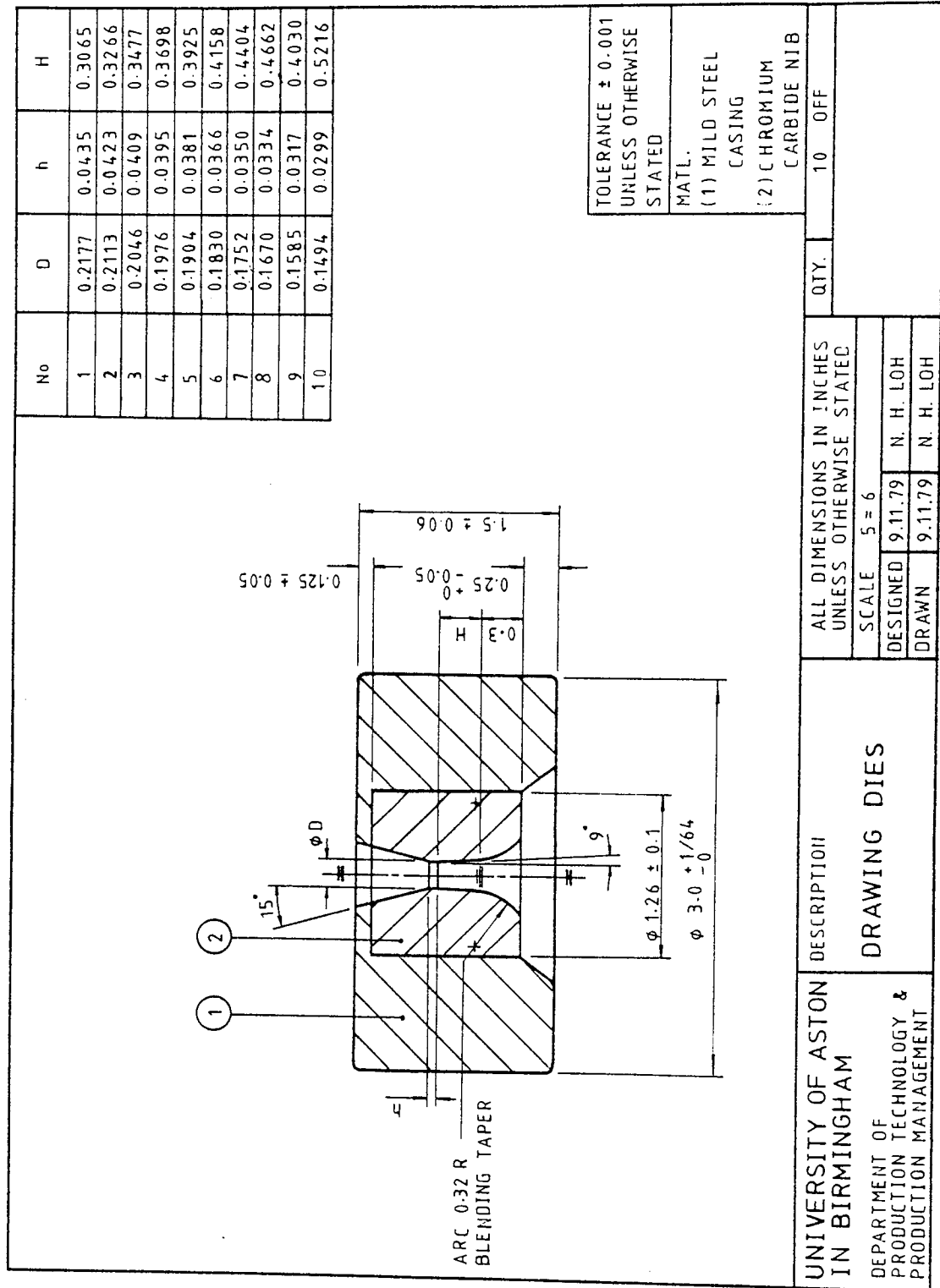


Figure 3.1: Drawing Dies

Four of the dies had to be polished due to severe pick-up on the die during the preliminary trials. Thus, new plastic replicas were made for the four dies and the diameters of the cold drawn wires were measured to establish the corresponding area of reduction. The die semi-angle was again checked on the Nikon profile projector and it was noticed that the die profile had altered, probably due to the polishing given by this inexperienced author. An example of one of the profiles is shown in figure 3.2. The conical section essentially consists of two parts: AB and BC. The angle made by BC with the draw axis has not changed significantly, whereas that of AB has. For each plastic replica, four measurements of the die semi-angle were taken along AD and EF where DF is the diameter of the undrawn wire. This method of measurement provides a better representative value of the die semi-angle. The measured values are shown in table 3.1.

The polished dies were used to draw mild steel wires only.

Die No.	2	3	4	5
Average die semi-angle	4.33°	4.13°	7.52°	6.33°
Diameter of cold drawn wire (in)	0.2260	0.2170	0.2074	0.2016
Area of reduction (%)	15.0	18.0	22.84	27.0

TABLE 3.1 Measurements of the chromium carbide die profiles after polishing

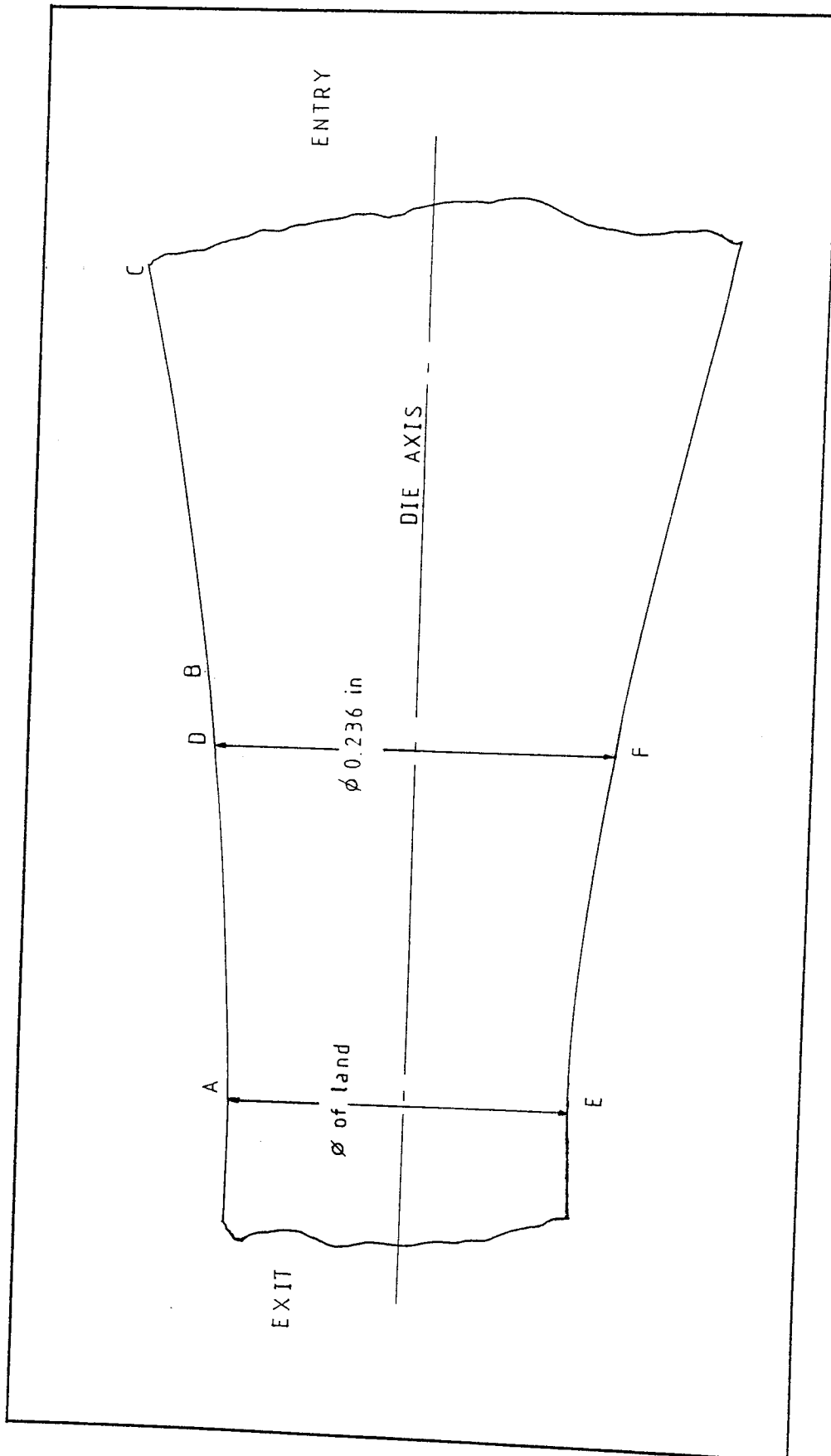


Figure 3.2: Profile of chromium carbide die No 5 after polishing (10 x magnifications)

3.2.1.3 'Syalon' Dies

Since chromium carbide dies were not suitable for drawing mild steel wires at elevated temperatures, and in view of the fact that more difficult to cold-draw metals were to be drawn, ceramic die materials were investigated and it emerged that the then new material 'Syalon' had properties which made it suitable for the projected draw trials. The manufacturer of 'Syalon' was approached - not a die manufacturer - and with his assistance the dies were made in collaboration.

'Syalon' is a member of the ceramic family and essentially consists of aluminium nitride, alumina and silicon nitride. Other elements can be added to make 'Syalon' display different properties.

This material was chosen because:

- (a) it remains stable at elevated temperatures and does not weld readily to ferrous alloys
- (b) it has high resistance to thermal shock. This is particularly important as water is sprayed onto the wire to increase its strength at the exit from the die.
- (c) it is easier to fabricate than other ceramics, thus reducing the cost of the die

The die design and the method of establishing the die profile were similar to that used in chromium carbide dies.

For both the die materials, the wires were cold drawn through the dies and the wire diameters were measured. The areas of reduction were calculated from these preliminary tests. For the 'Syalon' dies, the semi-angles and the measured diameters did not vary significantly from the specifications, thus, computations of the draw stresses were based on a die semi-angle of 9° and areas of reduction as specified in the drawing. This also applies to the two additional chromium carbide dies, 40 and 45% areas of reduction, used in the experiments.

3.2.2 Test Materials

Unlike well-established cold-drawing practices, elevated temperature wire drawing posed a number of problems; the art of drawing wire in the laboratory has to be established. Thus, easily cold drawn wires were the first test materials to be drawn at elevated temperatures. When the drawing procedures were routine for the mild steel, step-by-step the more difficult to deform alloys were drawn.

The test materials used in the research programme are listed below in the order in which they were investigated:

3.2.2.1 Mild Steel EN2B

The preliminary trials were carried out with mild steel EN2B as it can be deformed easily; it has a relatively low work hardening rate, is readily available and is not unduly expensive. Wire of 6 mm diameter was chosen as this is commonly available.

3.2.2.2 Medium Carbon Steel EN8 D

This alloy was selected as one of intermediate difficulty for drawing between mild steel and M2 'high speed' steel. Also, among the range of medium carbon steel available, the EN8 D type was readily available in 6 mm diameter, thus costing less to purchase.

3.2.2.3 M2 'High Speed' Steel

M2 'high speed' steel is an expensive material used increasingly as a tool material and for hack-saw blades. The cold drawing of the alloy does provide problems because the wire rapidly work-hardens when cold drawn. Pick-up on the die is often severe with high speed steel and therefore it is common practice to avoid high reductions of area per pass. This material was drawn at the request of a company whose traditional method of drawing was becoming increasingly expensive and would be more so with an increasing demand for this product. Wires of 5.5 mm diameter were supplied by the company.

In order to try to maintain uniform mechanical properties and surface finish, each type of wire was requested to be supplied from the same cast. The wires were supplied in the annealed condition, cleaned and limed.

The chemical compositions of the materials are shown in table 3.2.

Constituents Material	C	S	Si	P	Mn	Ni	Cr	Mo	Co	Ti	Nb	Cu	Sn
Mild steel EN2B	0.04	0.018	-	0.010	0.32	0.01	0.02	-	-	-	-	0.02	0.001
Medium carbon steel EN8D	0.39	0.016	0.18	0.013	0.71	0.01	0.03	-	-	-	-	0.03	0.001
M2 'high' speed' steel	0.81	0.008	0.44	0.018	0.33	0.05	4.13	4.7	.12	.01	.02	0.05	0.005

Table 3.2: Chemical compositions of mild steel, medium carbon steel and M2 'high speed' steel

3.2.3 Lubricants

Before the drawing process can be carried out, a lubricant must be specified which will perform efficiently at the draw temperature. Since most lubricants have been formulated for cold drawing, their constituents often decompose when used at elevated temperatures. A suitable high temperature lubricant must prevent pick-up, excessive die wear and reduce the draw force.

The problems incurred as a result of poor lubrication cannot be overlooked, thus advice and suggestions were sought from various lubricant manufacturers and the following lubricants were used:

3.2.3.1 Hot Rolling Oil RH12

This lubricant was recommended by the manufacturer as it is supposed to be capable of maintaining its lubricating properties up to 1300°C. It is essentially an ester blend with minor additions of lubricity and rust preventive additives. Initial trials on mild steel gave undesirable fumes and signs of breakdown were observed at about 350°C. The fumes emitted would be unacceptable in industrial practice.

3.2.3.2 Dag 2961

It is essentially a water-based lubricant, comprising graphite and molybdenum disulphide. This lubricant was chosen because:

- a) The lubricant could be used at ambient temperatures up to about 700°C, which covered the desired range in this

research

- b) The draw process and the lubricant developed by the lubricant manufacturer, eliminated the necessity to pre-coat the wire. The wire travels through the lubricator, into the induction heater and the die. As it is a water-based lubricant, the water evaporates when it is heated thus causing the graphite to adhere well to the wire, resulting in good lubrication.

All the tests on mild steel, medium carbon steel and M2 'high speed' steel were carried out with Dag 2961.

3.2.3.3 Dag 2543

Dag 2543 is a water-based semi-colloidal graphite of higher purity than Dag 2961. It is suitable for temperatures from 400°C - 1,000°C.

This lubricant was tried on mild steel wires only, at temperatures above 400°C. The main purpose was to compare the effects of using different lubricants.

Although the use of this lubricant produces a lower draw stress than Dag 2961 for the same drawing conditions, its disadvantage is that it could only be used for drawing at 400°C onwards, whereas Dag 2961 could cover the desired range of 20°C to about 700°C, and it is essential to be able to draw the first two or three feet cold, ie. until the temperature has been raised.

CHAPTER FOUR

DESIGN AND MANUFACTURE OF NON-MEASURING EQUIPMENT

IV. DESIGN AND MANUFACTURE OF NON-MEASURING EQUIPMENT

4.1 INTRODUCTION

The design, manufacture, assembly, installation and commissioning of the following items were undertaken during the preparatory period.

- (a) cooling systems for the wire, die and induction heating coils
- (b) lubrication system
- (c) heating system
- (d) instrumentation for the measurements of:
draw load, torque, speed and temperature

Items (a) - (c) are discussed in this chapter and item (d) will be discussed in the next chapter.

At this stage in the narrative it is felt pertinent to include a brief description of the drawing operation as this will assist in a better understanding of the equipment described in this chapter.

The set-up of the equipment used in the laboratory is shown diagrammatically in figure 4.1.

A set of five offset rollers was used to straighten and align the wire before entry to the lubricating system and the die. By this means a uniform coating of lubricant was obtained and the wire is kept within

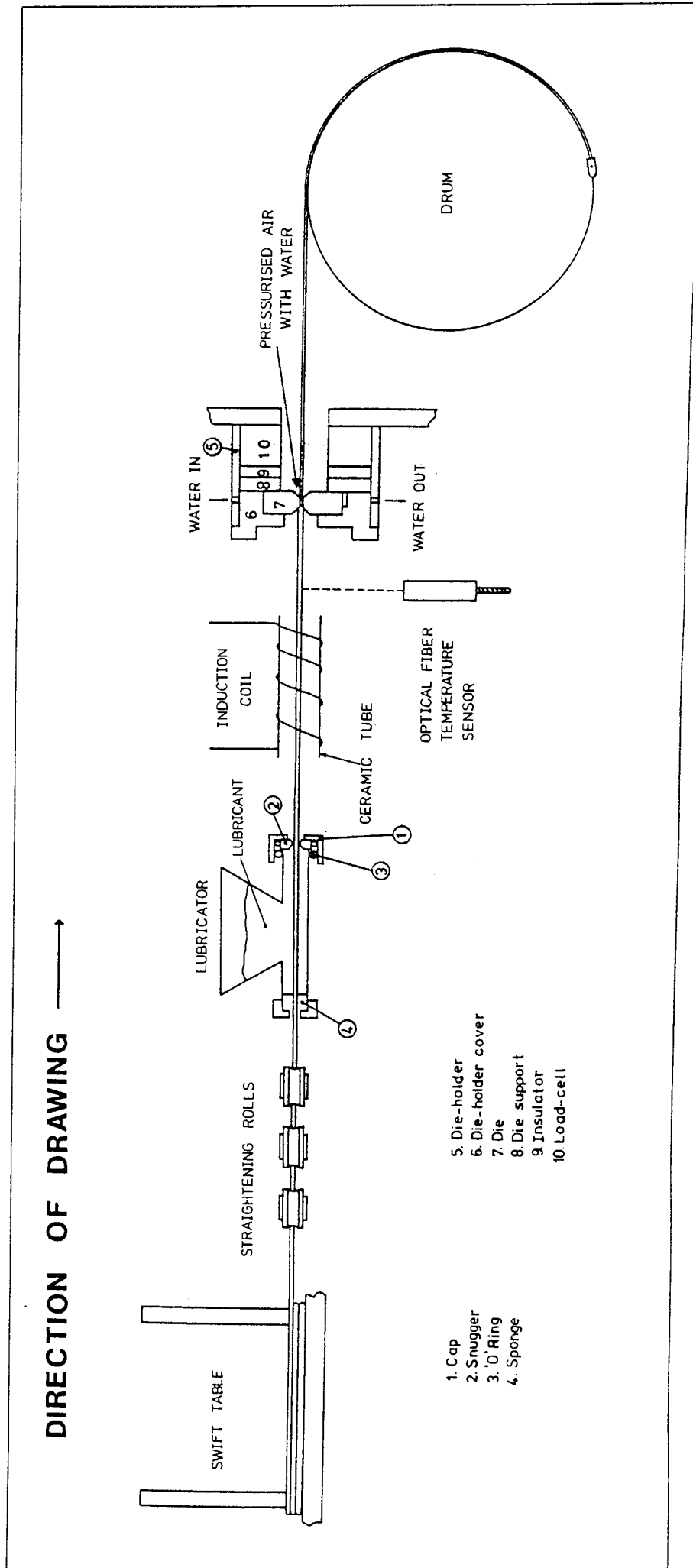


Figure 4.1: Schematic diagram of equipment set-up

the focus of the temperature measuring equipment - ie. the infra-red thermal monitor which used optical fibre.

The wire was straightened, immersed in lubricant, heated by the high frequency induction heater and drawn through the die. The die casing was directly cooled with water, as suggested by both Fuchs⁽⁷⁶⁾ and by companies employing such techniques. It is the author's experience that the cooling of the drawn wire is essential, particularly when drawing at higher temperatures and areas of reduction - when the strength of the drawn wire drops and rupture occurs. This view is supported by Schroder⁽⁷⁷⁾, who found that in the temperature range 600-800°C rupture and local necking in the titanium alloy often occurred. Thus, the wire emerging from the die was cooled immediately by two sprays consisting of a mixture of water atomised by compressed air at 40 lbf in⁻². This fine high pressure spray quenches the drawn wire increasing its strength and rendering it easier to handle. The die was also cooled thus maintaining the shrinkage stresses.

As a horizontal bull-block with a traversing table was used, it was essential for all the equipment for straightening, lubrication, induction heating, drawing and cooling, to move transversely in step with the wire accumulating on the drum. This was achieved by mounting all the necessary parts on a thick base plate (see appendix A7) which was driven by the traverse plate and its screw. Thus the whole system moves as one unit.

4.2 NON-MEASURING EQUIPMENT

The description of the non-measuring equipment used can be broadly divided into three categories, namely:

- (a) lubricator
- (b) induction heating assembly
- (c) die-holder assembly

The mechanical drawings of the various units will be found in the appendix and are filed according to the order in which they are mentioned.

4.2.1 Lubricator Assembly

Prior to entering the induction heater, the wire passed through a lubricator containing a well blended mixture of water and the appropriate lubricant. The lubricator assembly is shown in figure 4.2.

The lubricator container was made from brass plate and a brass tube. Brass was chosen because: it is relatively soft and easy to work on, it does not rust nor react with the lubricant. On the entry end of the lubricator was a piece of sponge which prevented the lubricant from overflowing. The sponge was prevented from slipping out of the lubricator by a brass cover; thus was held tightly over the end of the lubricator by a grub screw.

A 'snugger' was placed at the outgoing end of the lubricator tube. It had tapered ends and a parallel portion, the diameter of which is slightly larger than the diameter of the undrawn wire. This prevented both excessive overflow of the lubricant and excessive lubricant being carried with the wire. The 'snugger' was made from nylon material as this can be easily machined, is non-reactive to water or the lubricant, and being very soft it would not cause any damage to the wire surface. The 'snugger' was held in the nylon cap by an 'O' ring of 1/8 in cross-

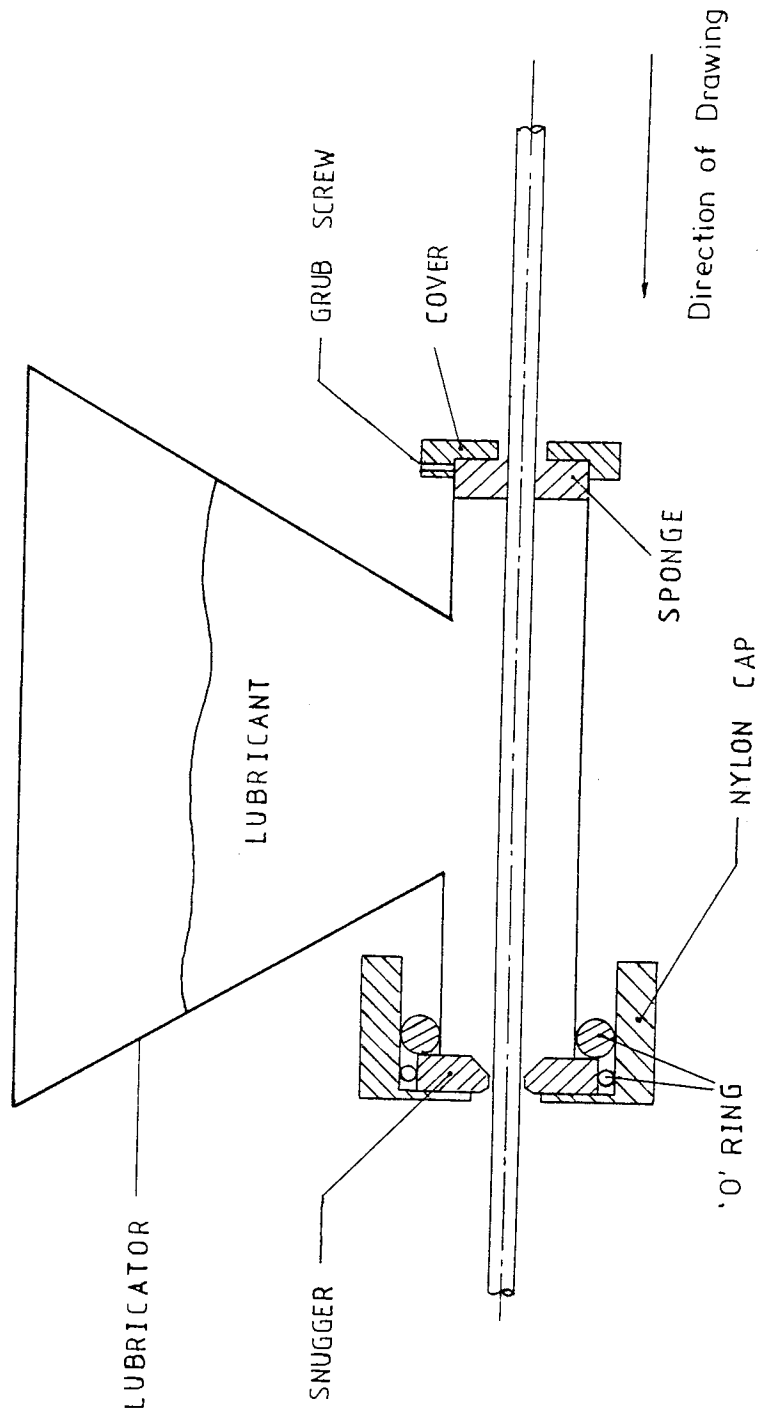


Figure 4.2: Lubricator assembly

sectional diameter.

The 'snugger' and the nylon cap were held tightly against the end of the lubricator by a bigger 'O' ring of 3/8 in cross-sectional diameter. This 'O' ring eased the mounting and dismounting of the nylon cap and also prevented the possibility of lubricant overflow.

The 'snugger' was easily machined and assembled to suit different wire diameters.

4.2.2 Induction heating assembly

It has been pointed out that a horizontal bull-block was used, thus the induction coil had to follow the movement of the traversing table on the bull-block. This was achieved by:

- (a) supporting the coil on the base plate
- (b) including a flexible extension connecting the induction heater and induction coil.

The flexible extension, which had to be made specifically for the purpose, enables the coil to follow the movement of the traversing table and at the same time provides the inductive effects from the induction heater; also it allows the coil cooling water to flow from the heater, through the coil, and back into the heater.

The components in this assembly can be sub-divided into three parts:

- (a) flexible extension
- (b) induction coil
- (c) support for the induction coil and ceramic tube

4.2.2.1 Flexible Extension

The assembly of the flexible extension is shown in the appendix, A7. Four holes of 3/16 in diameter were drilled on the smaller diameter copper tube. Slits from the holes down to the end of the smaller tube were made to allow for a better flow of water. The ends of the braided copper wires were silver soldered to the copper tube. Silver solder was used because of its strength.

A special type of tube used in brewing and which will be called a brewer's tube in this thesis, was placed over the length of the braided wires and part of the copper tube. The distinguishing feature of the brewer's tube is that it does not contain carbon which is conductive; thus it provides adequate insulation.

4.2.2.2 Induction Coil

The wires were drawn cold and in the temperature range of 100°C - 700°C in steps of about 100°C. As the drawing temperature range was rather wide, and the wire would be drawn at various areas of reduction at 20 ft min⁻¹, no single induction coil could be used for the whole experimental range. Thus, five copper coils were constructed from annealed copper tube of 1/4 in outer diameter. The design of an induction coil is shown in figure 4.3 and the dimensions of the coils are:

Coil internal diameter (d) in	Number of coil turns (N)	Coil length (L) in
	2	1.50
1.6	4	1.22
	8	2.80
1.25	12	4.25
0.7	16	5.87

It should be emphasized that optimisation of the input power to the induction heater is not the primary concern in this research, but rather achieving the desired draw temperature at a speed of 20 ft min^{-1} .

The coils were made by winding the copper tube round a mandrel held in a large lathe. Even though the coils were water cooled, and hence constrained to a low temperature, the outer surface might be exposed to a much higher temperature; so high conductivity copper was used. The gaps between two successive turns are each about $3/16$ in which provided adequate insulation between the turns.

A ceramic tube was placed in the induction coil to prevent the wire from touching the coil and to avoid causing shorts between adjacent turns in the coil and the undrawn wire.

By an appropriate combination of induction coil design and input power to the induction heater, the desired temperature could

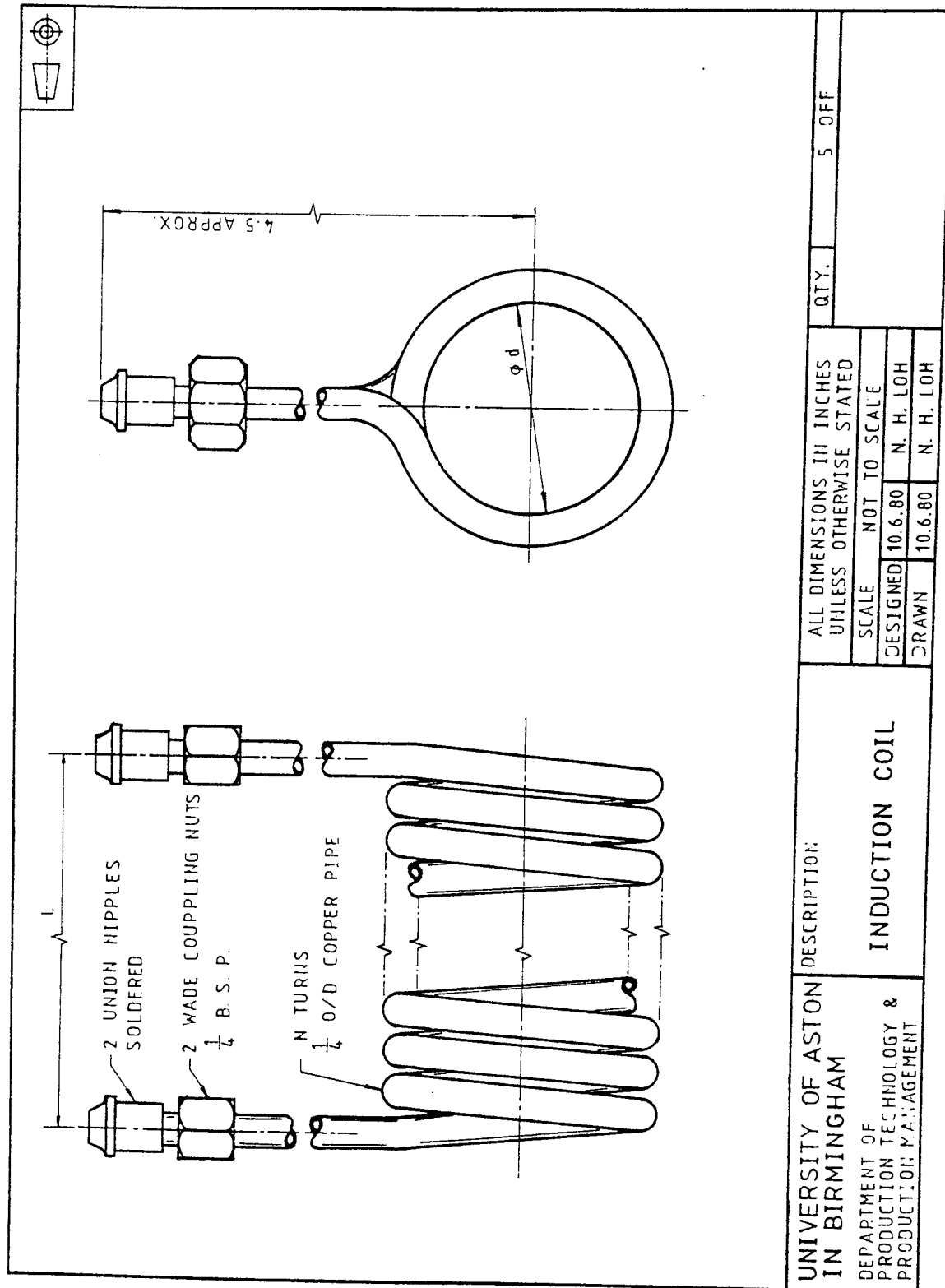


Figure 4.3: Induction coil

be obtained in the wire as it passed through the heater at a speed of 20 ft min⁻¹.

4.2.2.3 Support for the Induction Coil and the Ceramic Tube

The induction coil must be mechanically rigid and held firmly in place as there are substantial electromagnetic forces on the coil.

Holes of 3/16 in diameter were drilled at appropriate positions in a piece of Tufnol. The hole positions were designed to accommodate the free ends of the various induction coils. The Tufnol was divided into two halves through the horizontal centre line, thus producing two parts termed the upper and lower coil clamps. The bottom coil clamp was bolted to the coil support, which is also of a Tufnol material, with its cut surface uppermost. The coil support was held in position by screwing it onto an aluminium plate to allow for axial adjustment.

The induction coil was held in position by allowing its two free ends to sit in the appropriate holes, and by tightening the top and bottom coil clamps with brass nuts.

The ceramic tube was held rigidly by a ceramic holder which has a small slit along the upper part of its axis. This enables its grip on the ceramic tube to be tightened by means of a brass nut. A longitudinal slot was made on the ceramic holder to allow vertical adjustment for the alignment of the ceramic tube and the induction coil. Figure 4.4 shows the ceramic support assembly.

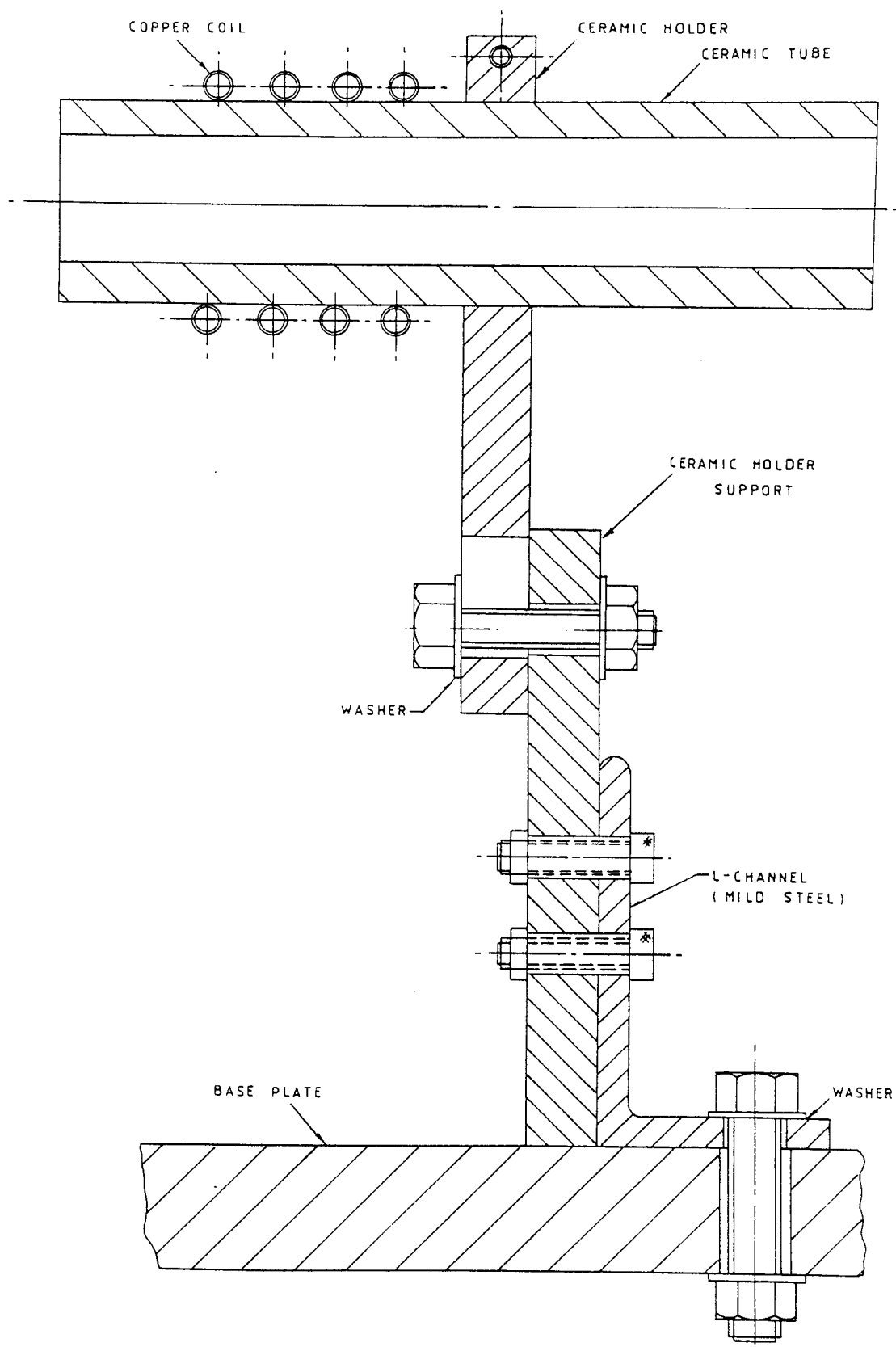


Figure 4.4: Assembly of the ceramic support

4.2.3 Die-holder Assembly

The die-holder assembly is shown in figure 4.5 and consists of five components, namely:

- (a) die-holder
- (b) die-holder cover
- (c) die support
- (d) cylindrical Sindanyo
- (e) load cell

To support the die on the loadcell, a die-holder was manufactured. It was designed so that it could be mounted on an angle block by 8 screws. The die-holder was made from a solid bar and it has inlet and outlet holes to water-cool the die.

The die was held against the die support by 3 pins, located over a 180° angle. The die support has an 'O' ring round its circumference to prevent the cooling water from penetrating into the load cell. A cylindrical tube was welded onto one face of the die support to drain away the water for cooling the wire at exit. Silicone grease was smeared over the surface of the 'O' ring and the inner surface of the die-holder to reduce friction between the die-holder and the 'O' ring. This frictional effect was further reduced by: ensuring that the inside of the die-holder was machined with a good surface finish, and allowing a small clearance between the die-holder and the 'O' ring.

The die-holder cover was screwed up to the die-holder by three screws which retain the die in position. The die-holder cover has two 'O' rings to prevent leakage of water during the tests.

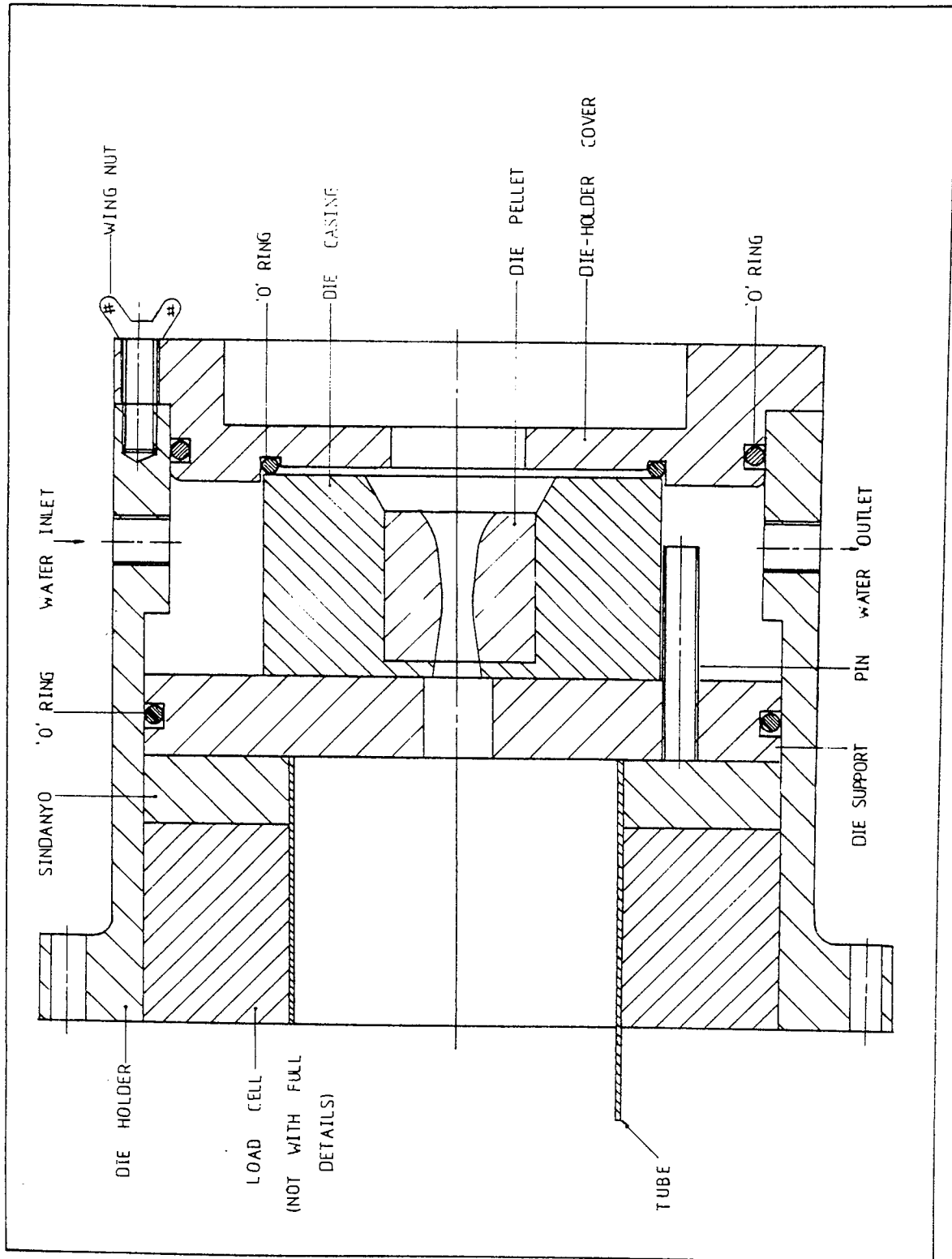


Figure 4.5: Die-holder assembly

The die-holder, die-holder cover and die support were all cadmium plated to prevent rusting.

The load cell was placed next to the angle block followed by a 1/2 in thick Sindanyo disc to insulate the die thermally from the load cell.

A reservoir supplied through a rubber tube, the die-cooling water and the water for cooling the drawn wire.

CHAPTER FIVE

DESIGN, INSTRUMENTATION AND CALIBRATION OF MEASURING EQUIPMENT

V DESIGN, INSTRUMENTATION AND
 CALIBRATION OF MEASURING EQUIPMENT

5.1 INTRODUCTION

The experimental investigations of the drawing of wires at elevated temperatures involved the measurement of the following process parameters:

- a) draw force
- b) draw speed
- c) draw temperature

Initially it was also planned to measure the torque but this was discarded due to friction in the bearings.

In all the electrical circuitry, any cross-coupling effects such as noise pick-up were minimised using continuously screened cables. Capacitors were also used to suppress 'electronic noise'. Fixed resistors of high values were used to prevent possible damage to the galvanometer.

All the calibrations were carried out with the incorporated damping circuits. Before calibration, the equipment was switched on for about an hour to achieve stability and any necessary zero adjustment of the Wheatstone bridge circuit was made.

5.2 THE LOADCELL

5.2.1 Design of the Loadcell

The axially compact ring loadcell designed by Basily and Sansome (78) works on the principle of measuring the axial thrust from bending strains.

The ring loadcell used in this research was designed for a maximum axial load of 2 tonf. The ring loadcell consists of a continuous ring of rectangular cross-section. On one side were four integral sectoral supports equally spaced, and on the other side a similar number of equi-spaced supports placed in positions equal to half the pitch. Consequently, the ring was formed from a continuous series of circumferentially shaped beams which strain in bending and torsion. When a compressive force is applied to the loadcell the active strain gauges, which were bonded to the ring on the face opposite to the sectoral supports, responded to a tensile bending strain. The positioning of the sectoral supports and strain gauges are shown in figure 5.1. Each of the strain gauges used had a resistance of 120 ohms and all were from the same batch. The inactive gauges were bonded to the inner and outer peripheral surfaces in the circumferential direction in line with the neutral surface. This arrangement was adopted to compensate for temperature variations around the ring and any distortion other than that caused by axial thrust. The stress and strain distribution and the stiffness of this type of loadcell is discussed elsewhere in detail by Basily and Sansome.

As the drawn wire was cooled with water, the ring loadcell was specially made to prevent the ingress of water which might cause

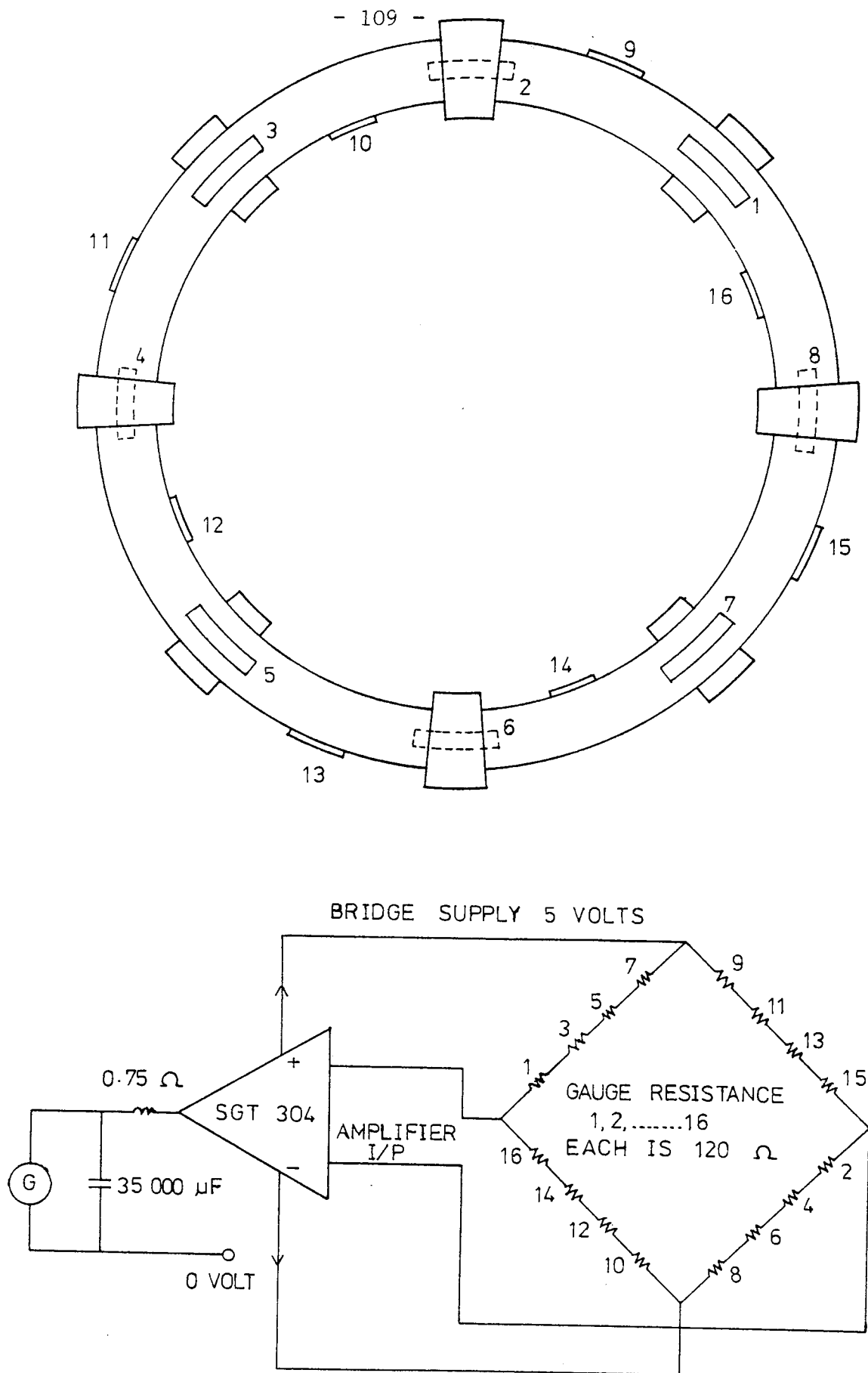


Figure 5.1: Alignment of the strain gauges and the circuit diagram of the load cell

possible damage to the strain gauges.

5.2.2 Instrumentation of the Loadcell

The circuit diagram of the loadcell is shown in figure 5.1.

An amplifier SGT304 was used to amplify the output of the loadcell and to supply a voltage to the Wheatstone bridge. This voltage was kept constant at 5 volts. Although a continuously screened cable was used, the signal from the loadcell suffered from 'pick-up' noise. This noise was suppressed by: connecting a 0.75 ohm choke in series with the amplifier output and a capacitor across the galvanometer, together with the use of a stiffer galvanometer.

5.2.3 Calibrating the Loadcell

The loadcell was calibrated by compression between two platens in a certificated 50 tonf Denison compression machine. The Denison machine had been re-calibrated by the appropriate personnel a few months prior to this loadcell calibration. Thus, the accuracy and reliability of the machine were ensured.

As a variety of metals would be drawn at different areas of reduction and temperatures, the loadcell was calibrated with five different load ranges: 0-0.4 tonf, 0-0.6 tonf, 0-0.8 tonf, 0-1.25 tonf and 0-2.0 tonf. The calibration graphs are shown in figures 5.2 - 5.6.

The loadcell was recalibrated but no detectable variation was found.

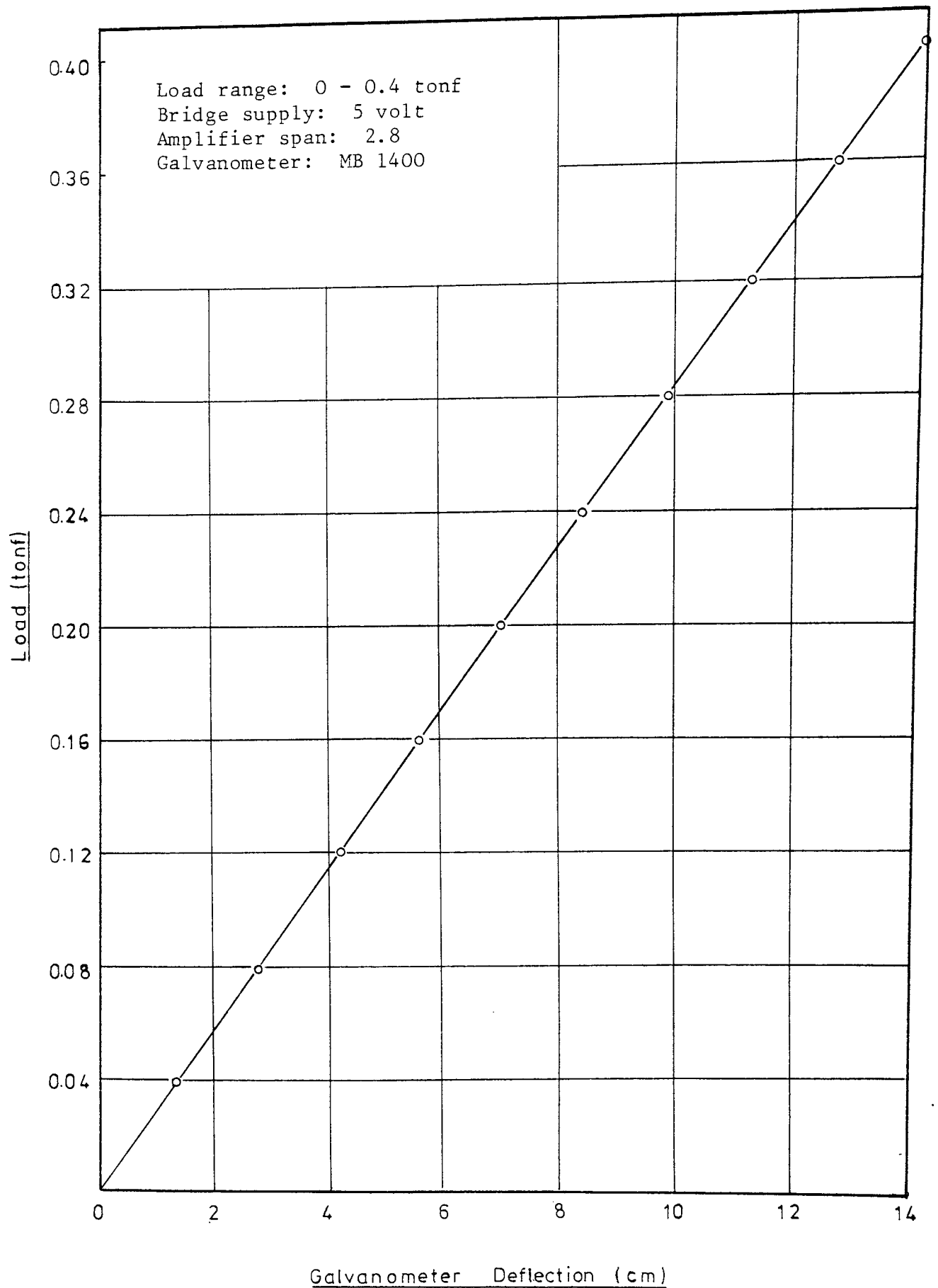


Figure 5.2: Calibration graph of the load cell for the load range 0 - 0.4 tonf

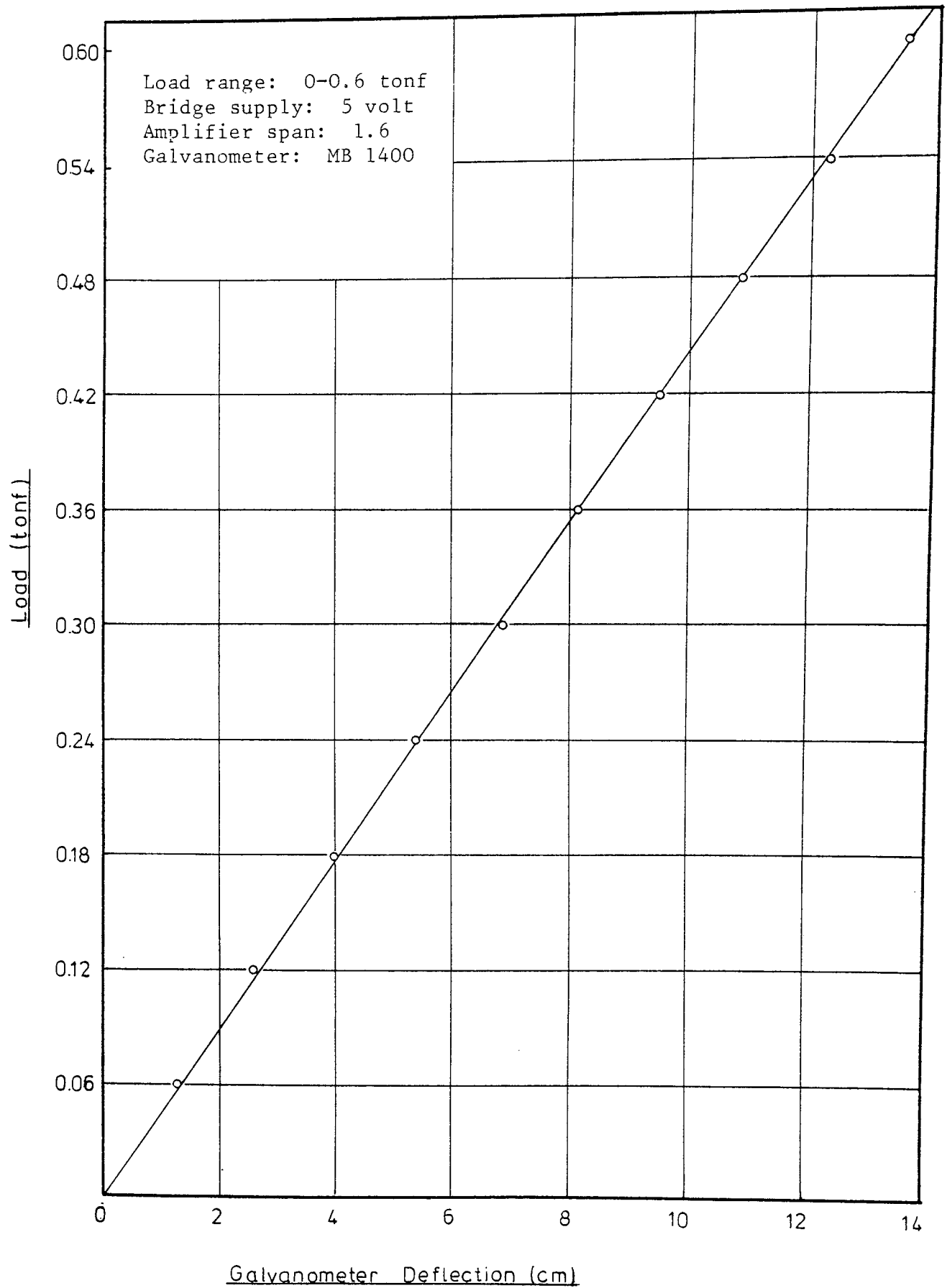


Figure 5.3: Calibration graph of the load cell for the load range 0 - 0.6 tonf

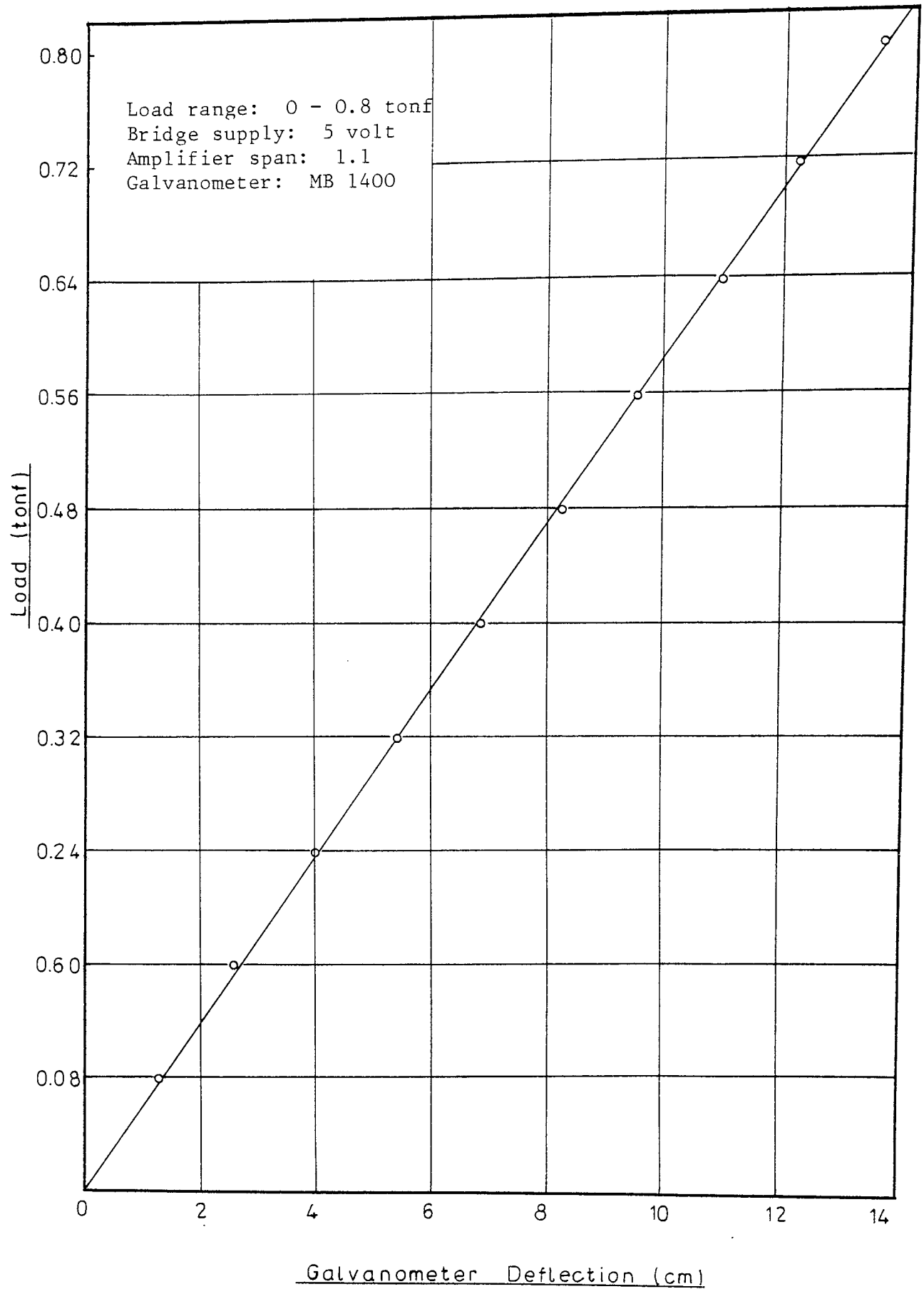


Figure 5.4: Calibration graph of the load cell for the load range 0 - 0.8 tonf

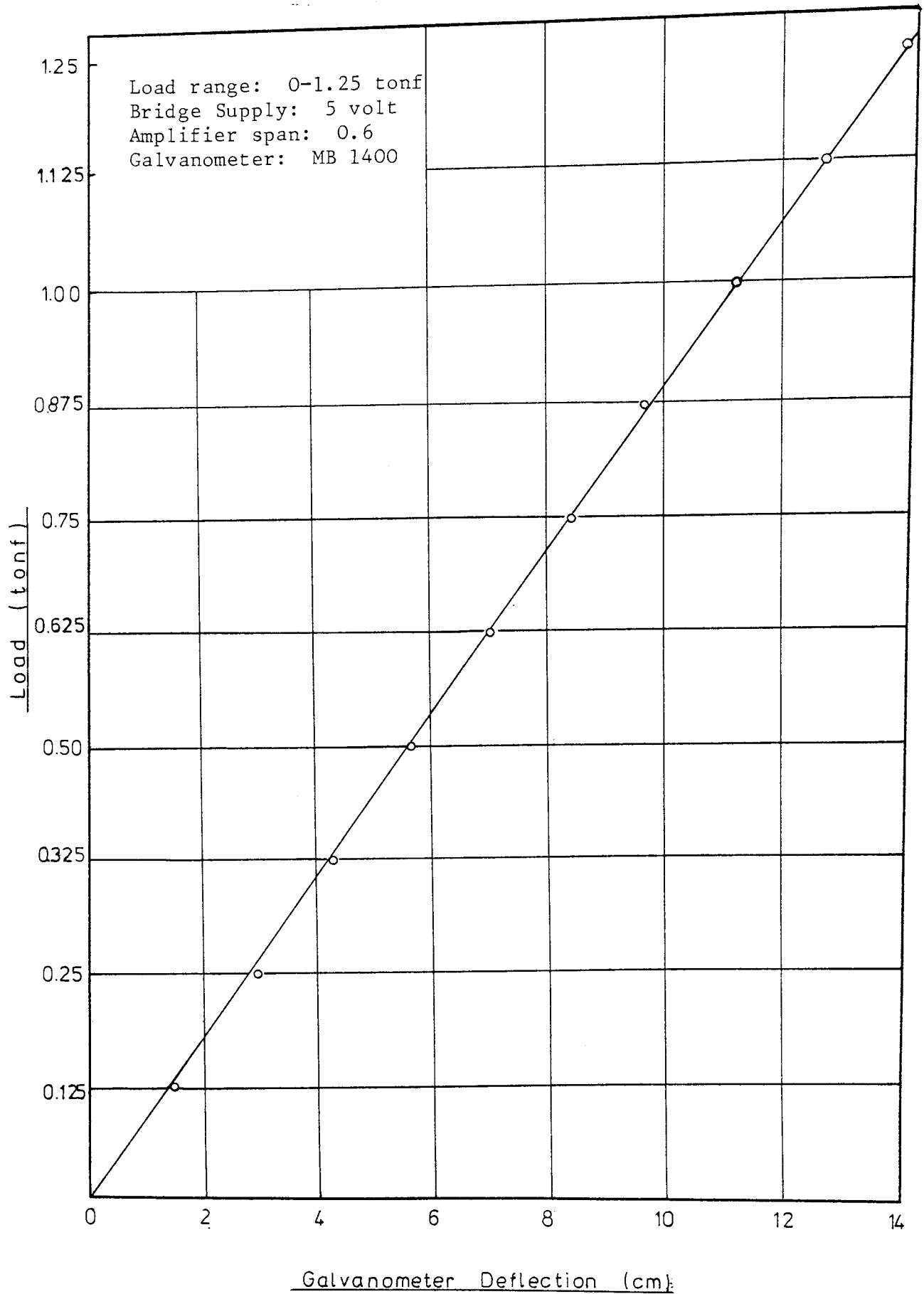


Figure 5.5: Calibration graph of the load cell for the load range 0 - 1.25 tonf

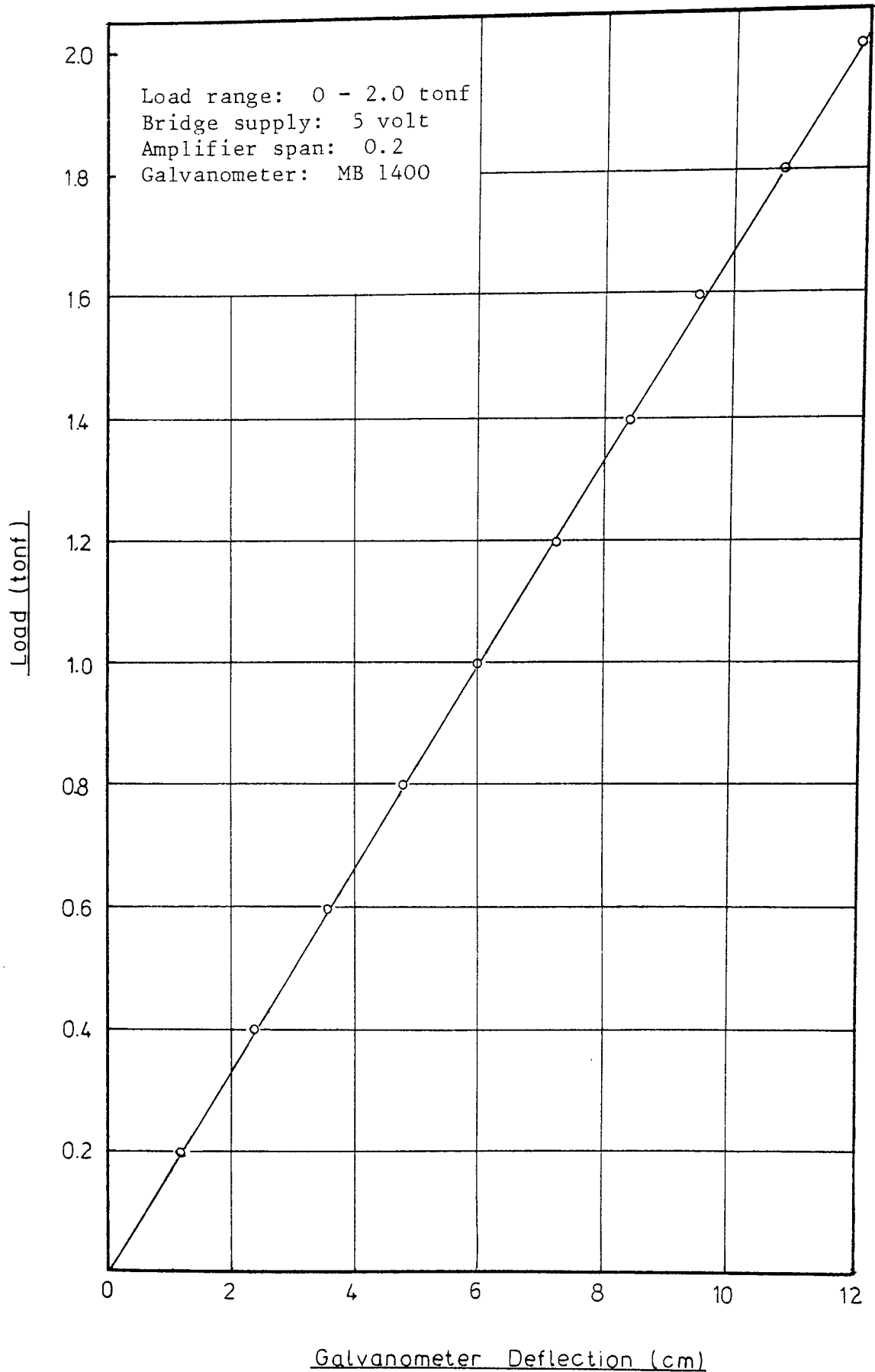


Figure 5.6: Calibration graph of the load cell for the load range 0 - 2.0 tonf

5.3 THE TORQUEMETER

5.3.1 Design of the Torquemeter

The torquemeter, originally installed by Winsper⁽⁷³⁾ and used subsequently by Dawson⁽⁷⁴⁾, was found to be faulty. Consequently, a new set of gauges was bonded on the drum shaft and re-calibrated.

The torquemeter details are shown in figure 5.7. Four torque foil gauges, each of 50 ohm, were bonded to the shaft of the bull-block drum. This particular arrangement of the strain gauges results in automatic temperature compensation for all gauges and the elimination of the effects of all strains other than torsional strains.

The procedure for bonding the gauges was as follows:

- a) The back of the gauges were roughened with fine emery paper and then degreased by Inhibisol.
- b) The shaft was also degreased and roughened with emery paper and the surface chemically cleaned by Inhibisol.
- c) The positions of the gauges on the shaft were marked and coated with cyanoacrylate adhesive. The gauges were bonded.
- d) After bonding, each gauge was checked for continuity and insulation resistance to earth.
- e) The gauges were sealed against moisture by lacquer and tape and again tested for continuity and insulation resistance.

5.3.2 Instrumentation of the Torquemeter

The loads from the torquemeter bridge were connected to a slip ring

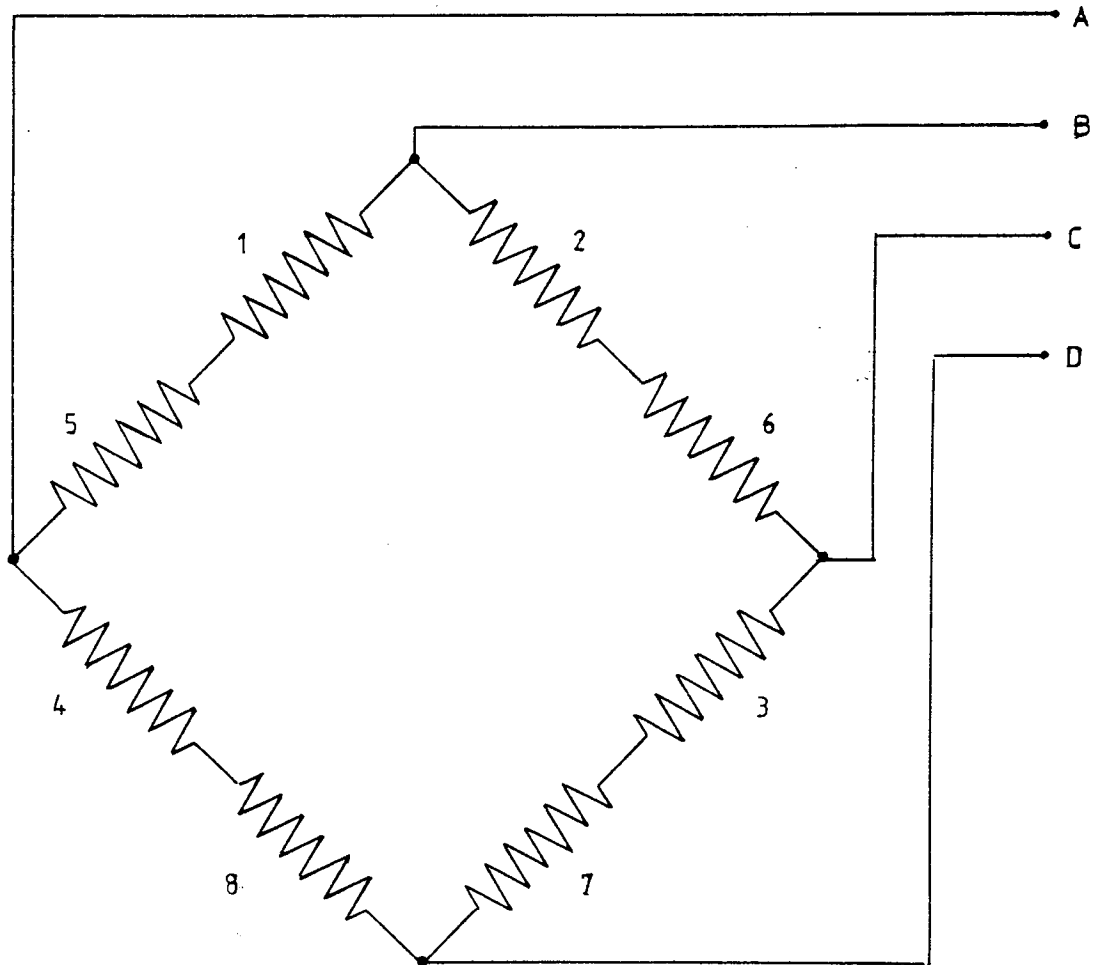
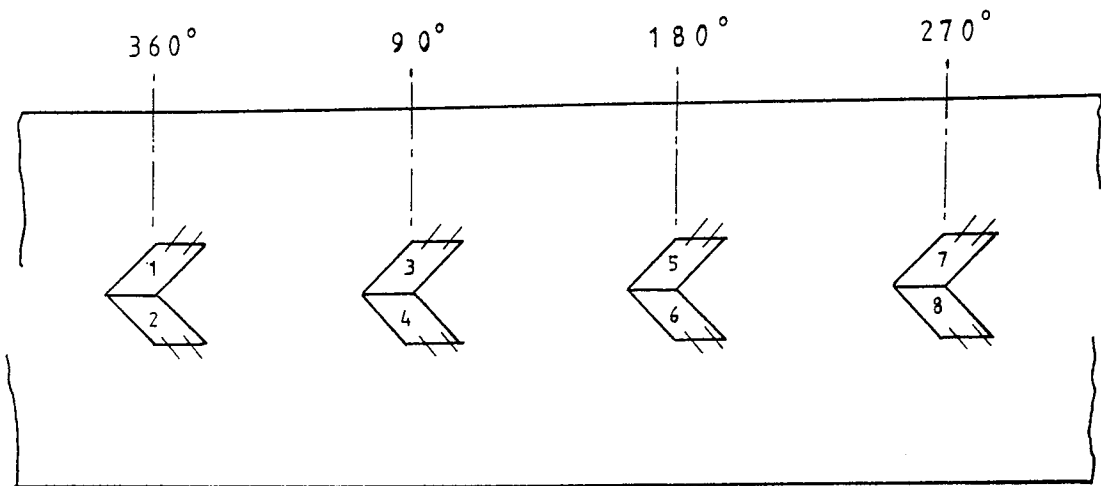


Figure 5.7: Alignment of the strain gauges and the circuit diagram of the torquemeter

which was mounted at the drive end of the shaft.

As the output from the torquemeter was very small an amplifier was used. A capacitor of 2500 μ F was connected in series with the ultra-violet recorder connections so as to reduce the level of 'electronic noise'. The bridge supply was 4 volt.

5.3.3 Static Calibration of the Torquemeter

The torquemeter was calibrated by loading dead weights on a torque arm which was fixed to the drum shaft. The torque arm had a radius of 2 ft and was mounted at the free end of the shaft. The whole set-up is shown in figure 5.8. To prevent rotation of the drum during loading, the shaft drive pinion was locked in position with the torque arm horizontal.

The loads were applied in increments of 90 lbf, up to a maximum of 720 lbf. The loads were decreased to zero in a similar manner. For each load increment a record was taken of the galvanometer deflection.

Initial calibration curves revealed an unacceptably high hysteresis loop, considered to be due to friction in the drum. This was also found by Dawson⁽⁷⁴⁾. In an effort to overcome this, an extra load was applied manually after each load change, and then removed gradually. Thus the torquemeter always approached the load from the same direction. This technique reduced the hysteresis in the calibration curve. The mean values were taken and the calibration curve for the torquemeter is shown in figure 5.9.

At that time it was still planned to employ the torquemeter, since it was hoped that the magnitude of the friction drag on the drum under test conditions would be reduced to an acceptable level. The

torquemeter readings obtained in the preliminary tests showed wide fluctuations of 'peaks and troughs', attributed to the friction in the drum bearings. Consequently, its use was discontinued as the readings would have been unreliable. Dawson found that the friction forces in the drum bearings rendered the measurements inaccurate and also stopped using it.

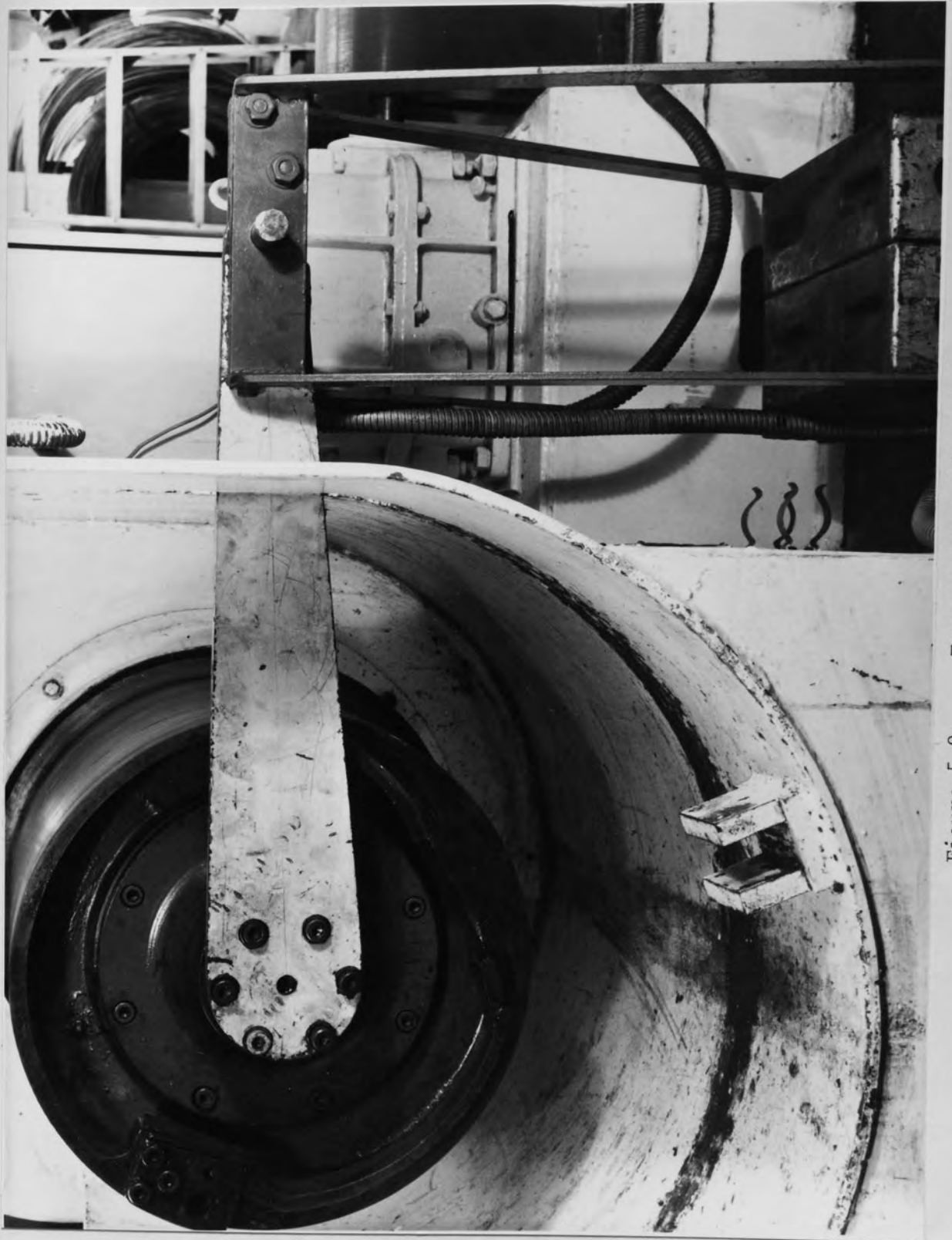


Figure 5.8: Torquemeter calibration

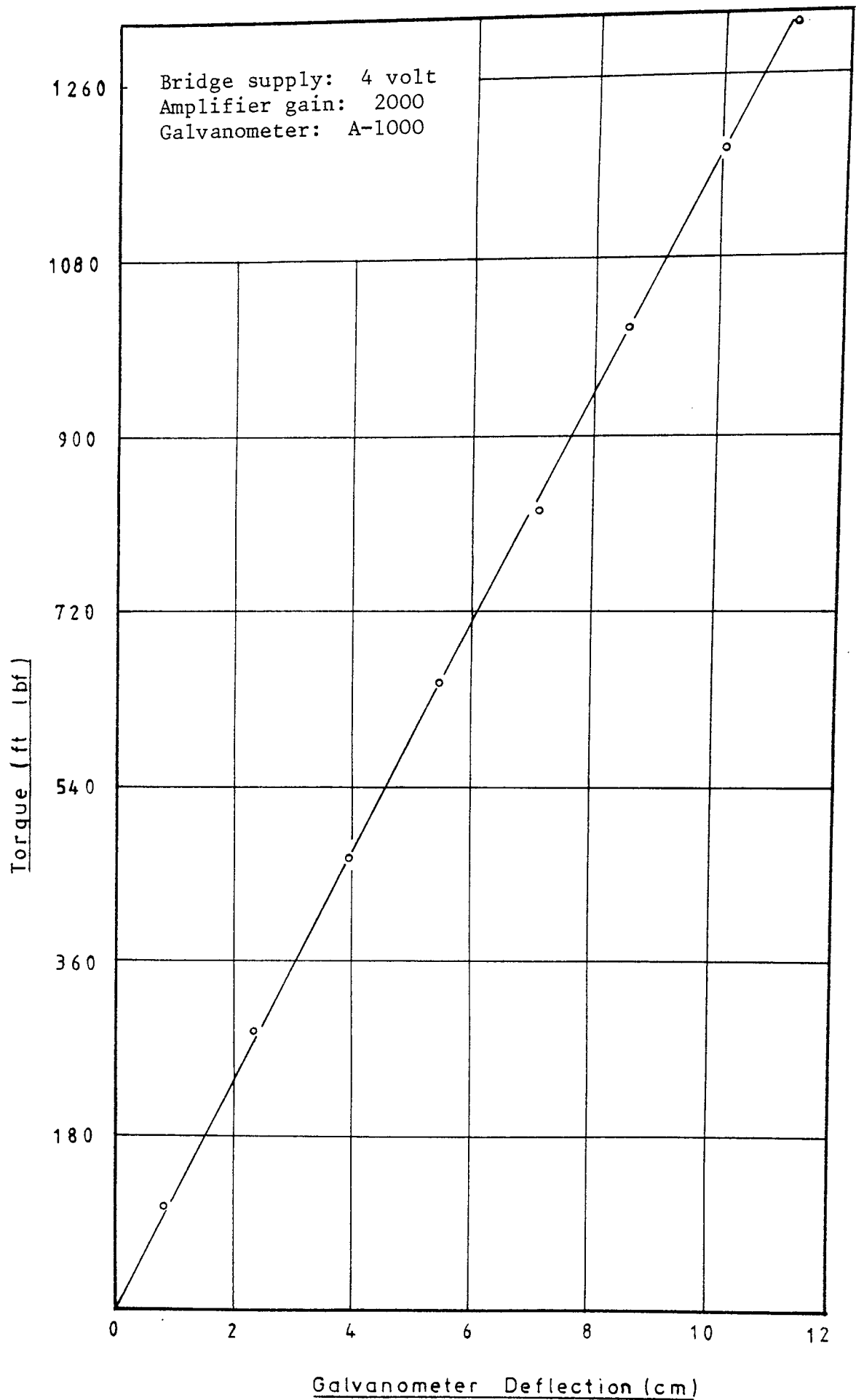


Figure 5.9: Calibration graph of the torquemeter

5.4 THE TACHOMETER

As mentioned earlier, the bull-block was driven by a 15 h.p. induction motor. This motor was connected to a Carter oil gear through a belt drive. The oil gear was coupled directly to a 4 speed gear box which was in turn coupled to the drum shaft by a worm and pinion gear. The speed of the worm shaft was determined by a tachometer which gives 20.8 volt per 1000 rev min⁻¹. Since the speed ratio of the worm shaft to the pinion is known, the speed of the pinion and subsequently the drum speed could be calculated.

A circular disc (see figure 5.10) was tightened to the end face of the worm shaft by three screws. The tachometer was held and supported in a vertical position by an L-plate, as shown in figure 5.11. The rotary motion of the circular disc was transmitted to the tachometer by a plastic tube. The ends of the tube were shrunk onto the shaft of the tachometer and the smaller end of the circular disc. These shrink fits prevented slipping between the parts in contact.

5.4.1 Instrumentation of the Tachometer

The voltage output from the tachometer was sufficiently high to be passed directly to the galvanometer, eliminating the use of an amplifier. The circuit diagram of the tachometer is shown in figure 5.12. Any damage to the galvanometer was avoided by connecting a fixed resistor of a high resistance value of 68K ohm in series with the galvanometer. The variable resistor of 100K ohm allows the galvanometer deflection to be adjusted.

A capacitor of 500 uF was connected across the tachometer to reduce

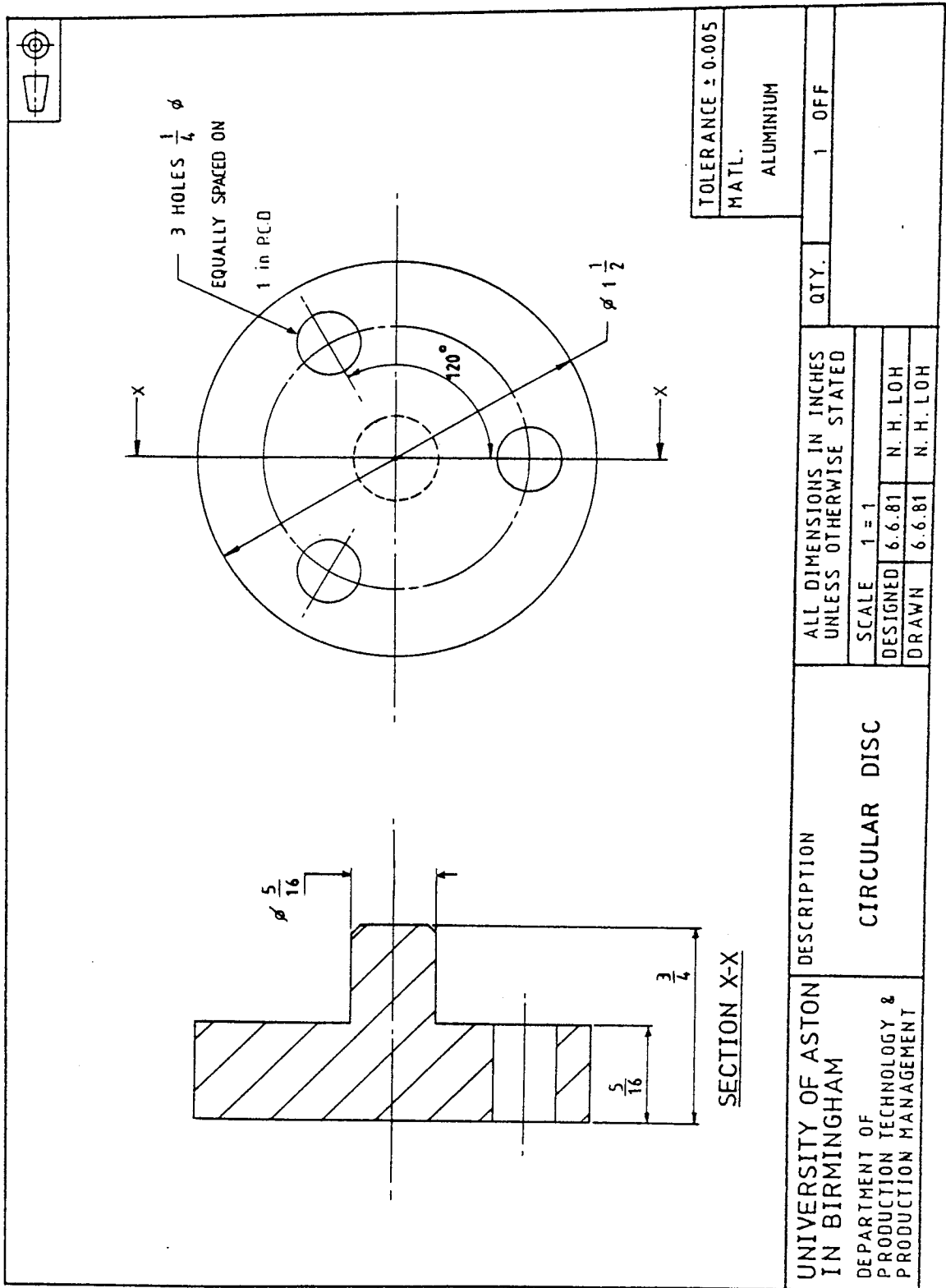


Figure 5.10: Circular disc

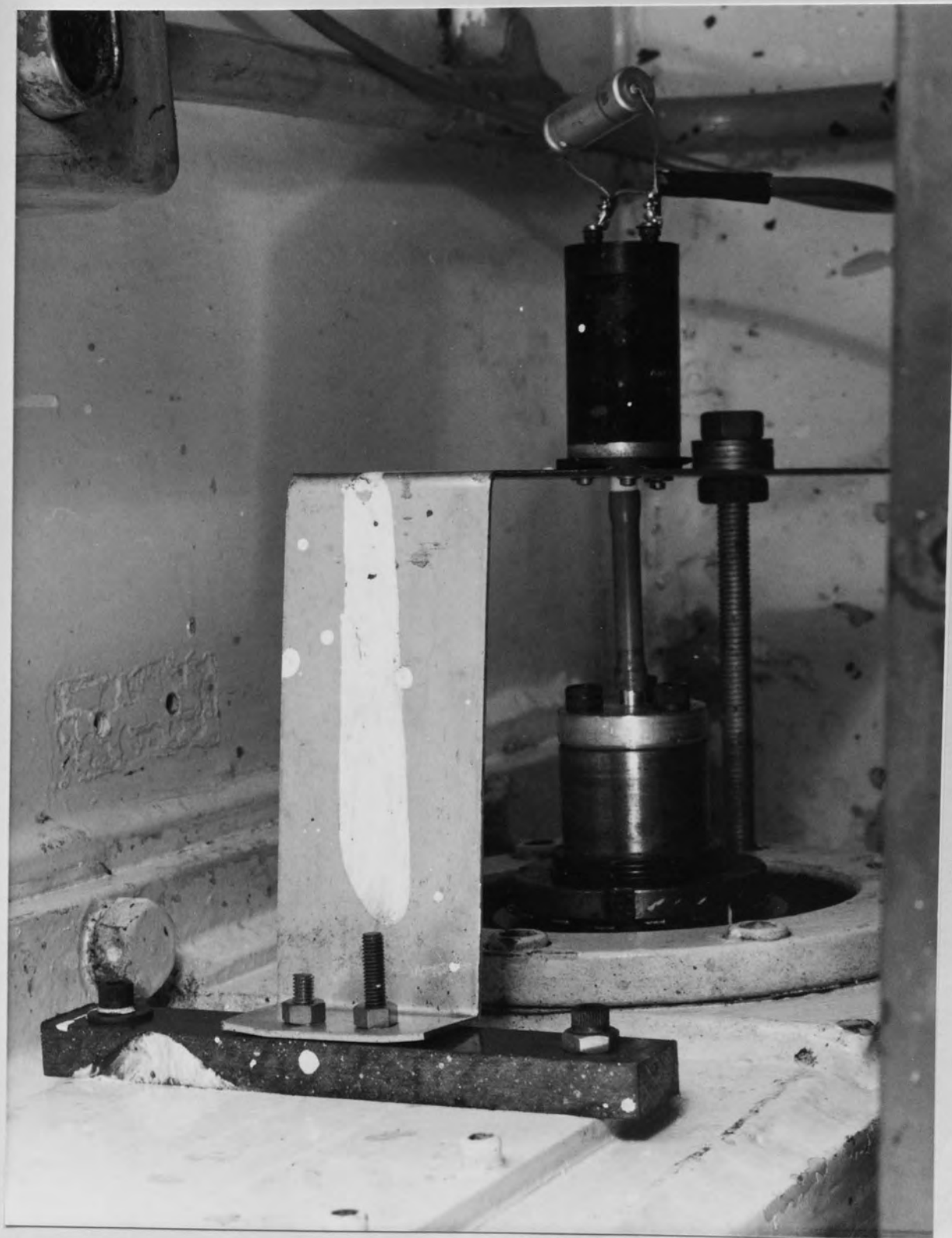


Figure 5.11: Mounting of tachometer

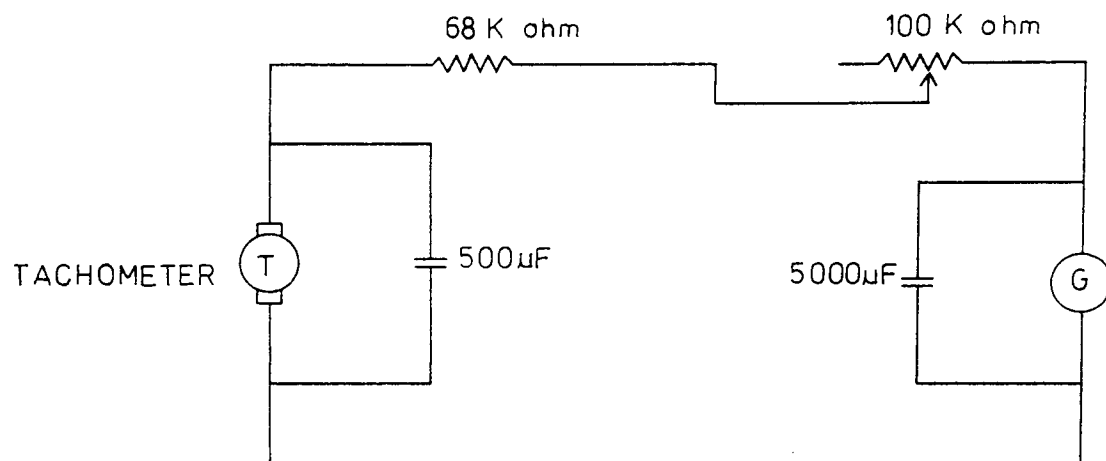


Figure 5.12: Circuit diagram of the tachometer

the noise made by its brushes. The 'electronic noise' affecting the galvanometer was suppressed by connecting a 5000 uF capacitor across it.

The output voltage of the tachometer was displayed on a digital voltmeter. This visual readout assisted in easing the adjustment of the draw speed.

5.4.2 Calibrating the Tachometer

As the tachometer had been used for other work before being used for this research, the accuracy of the tachometer was checked. This was carried out with a fixed field d.c. shunt motor which rotates at uniform speed. The shafts of the tachometer and the shunt motor were aligned axially and connected by a plastic tube, in the same manner as described earlier. The set-up was allowed to run for 3 minutes to attain stable conditions. The time taken to complete 50 revolutions was recorded by a stopwatch. The corresponding output voltage was noted from the digital voltmeter. The procedure was repeated 5 times; good accuracy and repeatability were found.

Before the calibration of the draw speed was carried out, the old oil in the Carter gear was replaced by a new supply. The bull-block was run under no-load conditions for about half an hour to stabilise the speed. The drum revolved in the same direction as that used in the drawing process. The calibration was carried out in increments of 0.5 volt. For each increment a record was taken of the galvanometer deflection. The same procedure was repeated for decrements of 0.5 volt. The calibration graph is shown in figure 5.13.

The tachometer was recalibrated at an appropriate time during the experimental work but no detectable variation was found.

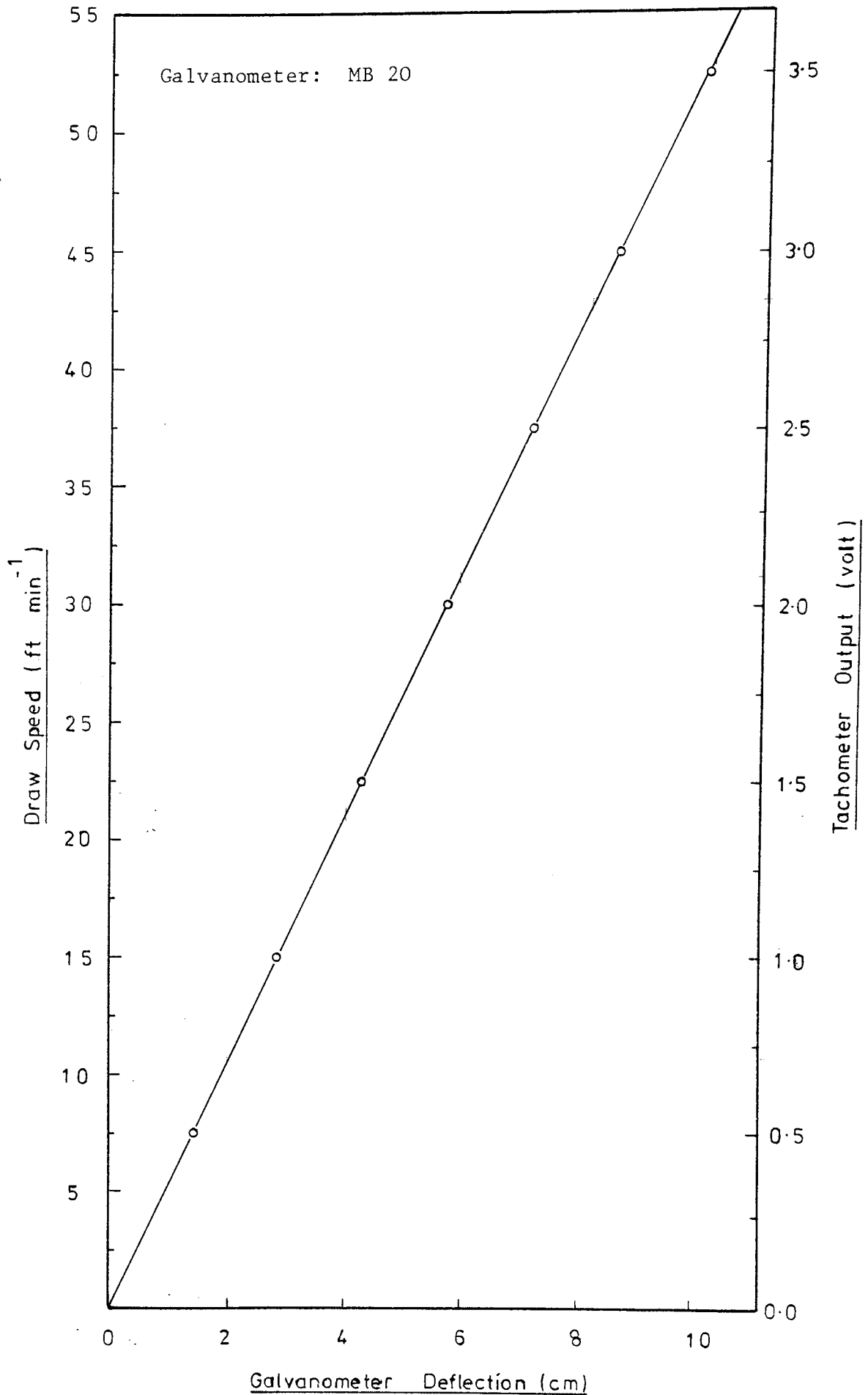


Figure 5.13: Calibration graph of draw speed against tachometer output and galvanometer deflection

5.5 THE INFRA-RED THERMAL MONITOR

5.5.1 Introduction

The temperature of the wire before entering the drawing die was measured by the Vanzetti infra-red thermal monitor. It is a non-contact temperature measuring system making use of a flexible optical fibre bundle to receive the radiation from the target. The system permits the observation of targets in remote or inaccessible places. The basic system consists of an optical detector head assembly with an optical fibre bundle connected by a cable, and an electronic chassis with a digital display. A light source and a calibration source were also available and their use will be mentioned later in the section.

As the temperature range measured (100°C - 700°C) was rather wide, two sets of optical fibre bundles - for convenience termed: 'low' and 'high' optical fibres - were used to give increased accuracy. The ranges covered were 80°C - 350°C and 300°C - 1000°C respectively. The optical fibre bundle detects the amount of radiation from a 'spot' of fixed dimension focussed within the wire. For the low optical fibre the diameter of the spot size is 0.125 in. A rectangular spot size of 0.055 in by 0.165 in was used for the high optical fibre.

5.5.2 Instrumentation of the Thermal Monitor

The temperature was indicated in digital form on the electronic chassis, remote from the drawing area. This temperature corresponds to a linear output voltage of one mV per degree Centigrade. The output was fed into an ultra-violet recorder. To increase the accuracy of the

galvanometer deflection for the lower temperature range, a two temperature contact switch was used, namely the 'low' and 'high' contact. The circuit diagram is shown in figure 5.14. The values of the fixed resistors used were rather high so as to prevent damage to the galvanometer due to excess current flowing through it.

Throughout the calibration and the experimental work, consistency was maintained by using the 'low' and 'high' contacts for the 'low' and 'high' optical fibres respectively.

Before the thermal monitor could be used in the experiments, the emissivities of the wires at different temperatures had to be determined, and this is described in section 5.5.4.

5.5.3 Calibration of the Thermal Monitor

The resistance heating unit described in section 5.5.4.1 was used to heat the wire for the calibration of the thermal monitor.

For each of the contact switches, the wire sample was heated to the maximum temperature required, with the spot of the optical fibre focussed within the boundaries of the heated wire. This focussing was made possible by a light source which illuminated the spot. The variable resistor was adjusted to give the desired maximum galvanometer deflection. The temperature was then decreased in steps of 100°C and the galvanometer deflection noted. For each temperature, the focussing of the spot was checked and adjusted when necessary. This is particularly important at the higher temperatures where the wire tends to sag.

The calibration curves are shown in figures 5.15 and 5.16.

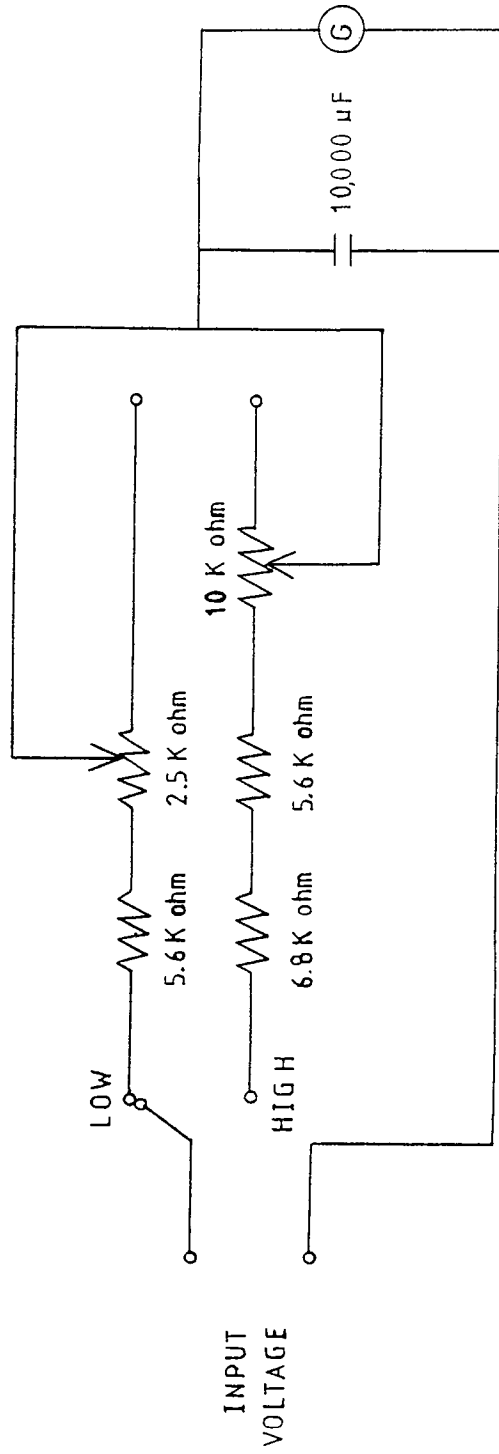


Figure 5.14: Circuit diagram of the Infra-red thermal monitor

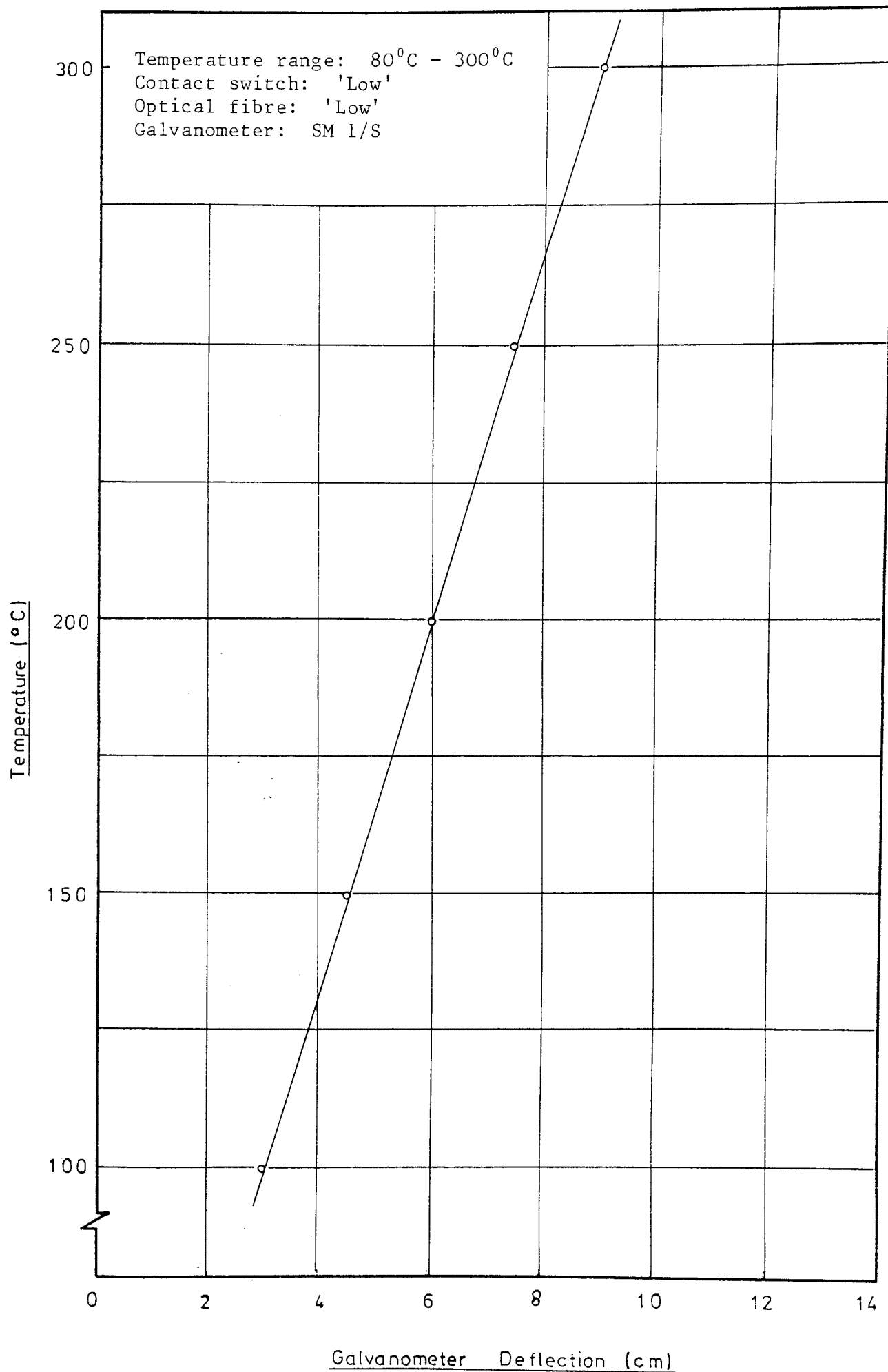


Figure 5.15: Calibration graph of the infra-red thermal monitor using the 'low' optical fibre

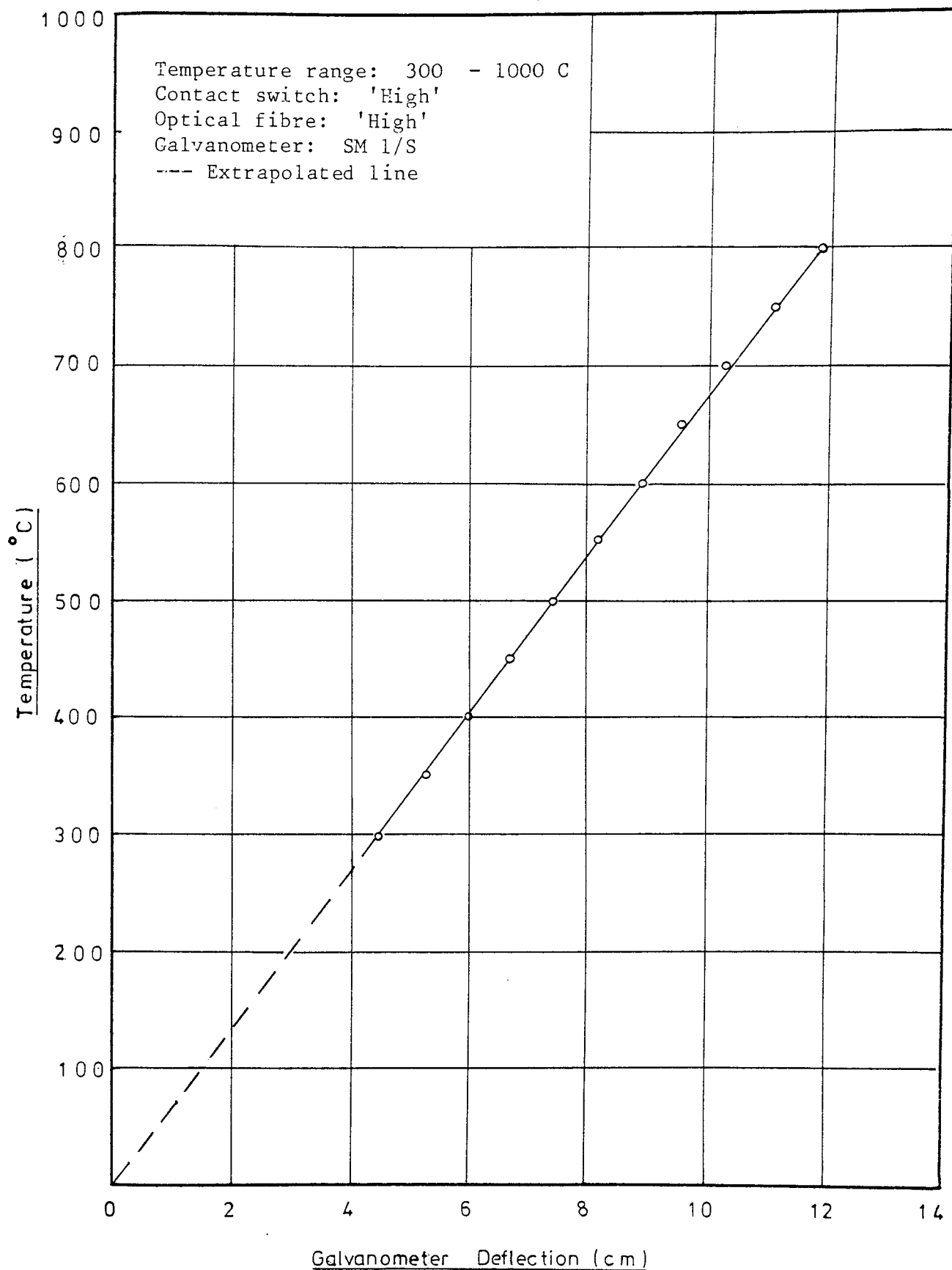


Figure 5.16: Calibration graph of the infra-red thermal monitor using the 'high' optical fibre

5.5.4 Emissivity Calibration

The emissivity calibration was carried out for each of the three types of wire materials for the temperature range of 100°C - 800°C, in steps of 100°C.

A special a.c. resistance heating unit had to be built to heat the wire sample because of the difficulties in measuring the temperature of the heated wire.

5.5.4.1 The Resistance Heating Unit

The circuit diagram of the resistance heating unit is shown in figure 5.17. Three turns of cable were wound round the transformer to give low voltage secondary windings.

The power required to heat the wire sample to the required temperature was measured. Although this is not used in the theoretical analysis, it gives an indication of the energy consumed.

The current flowing through the secondary windings was measured by an Avometer (model 7). As the test temperature increased, a 400 amperes shunt was used in place of the 200 amperes current transformer. An a.c. millivoltmeter was used to proportion the current flowing through the shunt. The voltage across the wire sample was measured by an avometer. Thus the power consumed could be calculated.

All the electrical wires used in the circuitry were twisted together to nullify any electromagnetic current pick-up.

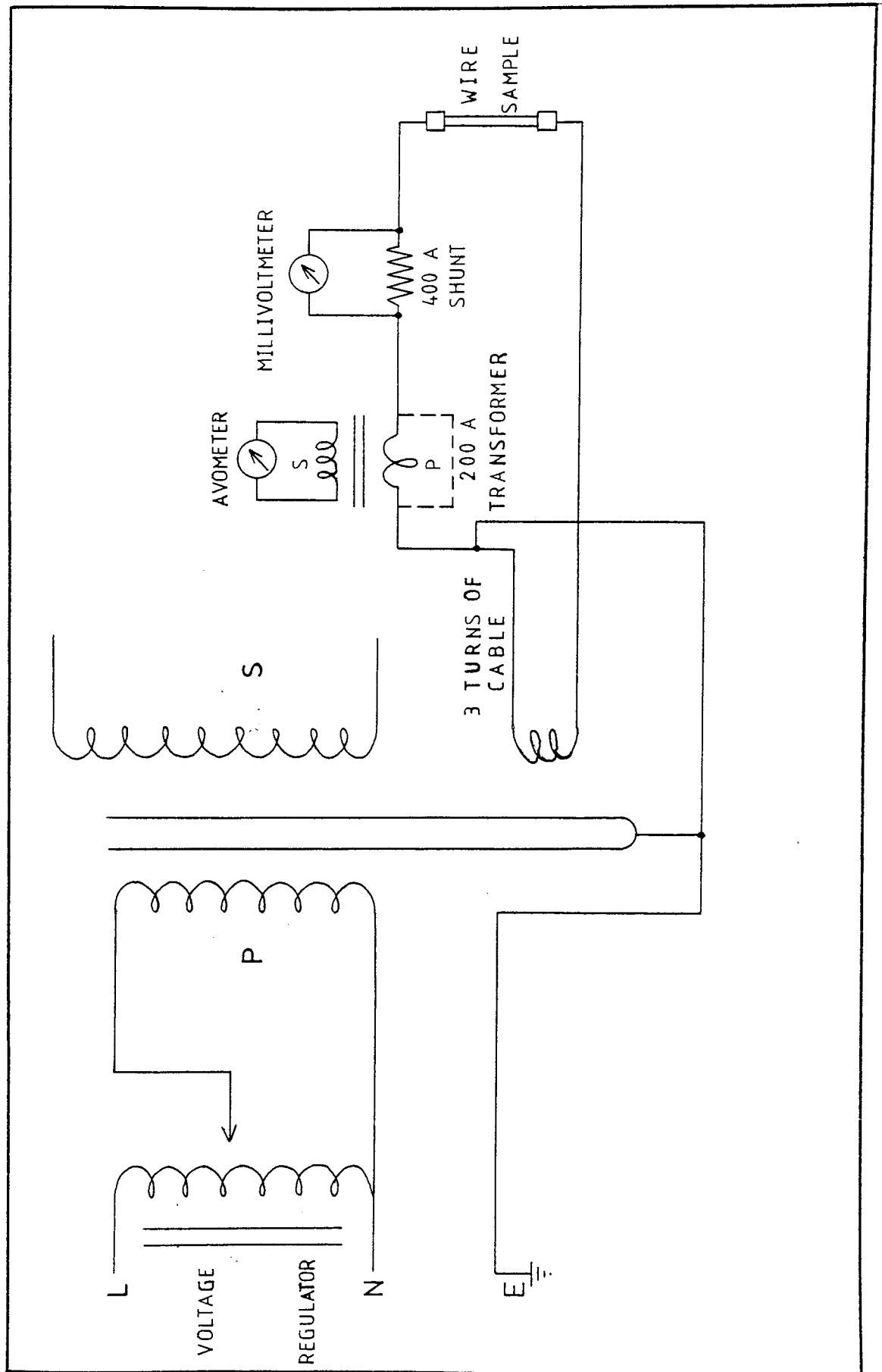


Figure 5.17: Circuit diagram of the resistance heating unit

5.5.4.2 Procedure for the Emissivity Calibration

The wire sample used for the emissivity calibration was selected to be representative of the wires to be drawn. Each end of the wire was brazed into an 'Enot' adaptor, as shown in figure 5.18.

A chromel-alumel thermocouple was used to measure the surface temperature of the wire sample. A small wire diameter of 7.48×10^{-3} in (0.19 mm) was chosen to reduce the heat conduction and to increase sensitivity.

The cleaned ends of the thermocouple were twisted together with about two turns. The end of the twisted wires was formed into a small bead by gas welding.

To measure the surface temperature accurately, the hot junction had to penetrate the surface scale. Thus the opposite surface of the central portion of the wire sample was filed and rubbed with fine emery cloth to give smooth 'flats' on both surfaces. The flats and the thermocouple bead were cleaned with Inhibisol. The head was welded to one of the 'flats' to give good thermal contact by capacitor discharge welding.

Both the ends of the thermocouple were cleaned before fastening to the temperature readout, to ensure good electrical contacts.

The calibration of the emissivity was as follows:

- a) The wire sample was coated with the appropriate lubricant at all the areas except the spot weld region. The lubricant mixture was similar to that used in the actual

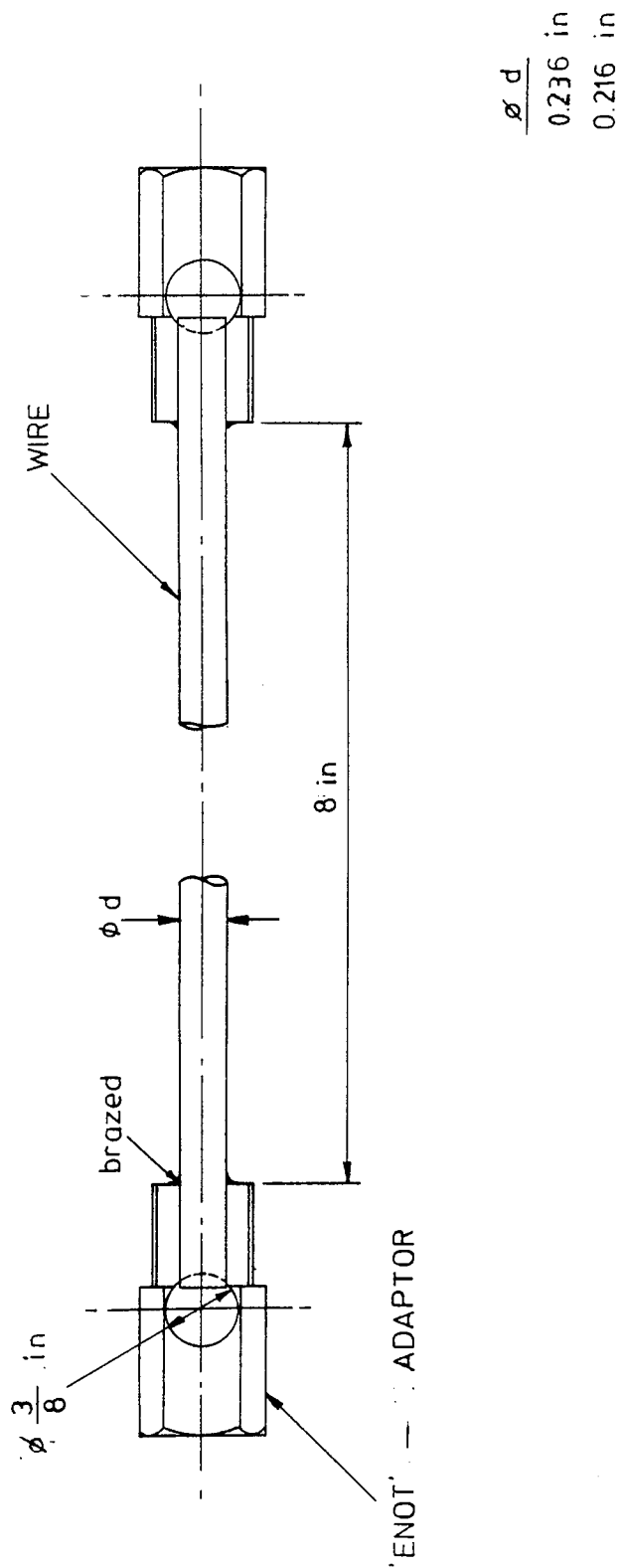


Figure 5.18: The wire sample

drawing tests.

- b) The spot of the optical fibre was focussed onto the wire sample at the lubricant coated area. The spot was brought very close to the thermocouple bead thus ensuring similar thermal conditions.
- c) The wire was heated by direct resistance heating and the temperatures adjusted by controlling the input voltage. This was achieved by means of a voltage regulator.
- d) When the temperature reached its steady-state condition, the emissivity was adjusted so that the temperatures indicated by the thermocouple and the infra-red thermal monitor agreed to $\pm 2^{\circ}\text{C}$.

By adjusting the input voltage to the resistance heating unit, the emissivity over the whole range of temperatures was found.

The focussing of the spot on the wire sample was checked for every temperature reading thus giving reliability to the results obtained.

The emissivity values of the 3 different wire materials at different temperatures are shown in Table 5.1.

	Temperature (°C)	Emissivity value		
		Mild steel	Medium carbon steel	M2 'high speed' steel
'Low' optical fibre	100	0.90	0.95	1.00
	200	0.90	0.91	0.90
	300	0.86	0.91	0.86
'High' optical fibre	400	0.86	0.91	0.86
	500	0.82	0.80	0.83
	600	0.80	0.76	0.80
	700	0.75	0.72	0.80
	800	0.70	0.70	0.79

Table 5.1: Emissivity values for mild steel, medium carbon steel and M2 'high speed' steel

CHAPTER SIX

STRESS-STRAIN DATA

VI. STRESS-STRAIN DATA

6.1 COMPRESSION TESTING OF MATERIALS

6.1.1 Introduction

The present experimental tests were carried out with materials for which there were insufficient stress-strain data. Therefore it was decided to conduct a test programme in order to obtain the required data. This was the most difficult task to be organised in this research.

The initial idea was to generate stress-strain data in the temperature range 100°C - 800°C , with at least three strain rate values. From the data it was intended to relate the stress, strain, strain rate and temperature mathematically as discussed in section 2.2.6.1.

Tension tests were studied and enquiries were made to locate suitable test equipment. The idea was eventually abandoned because:

- a) of the limitation in strain due to instability during necking. According to Sellars⁽⁷⁹⁾ the limiting strain normally varies from 0.15 to 0.25 for testing under hot deformation conditions
- b) the strain rate obtainable in many conventional tensile testing machines is considerably lower than the strain rate that prevails during deformation and that required in the theoretical analysis.

In view of the limitations of tension tests, compression tests were conducted on a cam plastometer. Two out of the four cam plastometers available in the UK were not in working condition and shortage of time did not permit further delay. Thus the tests were conducted on the 5 tonf cam plastometer at Sheffield Polytechnic.

6.1.2 The Cam Plastometer

The cam plastometer enabled uniaxial compression testing of materials at constant natural strain rates between 3 and 50 s⁻¹. The plastometer is described below.

The cam was driven by a 2 h.p. motor to the flywheel by a simple vee-belt pulley drive. An eccentric plate clutch mechanism was used to engage and disengage the cam shaft from the rotating flywheel. The cam had a logarithmic profile, thus imparting constant natural strain rate to the cam follower, providing the cam speed was constant. The rotational motion of the cam was converted into vertical movement of a piston mounted in a spring loaded guide block by means of a cam roller follower. The downward movement of the piston was transmitted through the upper moving platen of the die assembly to the specimen. The lower die platen was mounted rigidly in the die assembly which was mounted on an adjustable spacer assembly on top of the loadcell.

The die-assembly as shown in figure 6.1 consisted of a moving upper platen and a stationary lower platen, between which the cylindrical specimens were axi-symmetrically compressed.

The displacement of the piston was measured by means of a linear transducer. The speed of the cam shaft was measured by means of a slotted disc, which was mounted on one end of the cam shaft. The

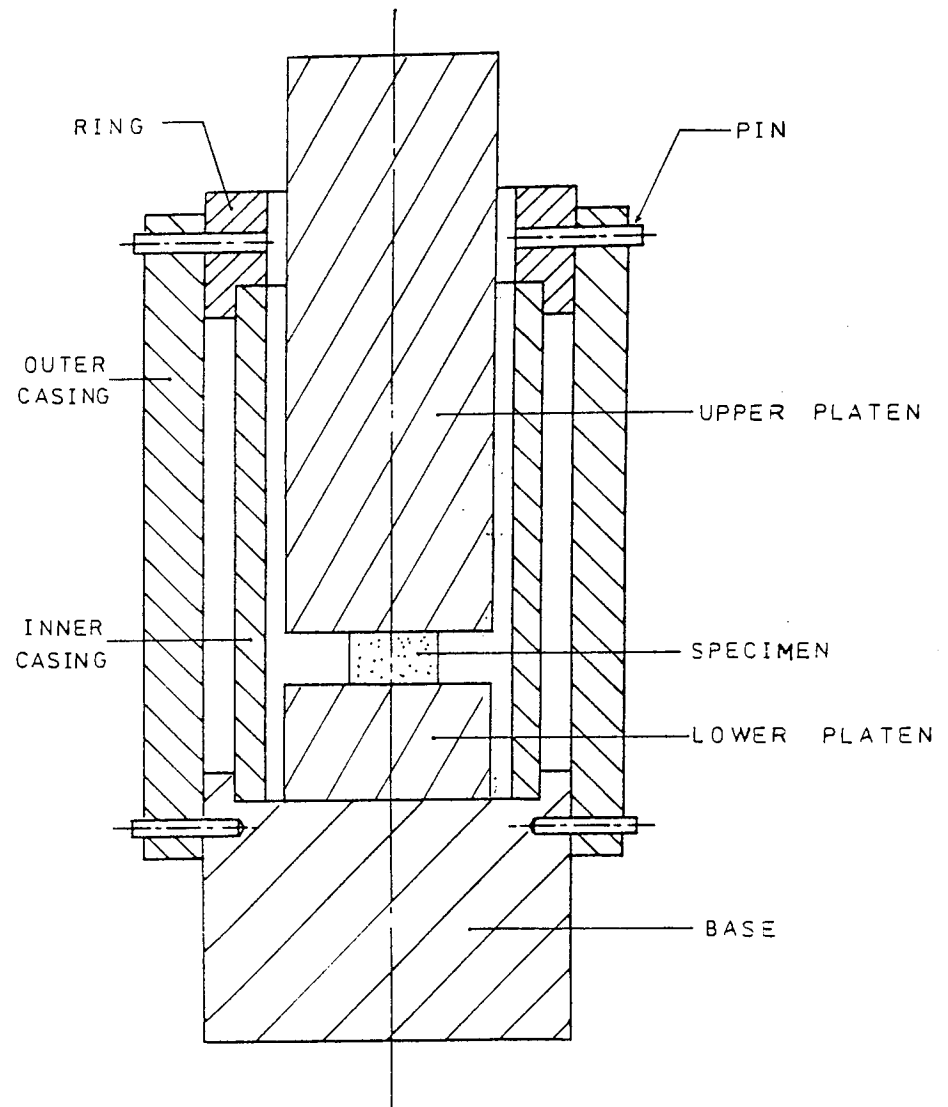


Figure 6.1: Die assembly

magnetic head picked up the slots on the disc as impulses.

The calibrations of the loadcell, linear potentionmeter and the magnetic head were performed by the personnel at Sheffield Polytechnic. The outputs from the loadcell, linear transducer and magnetic head were amplified and fed into an ultra-violet recorder to give a permanent record of the results.

Adjacent to the cam plastometer was a furnance for heating the specimens.

6.1.3 Preparation of Specimens and Test Procedure

Plain cylindrical specimens, 0.315 in. in diameter and 0.5 in in height were manufactured from specially purchased annealed stock material. The end faces of the specimens were surface ground to reduce the effects of friction during the compression tests.

The following test procedure was adopted. To minimise further the effects of friction, the specimen end faces were cleaned with Inhibisol and coated with lubricant Dag 2961 prior to loading them into the die assembly. The loaded die assembly was placed in the furnance which had earlier been switched on to the required temperature for about one hour. The specimen was allowed to soak for about 30 min at the required temperature. The main motor was switched on and the speed regulator was set to give a strain rate of 10 s^{-1} . The die assembly was removed quickly from the furnance and placed on the lower platen of the cam plastometer. The spacer was adjusted until the specimen was positively held between the platens. The ultra-violet recorder was started and the compression stroke initiated by engaging the cam. The ultra-violet recording contains 3 traces: load, displacement and speed.

After a few trials, the compression tests had to be discontinued because:

- a) the load capacity of the cam plastometer was exceeded when compressing M2 'high speed' steel at 700°C and medium carbon steel at 600°C
- b) the M2 'high speed' steel specimen sheared due to its relatively high height to diameter ratio of 1.5:1

6.2 STRESS-STRAIN DATA USED IN THE THEORETICAL ANALYSIS

6.2.1 Introduction

Continuous efforts were made to gather suitable published stress-strain data through: literature search, and making inquiries to the British Steel Corporation and various companies. As the efforts were futile, attempts were made to use the available data at hand. These are discussed in the following sections.

6.2.2 Mild Steel EN2B

Oyane⁽³³⁾ conducted high speed compression tests for a range of plain carbon steels at a constant strain rate of 450 s^{-1} . The results for 0.16% plain carbon steel are shown in figure 6.2. The results were assumed to fit the power relationship:

$$\sigma = B\epsilon^n$$

The graphs of $\log \sigma$ against $\log \epsilon$ are shown in figure 6.3. They were generally found to be linear for the strain range 0.2-0.4.

Using the specially written computer program discussed in section 2.3.2, suitable values of κ and $\dot{\epsilon}_0$ were found for the velocity-modified temperature equation. The graphs of σ against T_m for the various strains are shown in figure 6.4. The constant κ and standard strain rate $\dot{\epsilon}_0$ were taken as 0.08 and 2.0 s^{-1} respectively. The curves were similar in shape. A strain-ageing region and a peak stress at about $T_m = 500^\circ\text{K}$ were clearly evident in all the curves.

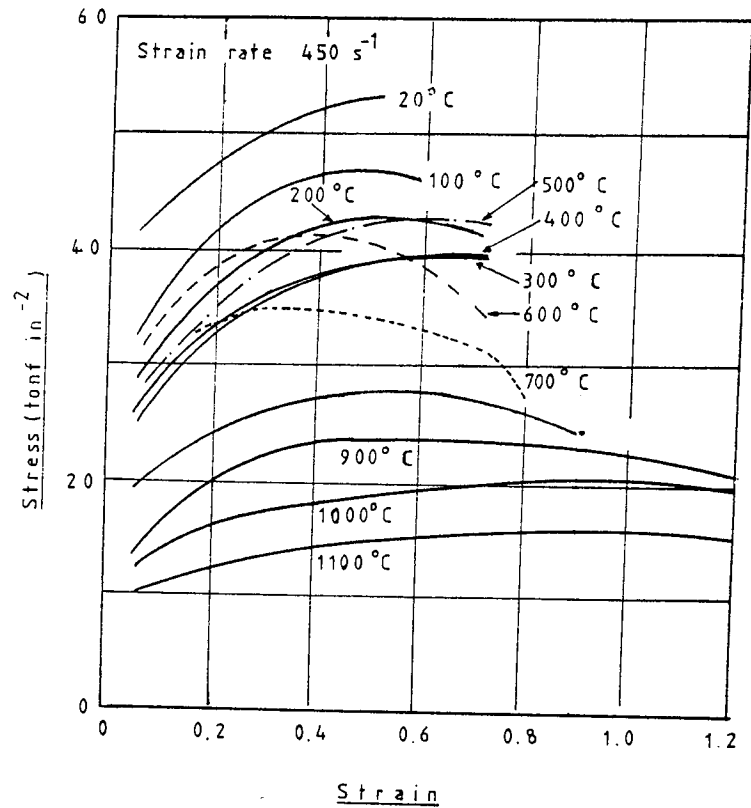


Figure 6.2: True stress-strain data for 0.16% C steel. After Oyane (33)

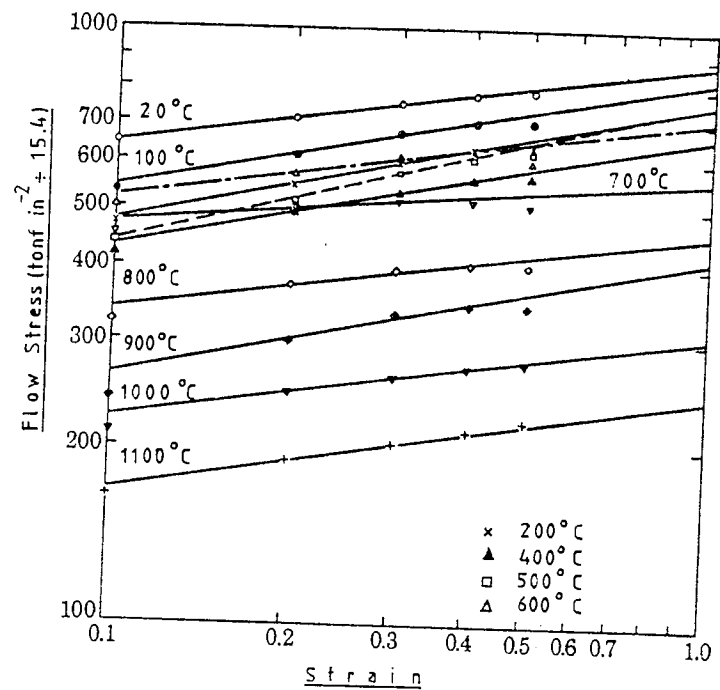


Figure 6.3: Graph of log stress against log strain for the 0.16% C steel of figure 6.2. After Hastings (80)

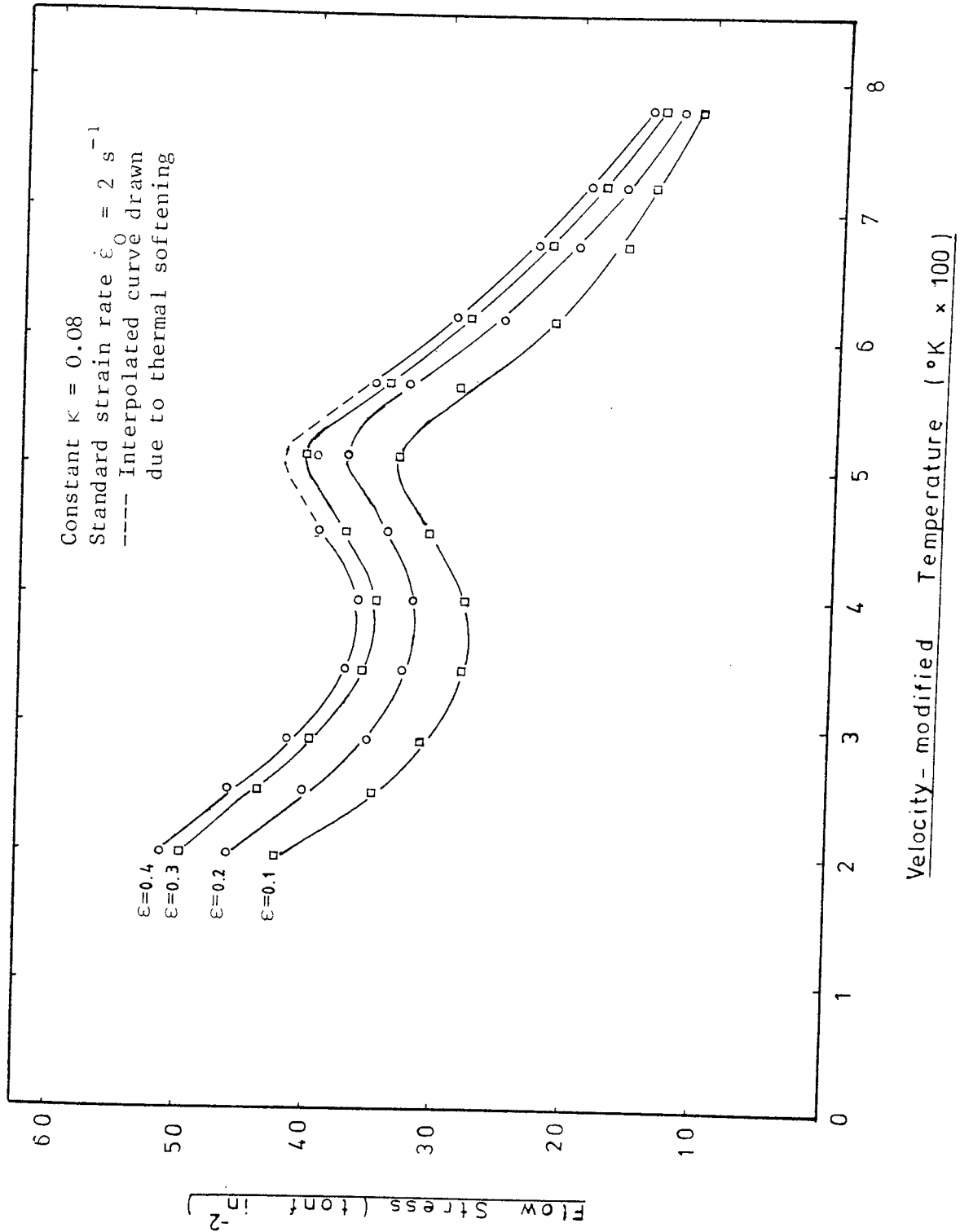


Figure 6.4: Flow stress as a function of the strain(ϵ) and velocity-modified temperature T_m for Oyane's data, 0.16% plain carbon steel

As the strain rate used in Oyane's data was constant, some results of Campbell⁽⁸¹⁾ were replotted against T_m . Campbell's results showed the effects of very wide ranges of strain rate and temperature on the lower yield point of a 0.12% plain carbon steel. Lower yield stress points taken from his results (see figure 6.5) at shear strain rates 1, 10 and 10^2 were replotted against T_m as shown in figure 6.6. The data was fitted reasonably well by a single curve, thus giving support to the use of the velocity-modified temperature concept.

The relationships between B , n and T_m are shown in figure 6.6. A strain-ageing region was evident. The curves were represented mathematically by polynomials. They were used in the theoretical computations for mild steel EN2B and medium carbon steel EN8D.

The assumed B and n for T_m greater than 780°K are shown as dotted lines.

6.2.3 Medium Carbon Steel EN8D

Studies were made on the plane strain compression data of Thomason⁽⁸²⁾ for EN8 medium carbon steel. Thomason's data were collected over a temperature range of 100°C - 600°C in steps of 100°C , and plane strain rate range of 3.12 s^{-1} to 52 s^{-1} . Although the temperatures and strain rates were suitable for use in the theoretical analyses, thermal softening was dominant. Consequently, it was difficult to represent the stress-strain data mathematically. The strain-ageing region was not evident as thermal softening and strain-ageing occurred simultaneously. Eventually, Oyane's data for 0.16%C as discussed in 6.2.2 was used.

Oyane plotted the graphs of stress against temperatures for various

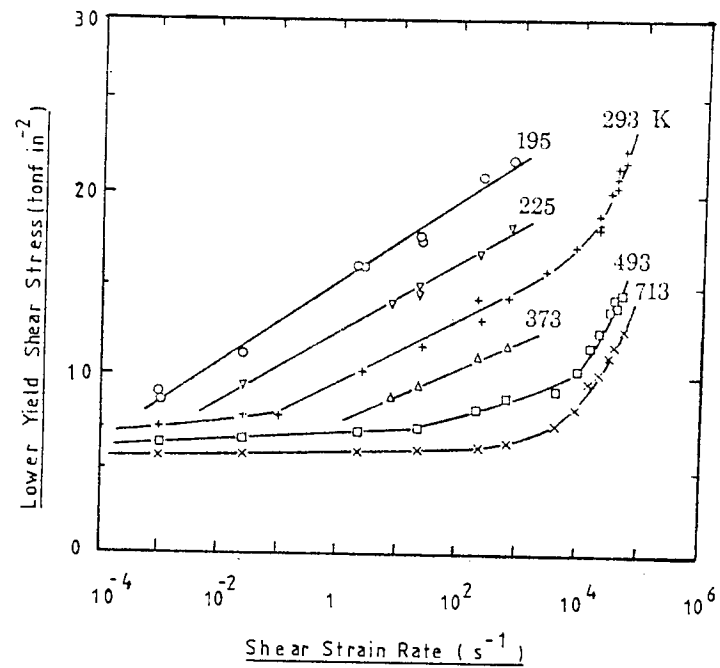


Figure 6.5: Effects of strain rate and temperature on the lower yield stress of 0.12% plain carbon steel. After Campbell (81)

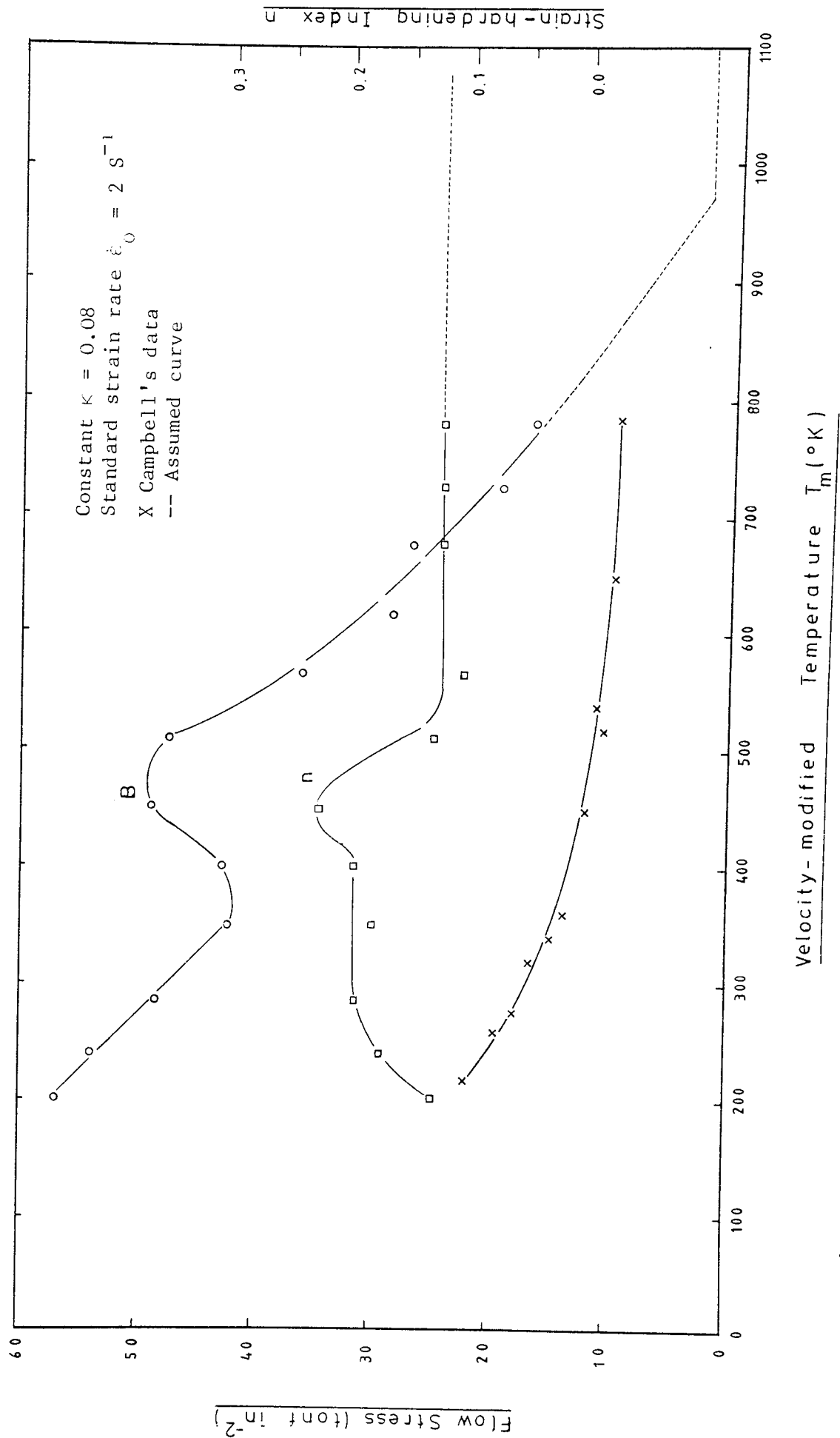


Figure 6.6: Relationship between B , n and T_m for Oyane's data, 0.16% plain carbon steel

carbon steels as shown in figure 6.7. A strain-ageing region and a peak stress at 600°C were clearly evident in all the materials.

Oyane's data for 0.16%C steel was used for the medium carbon steel EN8D (0.39%C) by:

- a) interpolating the stress in terms of the carbon content according to the relationship shown in figure 6.7. The stress was interpolated between 0.35%C and 0.45%C in intervals of 100°C
- b) expressing the interpolated value with that of the 0.16% plain carbon steel as a ratio.

From figure 6.7, the ratio of the flow stresses of the 0.39%C and 0.16%C at various temperatures can be found. Since the data for the various carbon steels was collected over similar strain rate and temperature ranges, the ratio was expressed with respect to T_m . The ratio could be represented by two straight lines as shown in figure 6.8. It is assumed that at all strains the ratio of the stresses can be correlated by the two straight lines for various values of T_m . Thus the stress for EN8D is expressed as:

$$\sigma = B\epsilon^n \times \text{a ratio}$$

The ratio is dependent on T_m . B and n were values of the 0.16% plain carbon steel.

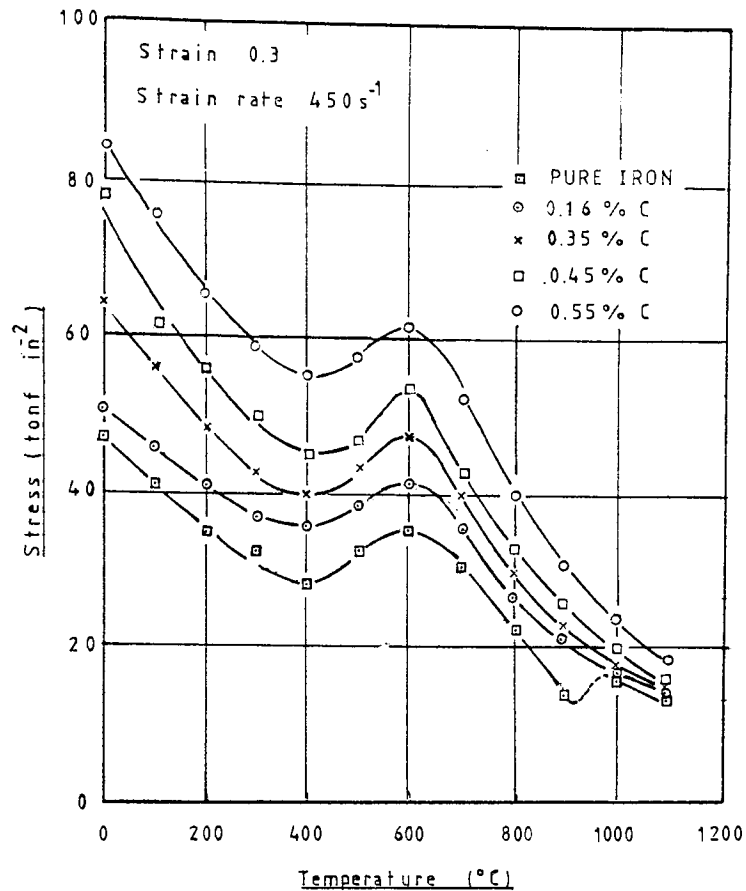


Figure 6.7: Effect of temperature on the stresses for pure iron and various carbon steels. After Oyane (33).

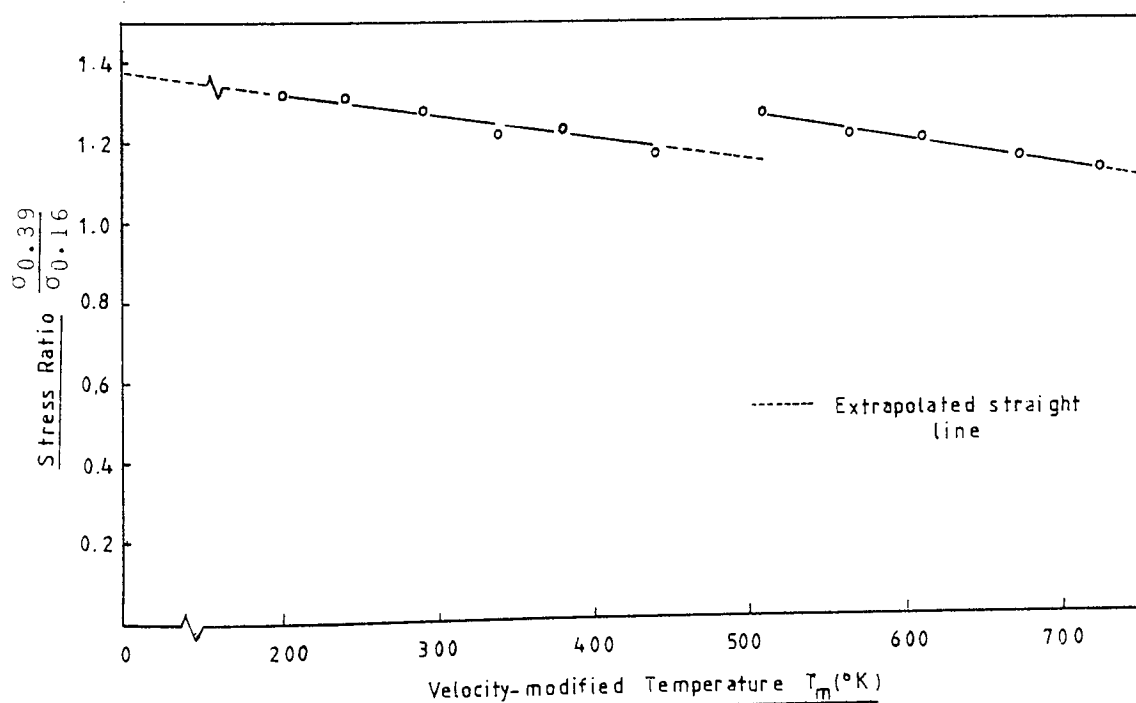


Figure 6.8: Stress ratio of 0.39% C and 0.16% C steels against velocity-modified temperature T_m .

6.2.4 M2 'High Speed' Steel

Attempts were made to use the stress-strain data of Samanta⁽³³⁾ for the theoretical computations. Samanta's data were conducted over a high temperature range of 524°C - 1055°C with strain rates of 450 s⁻¹ and 0.066 s⁻¹.

The graphs of B, n and T_m are shown in figure 6.9. Continuous curves were not obtained for B and n. It is suspected that there are boundary conditions to the velocity-modified temperature concept. In this particular case, the difference in strain rate could be the cause. Some of the values of T_m used in the theoretical analysis for the lower temperatures would be less than 470°K. As Samanta's data and information on the properties of the material at elevated temperatures were limited, the relationships of B, n and T_m could not justifiably be assumed. Thus with regret the theoretical analysis of this material was abandoned.

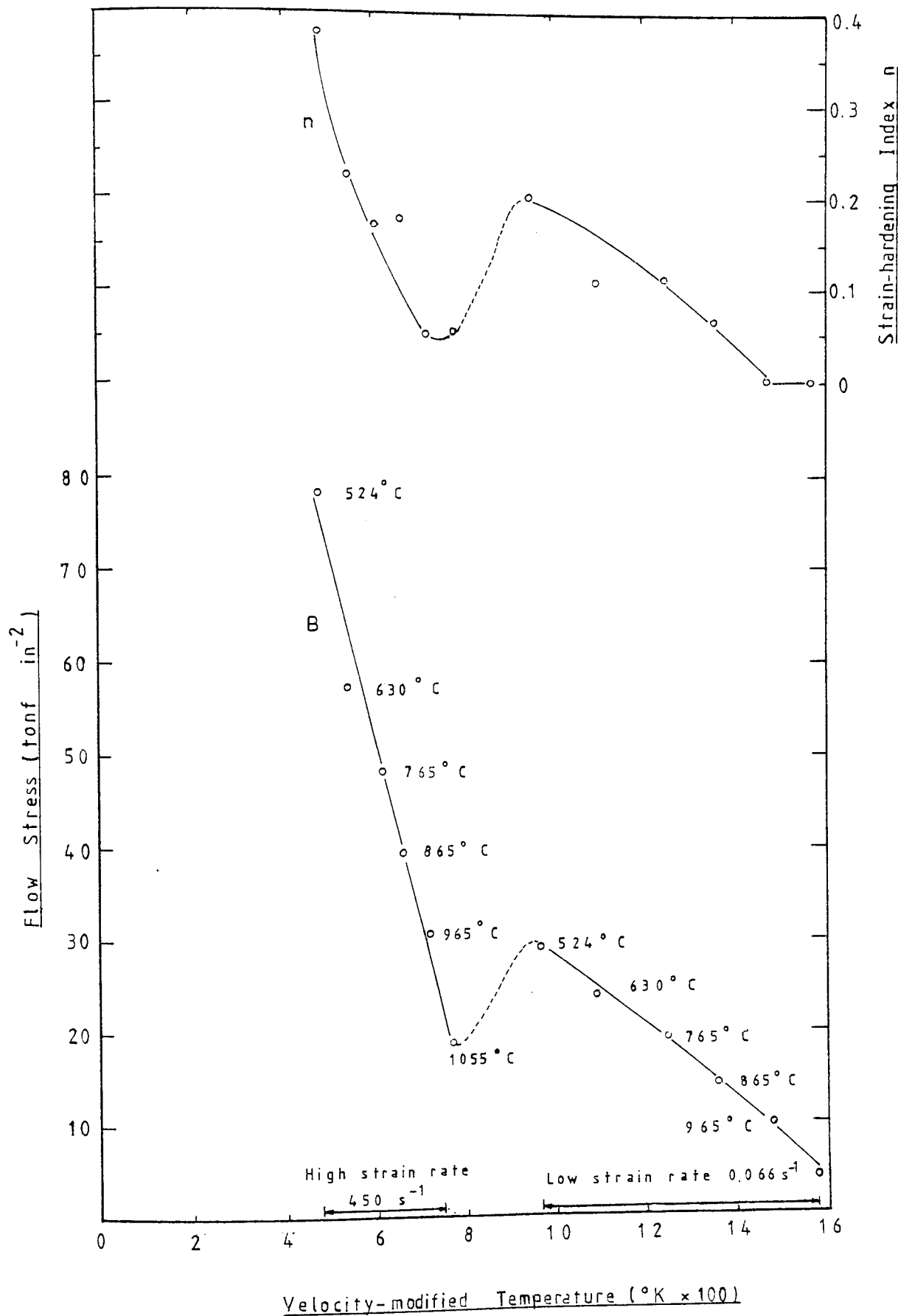


Figure 6.9: Relationships between B, n and velocity-modified temperature T_m for Samanta's data (83)

CHAPTER SEVEN

EXPERIMENTAL PROCEDURE AND TECHNIQUE

VII. EXPERIMENTAL PROCEDURE AND TECHNIQUE

7.1 INTRODUCTION

The first objective of the research was to develop a continuous in-line softening heat treatment draw process and to establish the art of wire drawing at elevated temperatures. A second objective was the theoretical development of an upper bound solution to predict the draw stresses at elevated temperatures.

In order to compare the upper bound solution developed in Chapter 2, with practical data, experimental tests were carried out.

Before the experiments were made, all the measuring equipment and the two air compressors were switched on for about one hour. This allowed the equipment to stabilise and the full capacity of the compressors to be attained. The latter ensured a steady supply of air during the drawing operation.

The loadcell supply voltage and the amplifier 'span' were checked and adjusted if necessary. The various settings on the infra-red thermal monitor were adjusted to the correct requirements.

7.2 PRELIMINARY PREPARATIONS

a) Preparing the wire before drawing

To enable the wire to be threaded through the die, the wire was swaged at room temperature by a rotary swager. Depending on the degree of reduction and the wire material used in the draw process, the wire was swaged down to 3 different diameters: 0.18 in, 0.15 in and 0.12 in.

To ensure that the lubricant would adhere well to the wire, the swaged section was cleaned with Inhibisol. A few turns of the wire were coated with lubricant Dag 2961 using a brush and they were allowed to dry in air.

b) Preparing the lubricant mixture

The lubricant used in the tests was mainly from the same drum. A fixed proportion of 1 volume of soap solution was added to 5 volumes of the lubricant. The mixture was stirred until well-blended. Although efforts were made to keep the viscosity of the lubricant uniform throughout the tests, some small variation was inevitable from one batch to another, nevertheless every effort was made to ensure consistency.

c) Preparing the drawing die

The drawing die to be used in a test was cleaned with Inhibisol and examined for pick-up; it was mounted on to the pins of the die-holder. To prevent the water used for cooling the die from overflowing, silicone grease was applied over the 'O' rings on the die-holder cover. The die

was securely held in the die-holder by 3 screws pulled up tight.

d) Instrumentation

With the die in position, the loadcell supply voltage and the amplifier 'span' were rechecked. The Wheatstone bridge circuit was balanced to zero.

The galvanometer positions of the loadcell, infra-red thermal monitor and the tachometer were recorded. These datum lines were set at convenient markings on the ultra-violet recorder paper.

7.3 THE DRAWING TECHNIQUE

When the lubricant coated on the undrawn wire had dried, the wire was threaded through the roller straightener, lubricator, induction coil and into the drawing die. The free end was pushed through the die and gripped by the jaw of the bull-block. The starting of the drawing operation is crucial especially in those circumstances in which the wire could not be cold drawn. One of the three techniques discussed below was adopted prior to the elevated temperature draw tests:

a) For small areas of reduction or softer material the wire was swaged once to the appropriate diameter

b) For larger areas of reduction or tougher materials the wire was swaged successively two or three times.

In both cases, the unswaged wire was cold drawn through the die for a short run and the drawing was stopped.

c) For wires that cannot be cold drawn, the point was swaged three times. Generally, part of the third stage of swaging, ie. 0.18 in diameter was drawn through the die and part of it passed through the induction coil. This enabled the unswaged wire to be heated right from the start of its length. This method was used together with a higher power setting on the induction heater so that the unswaged wire would be heated quickly to the safe drawing temperature.

It does not seem possible to draw M2 'high speed' steel wire below 300°C with a 40.5% area of reduction. Consequently,

starting of the drawing process was crucial.

Generally, the undrawn wire held between the die and the roller straightener had been straightened by the rollers. This enabled better and more accurate alignment of the wire in the induction coil and lubricator, and the focussing of the optical fibre. The 'spot' was focussed on to the stationary wire at a fixed distance of 1.5 in from the die-holder cover. When part of the wire had been drawn through the die, the water sprays were directed on to the drawn wire at exit and the water supply was turned on. Thus, the casing of the die and the wire were cooled.

Whenever possible, the wire was cold drawn for a short run with the illuminated 'spot' of the optical fibre focussed on to the wire and the lubricator filled with lubricant. This served to check two points: namely that the 'spot' was focussed within the wire during the drawing operation, and that the wire was thoroughly coated with the lubricant. The lubricator was filled to the brink with the lubricant mixture to ensure adequate supply during the drawing process.

Before the start of the drawing test, the galvanometer positions of the thermal monitor and the tachometer were rechecked to ensure that the zero datum lines had not shifted. Since the loadcell was now subjected to a load, an ultra-violet recording was taken.

Having been satisfied that all the equipment had been set to the correct requirements, the induction heater was switched on for warming up. When the heater was ready, compressed air was supplied together with the water for cooling the wire at exit. The set-up was ready for drawing. The bull-block was started, followed immediately by the induction heater coil.

When the desired temperature was reached the wire was allowed to run for several turns of the swift and an ultra-violet recording taken. The moving drawn wire was marked with white paint. The emissivity value, power input and speed were adjusted for the next desired temperature. The recording and marking procedures were repeated.

The drawn wire was allowed to cool, the marked portion cut off, labelled and examined for defects, and the diameter measured.

CHAPTER EIGHT

OBSERVATION AND DISCUSSION OF RESULTS

VIII. OBSERVATION AND DISCUSSION OF RESULTS

8.1 INTRODUCTION

This chapter presents an account of observations and a detailed discussion of results in the study of wire drawing at elevated temperatures. The discussion of the results is dealt with under two main headings, namely the experimental results and the theoretical results.

8.2 OBSERVATIONS

In general, the process of drawing wire at elevated temperatures up to about 700°C was successfully achieved. Mild steel wire and medium carbon steel wire were drawn up to 45% area of reduction. It is anticipated that the materials could be drawn with higher areas of reduction. M2 'high speed' steel wire which could not be cold drawn for a 40.5% area of reduction was drawn at temperatures above 300°C.

Pick-up on the chromium carbide dies was evident during the preliminary trials. This was almost absent when the draw technique was established and suitable lubricants used. A smooth continuous sleeve of graphite was deposited uniformly thereby causing drawing to occur smoothly. No pick-up was noticed with 'Syalon' dies. Generally, the drawn wire has a 'graphoid coat' resulting from traces of graphite being drawn through the die. At the higher temperatures, about 400°C upwards, the drawn wire has a smooth shiny surface as found by other investigators.

The chromium carbide dies were not suitable for elevated tempera-

ture wire drawing as crack lines were formed in the dies, probably due to the thermal stresses set up in the dies. Although crack lines were not seen on the 'Syalon' dies, wear rings and wear developed at the die entry and the conical section. This indicates that the frictional work at the die-wire interface must be of considerable magnitude.

Wire breakages were generally due to: insufficient cooling on the drawn wire or excessive load on the first swaged section when the wire was given three swages.

Generally, the diameters of the drawn wires were undersized, especially at the higher temperatures. This was because the wire expands when heated and contracts when cooled.

8.3 DISCUSSION OF THE EXPERIMENTAL RESULTS

The experimental results for mild steel EN2B and medium carbon steel EN8D are shown in figures 8.1 and 8.2 respectively. It is clear that generally as the temperature increases the draw stress decreases except in the approximate temperature range of 150°C - 400°C . This increase in stress is attributed to strain-ageing; the range depends on the material properties and the area of reduction.

Samanta⁽⁸³⁾ found the strain-ageing region of low carbon steel (0.11% C), for a mean strain rate of 0.066 s^{-1} , to be between 150°C and 300°C . Manjoine⁽¹⁸⁾ conducted slow tension tests on mild steel at a strain rate of 0.5 s^{-1} and found the strain-ageing region to lie between 150°C and 350°C .

In the experimental tests, the speed of drawing was 20 ft min^{-1} . The mean strain rate calculated using the formula proposed by Atkins⁽⁸⁴⁾ was in the region of 10 s^{-1} . As the tests conducted by Samanta and Manjoine were also performed at moderately low strain rates, the strain-ageing range found experimentally for mild steel is in reasonable agreement with their range. The shape of the curves shown in figure 8.1 is similar to that obtained by Manjoine.

Thomason⁽⁸⁵⁾ found that medium carbon steel of 0.41% C showed low ductility in the temperature range of 200°C - 300°C , for a mean strain rate of approximately 2.7 s^{-1} . This was supported by Glen⁽⁸⁶⁾ who performed tension tests on medium carbon steel. Thus, the strain-ageing region found experimentally for the medium carbon steel is in reasonable agreement with the results of others.

The deformation mechanism involved in the drawing of wire at elevated temperatures is indeed complicated as strain-ageing, strain-

hardening, recovery and recrystallisation may have significant effects. Generally for mild steel and medium carbon steel, at temperatures above 400°C , the stress variations between each area of reduction decreases, indicating that recovery and perhaps recrystallisation predominate. The draw stress drops as the temperature increases.

In summary, the three types of response to elevated temperature drawing of mild steel and medium carbon steel are:

- i) a gradual softening after a normal degree of work hardening at ambient temperatures
- ii) a strain-ageing region at about $200^{\circ}\text{C} - 400^{\circ}\text{C}$
- iii) a rapid rate of softening after the peak strain-ageing stress has been passed.

The experimental results for M2 'high speed' steel are shown in figure 8.3. A low ductility range was observed between the temperature range of $100^{\circ}\text{C} - 400^{\circ}\text{C}$. As there is insufficient information on the properties of M2 'high speed' steel at elevated temperatures, it is suspected that the low ductility was due to strain-ageing. In this case, the strain-ageing was not pronounced enough to show the effects clearly.

8.3.1 Effects of the Developed Lubricants

The use of an appropriately formulated lubricant reduces the draw stress further as shown in figure 8.4. It is clear that 'Dag 2543' is a 'better' lubricant at the higher temperatures; its composition, which consists mainly of graphite, has been formulated for use at

high temperatures. On the other hand, 'Dag 2961' consists of a mixture of graphite and molybdenum disulphide which renders it most suitable for a wider range of temperatures.

8.4 DISCUSSION OF THE THEORETICAL RESULTS

An upper bound solution for the drawing of wire at elevated temperatures was derived in Chapter Two. The initial plan was to use the mean flow stress Y_f at the die-wire interface to calculate the frictional power as defined in equation (50). Figure 8.5 shows the results for a 45% area reduction. As the constant friction factor increases, the difference in draw stress for a particular temperature decreases. The correlation between the experimental and theoretical results was poor; the constant friction factor is much greater than one. The cause of such an anomaly can be explained as follows. As the constant friction factor increases the temperature at the die-wire interface increases tremendously, especially when heat conduction is neglected. It is felt that the velocity-modified temperature concept proposed in section 2.2.6.1 does not relate well at higher values of T_m thus giving lower flow stresses. As a result, the mean flow stress Y_f decreases which gives a lower frictional power. Eventually, Y_f was replaced by the mean flow stress in the deformation zone Y_d (see section 2.2.9), for all the theoretical computations.

The effect of variation of the constant friction factor on the optimum die semi-angle

The upper bound solution for two different draw speeds is shown in figures 8.6 to 8.11. The upper bound solution shows a tendency for the value of the optimum die semi-angle to increase, as the value of the constant friction factor increases for a given draw condition. This may be explained as follows: the friction force component of the draw

force increases with the increasing value of the constant friction factor, causing a higher draw stress. This higher draw stress produced by the increase in friction, may be minimised by reducing the contact length of the die, ie. by increasing the die semi-angle.

From figures 8.7 and 8.11 it is seen that the curves are rather irregular. Figure 8.7 seems to deviate from the other results in that the optimum die semi-angle remains almost constant as the constant friction factor increases from 0.15 to 0.3. The reasons for this irregularity will be explained later.

The effect of variation of temperature and strain rate on the optimum die semi-angle

Figures 8.6 to 8.11 indicate that the optimum die semi-angle is dependent on the draw speed and temperature.

Figures 8.7 and 8.11 indicate that at the peak of the strain-ageing region, the curves of draw stress against the optimum die semi-angle are rather irregular. This can be explained as follows. The peak stress for a draw speed of 300 ft min^{-1} is at about 500°C , and the flow stress distribution in the deformation zone for the various die semi-angles varies over this peak region. As a result, the mean flow stress for the different die semi-angles varies in stages. This affects the draw stress. For clarity, take for example the case of $m = 0.1$ for figure 8.11. The mean flow stress increases as the die semi-angle increases up to about 12° . The frictional and redundant work balance each other and a minimum draw stress is seen. As the die semi-angle increases to 14° , the mean flow stress drops suddenly causing a decrease in draw stress. For angles above 14° , the mean flow stress

does not vary much and the draw stress increases as the die semi-angle increases.

As the draw speed was reduced to 20 ft min^{-1} , the same effects were observed, except that the curves were irregular at 300°C instead of 500°C . This is because for a speed of 20 ft min^{-1} and an area of reduction of 35%, the peak stress is at about 300°C .

Such irregularities in the curves can be expected also near the 'valley' of the strain-ageing region.

The effect of variation of area of reduction on the optimum die semi-angle

Another tendency revealed by the upper bound solution is for the optimum die semi-angle to increase with an increase in area of reduction.

This may be explained as follows: for a fixed inlet wire diameter and die semi-angle, the contact length at the die-wire interface increases as the area of reduction increases. Thus the frictional work increases. Hence, in order to reduce the frictional work the contact length at the die-wire interface needs to be reduced. This could be achieved by an increase in the die semi-angle.

Figures 8.12 to 8.17 show the results for two different draw speeds of 20 ft min^{-1} and 100 ft min^{-1} .

The effect of strain rate on the draw stress

As seen in figures 8.18 to 8.21, the strain-ageing region shifts to higher temperatures as the draw speed increases, that is as the strain

rate increases. Since strain-ageing is a time dependent phenomenon, the 'hump' can be shifted to a higher temperature with increasing strain rate. This shift was also found by Manjoine⁽¹⁸⁾, Oyane⁽³³⁾ and Samanta⁽⁸³⁾.

Figures 8.18 and 8.19 show that as the area of reduction increases, the strain-ageing region is narrowed. This is also seen for medium carbon steel in figures 8.20 and 8.21. Similar observations were also noticed by Manjoine.

The mean strain rates calculated using the formula proposed by Atkins⁽⁸⁴⁾ for the various draw speeds are indicated in the figures.

For mild steel, the strain-ageing regions shown in figures 8.18 and 8.19 for a draw speed of 5 ft min^{-1} (approximately 2 s^{-1}) are reasonably close to that found by Oyane, Manjoine and Samanta for slow strain rates. Osakada⁽⁸⁷⁾ conducted tests on 0.03% C steel at a strain rate of 0.003 s^{-1} and 380 s^{-1} . For a strain of 0.16, he found that the strain-ageing regions were about $100^{\circ}\text{C} - 240^{\circ}\text{C}$ and $400^{\circ}\text{C} - 600^{\circ}\text{C}$ respectively. The strain-ageing regions for a draw speed of 300 ft min^{-1} are also close to those found by Manjoine for a strain rate of 300 s^{-1} .

The strain-ageing region for medium carbon steel for a draw speed of 5 ft min^{-1} , as shown in figures 8.20 and 8.21, is also in reasonable agreement with that of Thomason⁽⁸⁵⁾ and Glen⁽⁸⁶⁾. Thomason performed the heading operation at a strain rate of about 2.7 s^{-1} . The strain-ageing region extends from about 200°C to 300°C .

The effects of temperature, constant friction factor and area of reduction on the theoretical draw stress

The theoretical results for mild steel and medium carbon steel are shown in figures 8.22 to 8.32. The experimental results are superimposed onto the theoretical results. This is done in order to show clearly the three different regions mentioned earlier, that is gradual softening, strain-ageing and rapid softening.

It is evident from the figures that the response of the two materials to temperature is similar to that found experimentally, although the strain-ageing regions do not coincide.

As the constant friction factor is increased, the draw stress increases also. Apparently the constant friction factor does not affect the strain-ageing region.

Generally, the experimental results of mild steel fall below the theoretical results at temperatures below 350°C and the strain-ageing regions do not coincide. The first discrepancy could be due mainly to the use of a 0.15% C stress-strain data in the theoretical computations. The wire material used in the experiments was a 0.04% C. Osakada⁽⁸⁷⁾ indicated that an increase in carbon content will increase the flow stress. Consequently, the theoretical results are higher than the experimental results. Another possible reason could be the form of the assumed relationships between, B , n and T_m as shown in figure 6.6. It is suspected that the actual values of the flow stress are lower than those shown in figure 6.6 for the T_m range of 275°K - 400°K. For a draw speed of 20 ft min⁻¹ and draw temperatures of about 300°C and below, the T_m values are generally below 400°K. Thus the values of the draw stress were over-estimated for temperatures of 300°C and

below. The second discrepancy could be attributed to one or several of the following factors:

- a) the use of stress-strain data of a different material. Glen⁽⁸⁶⁾ showed that the addition of alloy elements affects the strain-ageing region
- b) the velocity-modified temperature concept discussed in Chapter Two introduced error especially at higher values of T_m
- c) heat conduction and cooling of the wire were neglected in the theoretical studies, thus the theoretical strain-age region is displayed over a lower range of temperatures than occurs in practice.

Figures 8.22 to 8.27 show that as the temperature increases from 400°C upwards, the constant friction factor also increases. If the stress-strain data for the actual condition of the material was used, the constant friction factor would be higher than that shown in figures 8.22 to 8.27. This is because the flow stress would then be lower.

The theoretical and experimental results for medium carbon steel shown in figures 8.28 to 8.32 are replotted, as shown in figures 8.33 to 8.40. As the area of reduction increases, the draw stress increases for a given draw temperature, draw speed, die semi-angle and constant friction factor.

At a temperature of 100°C, (see figure 8.34) a good fit between the experimental and theoretical results was found for $m = 0.03$. In the strain-ageing region of 200°C - 300°C, the experimental results fall below the theoretical results (see figures 8.35 and 8.36), for areas of reduction up to 40%. This is because the predicted strain-ageing regions do not coincide with the experimental strain-ageing

regions. The cause could be attributed to the factors mentioned for mild steel.

As the temperature increases to 400°C and 500°C , the constant friction factor also increases. The increase is more significant for an area of reduction of 45%. This is probably due to a greater increase in temperature at the die-wire interface causing the lubricant to be less effective.

The constant friction factor continues to increase as the temperature increases. It is thought that at temperatures of 600°C and above the velocity-modified temperature concept does not hold well, predicting lower flow stress. Although the flow stress of the medium carbon steel was derived from that of a 0.16% steel, as discussed in section 6.2.3, the error introduced would be small by comparison with that incurred in using the velocity-modified temperature concept.

Figure 8.41 shows the true stress-strain curves for medium carbon steel based on the assumptions made in section 6.2.3 and used in the theoretical computations. The results of Dean⁽⁸⁸⁾ for medium carbon steel EN8 at temperatures of 600°C were also shown on the same figure. It is clear that the flow stresses calculated were much lower than those of Dean. This explains the high values of constant friction factor at the temperatures of 600°C and 700°C (see figures 8.39 and 8.40).

The presence of wear on the dies and the shiny surface finish of the drawn wire for temperatures above 400°C suggested that the frictional resistance is rather high. The upper working temperature of Dag 2961 is about 700°C . Thus it can be concluded that the friction at the die-wire interface increases at draw temperatures above 400°C . The value of the constant friction factor was increased

further due to the error introduced by the velocity-modified temperature concept.

The theoretical and experimental results for mild steel EN2B could not be confidently compared because of the the lack of appropriate experimental stress-strain data for the material. Nevertheless, the shape of the theoretical curves was similar to that of the experimental curves. This gives some support to the theoretical analysis developed in Chapter Two. Further, figures 8.22 to 8.27 show that the constant friction factor increases as the temperature increases from 400°C upwards. This was to be expected as the frictional resistance tends to increase with temperature.

The theoretical results obtained from the upper bound solutions for the medium carbon steel generally agreed satisfactorily with the experimental results (see figures 8.33 to 8.40). The experimental results can be relied on because they were obtained with reliable instruments which were accurately recalibrated using established procedures. Hence, it can be concluded that the upper bound solution derived can be used to predict the draw stress with reasonable accuracy, if the constant friction factor is known.

The upper bound solutions developed were dependent on several assumptions. The main ones were:

- a) the relationships between B , n and T_m

As explained earlier, it was not intended to correlate the relationships over a wide range of strain rates. However, as suitable stress-strain data is non-existent, the high speed compression data of Oyane⁽³³⁾ was used. The strain rate used in this test was 450 s^{-1} .

The velocity-modified temperature concept does have limits.

Since the mean strain rates that prevail in the drawing process is about 10 s^{-1} , the error introduced in using Oyane's data could be significant.

- b) the relationship between the stress-strain data of the 0.16% C steel and that of the medium carbon steel (see section 6.2.3)
- c) the shape of the shear surface. The assumed surface was chosen to facilitate theoretical analysis. In reality, the shear surface is more complex as seen in visoplasticity test patterns.

Retrospectively, as the theoretical and experimental results for medium carbon steel were in adequately close agreement it is concluded that: the main assumptions made were not significant enough to impair the validity of the theoretical solutions, except perhaps for draw temperatures 600°C and above, where the velocity-modified temperature concept does not relate very well.

8.5 CONTOUR PLOTTINGS

The contour plottings of strain, strain rate, temperature and flow stress in the deformation zone are shown in figures 8.42 - 8.53. The x-axis is the axis of the drawing die. The numerical values on the x-axis represent the distance (in) from the virtual apex of the die. The value on the y-axis represents the radius (in) of the wire in the deformation zone. The inlet shear surface is represented by a contour of zero value.

The contours are compared under identical conditions with one only variable. The variables studied are: exponential constant c , constant friction factor m , material properties, area of reduction, draw speed and die semi-angle. In all the contour plottings, the following parameters are assumed unless otherwise specified:

Mild steel wire of 0.236 in diameter

9° die semi-angle

Draw speed of 20 ft min⁻¹

Draw temperature of 100°C

Exponential constant c is 0.2

Constant friction factor m is 0.1

Effects of the exponential constant

The strain, strain rate, temperature and flow stress distributions in the deformation zone are shown in figure 8.42 - 8.45 for different values of c . The shape of the exit shear surface is represented by the largest contour shown in figure 8.42.

The sign of the exponential constant c affects the shape of the shear surface as shown in figure 8.42. For negative values of c : the radius from the inlet shear surface to the virtual apex increases as its inclination with the die-axis decreases, the equivalent strain increases as c decreases. When c is positive, the reverse is true. The shapes of the various strain and strain rate contours are similar to the shear surfaces because of volume constancy.

The temperature distribution is shown in figure 8.44. Temperature is greatest at the die-wire interface due to localised heating. The temperature developed in the deformation zone is highest for $c = -1$. This is because the deformation and frictional power increases as the strain increases.

Among the three temperature distributions shown in figure 8.44, that of $c = 0.2$ is the most likely temperature distribution to be found in the deformation zone. This is because the temperature increases from the die-axis to the die-wire interface. When c is negative, the reverse happens and this is most unlikely for steel.

Figure 8.46 shows the temperature distribution calculated by Altan⁽⁴¹⁾. Heat conduction was taken into account, according to the method proposed by Bishop⁽³⁷⁾. The shape of the contours of figure 8.44(i) and figure 8.46 are quite similar. In Altan's work the temperature increases from the centre to the die-wire interface.

The theoretical computations of the draw stress for the four values of c shown in figure 8.42, indicated that the draw stress for $c = 0.2$ is the lowest. This supports the argument that the isothermals of $c = 0.2$ is the most likely to be found in the deformation zone.

(The temperature and flow stress distributions for $c = 1.0$ are not plotted because the contours were very irregular; the computer program

does not smooth the curves. The temperature and flow stress values are greater than that for $c = 0.2$.)

Figure 8.45 shows the flow stress distributions for different values of c . The flow stress distributions is greatest for $c = -1.0$. This is because the strain values for $c = -1.0$ are greater than those for the other two values of c (see figure 8.42). Another possible factor is due to the higher strain rate values for $c = -1.0$. For a draw temperature of 100°C , an increase in strain rate will give a lower value of T_m . This probably gives higher values of B and n . Consequently the flow stress will increase.

Effects of the material properties

The mechanical properties of the wire affect the magnitude of the heat generated due to deformation and frictional work. The temperature distributions of mild steel and medium carbon steel are shown in figure 8.47. The strain and strain rate distributions are the same for the same draw conditions. The temperature developed in the deformation zone for medium carbon steel is higher than mild steel. This is because the former is a stronger material and thus has a higher flow stress. Consequently, the deformation and frictional work are greater than mild steel, giving a higher temperature rise at exit.

Effects of the constant friction factor m

The important factor determining the heat generation at the die-wire interface is the constant friction factor. Figure 8.48 shows the temperature distributions for various values of m . The frictional

effect is represented by a localised temperature rise at the die-wire interface, especially when heat conduction is neglected in the theoretical analysis. As m increases the temperature at the interface increases too.

The emerging wire is hotter at the surface than at the centre and the highest temperature occurs at the die exit.

Effects of the speed of drawing

As the speed of drawing increases, the equivalent strain rate increases as shown in figure 8.49. The equivalent strain is not affected by a change in speed. The temperature rise increases with increasing draw speed (see figure 8.50). This is because the deformation and frictional work increase with increasing draw speed.

Figure 8.51 shows the flow stress distributions for the two draw speeds. In this particular study, the flow stress distribution increases as the speed increases. This cannot be generalised as both the temperature and strain rate must be considered together.

Effects of the area of reduction

The effect of the area of reduction on the temperature distribution is shown in figure 8.52. In the case of the larger area of reduction, the exit temperatures are higher due to greater deformation work, and higher frictional work as the contact length at the die-wire interface is increased.

Effects of the die semi-angle

As the die semi-angle decreases, the strain and strain rate also decrease in magnitude. Figure 8.53 shows the temperature distributions for two different die semi-angles. Although the temperatures at exit (excluding the die-wire interface) do not seem to differ as shown in the figure, the exit temperatures for the 9° die semi-angle are only slightly higher than those for the 6° die semi-angle.

The temperature rise at the die-wire interface is greater for the smaller die semi-angle. This is because the contact length between the die-wire interface increases as the die semi-angle decreases. The exit temperature for the 6° die semi-angle is 482°C , this is about 90°C higher than that of the 9° semi-angle. This great difference in temperature is because of the assumed constant friction factor of 0.1.

Section 8.6: Graphical results and contour
 plots.

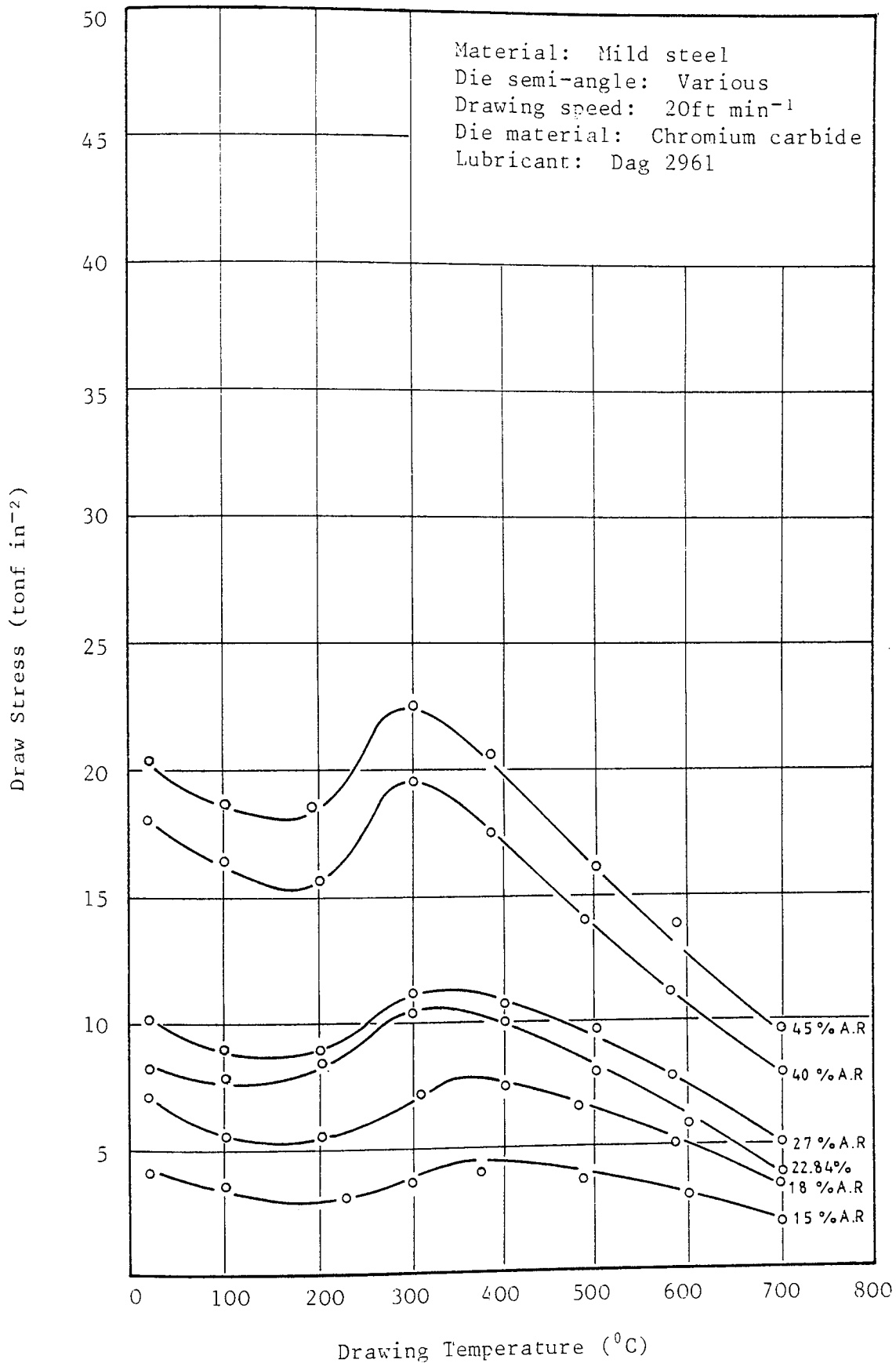


Figure 8.1: Experimental draw stress of mild steel at various areas of reduction (AR) and temperatures

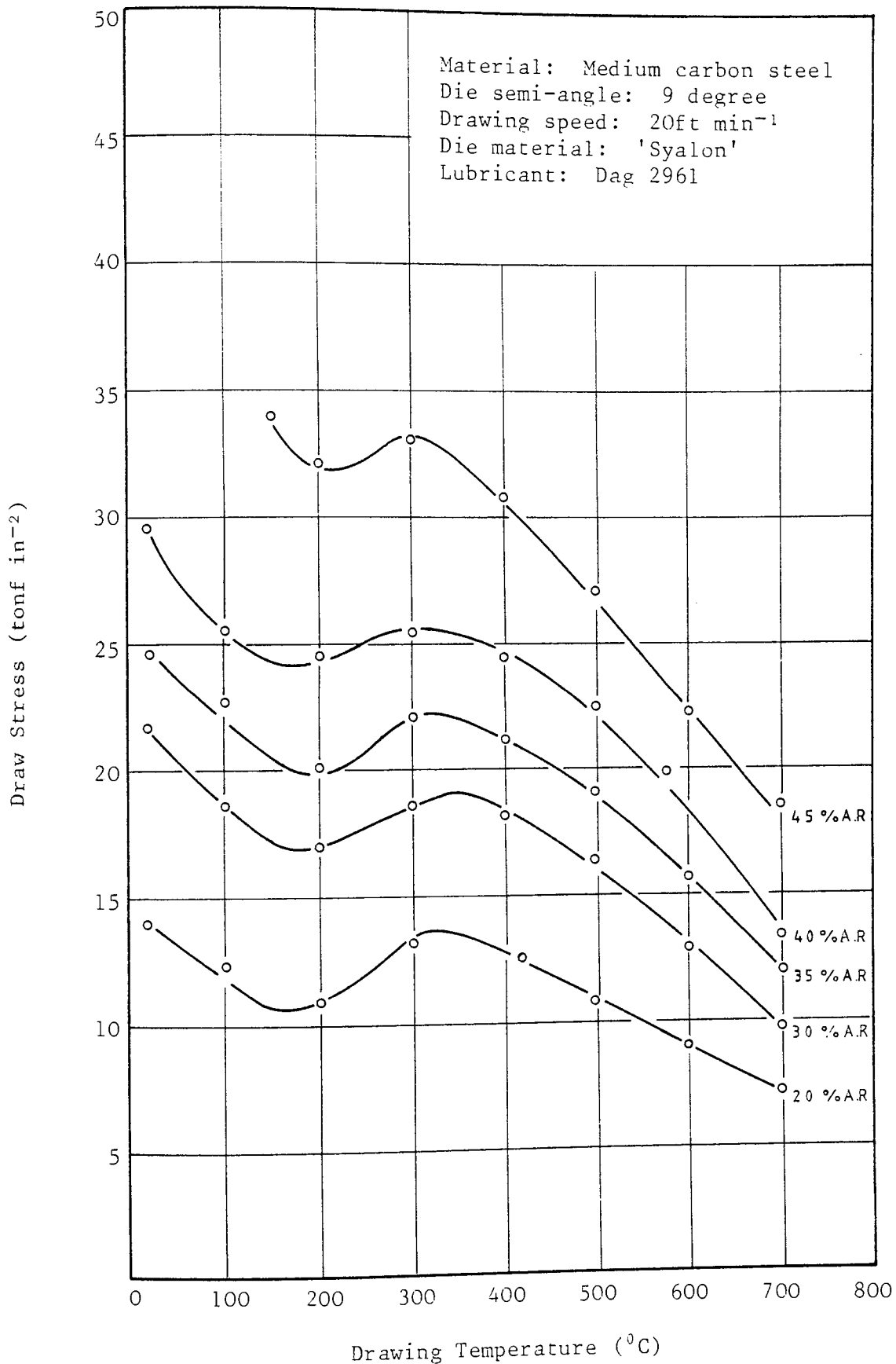


Figure 8.2: Experimental draw stress of medium carbon steel at various areas of reduction (AR) and temperatures

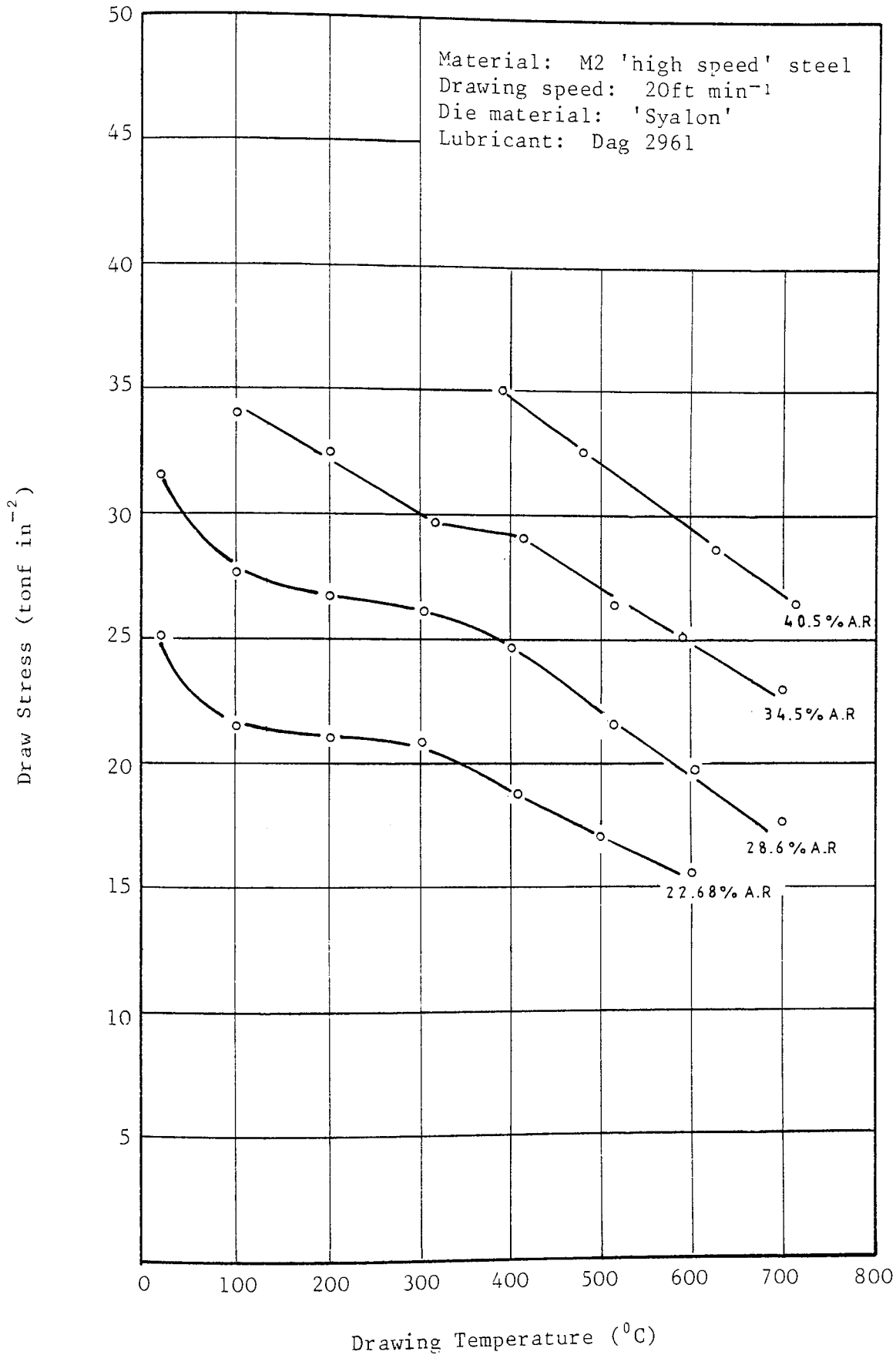


Figure 8.3: Experimental draw stress of M2 'high speed' steel at various areas of reduction (AR) and temperatures

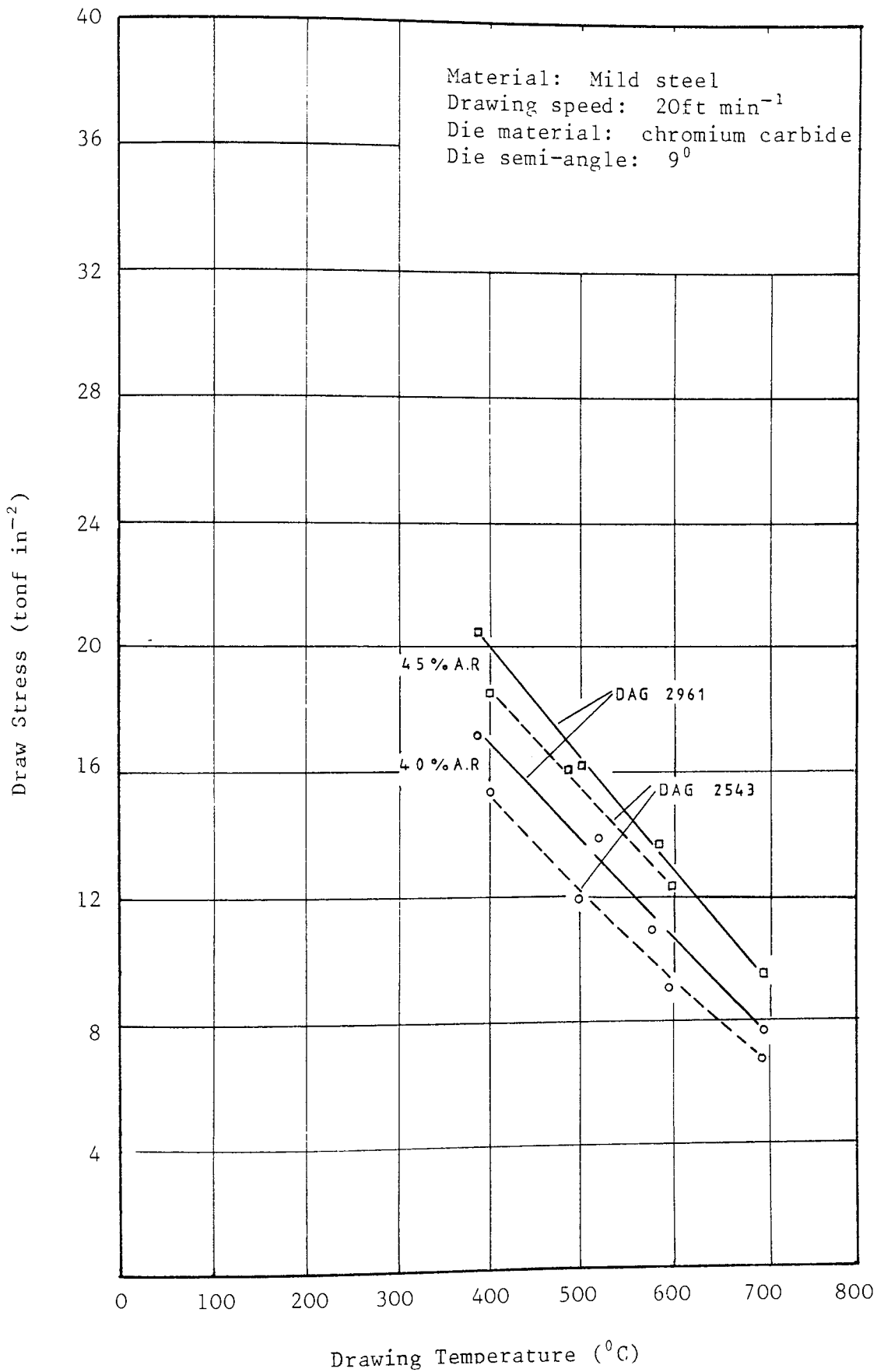


Figure 8.4: Comparison of experimental draw stress for lubricants 'Dag 2961' and 'Dag 2543' for various areas of reduction (AR) and temperatures

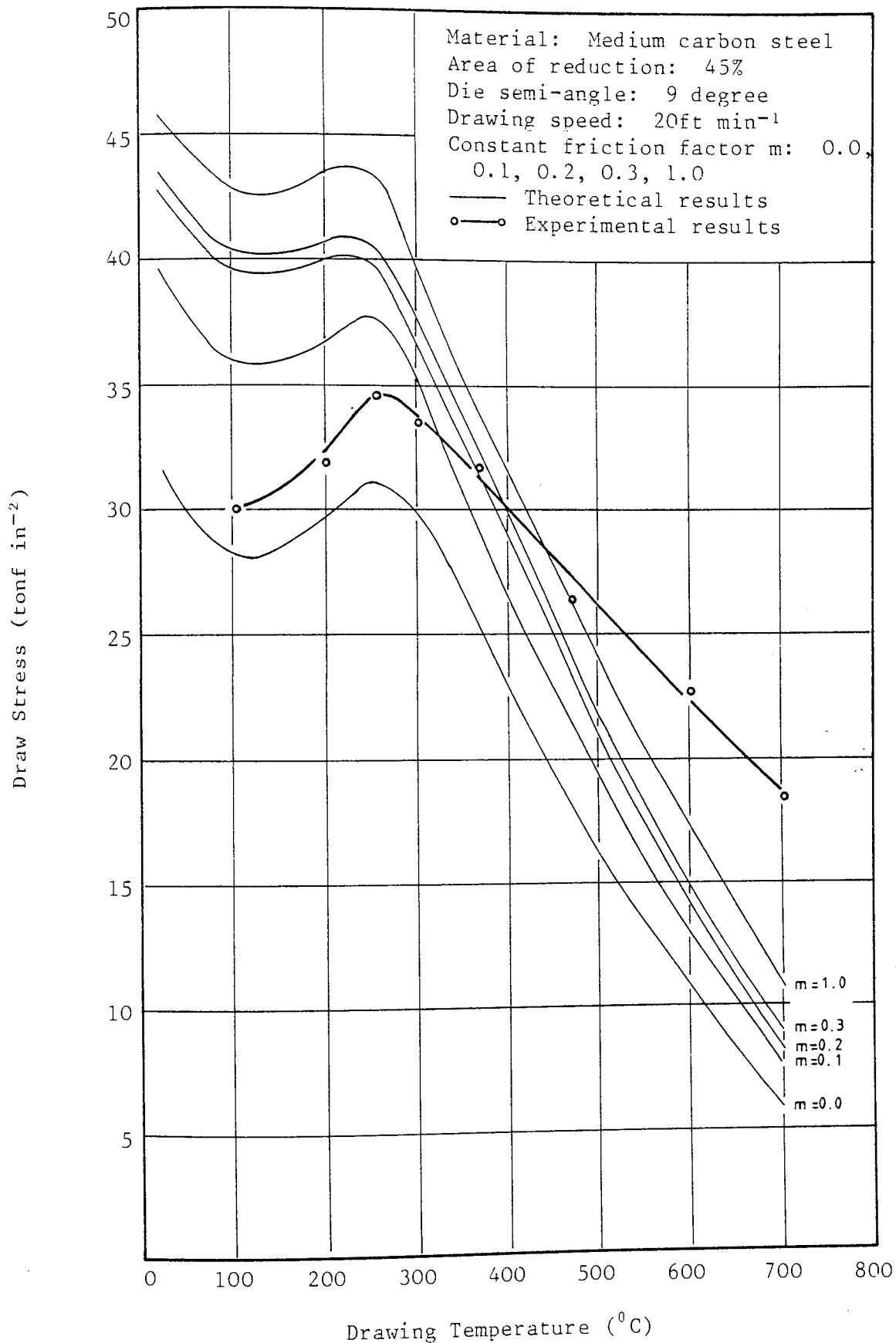


Figure 8.5: Comparison of the experimental and the theoretical results using the mean flow stress at die-wire interface to calculate the frictional power

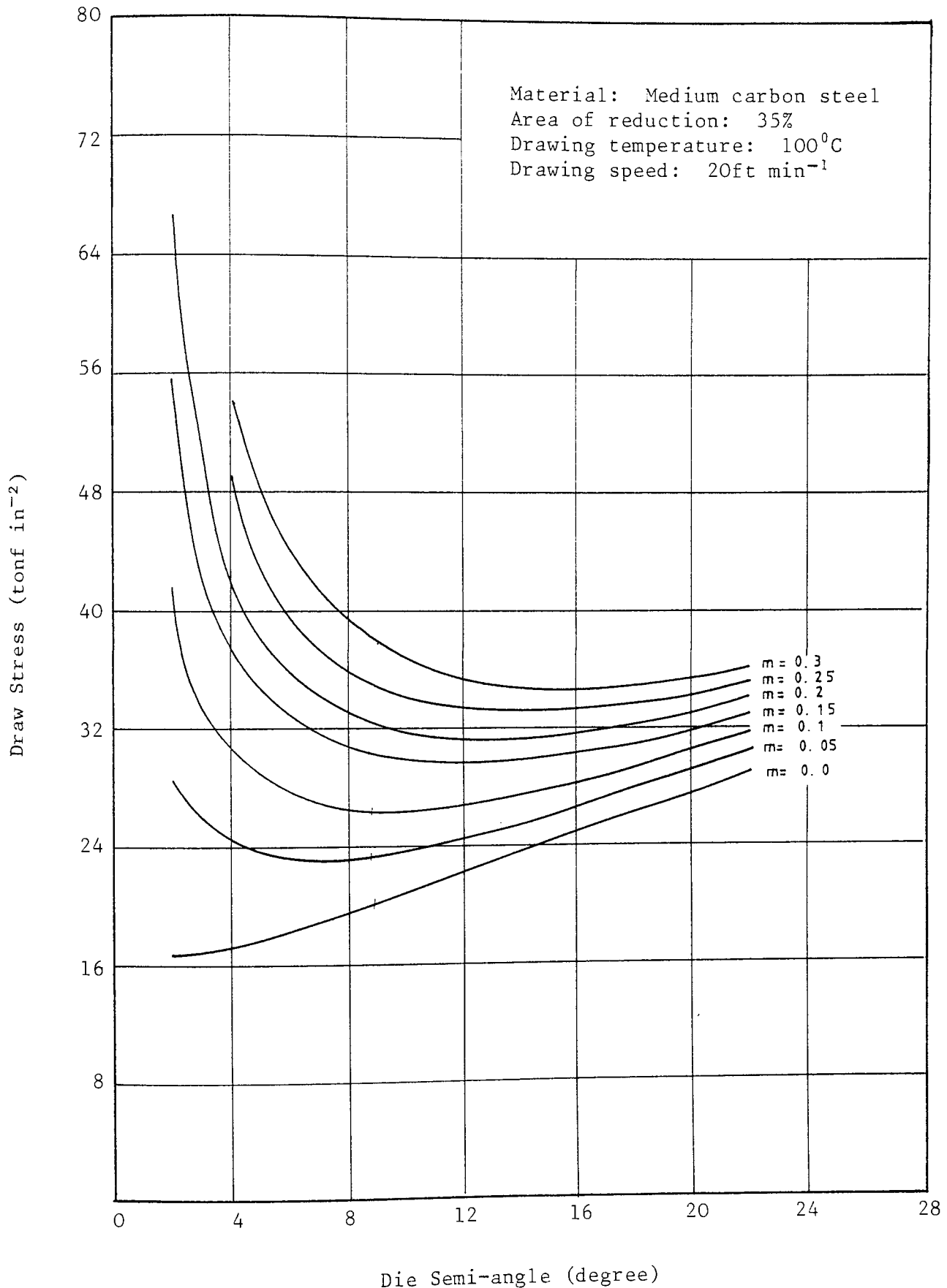


Figure 8.6: Variation of the draw stress against the die semi-angle for various values of constant friction factor m

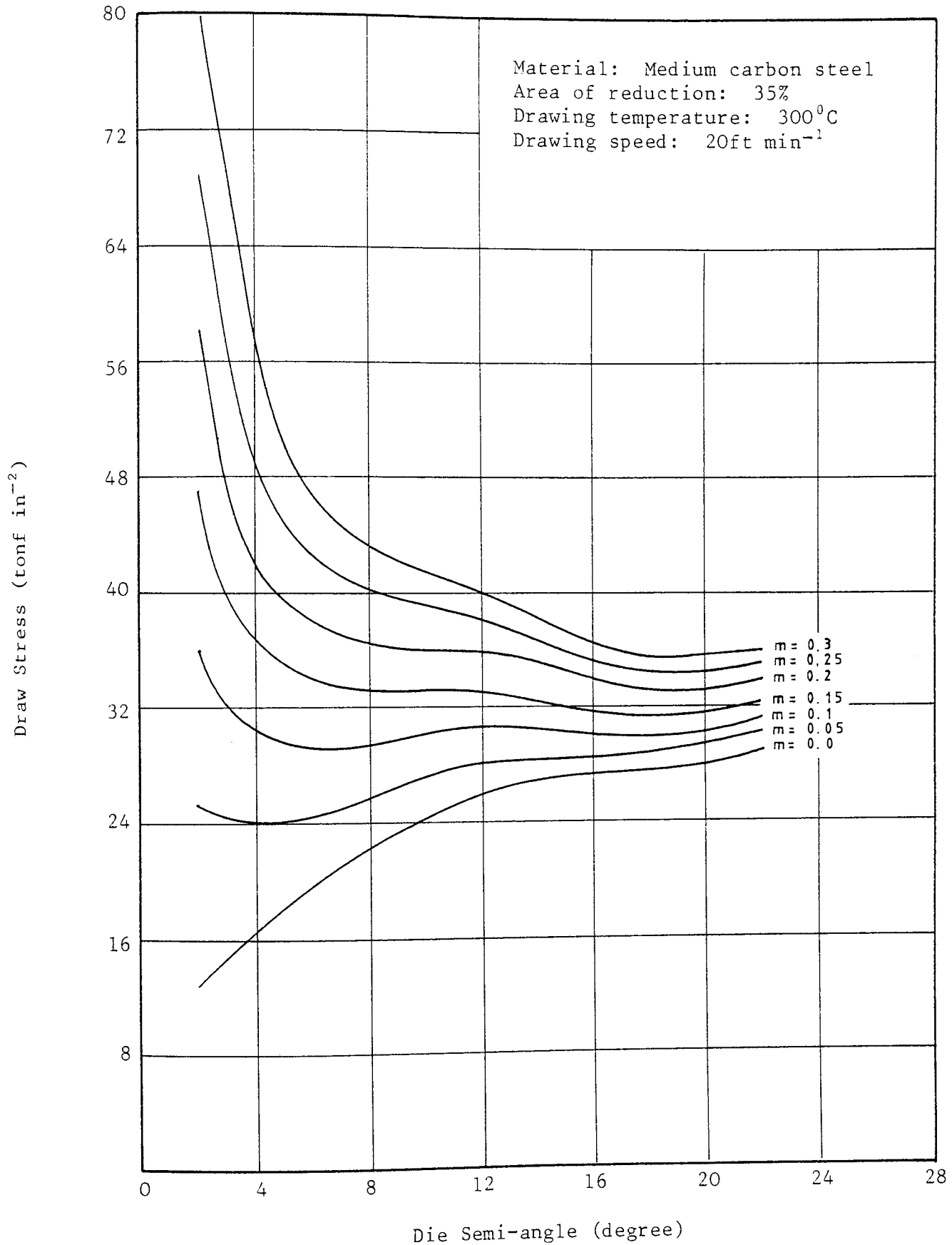


Figure 8.7: Variation of the draw stress against the die semi-angle for various values of constant friction factor m

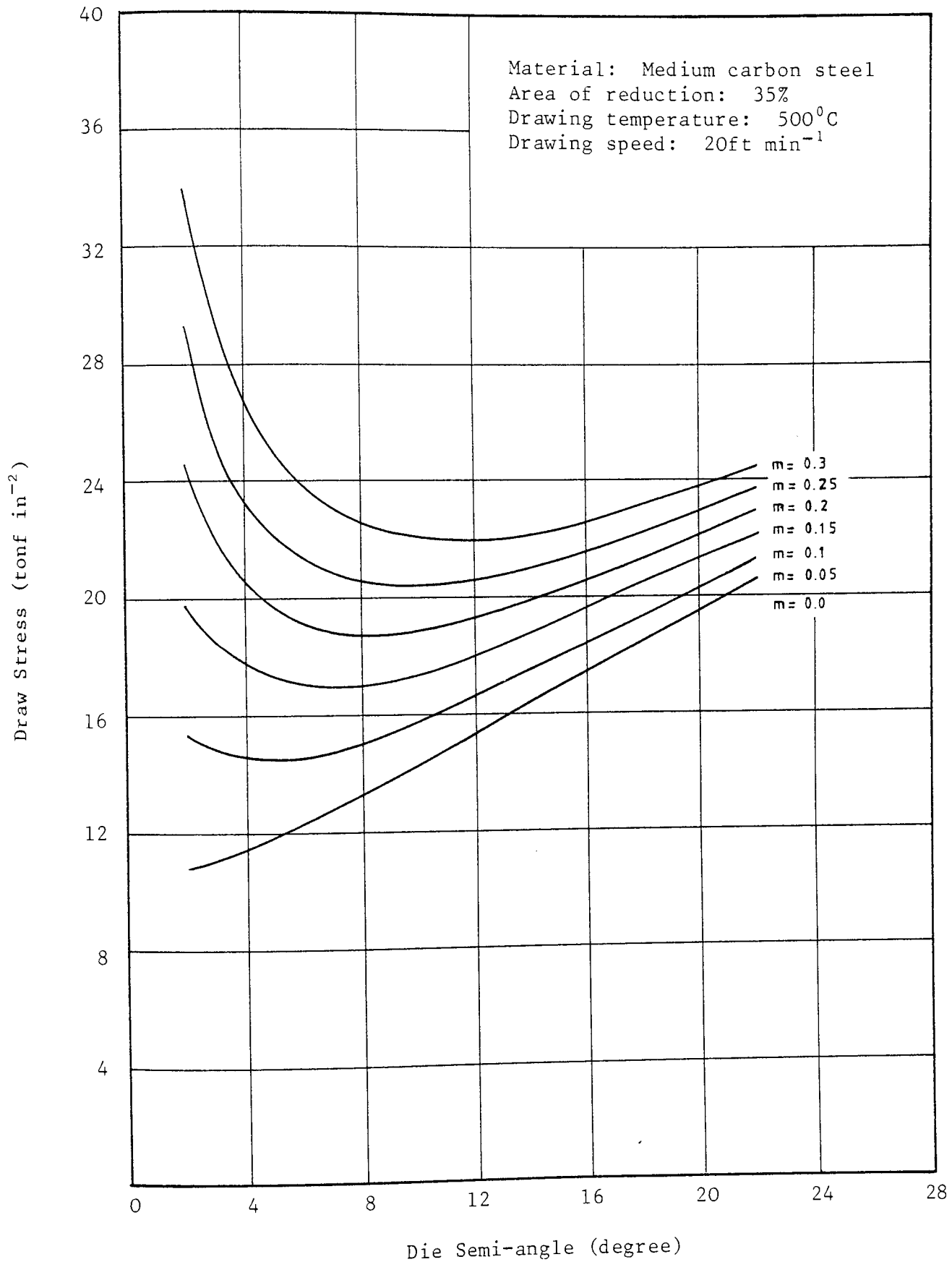


Figure 8.8: Variation of the draw stress against the die semi-angle for various values of constant friction factor m

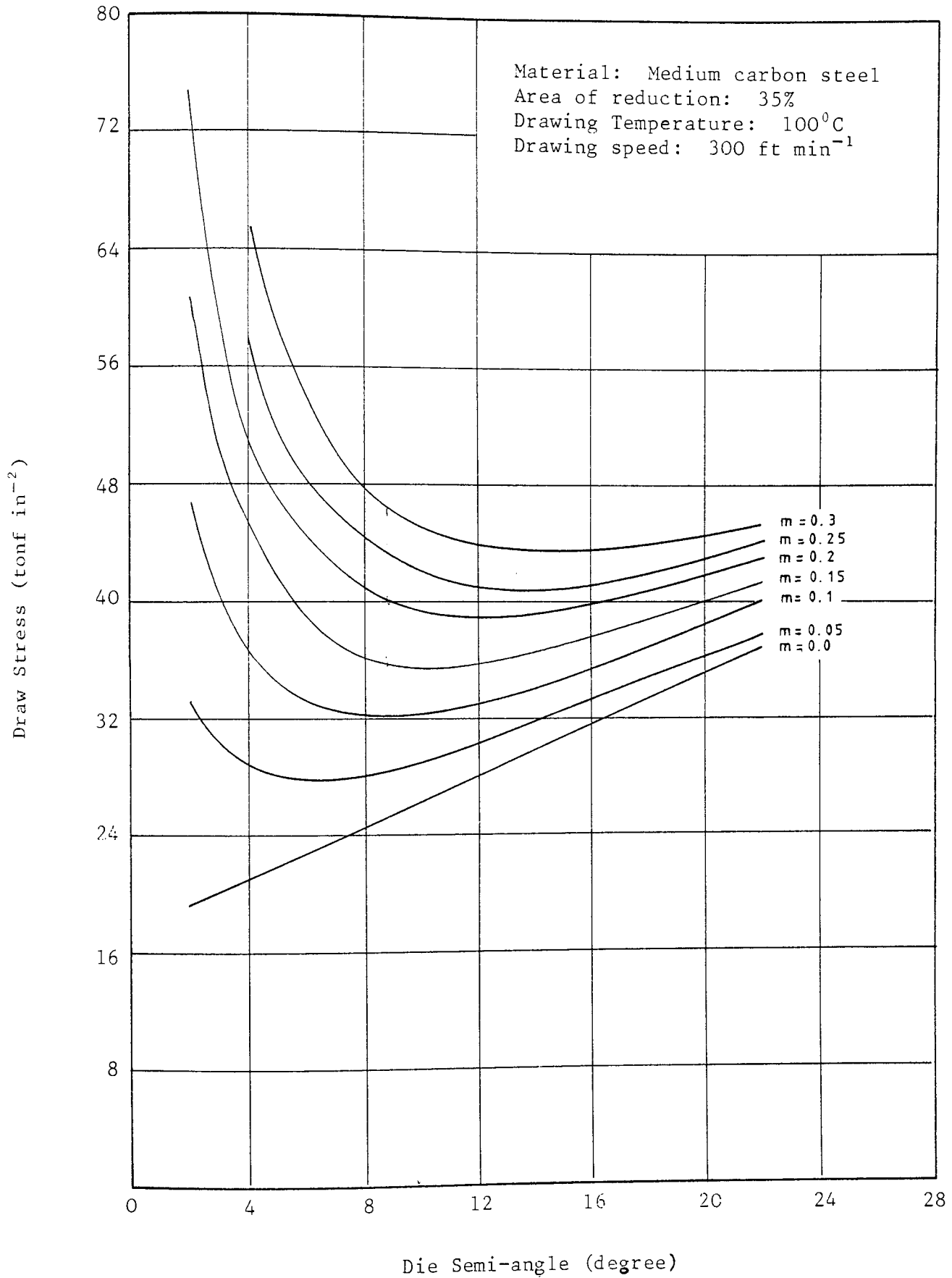


Figure 8.9: Variation of the draw stress against the die semi-angle for various values of constant friction factor m

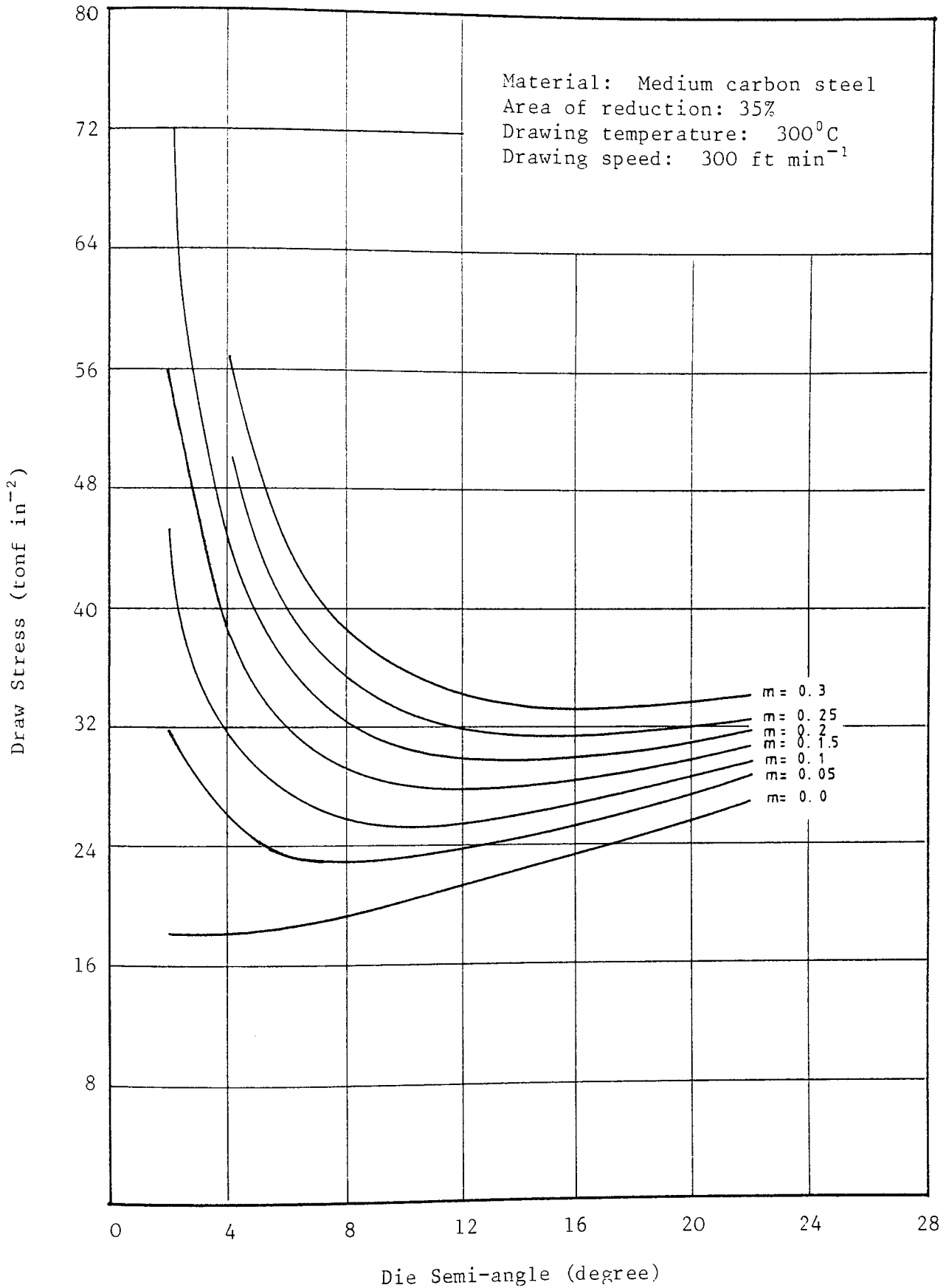


Figure 8.10: Variation of the draw stress against the die semi-angle for various values of constant friction m

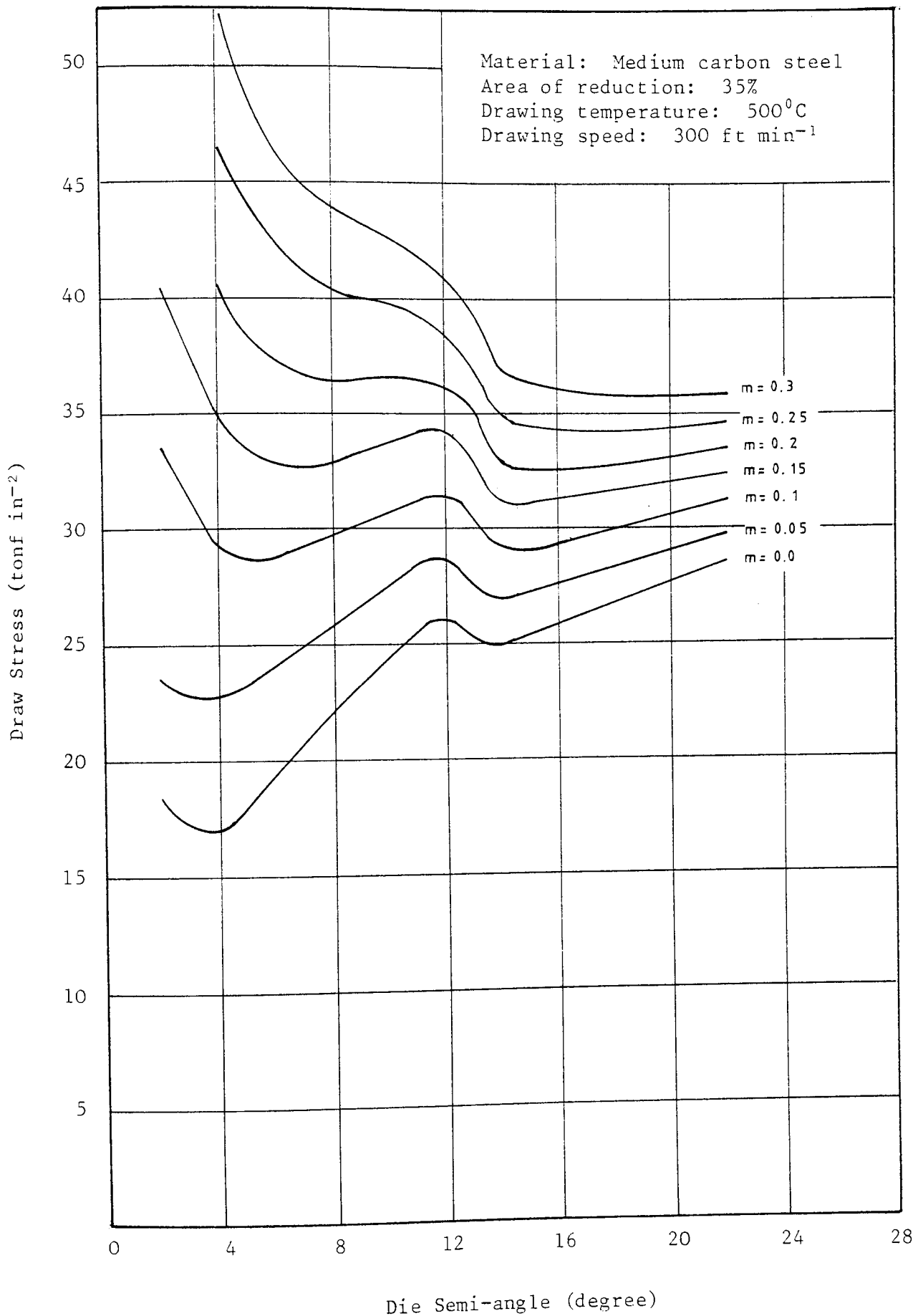


Figure 8.11: Variation of the draw stress against the die semi-angle for various values of constant friction factor m

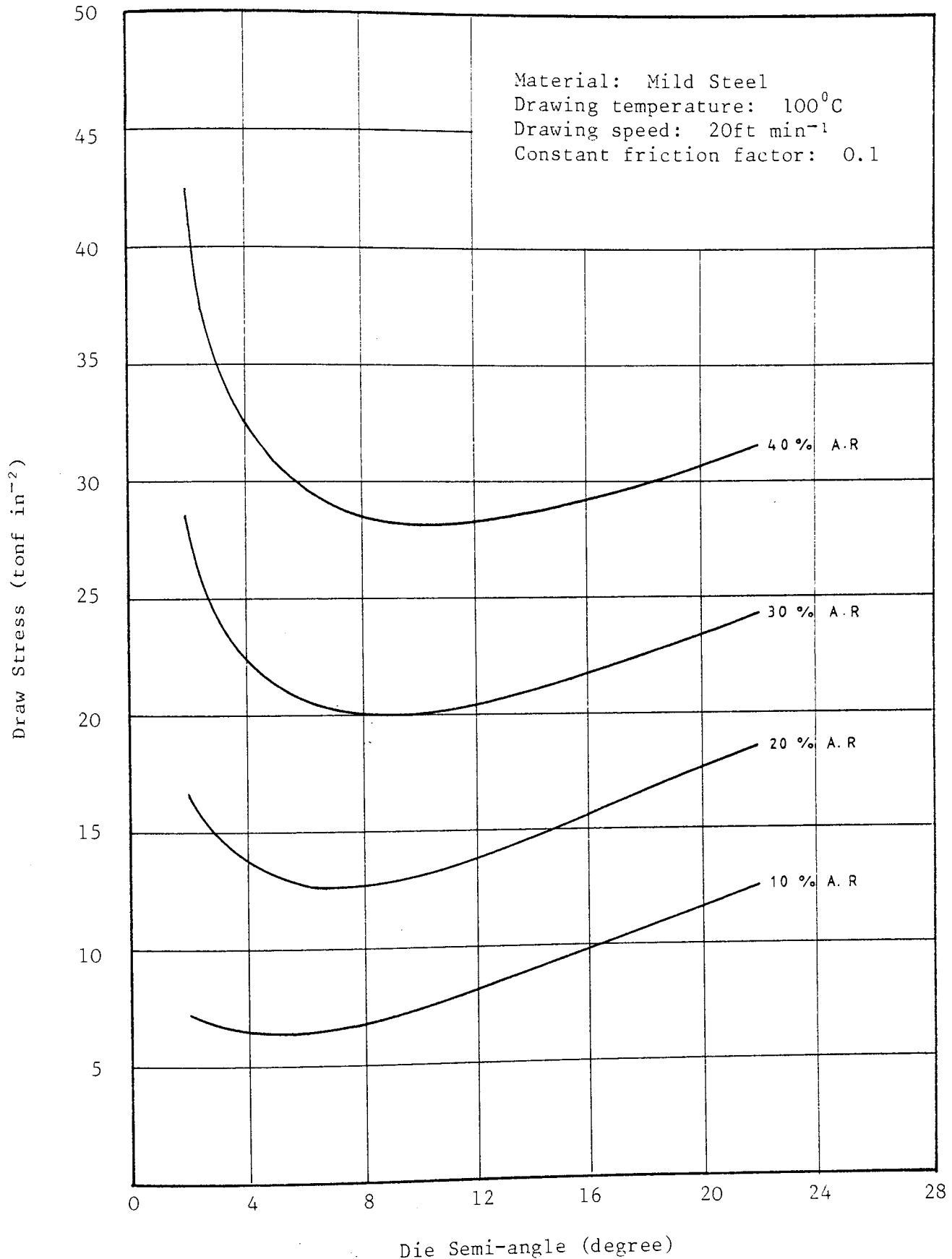


Figure 8.12: Variation of the draw stress against the die semi-angle for various areas of reduction (AR)

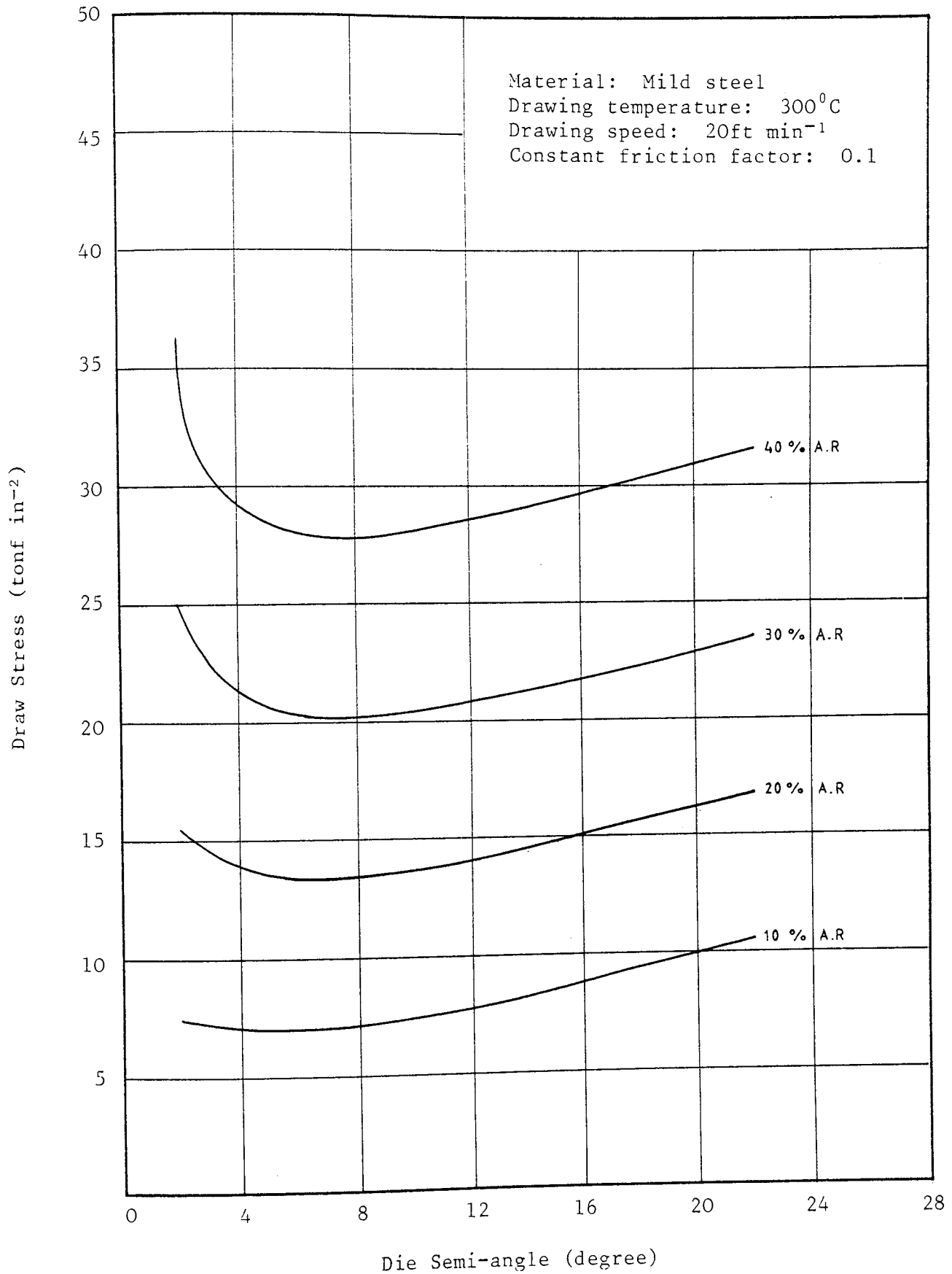


Figure 8.13: Variation of the draw stress against the die semi-angle for various areas of reduction (AR)

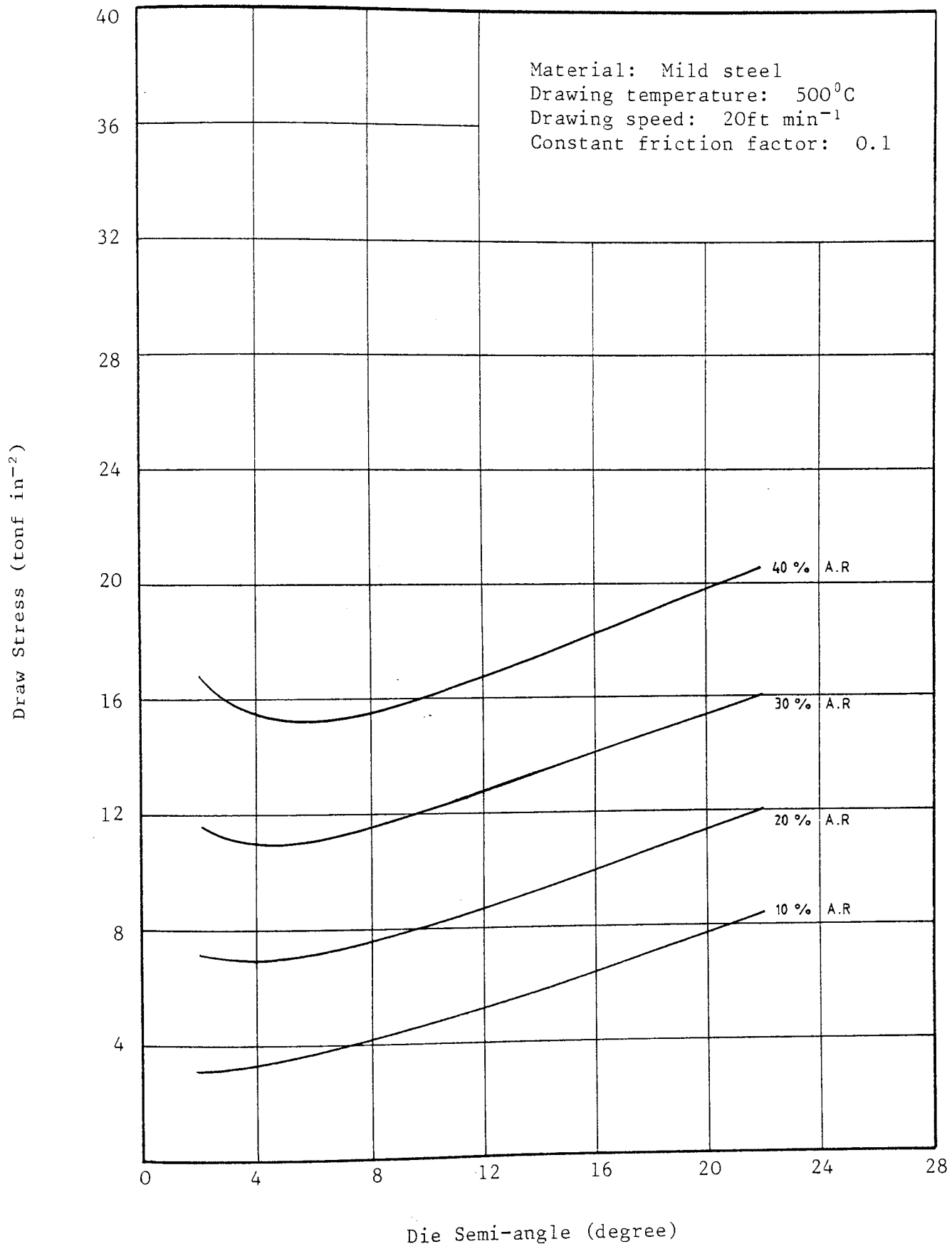


Figure 8.14: Variation of the draw stress against the die semi-angle for various areas of reduction (AR)

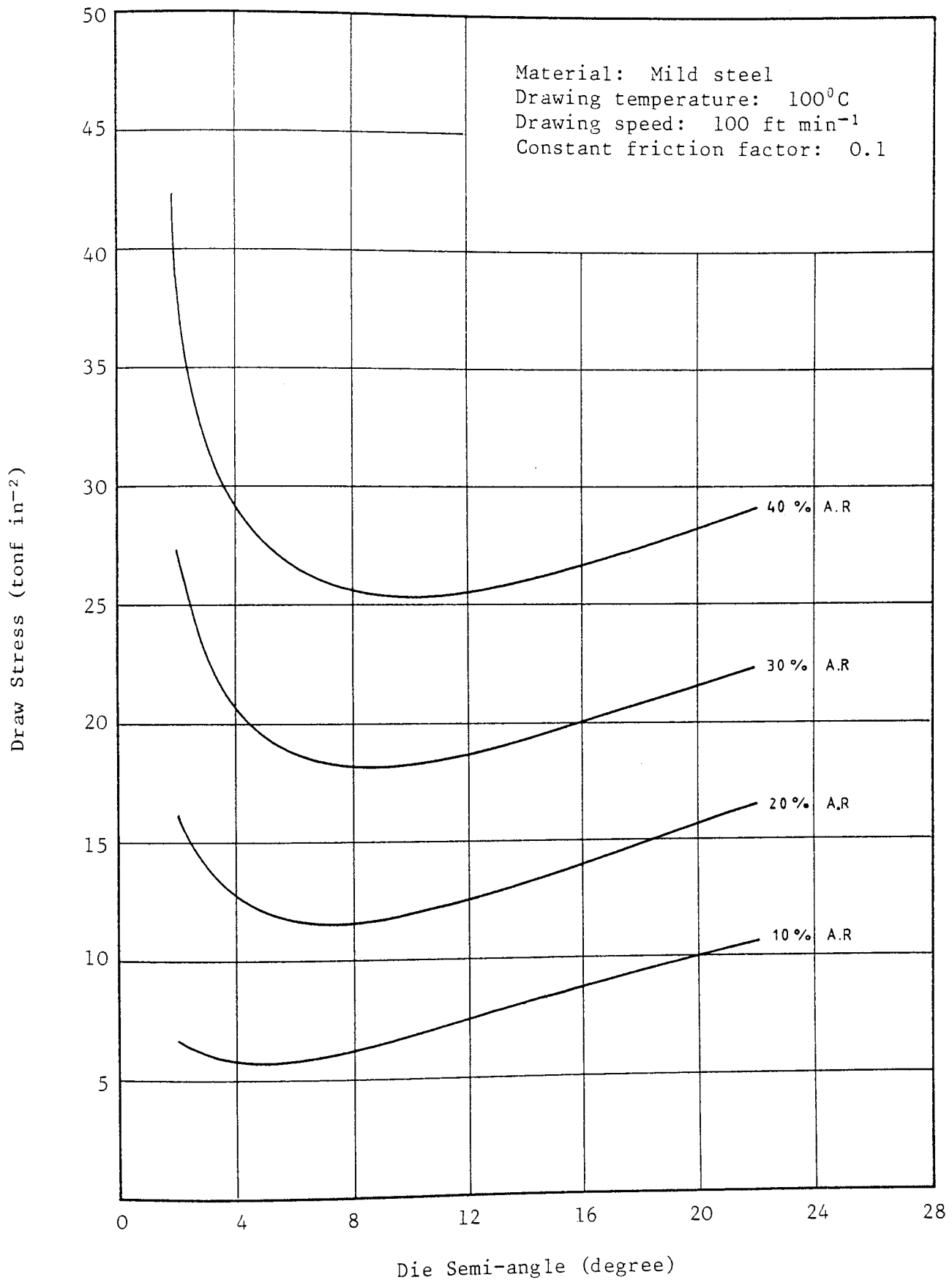


Figure 8.15: Variation of the draw stress against the die semi-angle for various areas of reduction (AR)

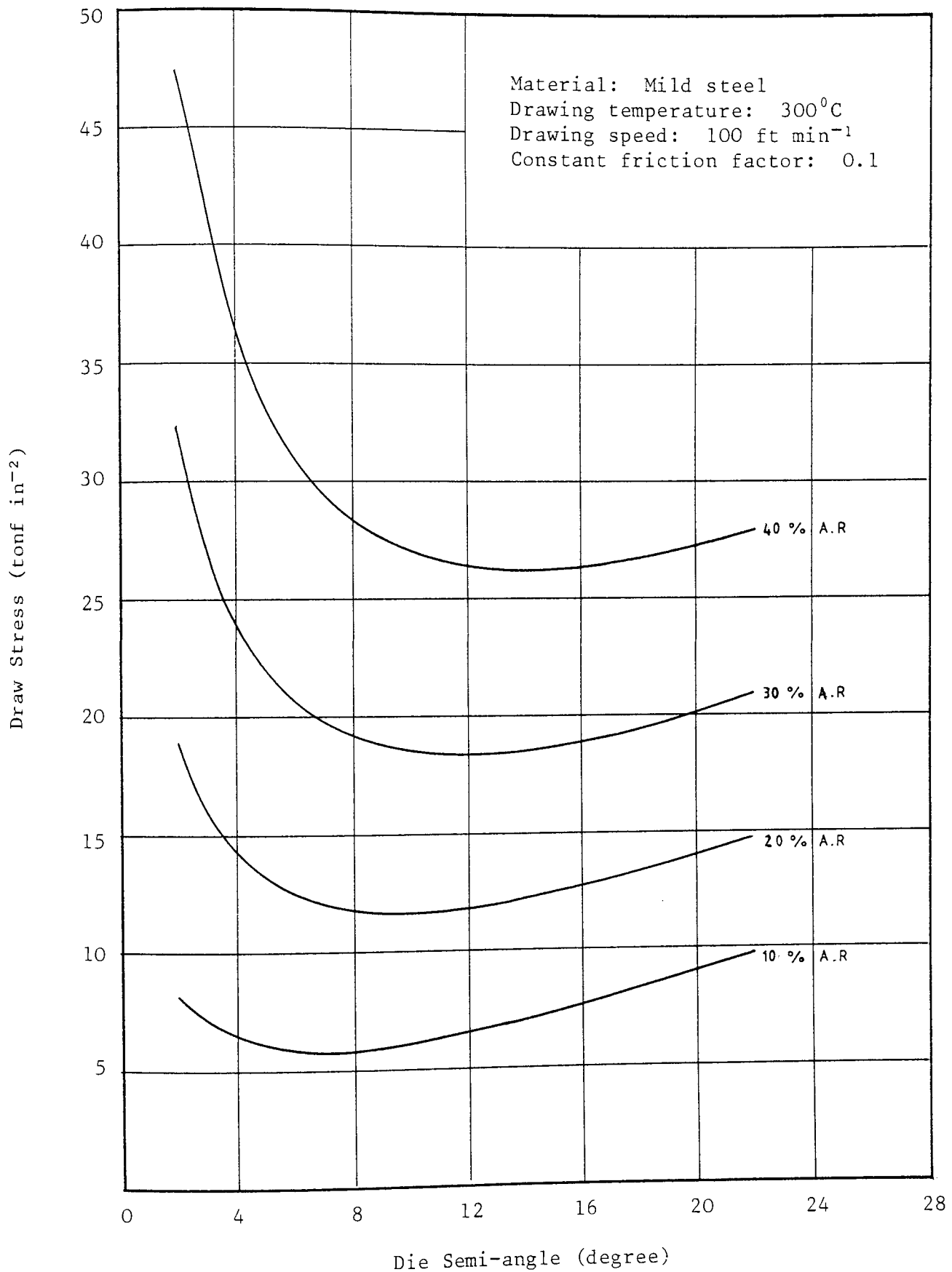


Figure 8.16: Variation of the draw stress against the die semi-angle for various areas of reduction (AR)

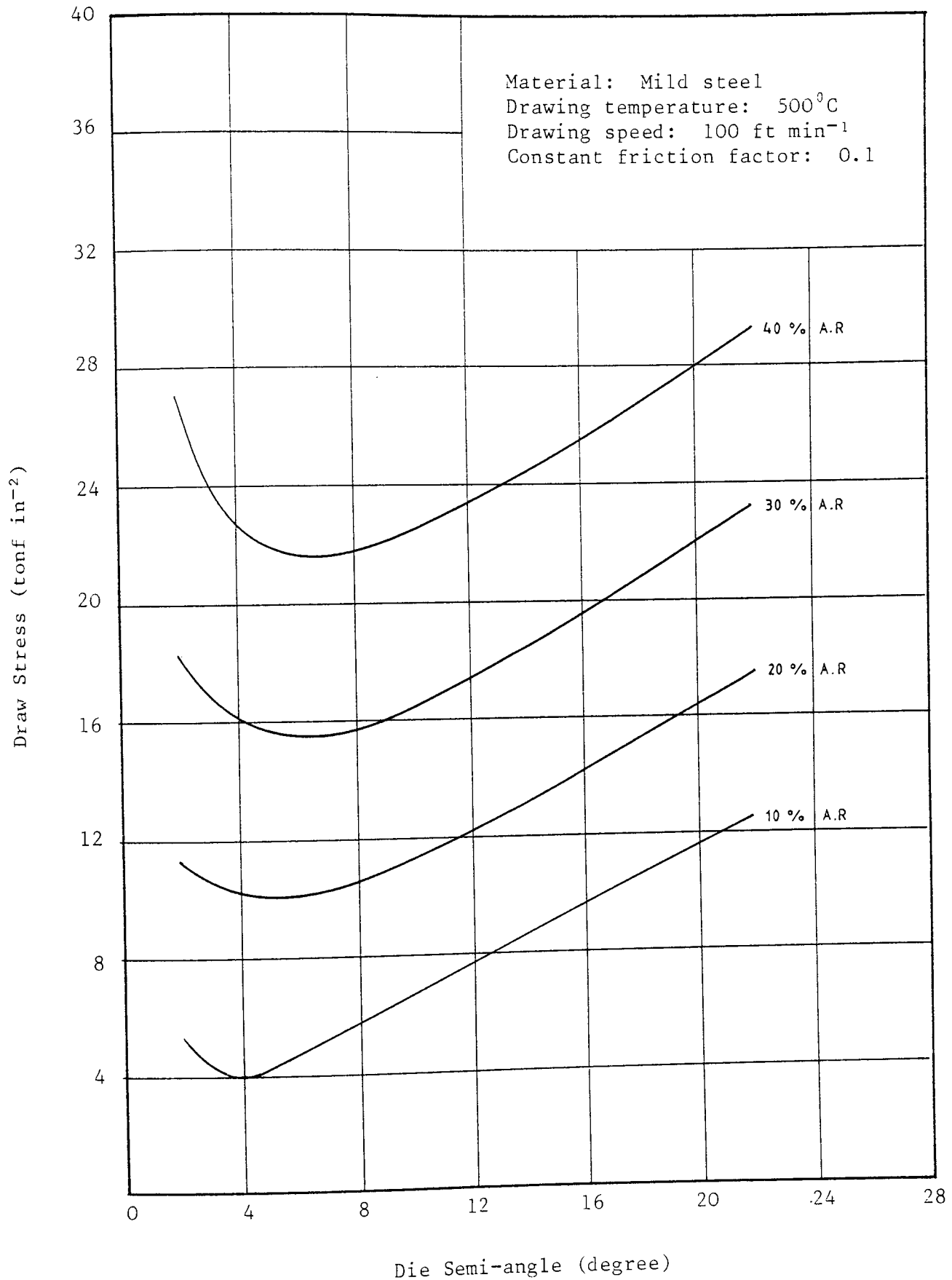


Figure 8.17: Variation of the draw stress against the die semi-angle for various areas of reduction (AR)

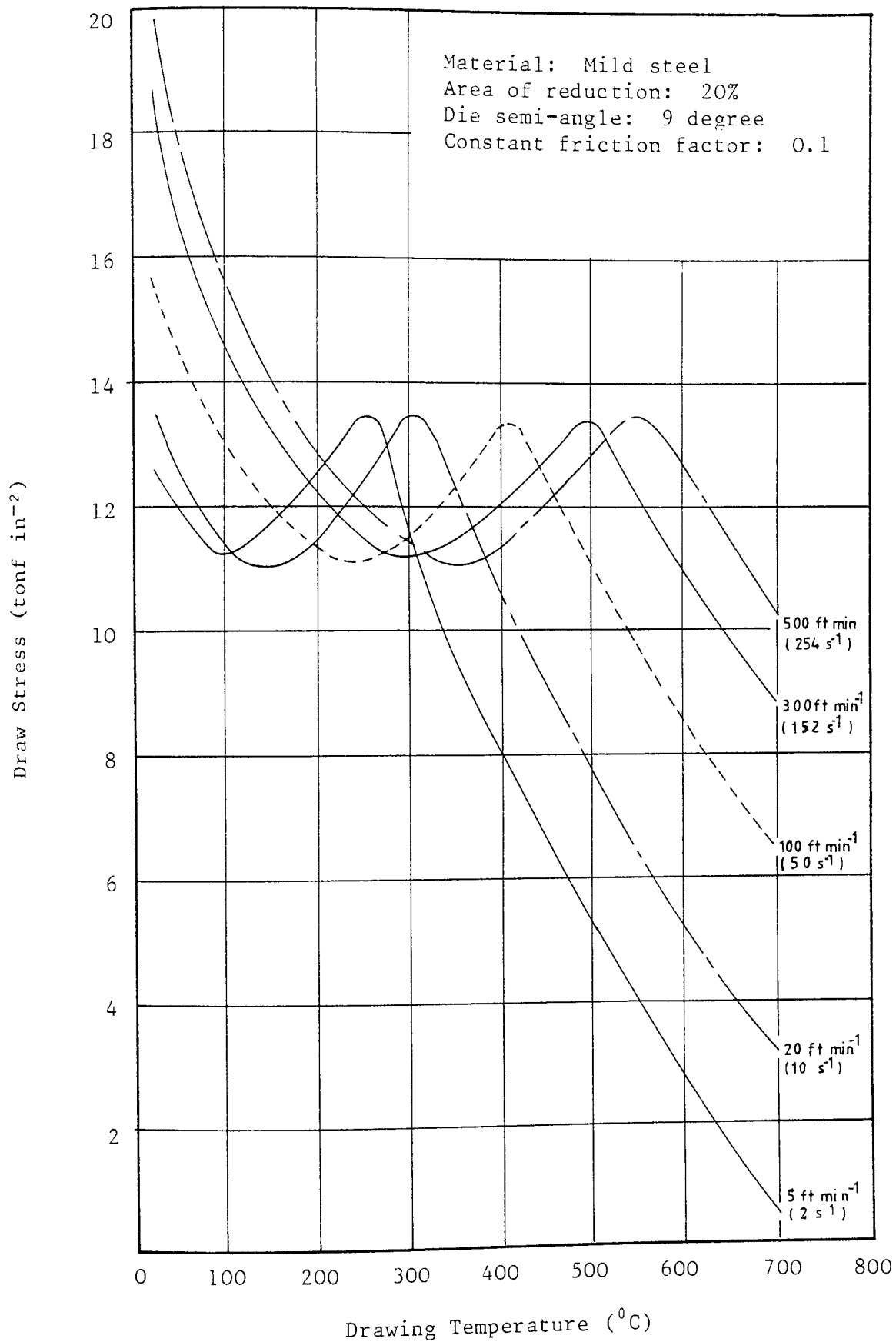


Figure 8.18: Theoretical results for various draw speeds and temperatures

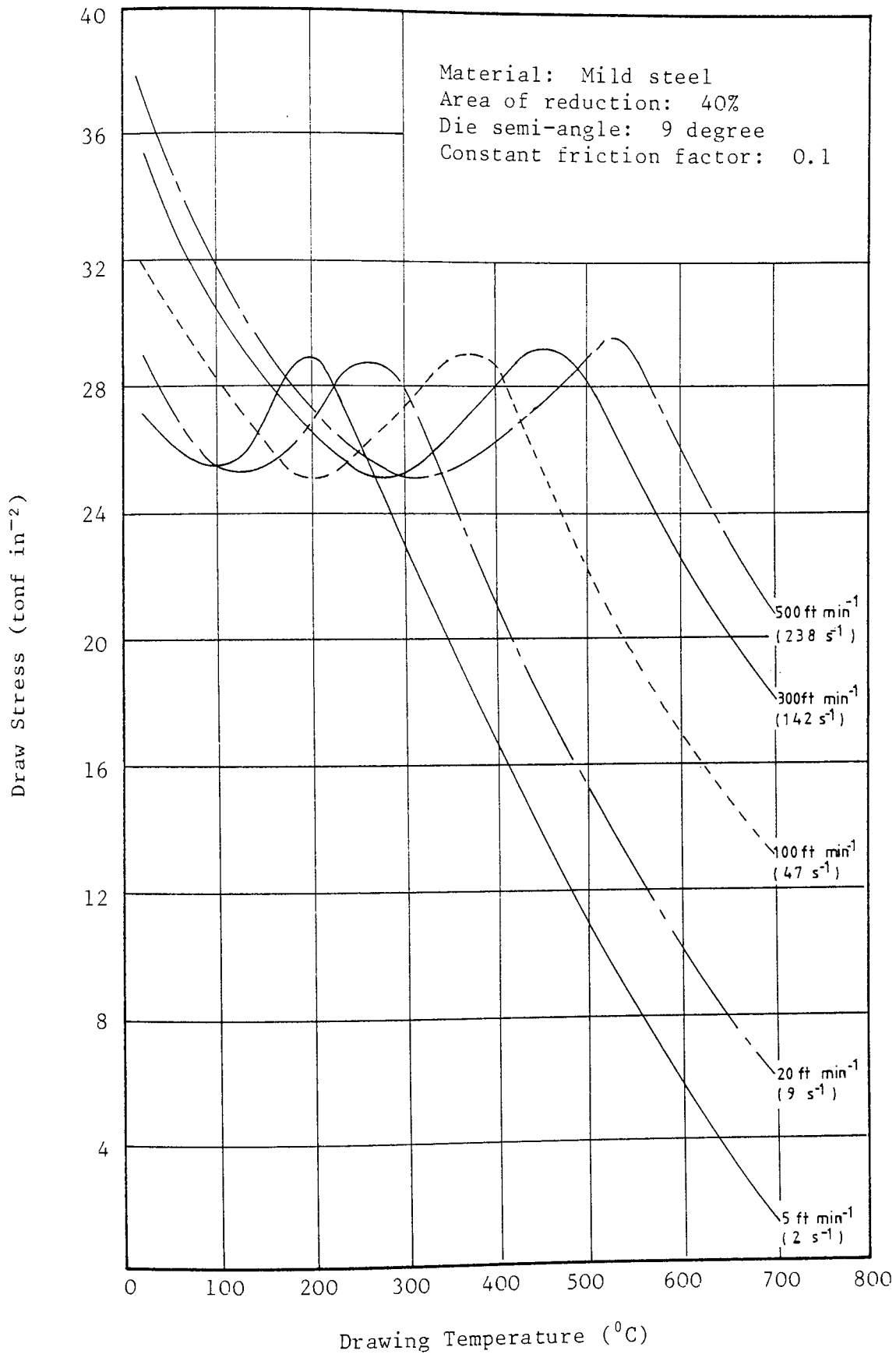


Figure 8.19: Theoretical results for various draw speeds and temperatures

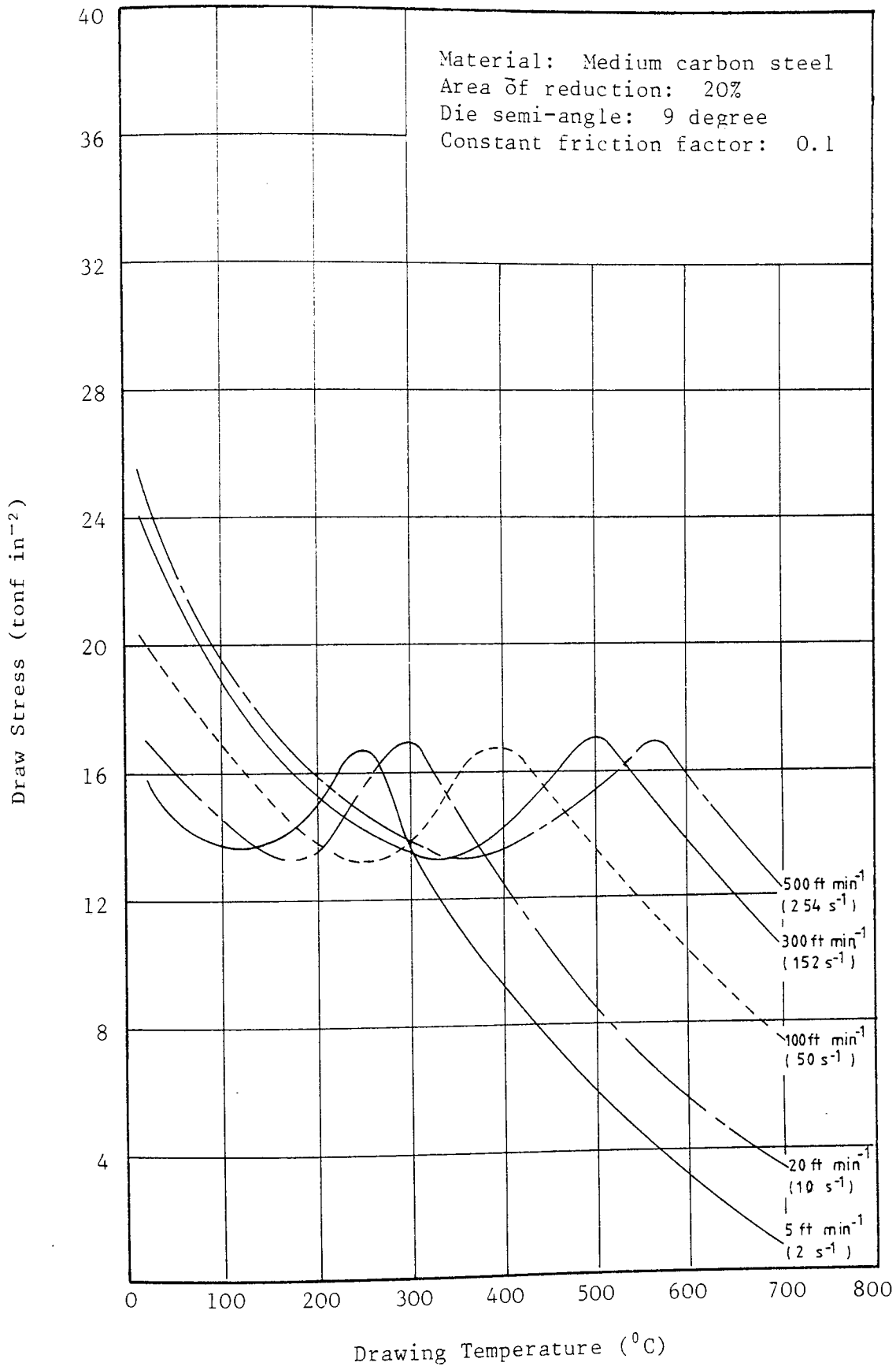


Figure 8.20: Theoretical results for various draw speeds and temperatures

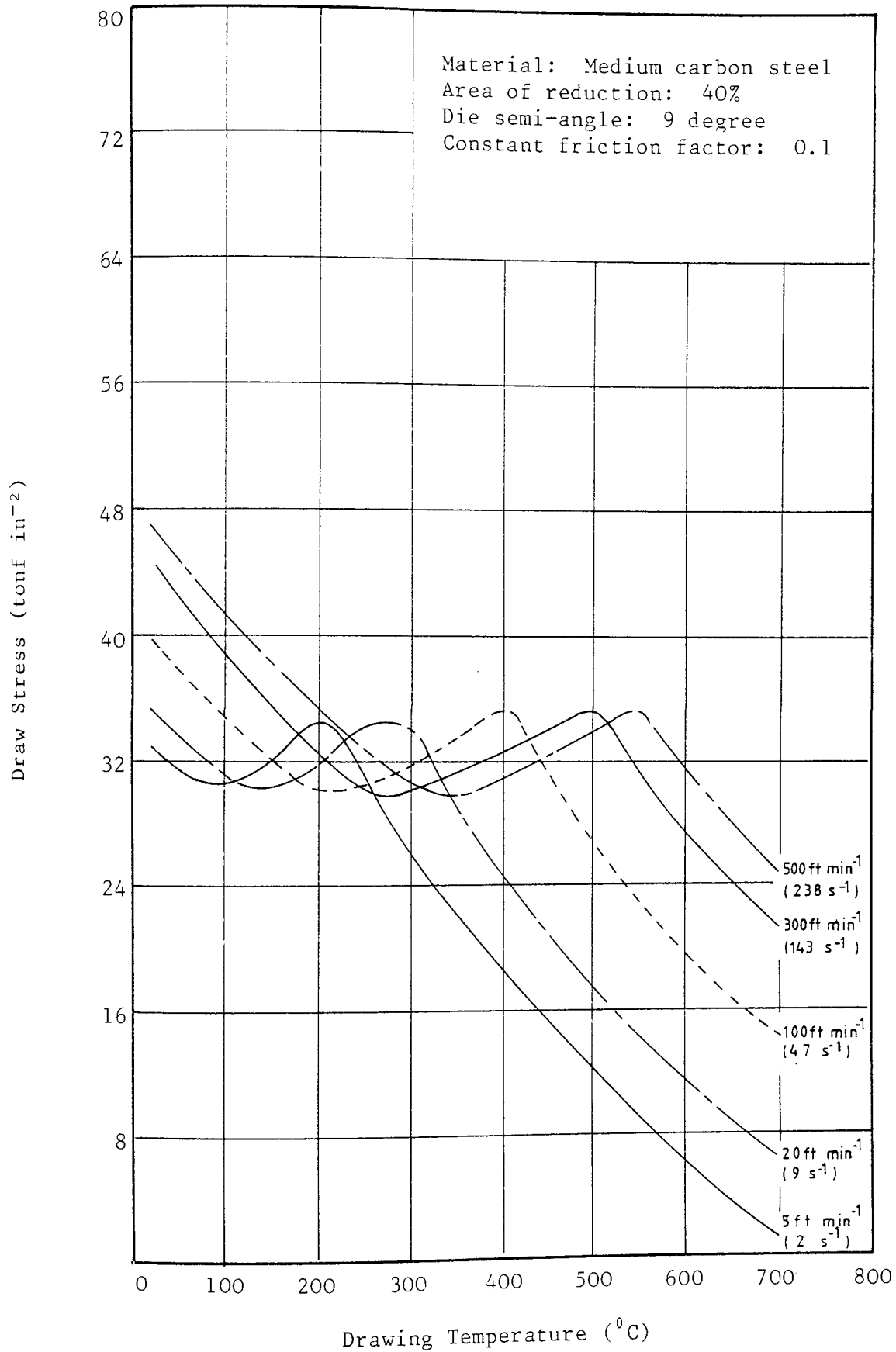


Figure 8.21: Theoretical results for various draw speeds and temperatures

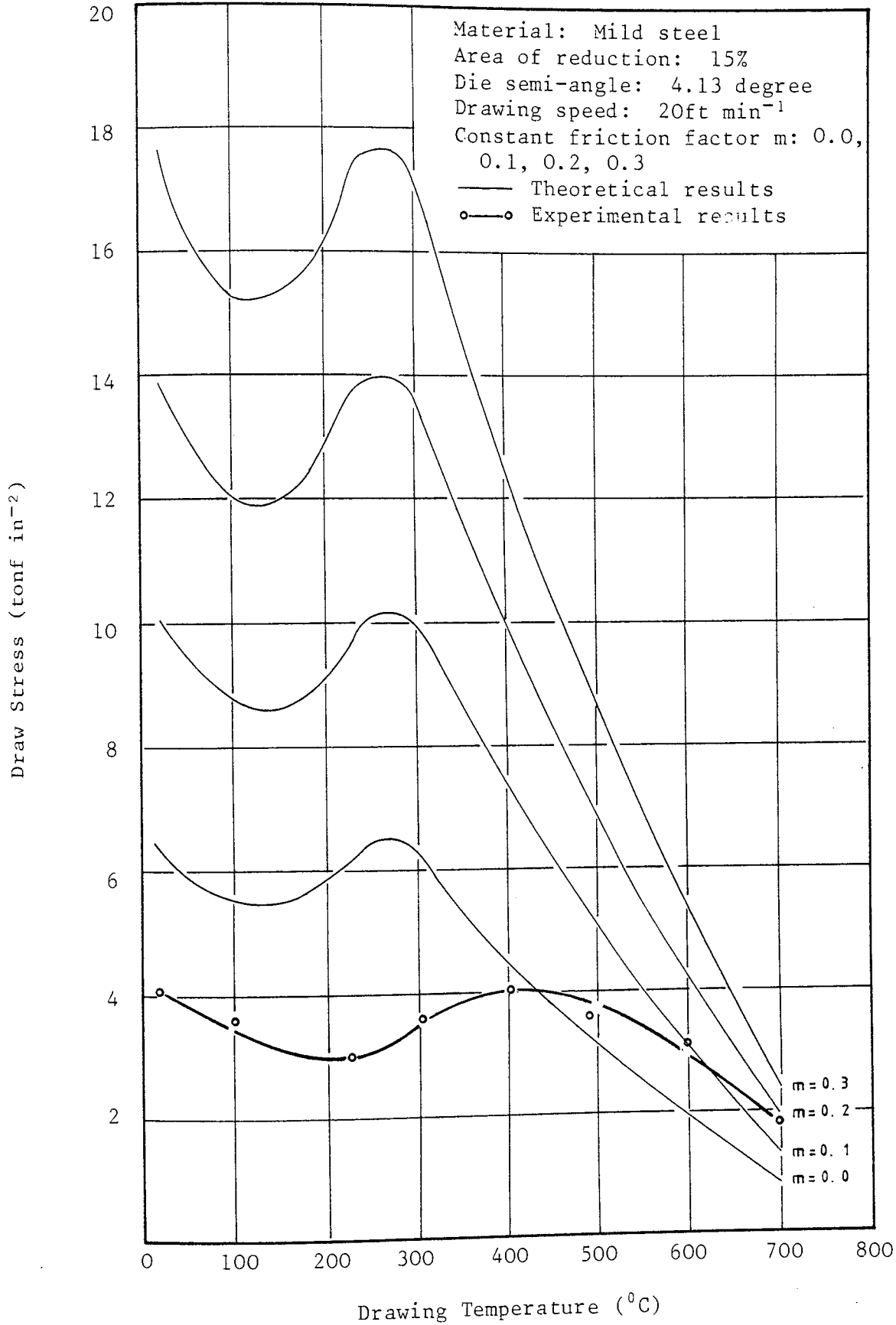


Figure 8.22: Comparison of experimental and theoretical results at various temperatures

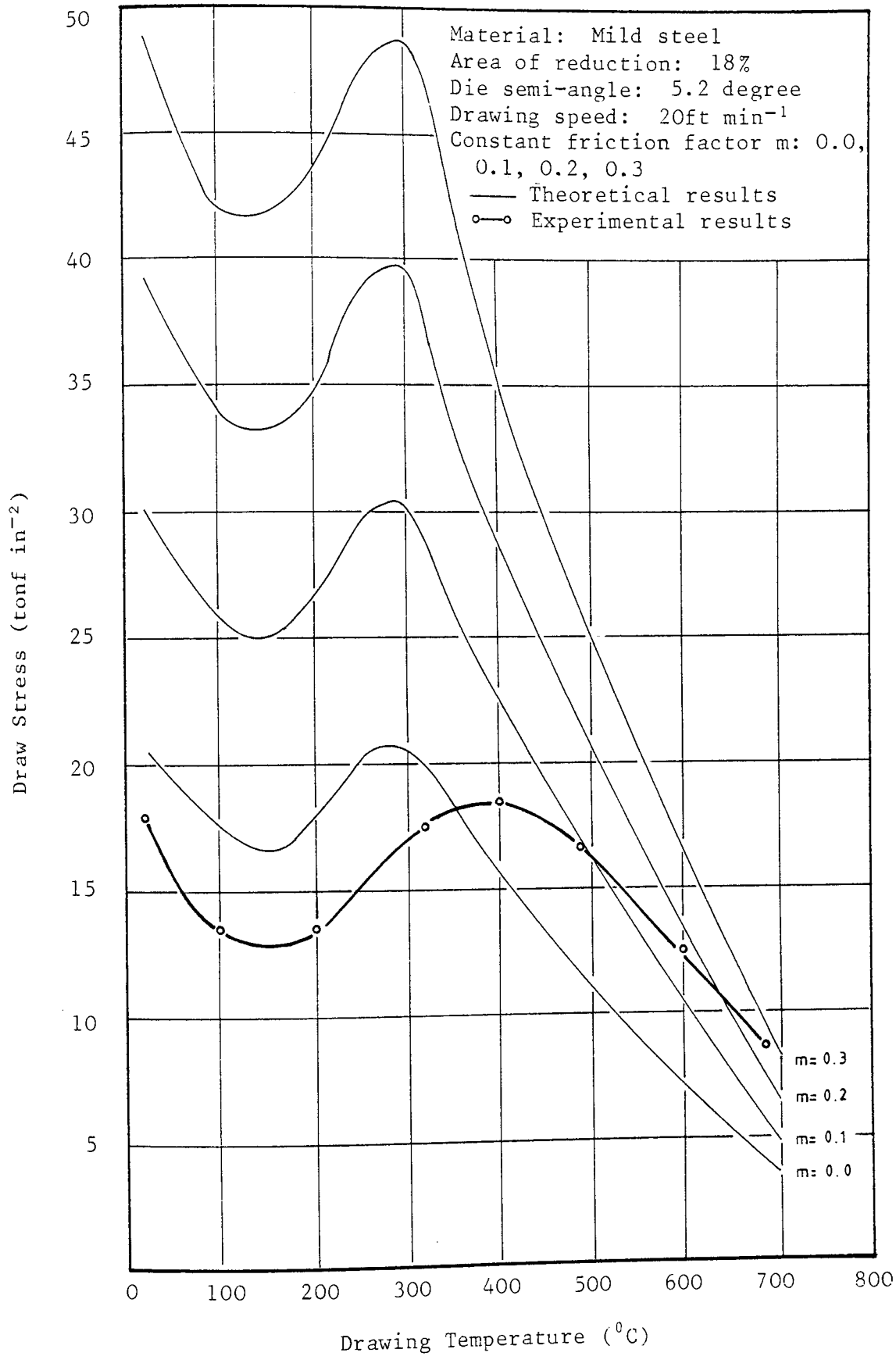


Figure 8.23: Comparison of experimental and theoretical results at various temperatures

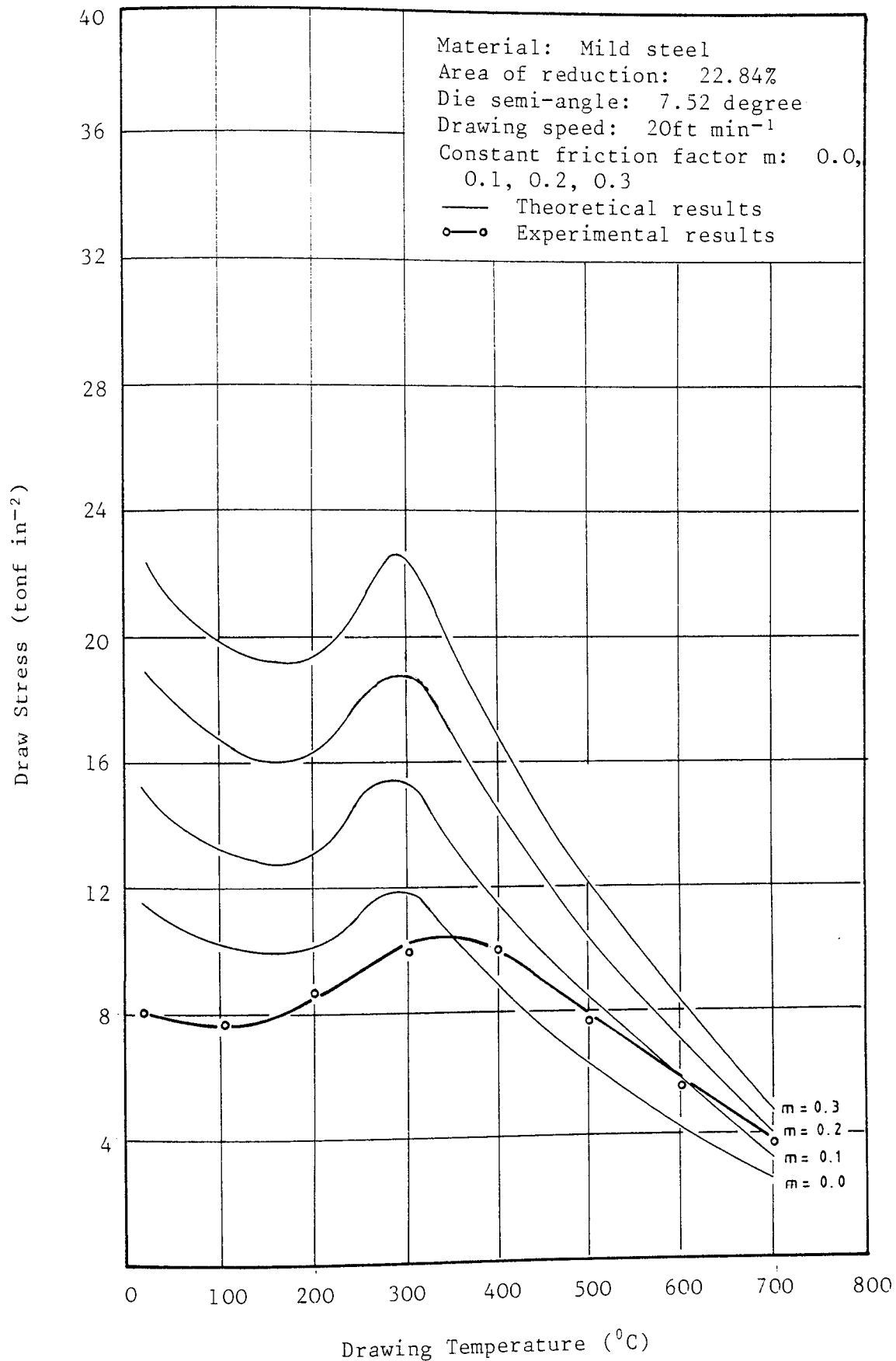


Figure 8.24: Comparison of experimental and theoretical results at various temperatures

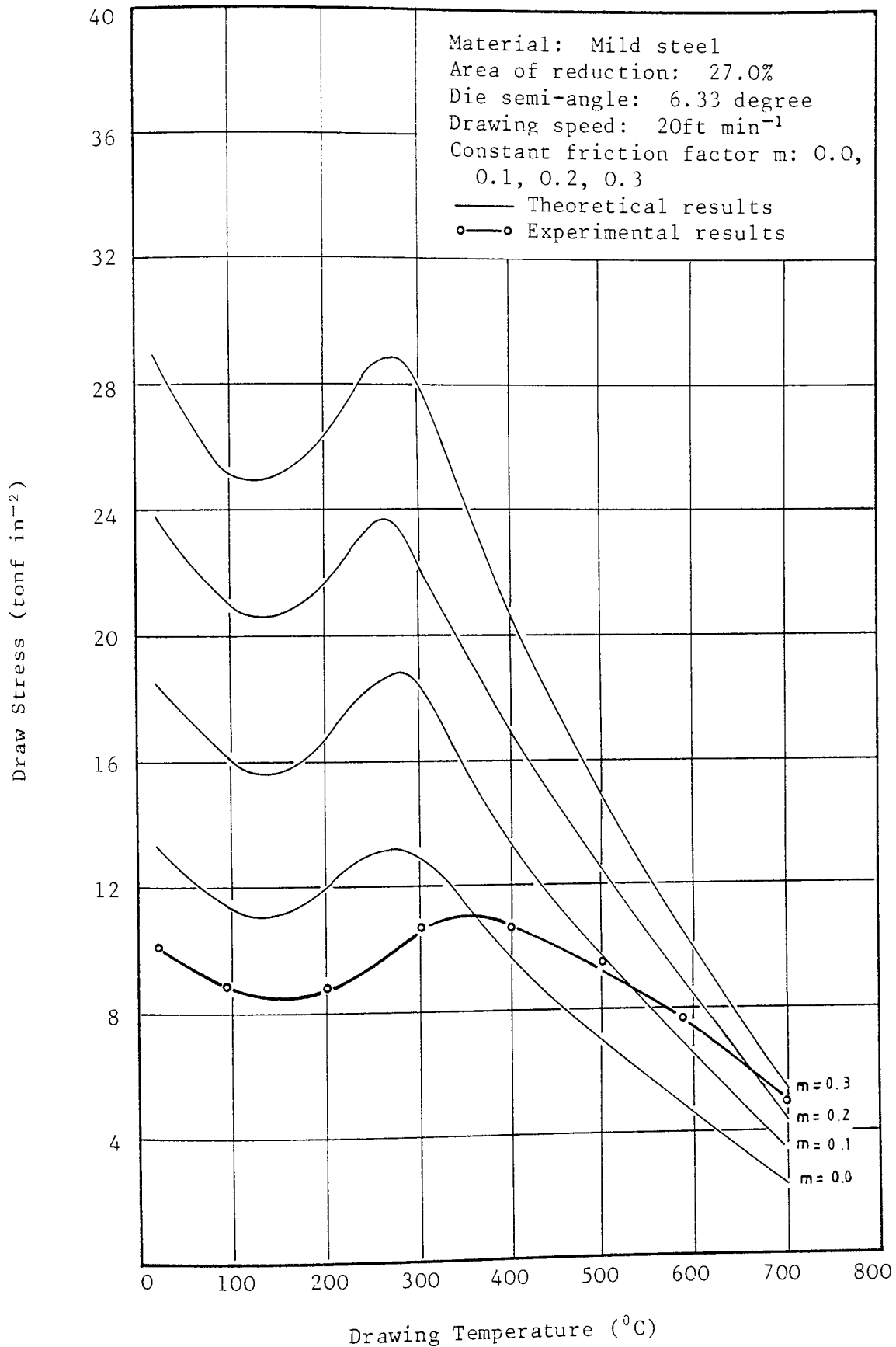


Figure 8.25: Comparison of experimental and theoretical results at various temperatures

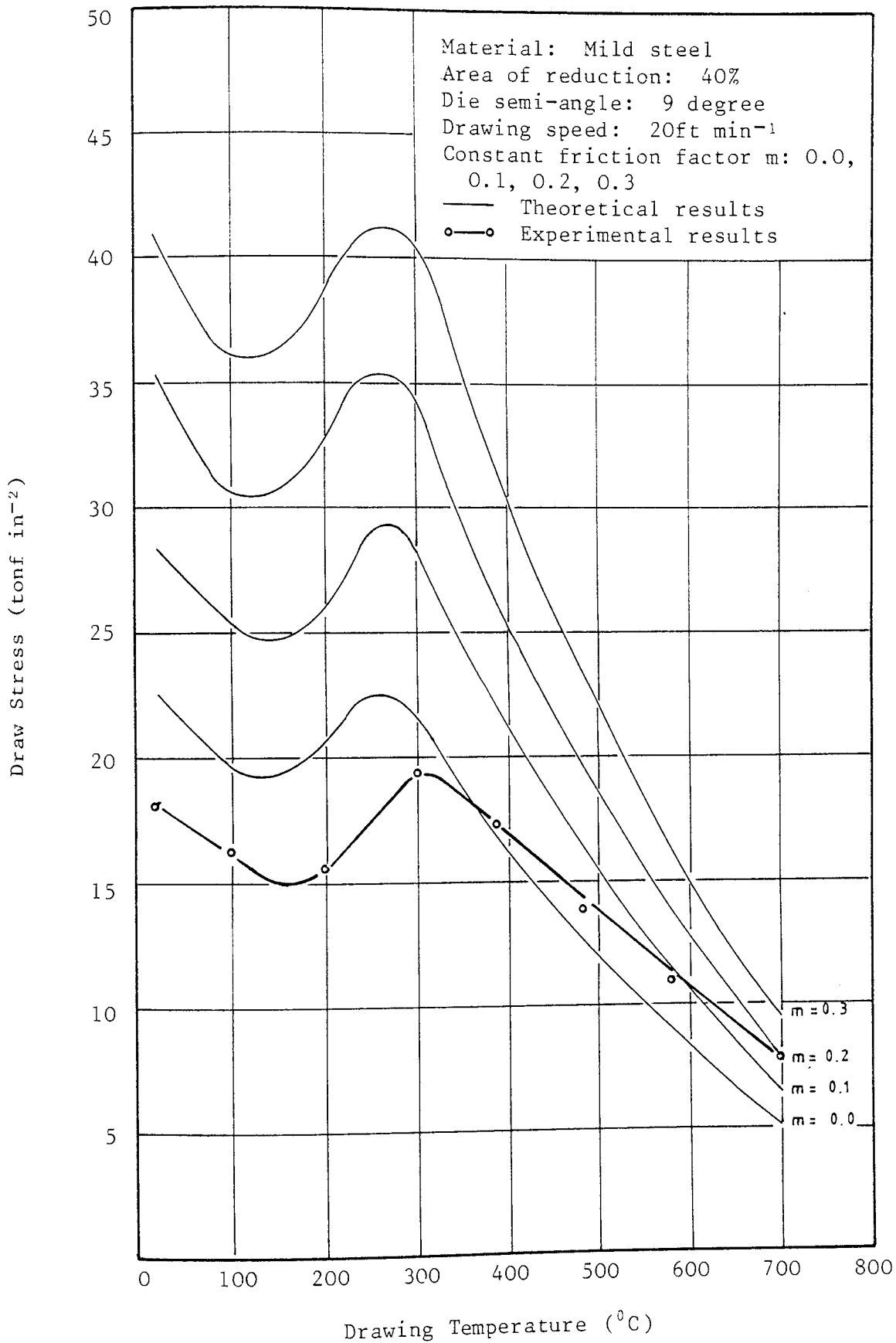


Figure 8.26: Comparison of experimental and theoretical results at various temperatures

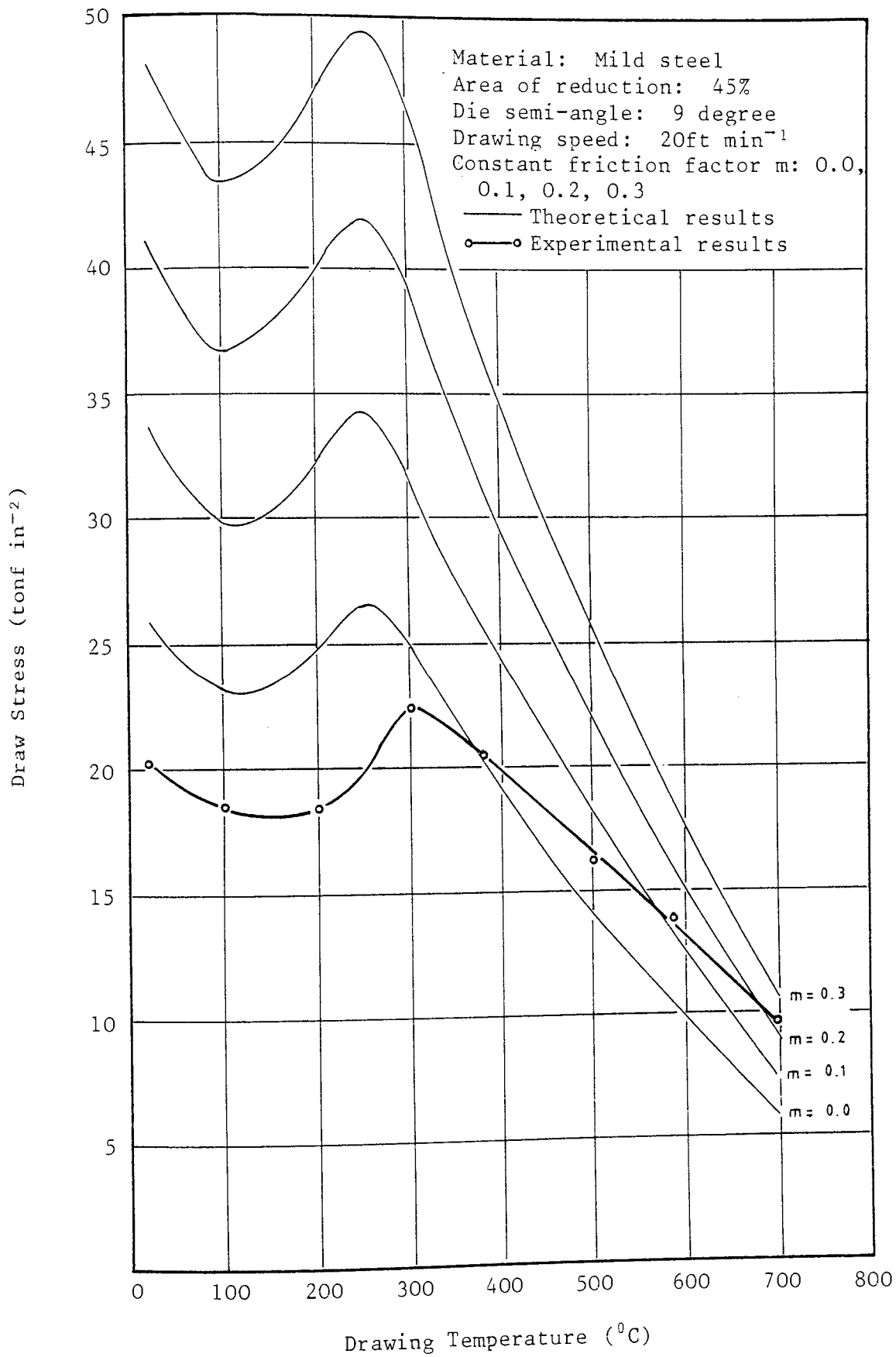


Figure 8.27: Comparison of experimental and theoretical results at various temperatures

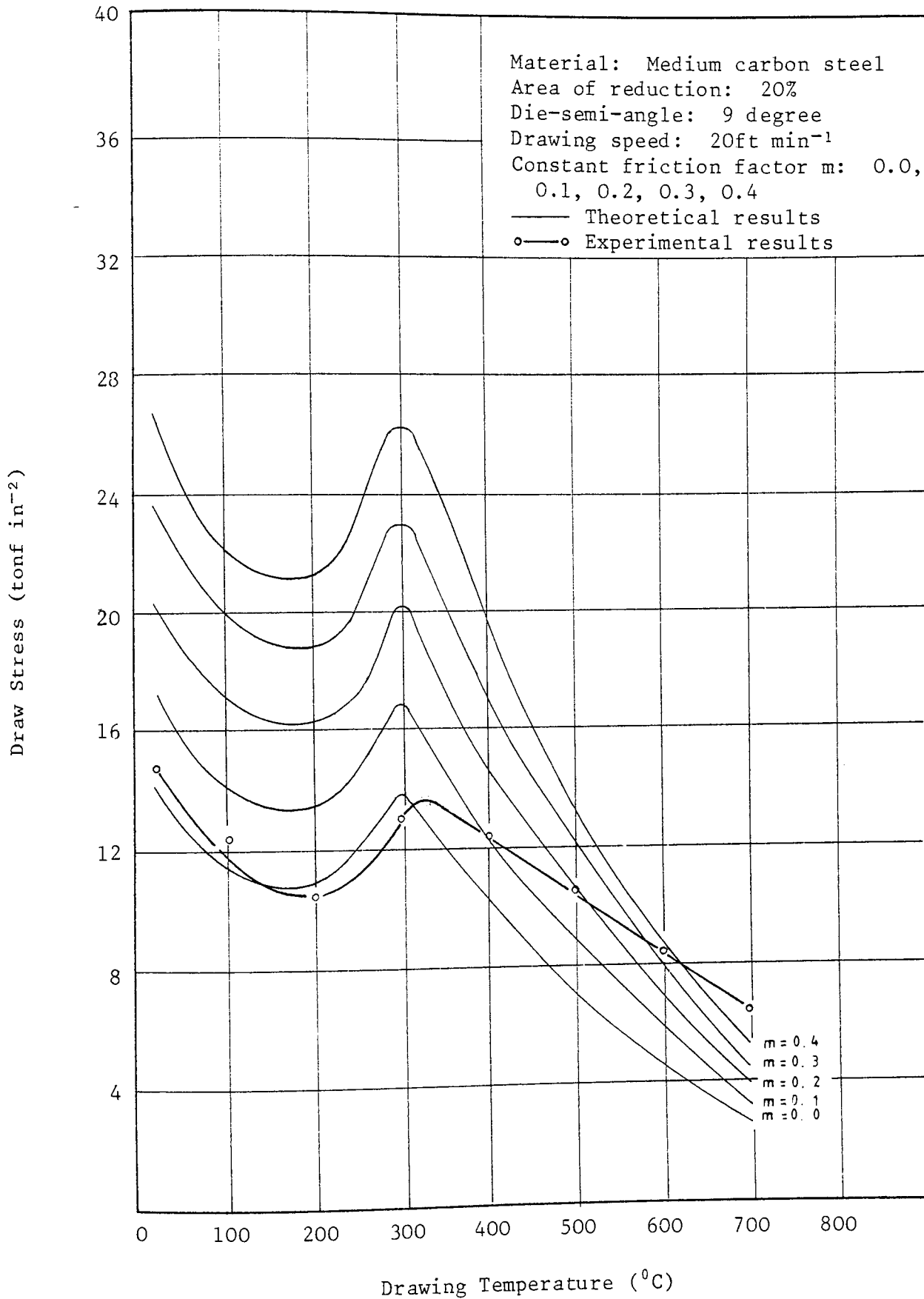


Figure 8.28: Comparison of experimental and theoretical results at various temperatures

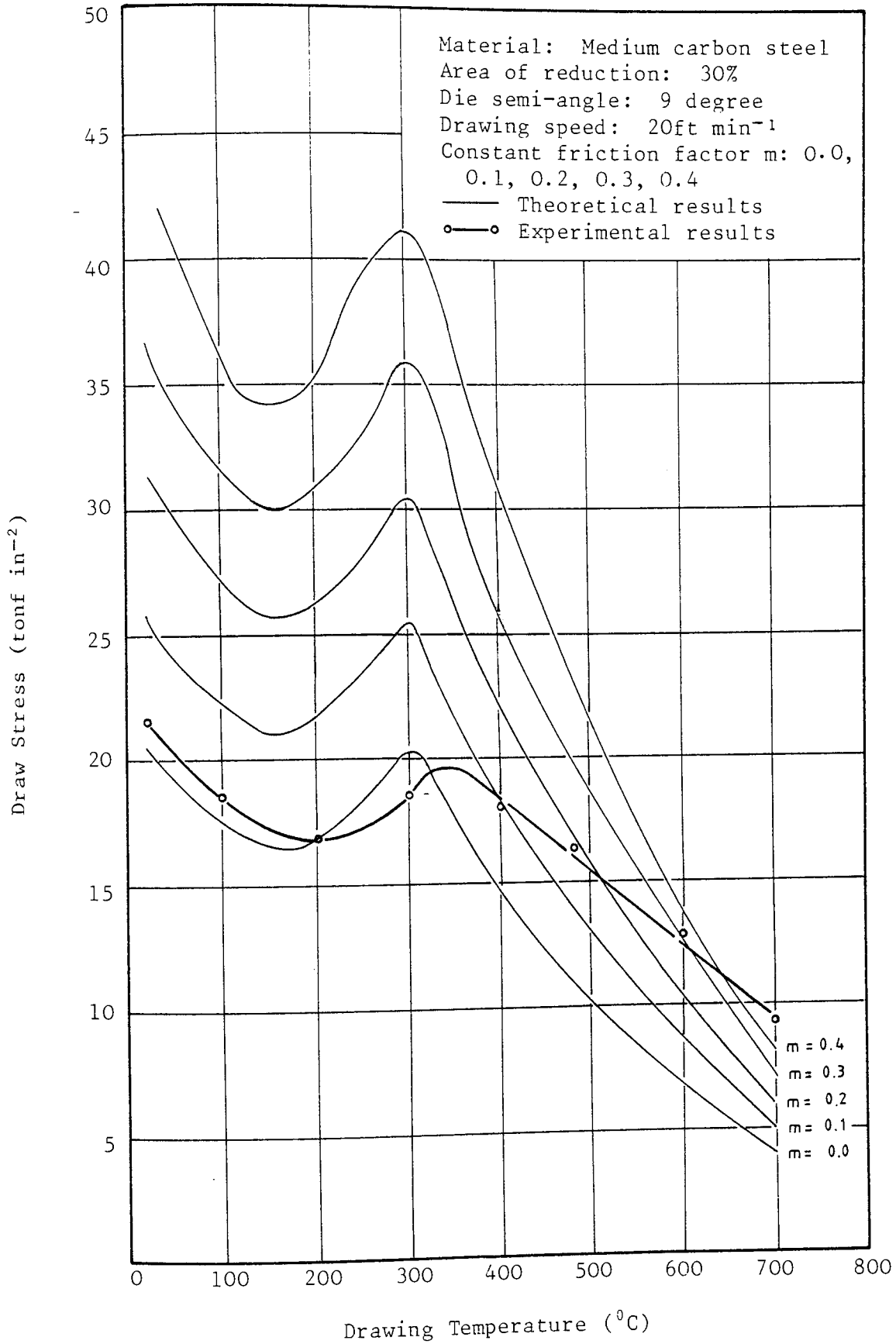


Figure 8.29: Comparison of experimental and theoretical results at various temperatures

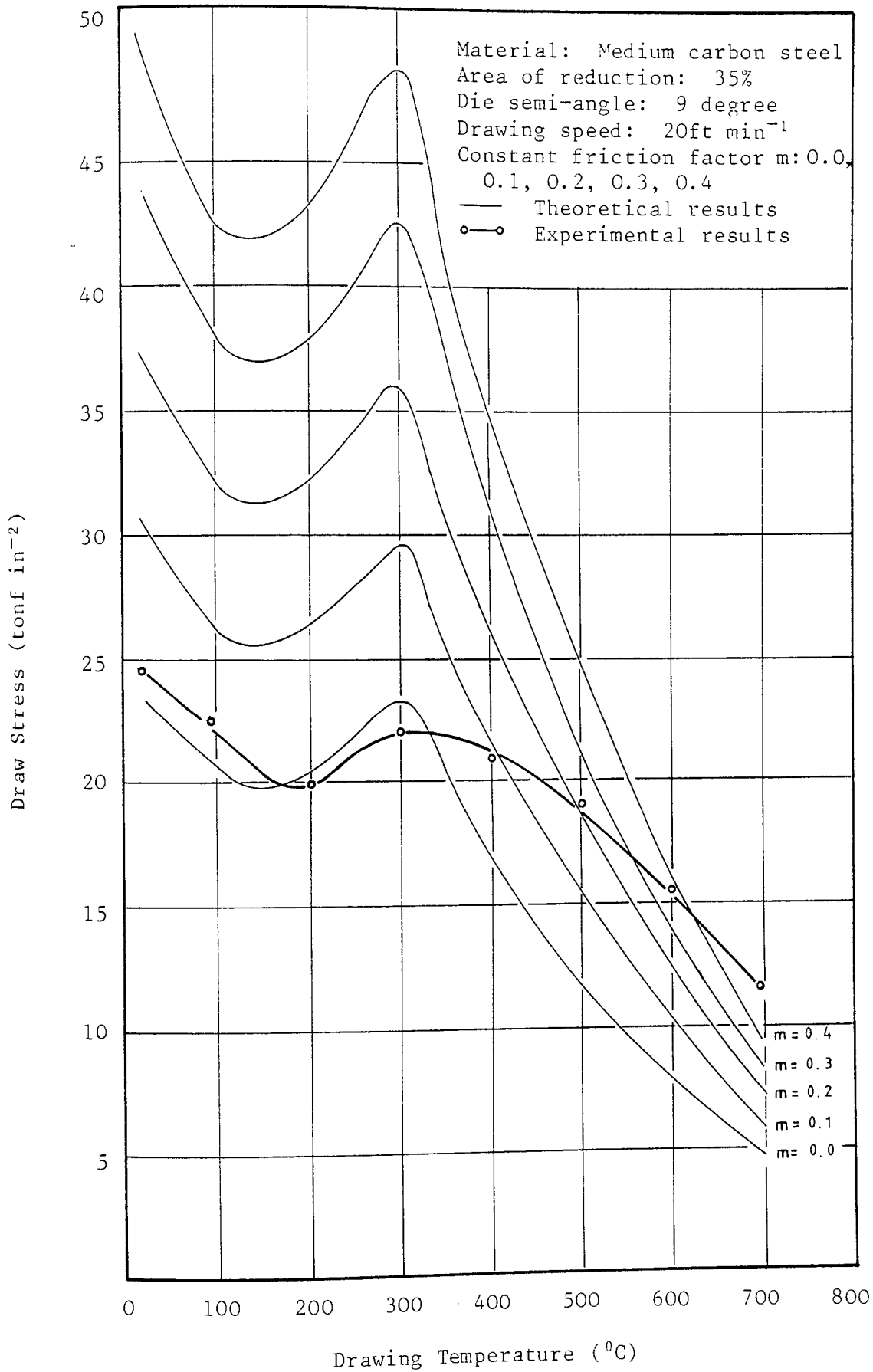


Figure 8.30: Comparison of experimental and theoretical results at various temperatures

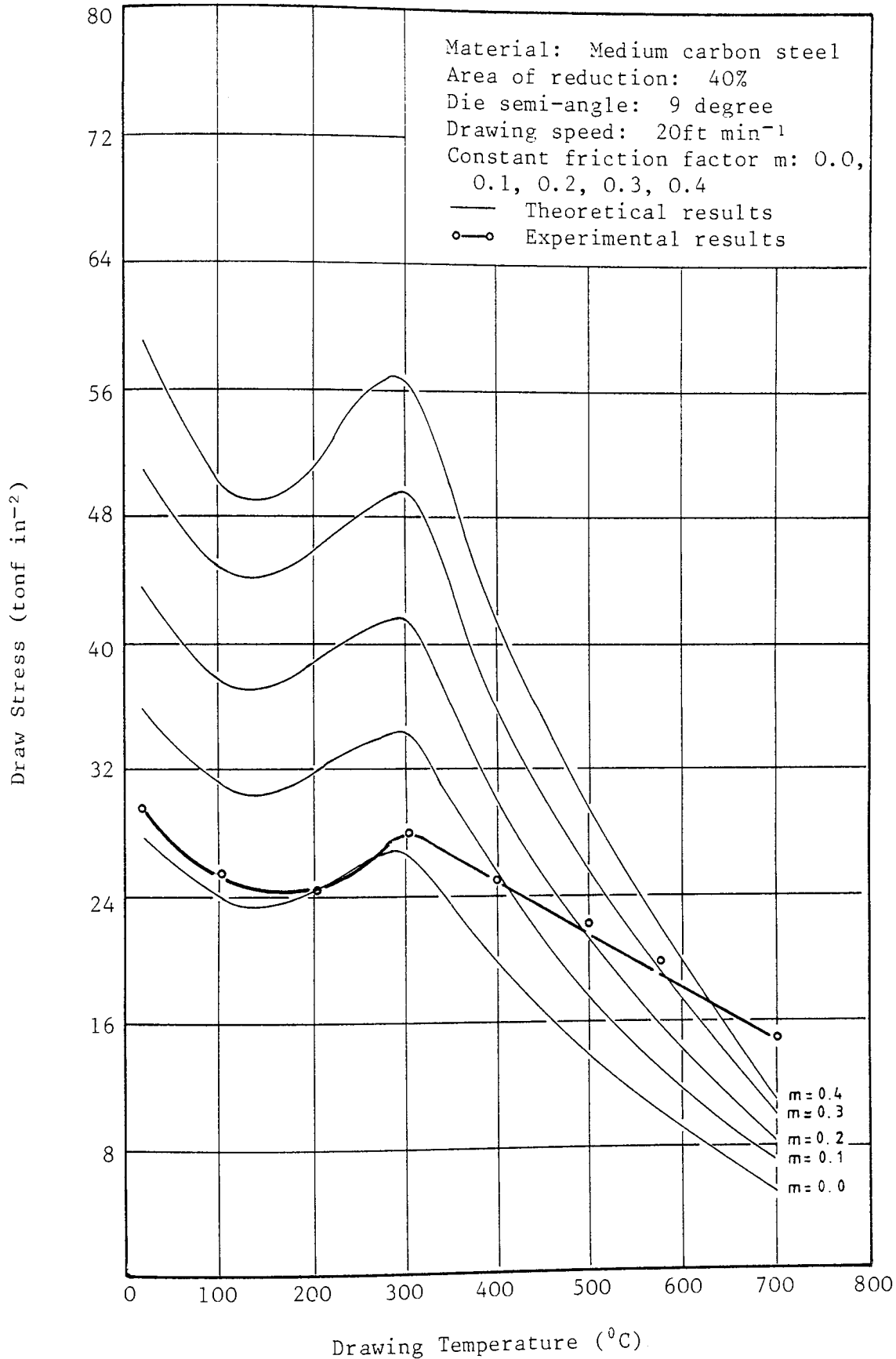


Figure 8.31: Comparison of experimental and theoretical results at various temperatures

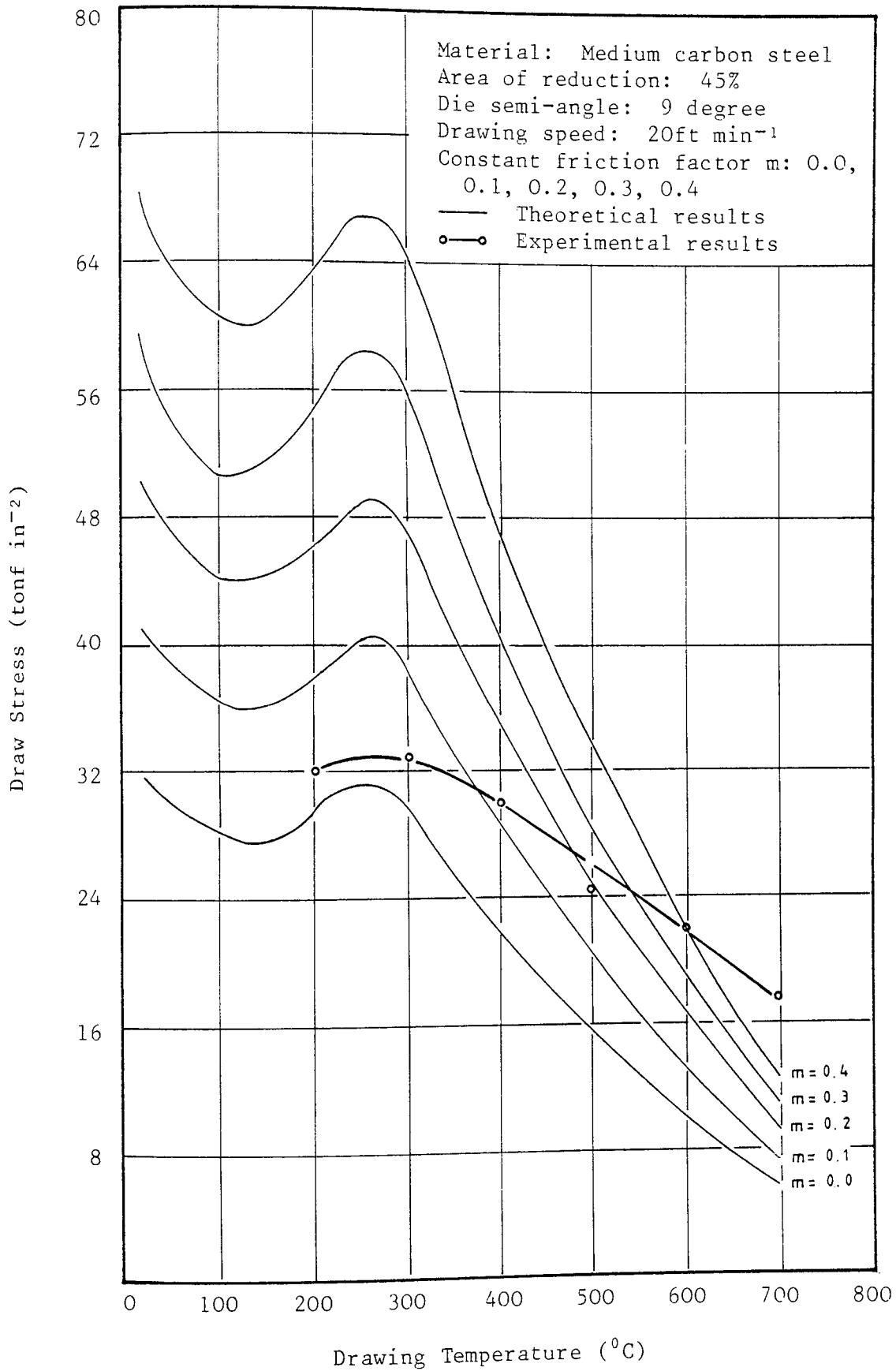


Figure 8.32: Comparison of experimental and theoretical results at various temperatures

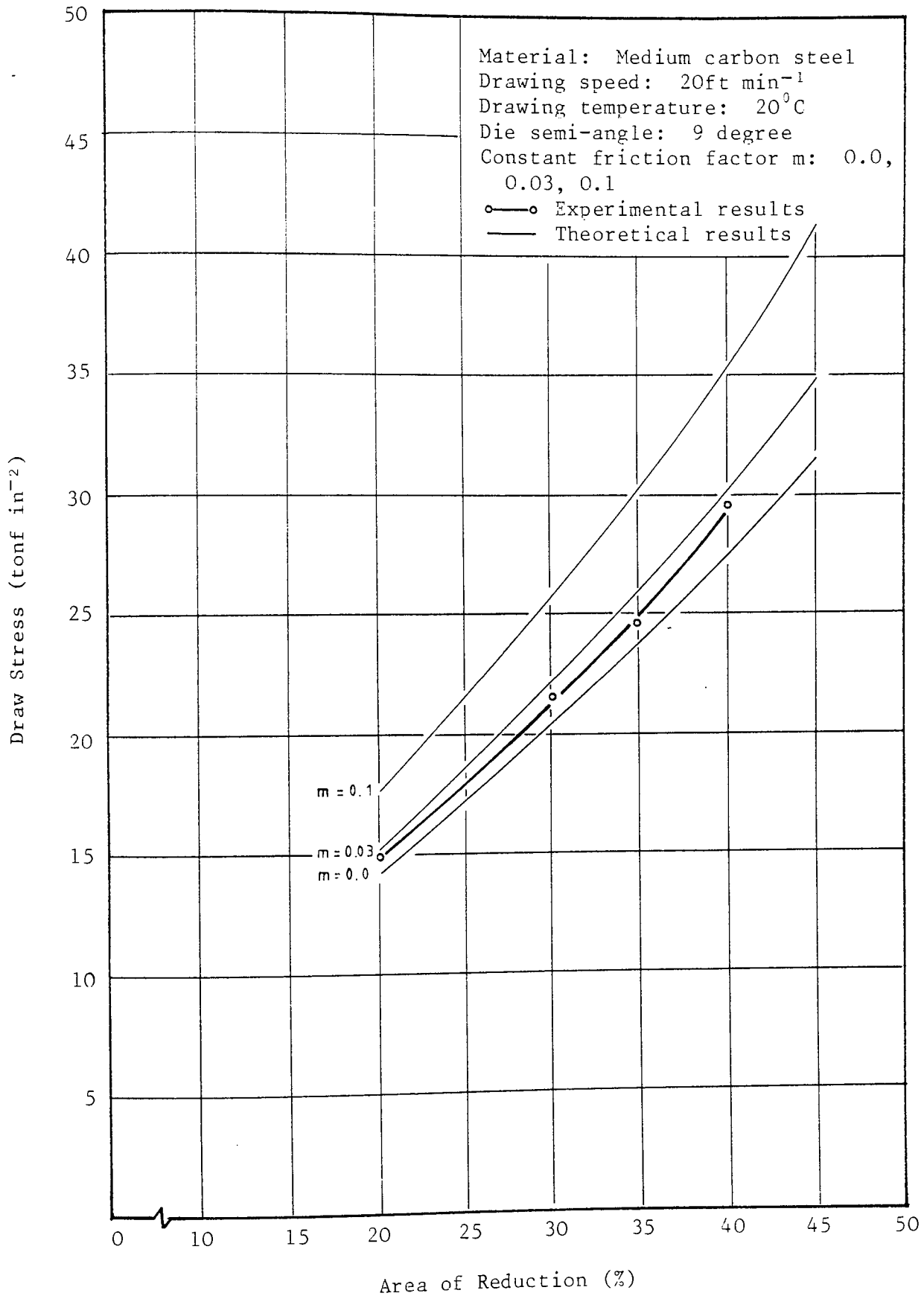


Figure 8.33: Comparison of experimental and theoretical results for different areas of reduction

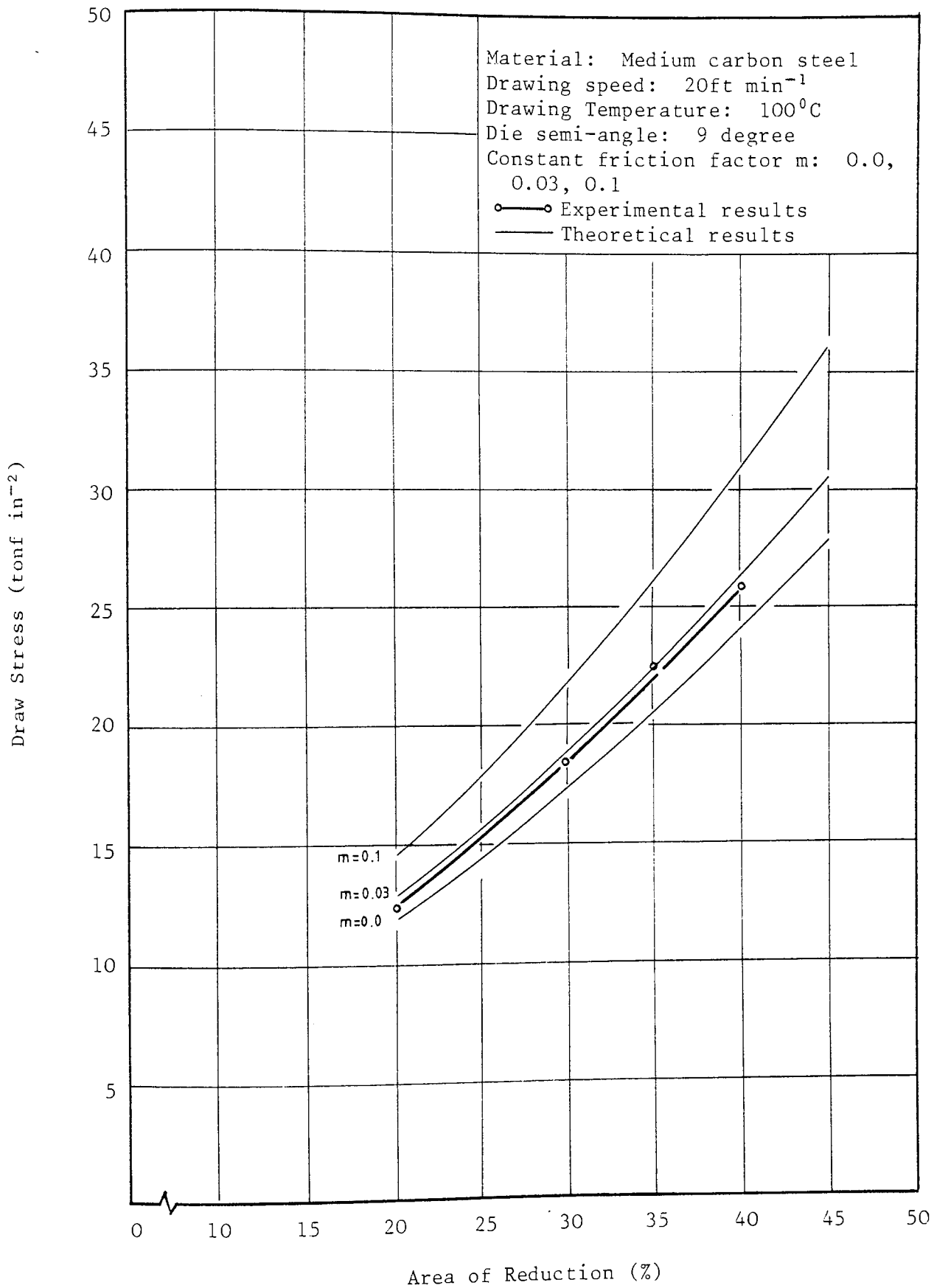


Figure 8.34: Comparison of experimental and theoretical results for different areas of reduction

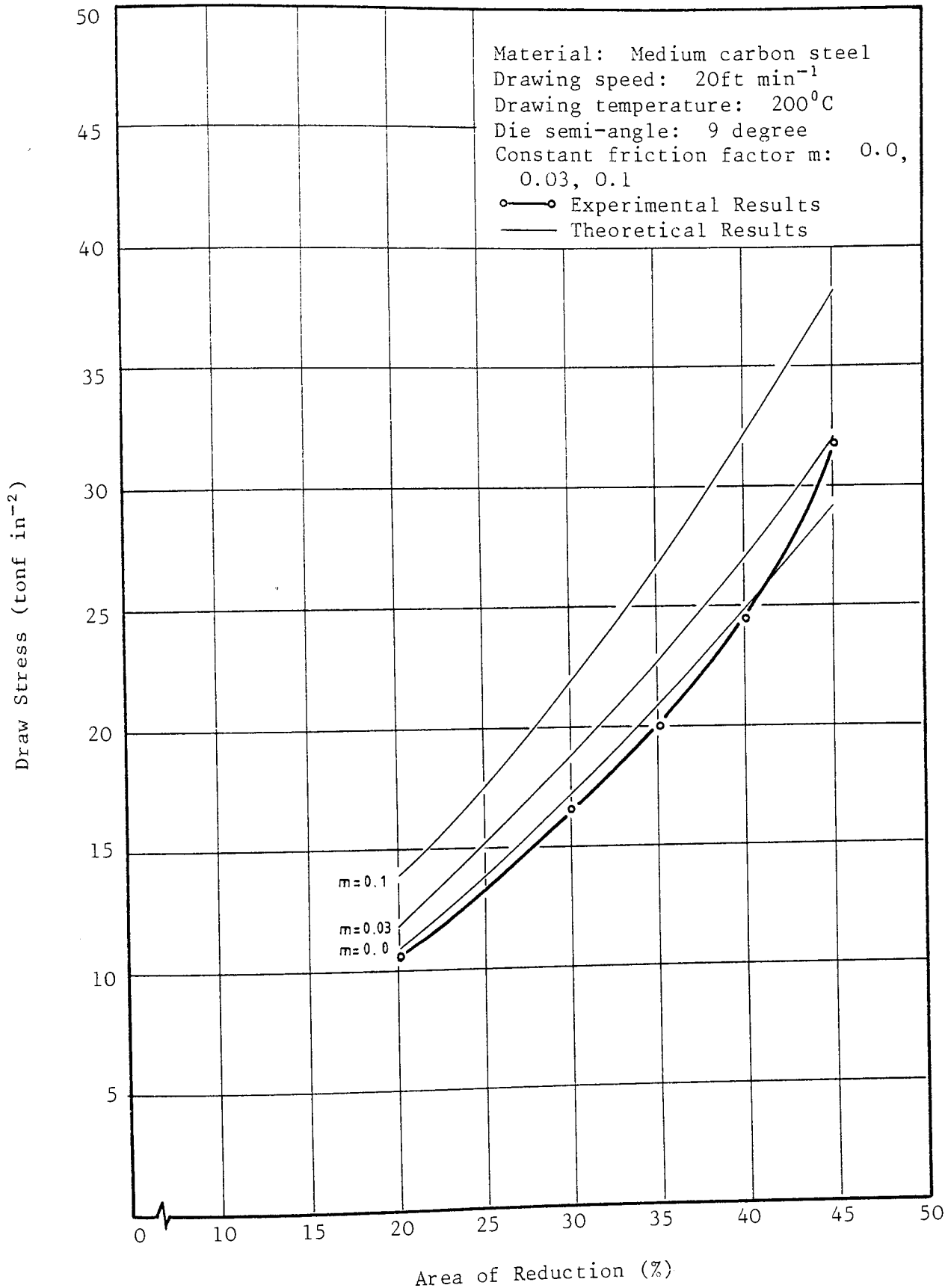


Figure 8.35: Comparison of experimental and theoretical results for different areas of reduction

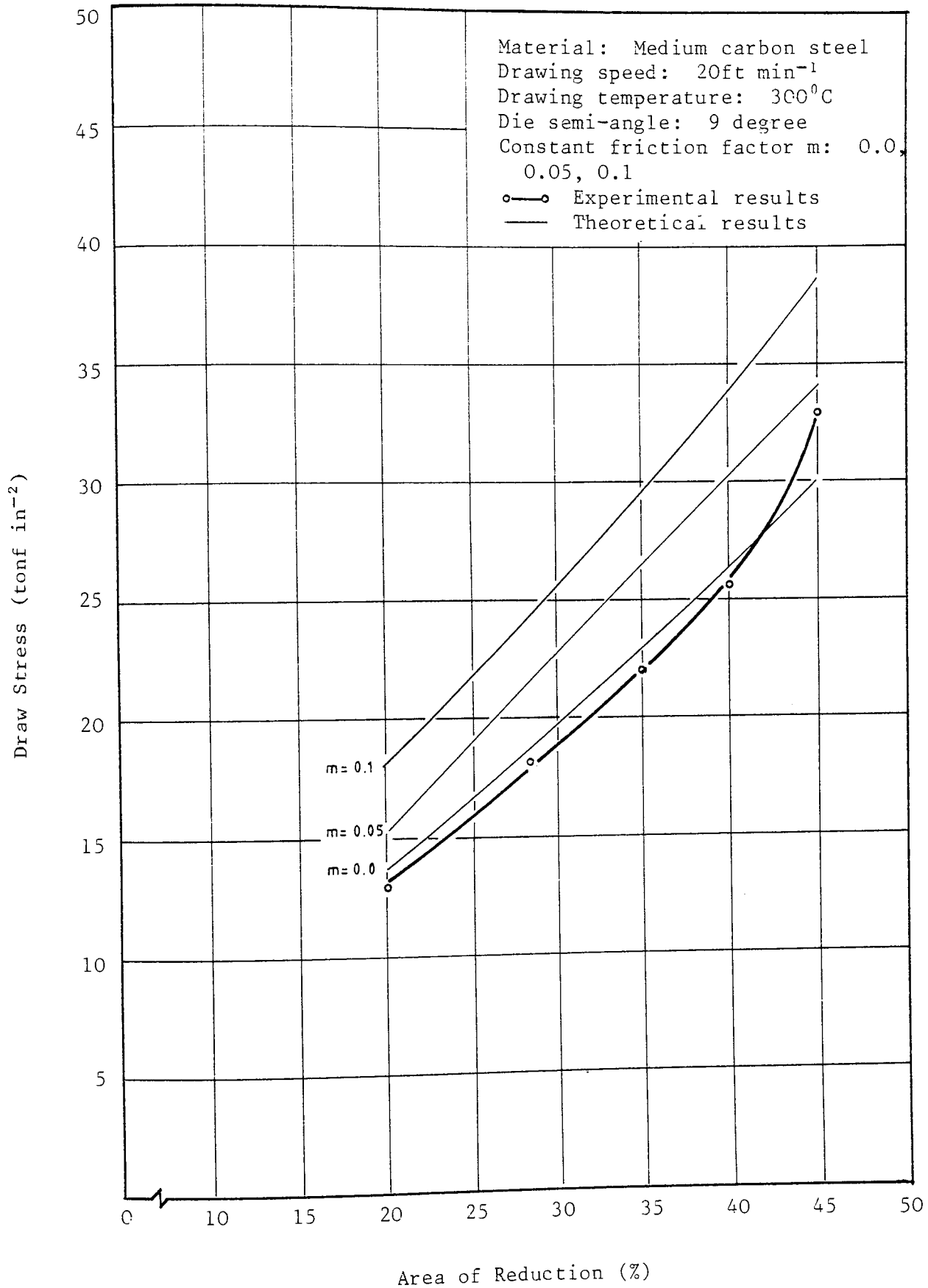


Figure 8.36: Comparison of experimental and theoretical results for different areas of reduction

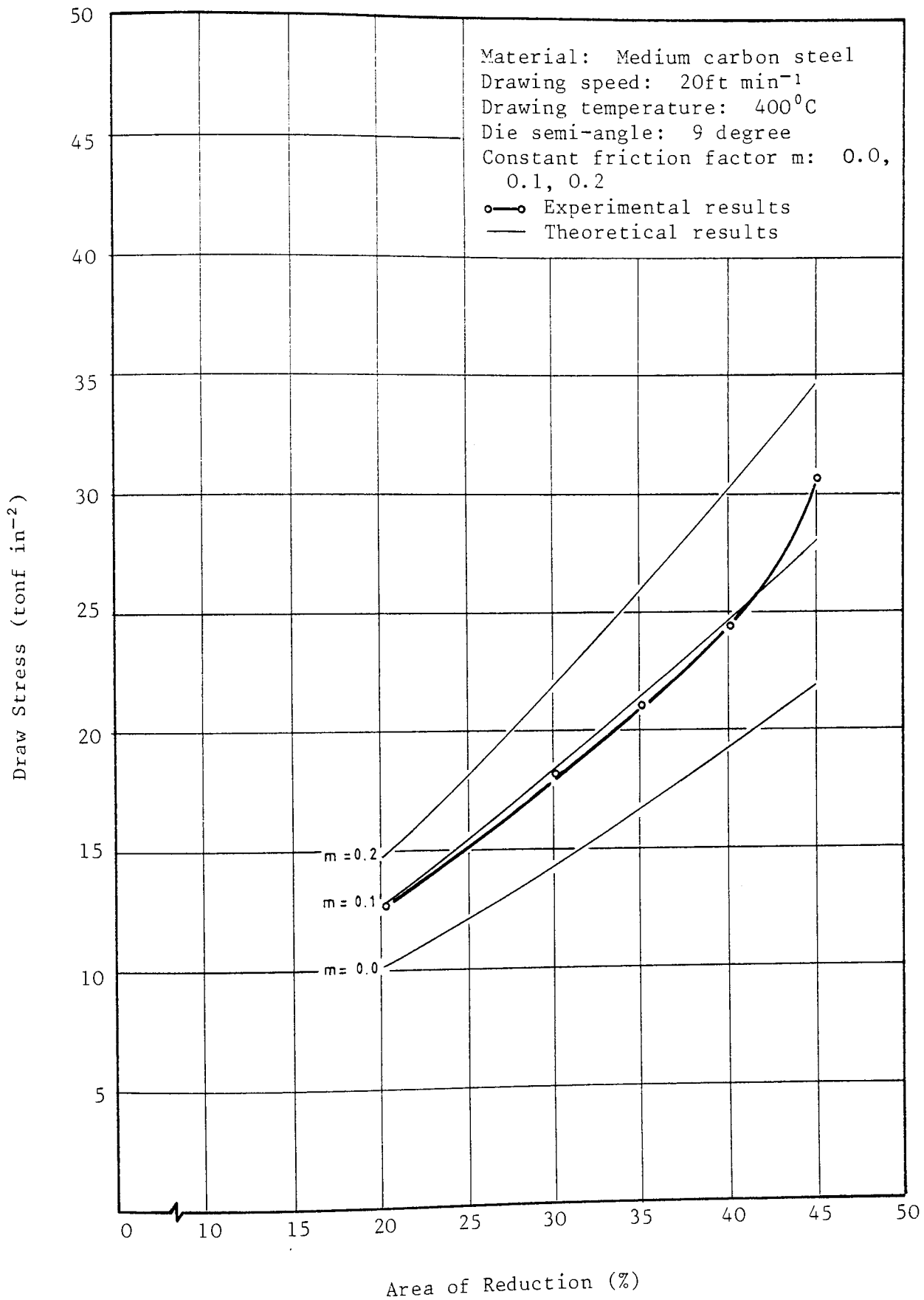


Figure 8.37: Comparison of experimental and theoretical results for different areas of reduction

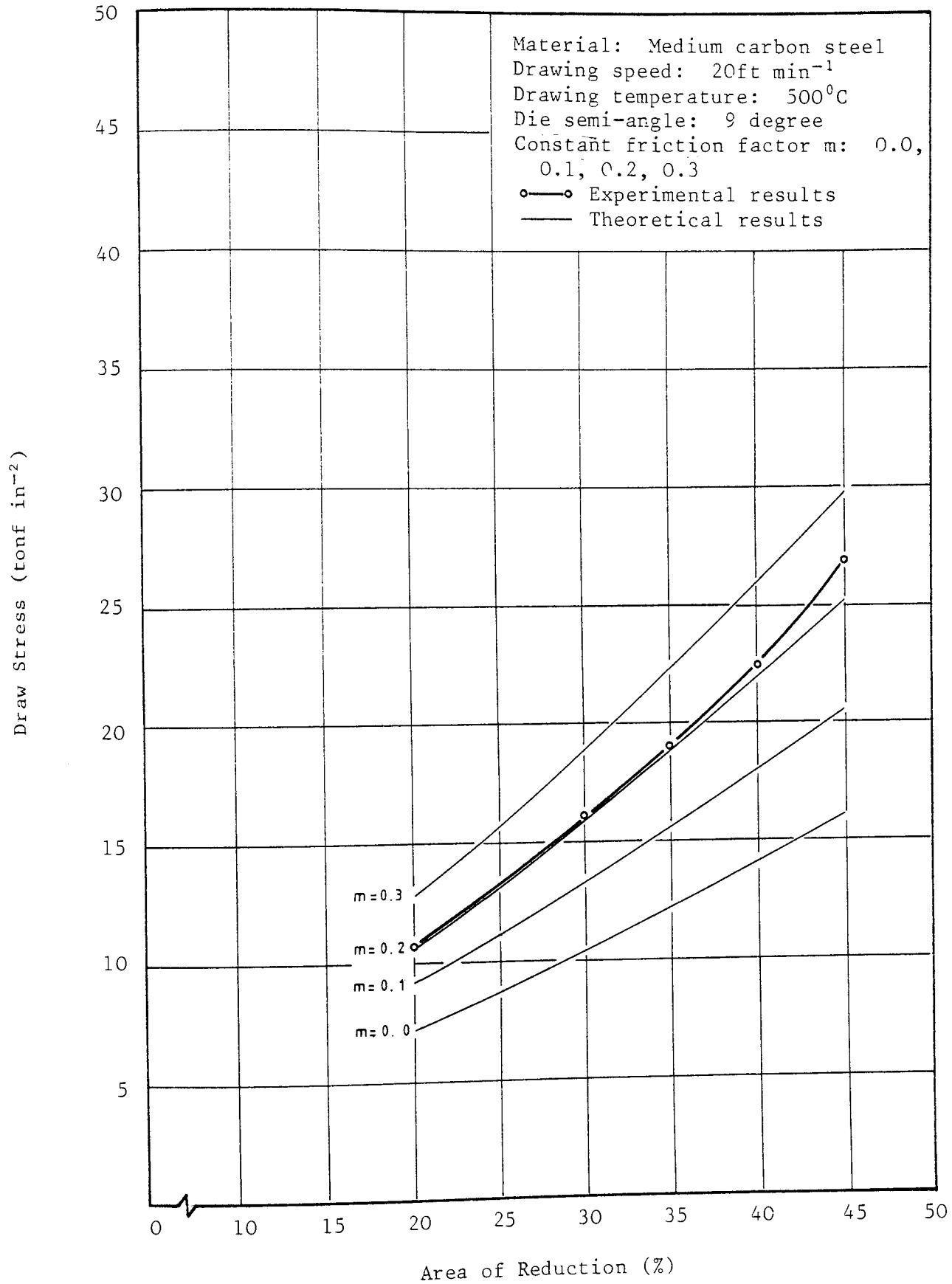


Figure 8.38: Comparison of experimental and theoretical results for different areas of reduction

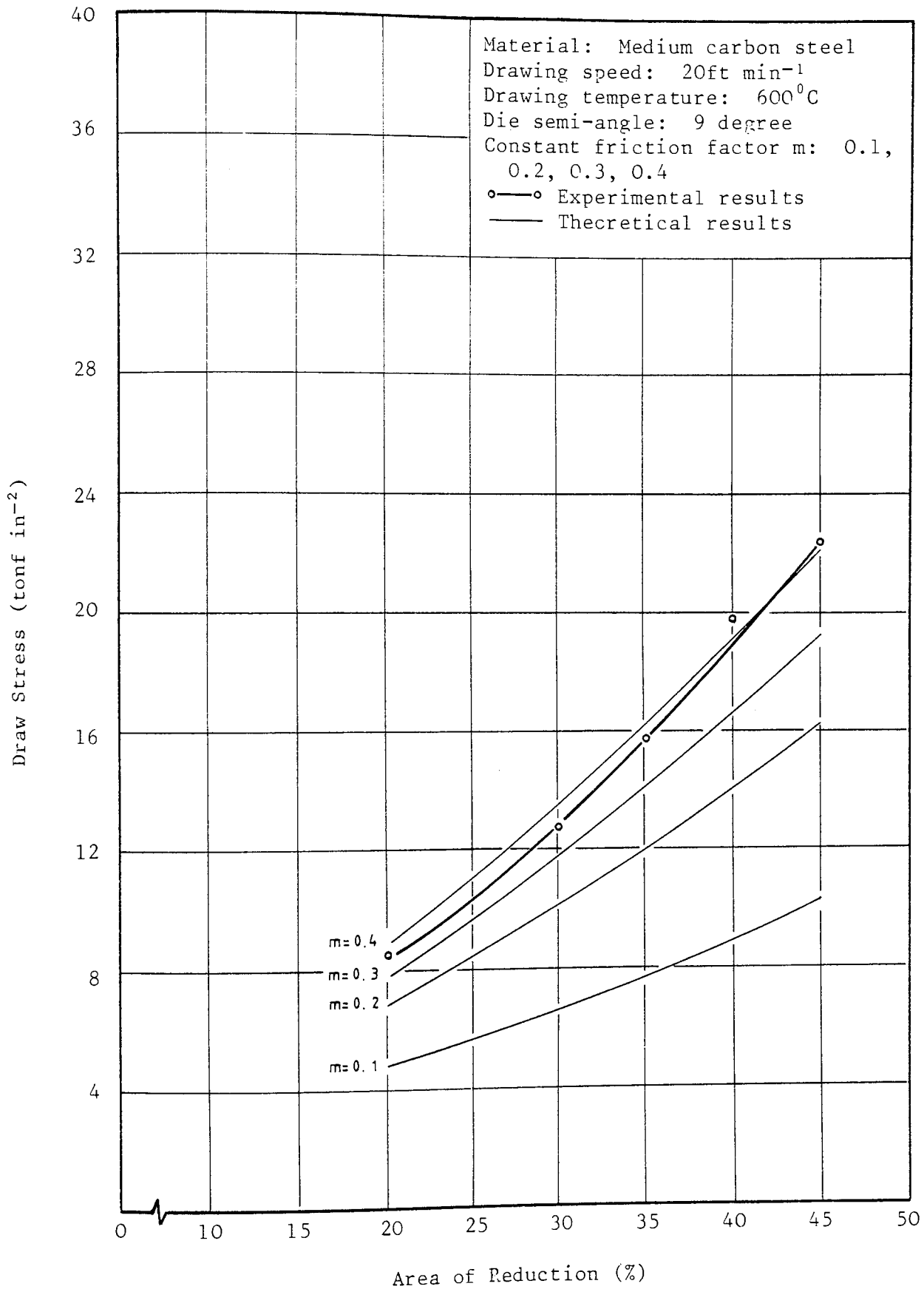


Figure 8.39: Comparison of experimental and theoretical results for different areas of reduction

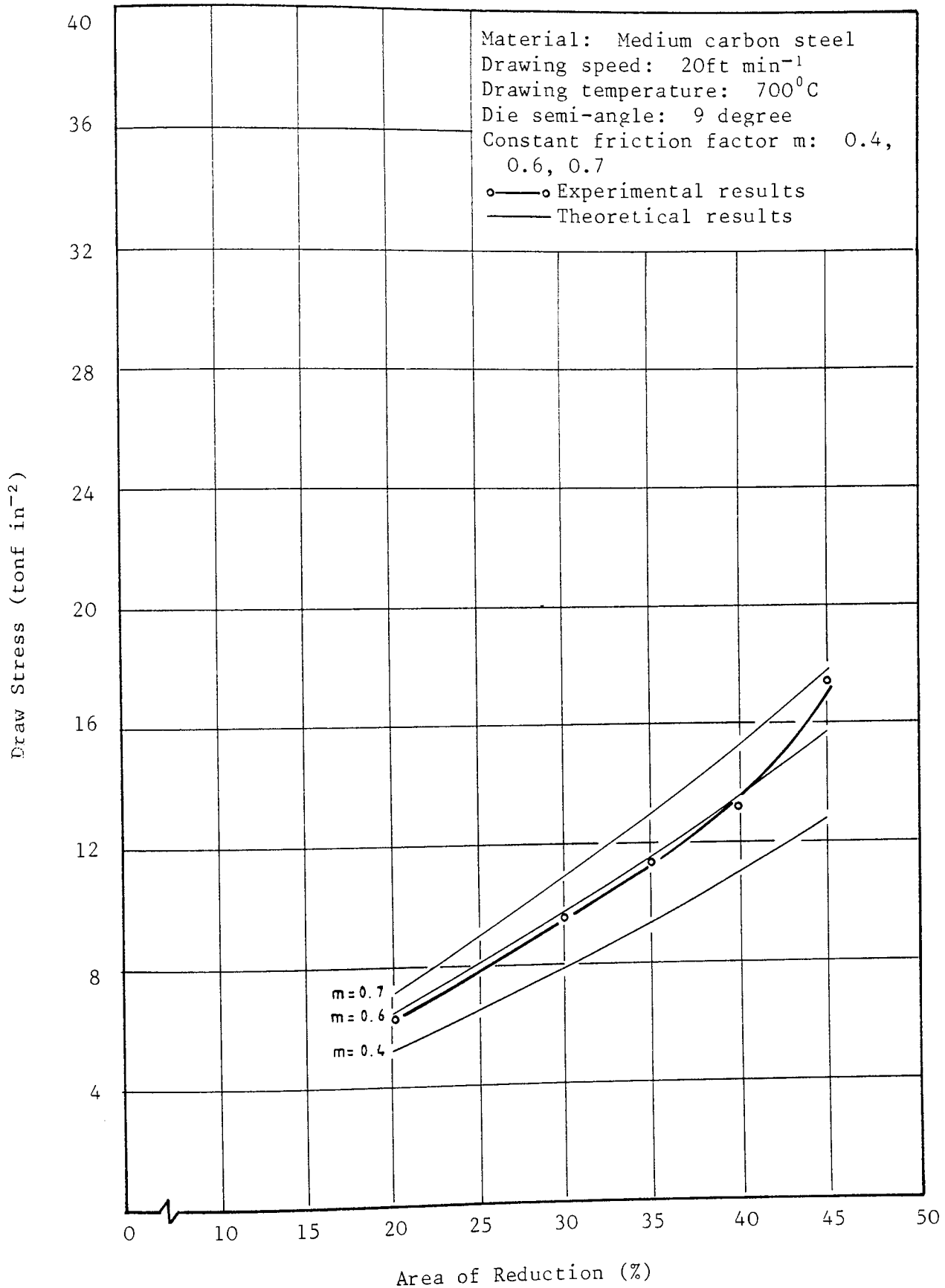


Figure 8.40: Comparison of experimental and theoretical results for different areas of reduction

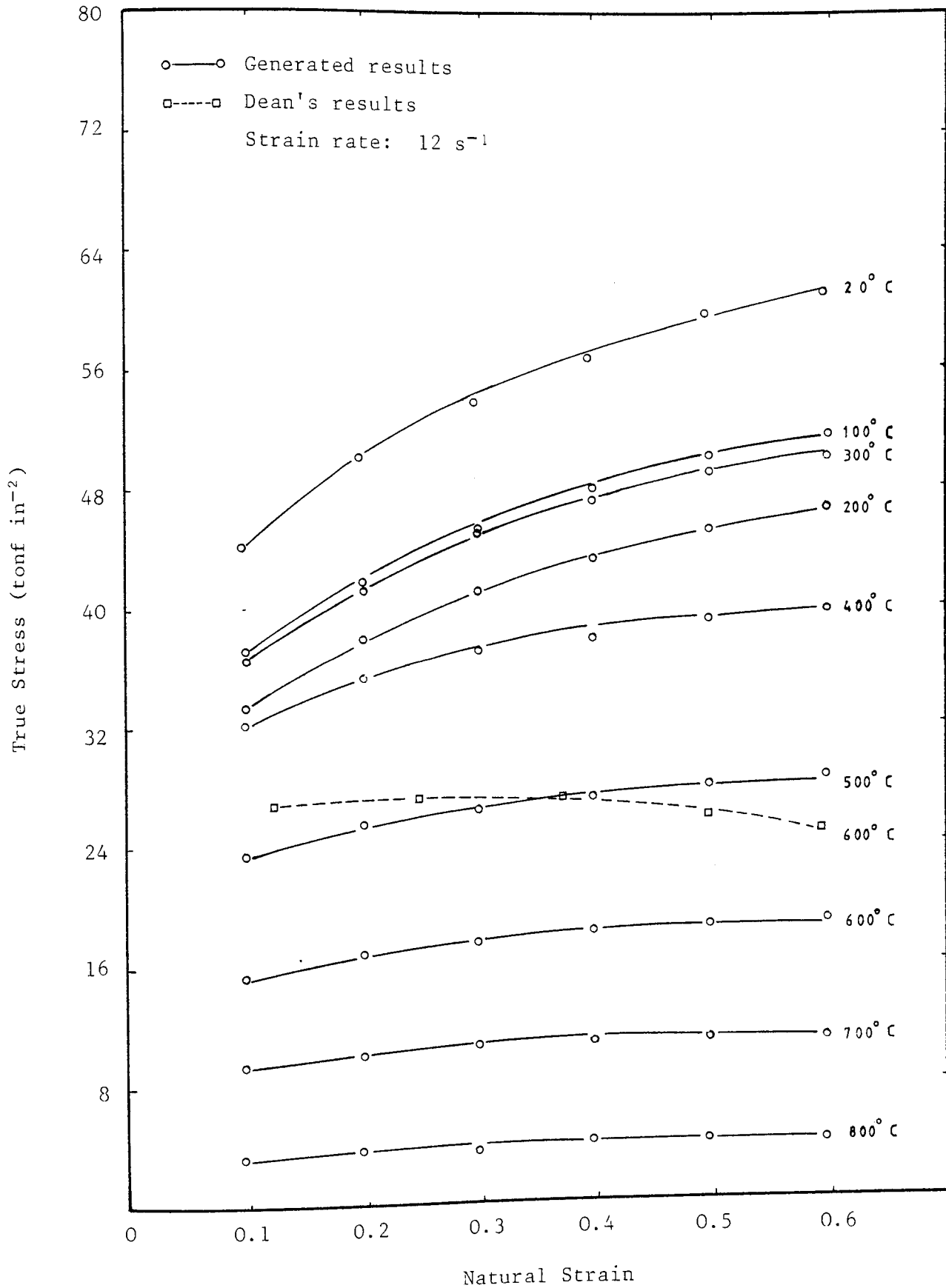
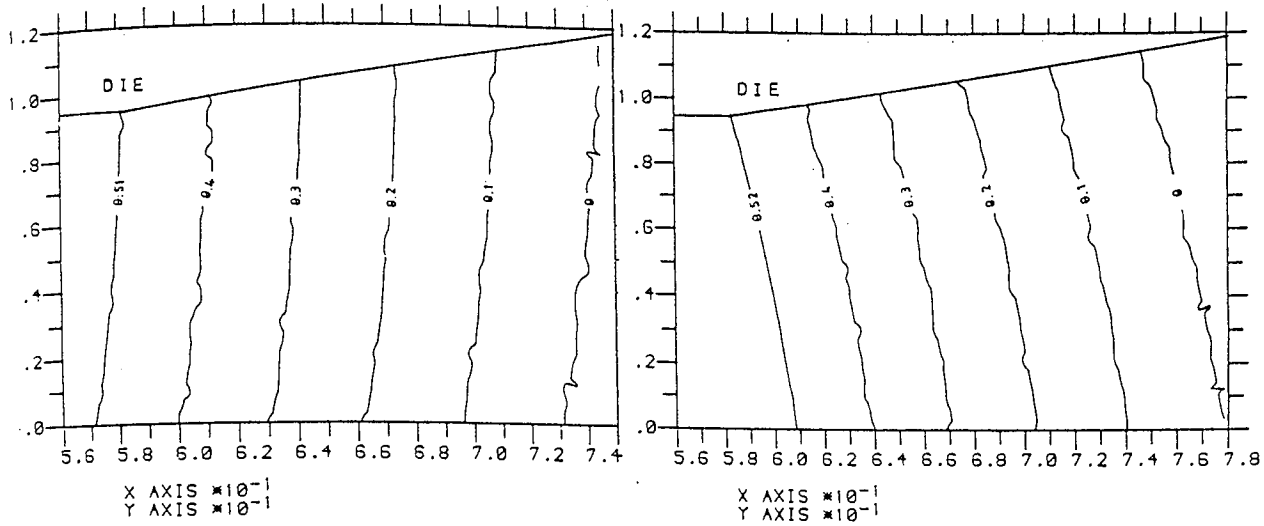
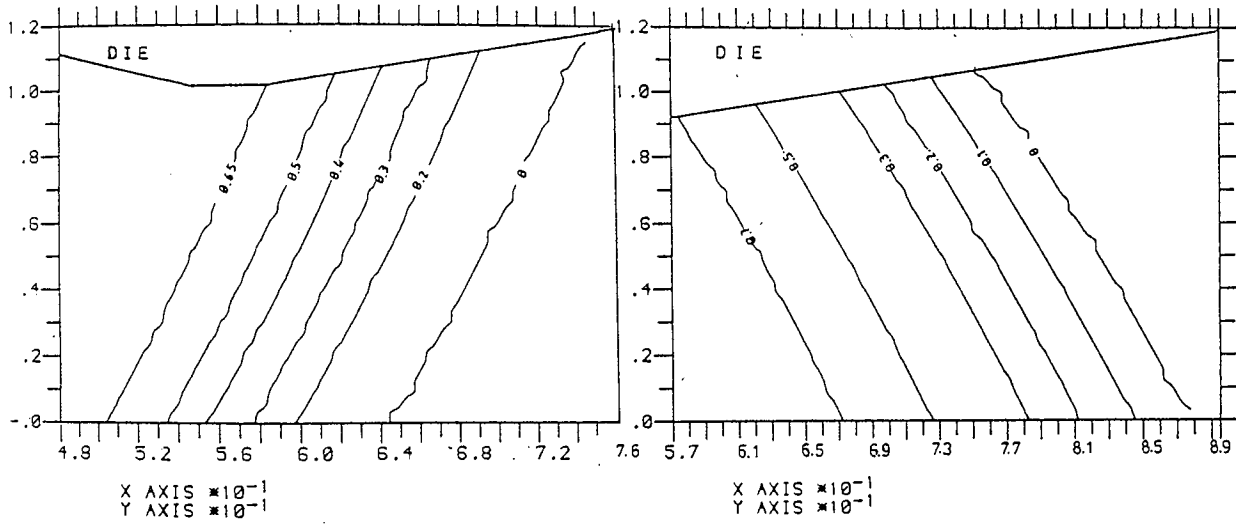


Figure 8.41: The generated stress-strain curves for medium carbon steel



i) $C = 0.2$

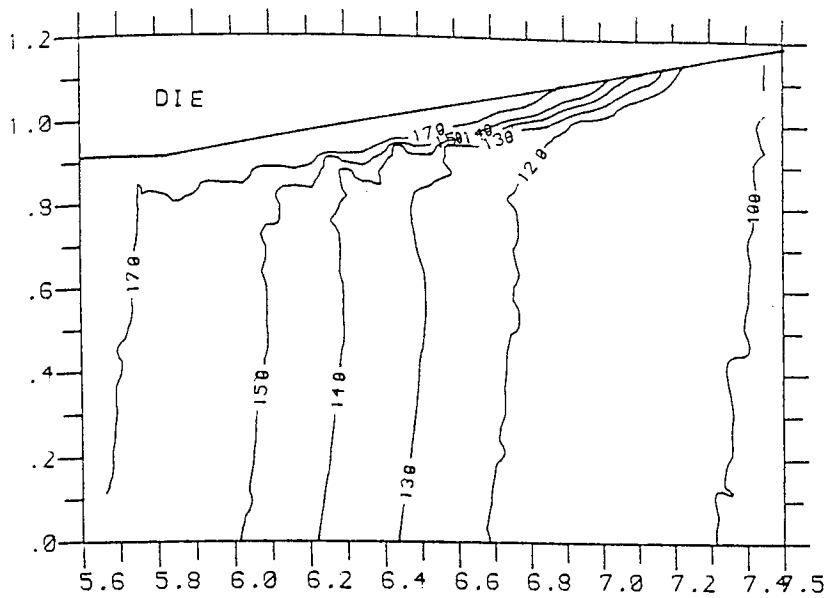
ii) $C = -0.2$



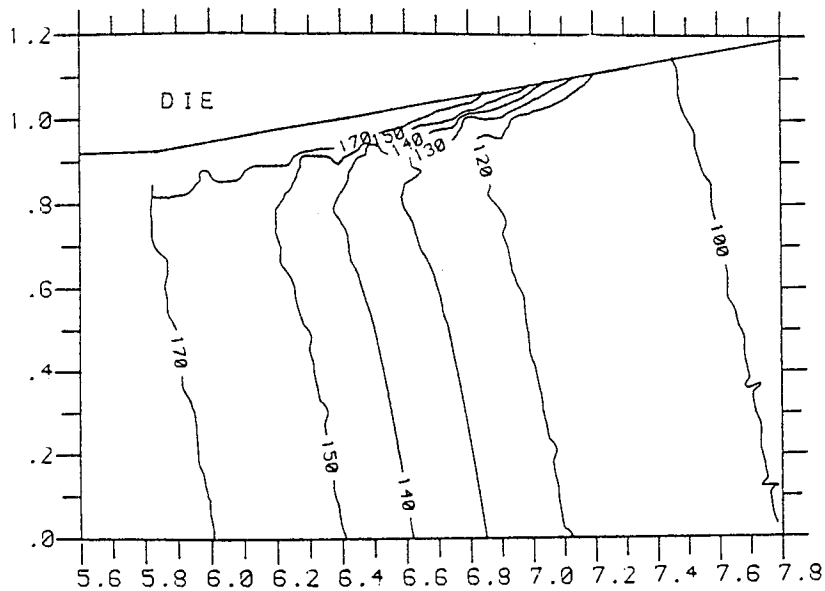
iii) $C = 1.0$

iv) $C = -1.0$

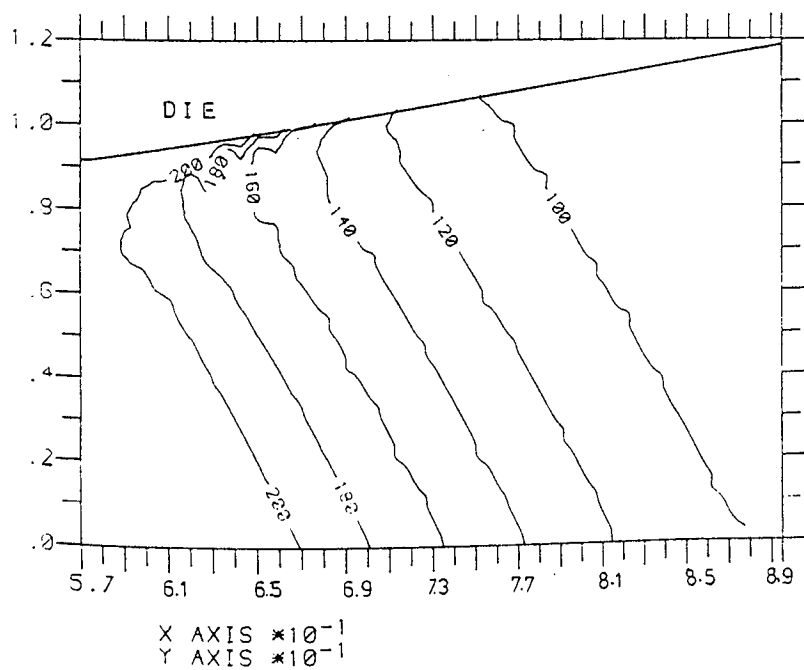
Figure 8.42: Strain distributions for different values of exponential constant c



i) $c = 0.2$

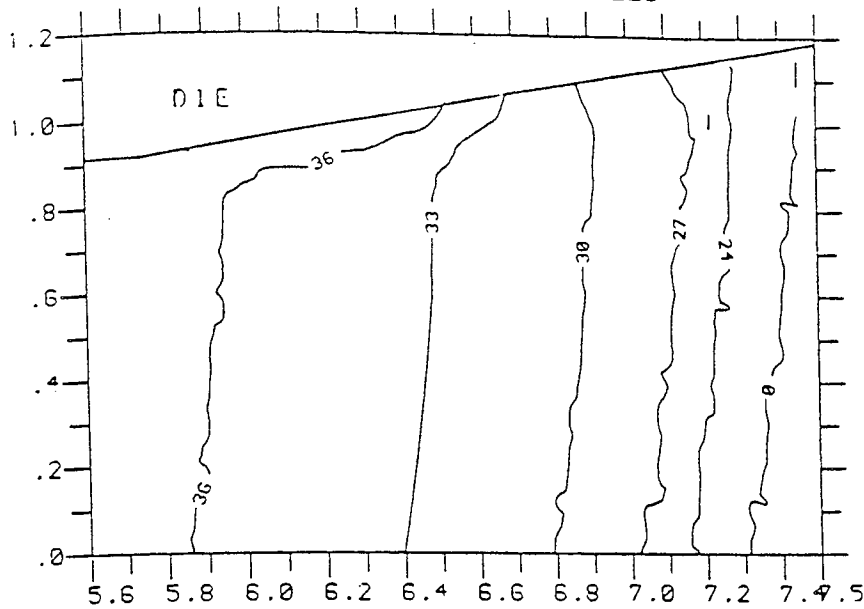


ii) $c = -0.2$

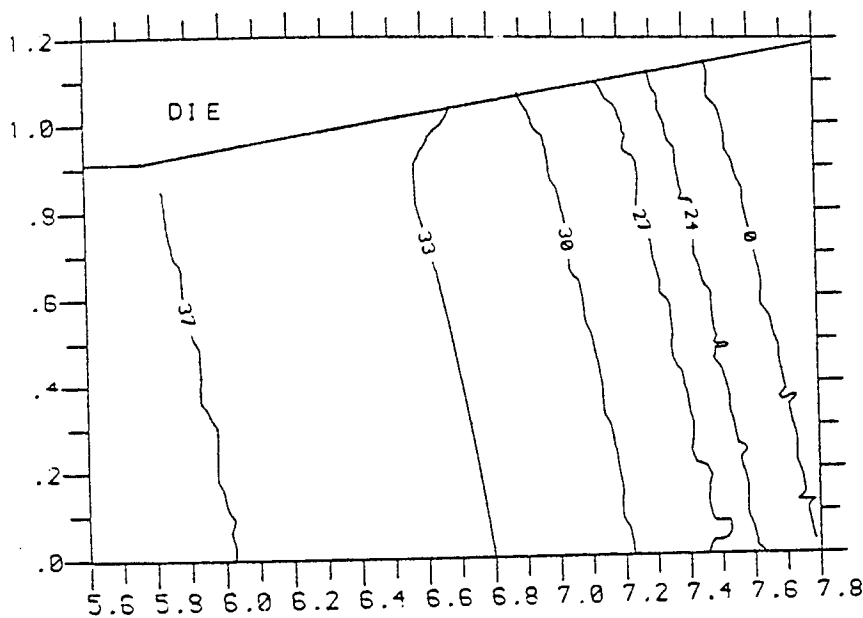


iii) $c = -1.0$

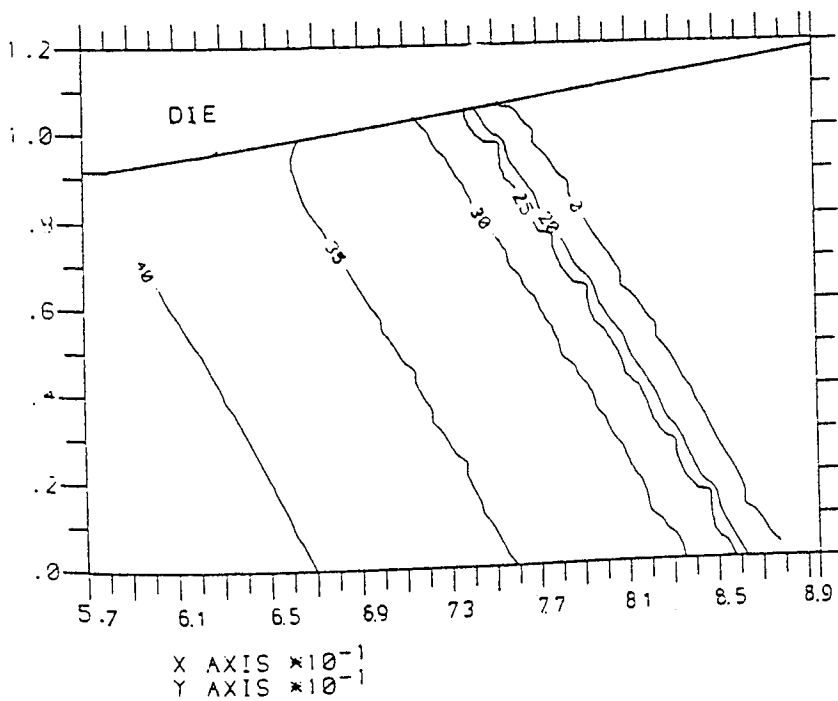
Figure 8.44: Temperature ($^{\circ}\text{C}$) distributions for different values of exponential constant c



i) $c = 0.2$



ii) $c = -0.2$



iii) $c = -1.0$

Figure 8.45: Flow stress (tonf in^{-2}) distributions for values of exponential constant c

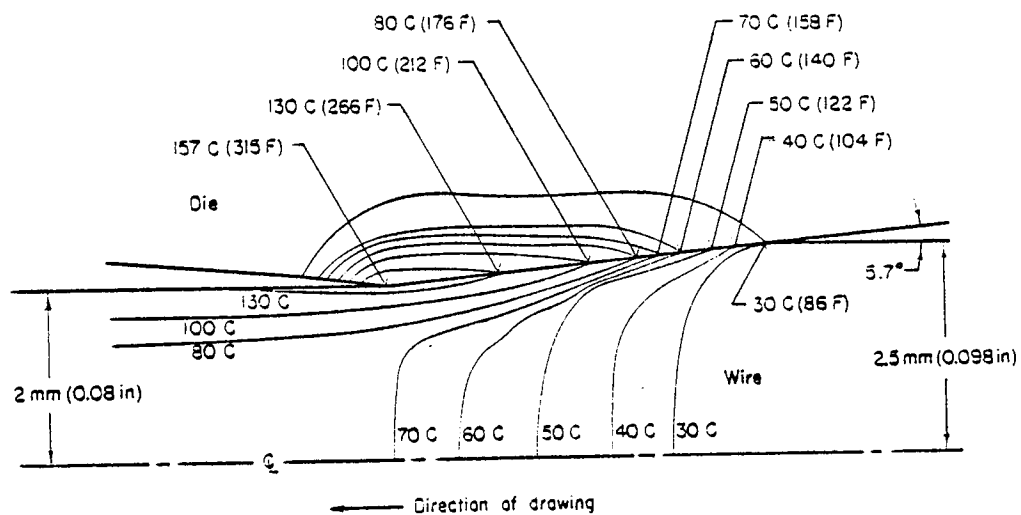
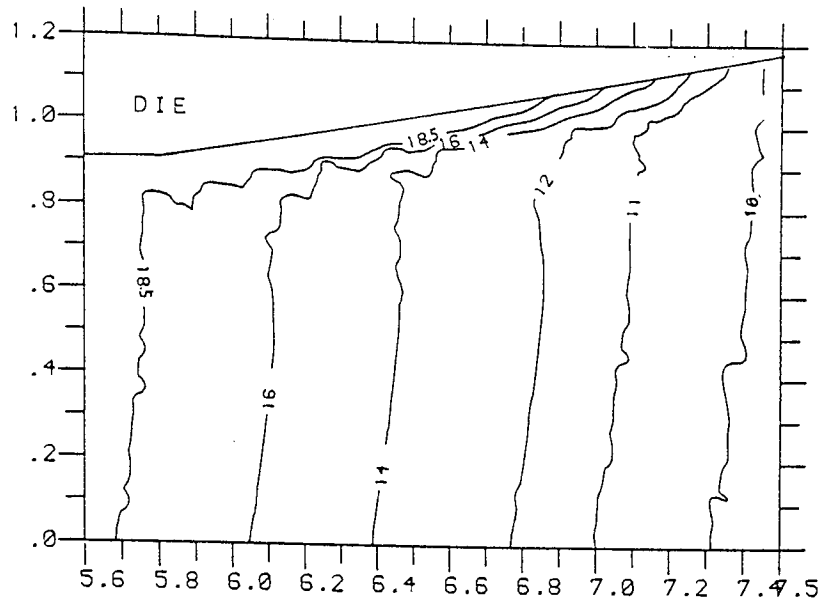
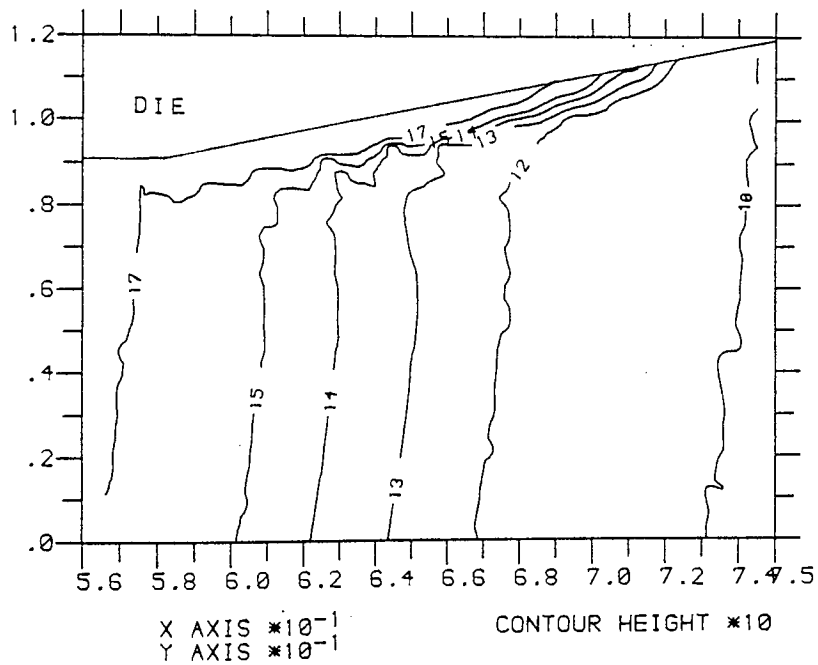


Figure 8.46: Temperature distribution in drawing steel wire from 0.2 in to 0.16 in with a speed of $196.8 \text{ ft min}^{-1}$, and coefficient of friction of 0.05. After Altan (7)

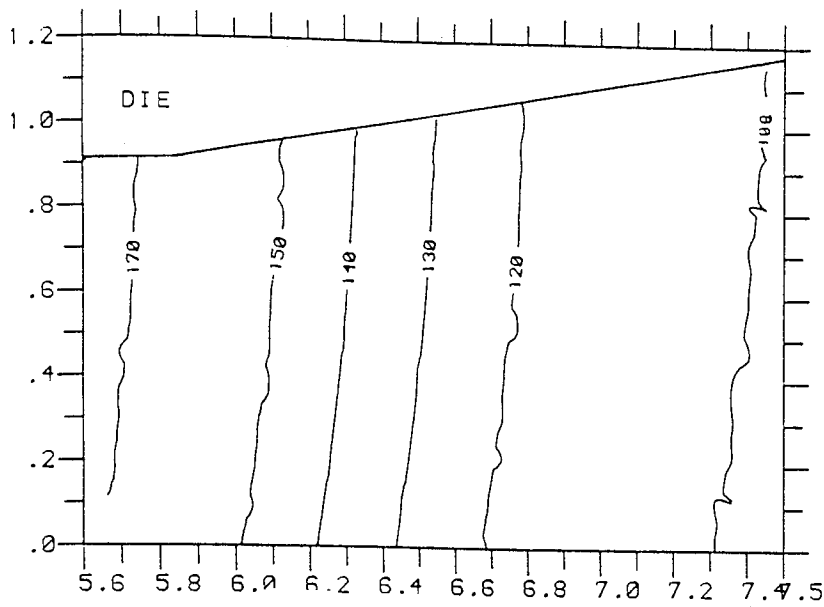


i) MEDIUM CARBON STEEL

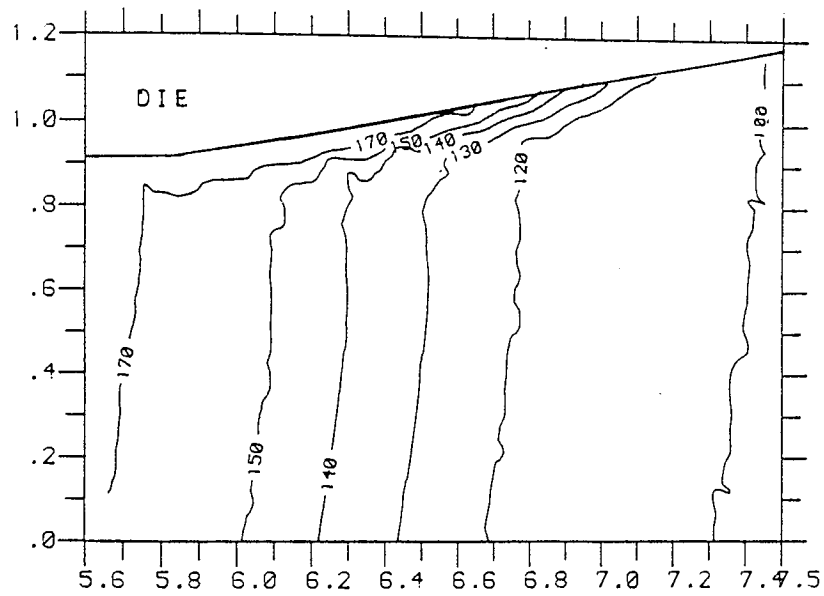


ii) MILD STEEL

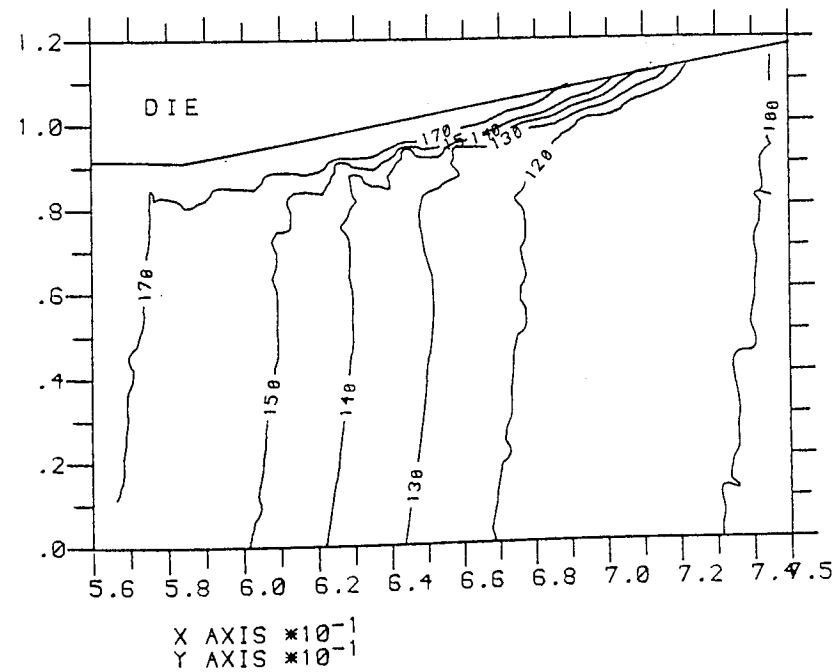
Figure 8.47: Temperature ($^{\circ}\text{C}$) distributions for different wire material



i) $m = 0$

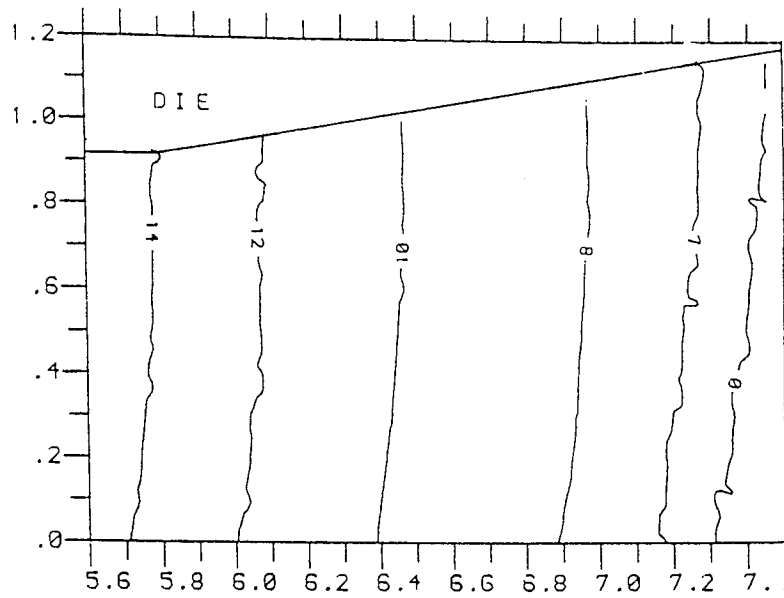


ii) $m = 0.05$

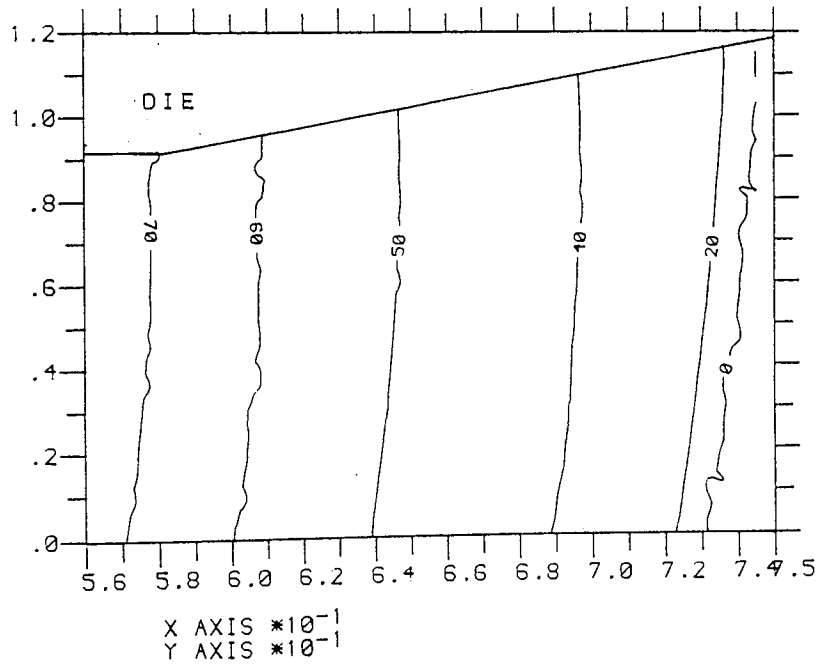


iii) $m = 0.1$

Figure 8.48: Temperature ($^{\circ}\text{C}$) distributions for different values of constant friction factor m

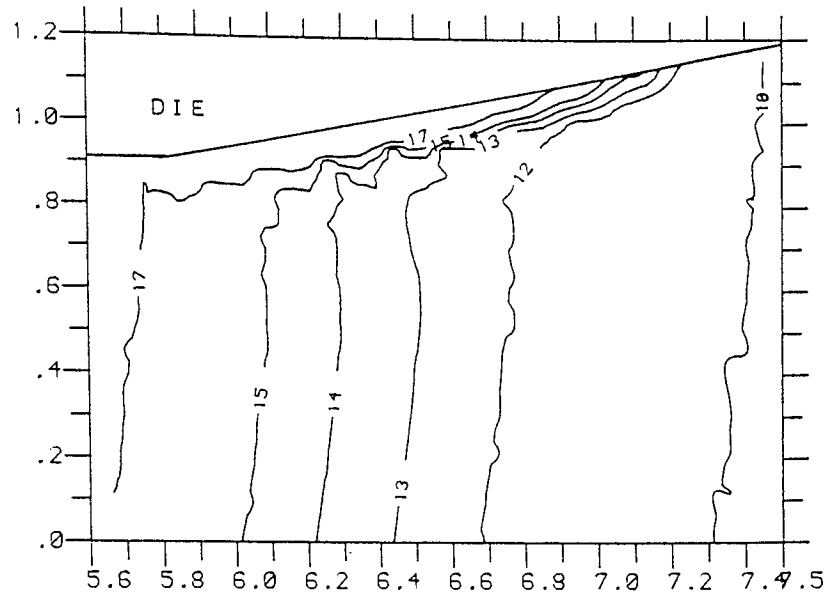


i) 20 ft min^{-1}

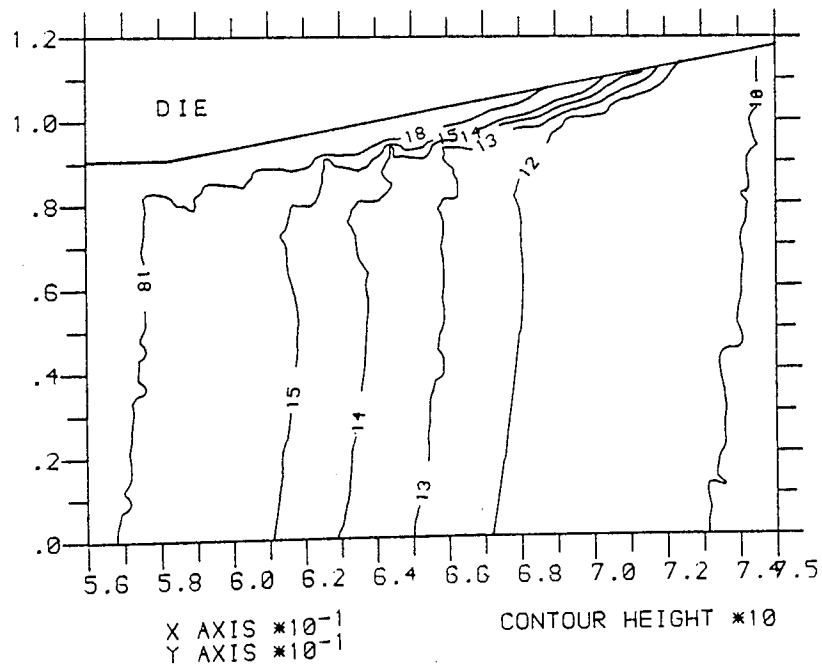


ii) 100 ft min^{-1}

Figure 8.49: Strain rate distributions for two different draw speeds

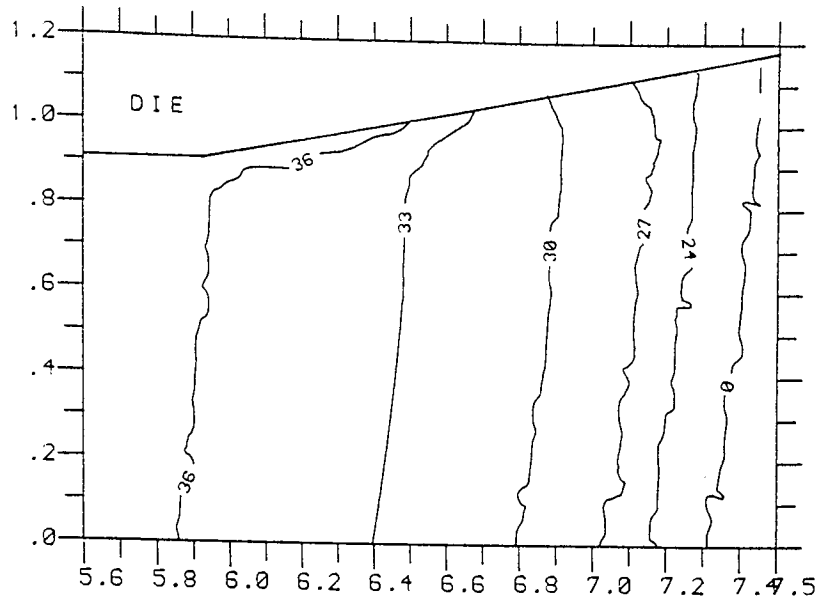


i) 20 ft. min^{-1}

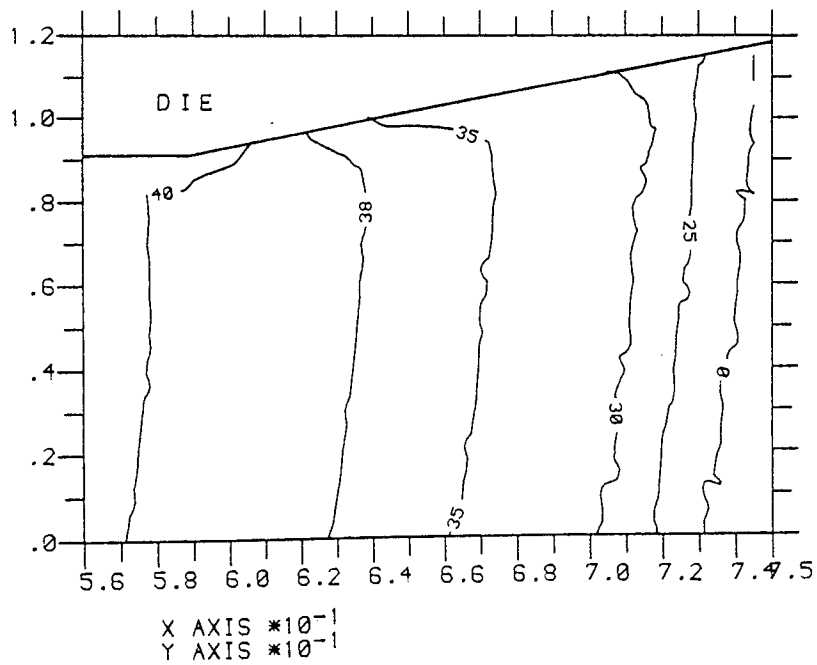


ii) 100 ft. min^{-1}

Figure 8.50: Temperature ($^{\circ}\text{C}$) distributions for two different draw speeds

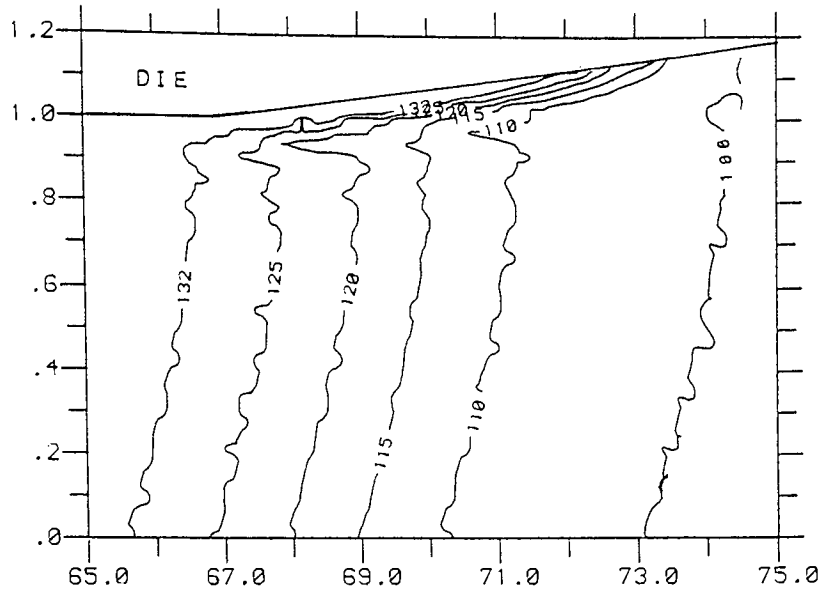


i) 2.0 ft. min^{-1}

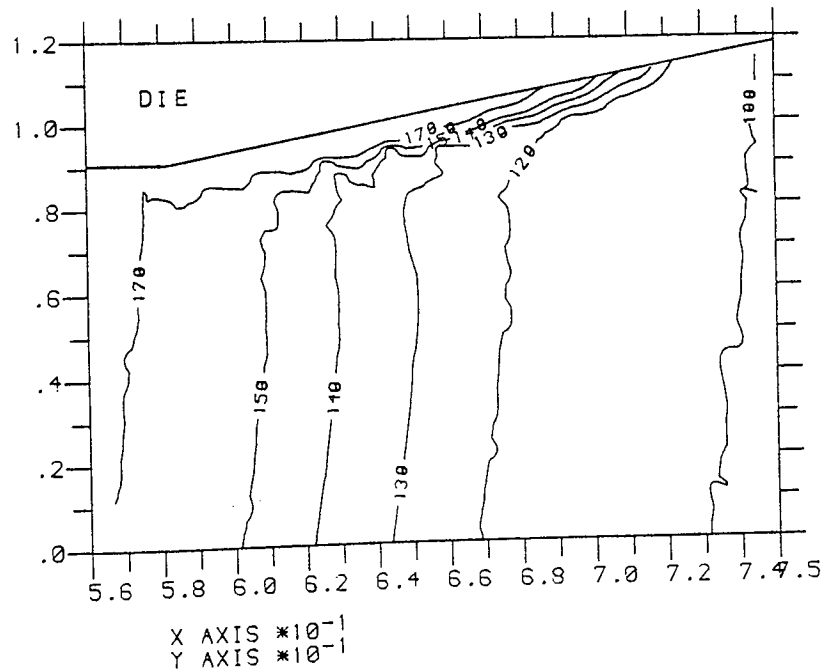


ii) 100 ft. min^{-1}

Figure 8.51: Flow stress (tonf in⁻²) distributions for two different draw speeds

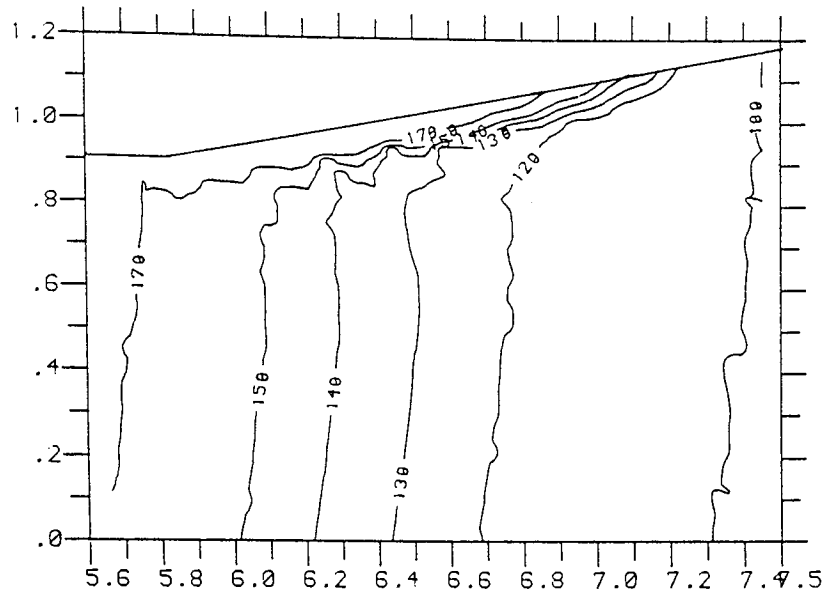


i) 20 % AREA REDUCTION

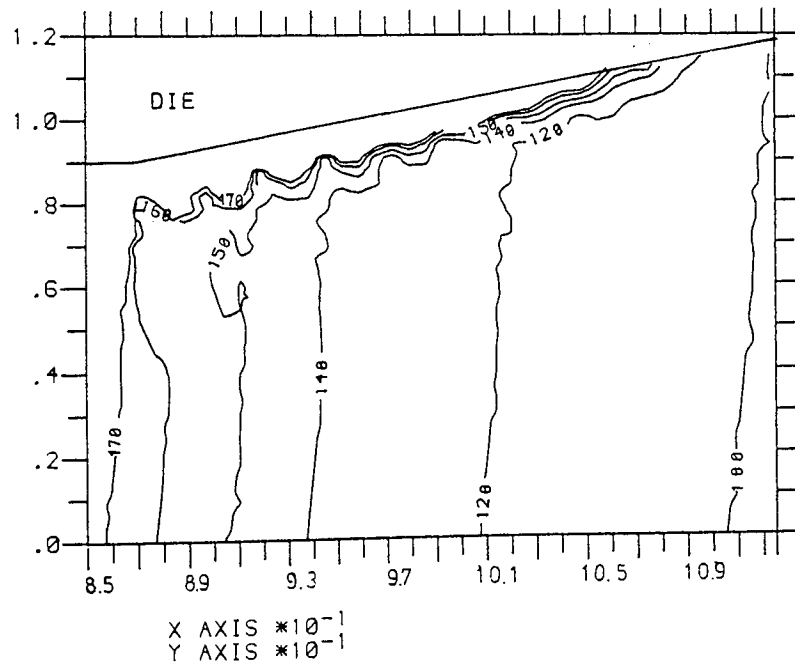


ii) 40 % AREA REDUCTION

Figure 8.52: Temperature ($^{\circ}\text{C}$) distributions for different areas of reduction



i) 9°



ii) 6°

Figure 8.53: Temperature ($^\circ\text{C}$) distributions for two different die semi-angle

CHAPTER NINE

CONCLUSIONS

IX. CONCLUSIONS

Since an extensive study has been conducted both experimentally and theoretically, on the drawing of a selection of wire at elevated temperatures and at a variety of reductions of area, and since the process and lubrication were developed specifically for the research programme, the following conclusions can be drawn:

1. The art of wire drawing at elevated temperatures had been successfully developed in the laboratory.
2. Mild steel and medium carbon steel wires were drawn up to 700°C and 45% area of reduction without rupture. M2 'high speed' steel wire which could not be cold drawn for a 40.5% area of reduction was successfully drawn at temperatures above 300°C . In general, the experimental draw stress at elevated temperature is lower than that at room temperature, for corresponding draw conditions.
3. The draw stress and surface finish were noticeably affected by the lubricant; the draw stress was reduced when a 'better' lubricant was used.
4. For mild steel and medium carbon steel wires, the experimental draw stress decreased as the temperature increased up to about 200°C . In the temperature range of 200°C - 400°C the draw stress increased with temperature. This is attributed to the strain-ageing phenomenon. Above 400°C , the draw

stress decreased rapidly with temperature.

5. Low ductility was observed for M2 'high speed' steel in the temperature range of 100°C - 400°C .
6. In general, the process of wire drawing at elevated temperatures was successfully analysed both theoretically and experimentally.
7. There was satisfactory agreement between the theoretical and experimental results on medium carbon steel for draw temperatures below 600°C . At higher temperatures, the velocity-modified temperature concept does not seem to relate well.
8. Although the results for mild steel could not be compared under identical conditions, nevertheless, the theoretical results showed a similar trend.
9. Logically accountable trends were observed in the derived upper bound curves which supports the validity of the theoretical solutions.
10. The theoretical results showed that:
 - a) An increase in the constant friction factor does not affect the strain-ageing region. Increases in the area of reduction narrowed the strain-ageing region.

- b) The draw speed affects the strain-ageing region; as the speed increases the strain-ageing region shifts towards the higher temperature. Thus, the effects of temperature and strain rate on the flow stress must be considered together.
 - c) The optimum die semi-angle was affected by area of reduction, constant friction factor, temperature and speed of drawing.
 - d) Frictional resistance at the die-wire interface was generally high (this was supported by the presence of a wear ring at die entry) and as the temperature was raised the frictional resistance increased.
11. The isothermal graphs showed that:
- a) In general, an increase in the following variables will increase the temperature at exit
 - i) the strength of the material
 - ii) the area of reduction
 - iii) the exponential constant c , if c takes positive valuesIf c is negative, then a decrease in c will increase the temperature at exit.
 - b) An increase in the constant friction factor will increase the temperature at the die-wire interface. As the die

semi-angle decreases the temperatures developed at the die-wire interface increases.

c) The temperature for mild steel and medium carbon steel was highest at the die-wire interface but it decreases towards the die-axis.

12. The proposed theory could also predict the effects of a change in speed on the draw stress. However, this has not been verified experimentally.

13. The process of drawing wire at elevated temperatures is technically feasible. Since the draw stress can be predicted within reasonable accuracy, the work can be scheduled effectively on bull blocks.

CHAPTER TEN

SUGGESTIONS FOR FURTHER WORK

X. SUGGESTIONS FOR FURTHER WORK

This research is one of the first into the mechanics and practice of wire drawing at elevated temperatures. There is a necessity for further investigations and original work to gain a wider and deeper understanding of the process and its mechanics, and thus to enable the industry to benefit from new technological developments.

In the light of the experience gained and conclusions formulated from this research programme, further work is suggested in the following directions:

1) Experiments with different wire materials

The draw material used in this project was limited to mild steel, medium carbon steel and M2 'high speed' steel. It would be valuable to extend the draw technique to austenitic and stronger ferrous and non-ferrous materials. Also, since the workpiece diameter was 6 mm and since there is interest in drawing fine wire or filaments at elevated temperatures it is suggested that research be initiated in that valuable area.

Non-ferrous materials such as aluminium bronze, niobium bronze, some nickel alloys and some brasses are difficult to cold draw and require frequent interstage annealing operations. Consequently, it may well be advantageous to draw these materials at elevated temperatures. Other forms of heating, such as resistance heating might be more suitable for heating non-ferrous

materials but much work needs to be done to advise on the appropriate method of heating the wire.

- 2) Experimentation with 'better' die materials and lubricants, higher draw temperatures and areas of reduction, and a range of draw speeds.

The draw stress is affected by: die material and design, lubricant, draw temperature, area of reduction and draw speed. Thus, by an appropriate combination of the various variables, the optimum draw condition can be established.

The chromium carbide and 'Syalon' dies used in the experimental work were unsuitable or not wholly suitable for elevated temperature wire drawing. Crack lines were formed on the chromium carbide dies, and wear at die entry was clearly visible on the 'Syalon' dies which in other respects was promising. It is felt that other forms of silicon nitride might prove to be a 'better' material. The wear could be reduced also by improvements in the lubricant. It was shown earlier that a 'better' lubricant will decrease the draw stress.

In this research, the wires were drawn up to 700°C with a constant speed of 20 ft min^{-1} . It would be valuable industrially and academically to see the effects of temperature and strain rate on the draw stress by drawing wires at different speeds and at a range of temperatures.

It is felt that it may be inadvisable to draw the wires at very much higher temperatures because: the wire is subjected to tensile stress and will neck easily if there is insufficient

cooling, and phase transformation may occur giving a higher draw stress.

- 3) Experimenting with redrawing the wires at elevated temperatures without interstage annealing.

If the wires could be repeatedly redrawn without interstage annealing, production routes and costs would be further reduced and the technology of in-line processing substantially advanced.

- 4) Developing the techniques of warm drawing of tubes, which are difficult-to-cold draw.

The warm drawing of stainless tubes has been studied elsewhere⁽⁶¹⁾. The draw stress was reduced to 60% - 70% of that in cold tube drawing.

- 5) Production of wires with a unique combination of physical and mechanical properties

There is a continual demand for wire possessing a wider range of mechanical properties than those currently catalogued. Some of these properties, which are unobtainable by cold-drawing, can be achieved by drawing wire at the specific temperatures and area reductions which give the desired metallurgical properties. Heat treatments can also be used in conjunction with elevated temperature wire drawing to yield microstructures having high tensile properties which are not possible with cold drawing alone.

- 6) Refinement of the proposed theory and extending it to include other wire materials.

Improvements in the theoretical analysis could be made by:

- a) generating stress-strain data of the actual wire material over appropriate temperature and strain rate ranges. Attempts could then be made to relate the stress, strain, strain rate and temperature mathematically. The formulae for relating the four variables would probably be different for different wire materials

- b) taking into consideration heat conduction, back tension and the effects of the land.

The cooling of the die casing and the wire at exit should also be taken into consideration. This would give better estimates of the temperature and flow stress distributions in the deformation zone.

The estimation of the temperature distribution could also be extended into the die region.

- c) improving the velocity-modified temperature concept
 - d) the use of more realistic shear surfaces and velocity flow, eg those seen in slip-line field solutions.
- 7) The value of the constant friction factor for specific draw conditions could be established by suitable techniques, such

as the rotating die method. This will provide a check on the accuracy of the theoretical analysis.

CHAPTER ELEVEN

APPENDICES

ACKNOWLEDGEMENTS

To my supervisor, Professor D H Sansome, I wish to express my thanks for his encouragement, guidance and patience throughout the course of this work.

I am grateful to the Science^{and} Engineering Research Council for their financial support and Mr N Marsh for reading through the manuscripts.

I would also like to thank:

Members of the technical staff in the Department of Production Technology and Production Management for their assistance, especially Messrs G M Jones, T Rudge and P McGuire

Mr T Hopper of Acheson Colloids, Mr N Cother of Lucas Industries and Mr Bolam of Peter Stubs Company for the supply of lubricants, dies and wire material

Dr Hashmi of Sheffield Polytechnic for making the arrangements to use the cam plastometer.

I am indebted to Mrs J Neale for typing this thesis and Miss S N Lau for helping in some of the drawings.

To my brothers and sisters in Christ who have given their encouragement and support during this work; space does not allow me to mention them all, but to them also I wish to express my thanks.

Finally, I wish to express my deep appreciation to my mother, brothers and sisters for their understanding, encouragement and unfailing support throughout this work.

APPENDIX A2

Supporting Papers

Two papers entitled:

- 1) 'A review of the warm drawing of wire'

Presented by N H Loh and D H Sansome at the Fine Wires International Conference, 30th-31st October 1980, Aachen, West Germany.

- 2) 'Drawing of wire at elevated temperatures'

Wire Industry, 1983, March, 148-153

The above paper was also presented earlier at the Wire Asia 82 Conference held in Singapore, 4th-8th October 1982, sponsored by the International Wire and Machinery Association.

APPENDIX A3

Supplementary Proofs

A3.1 Derivation of Strain Rates in Terms of the Velocity Components

From Equation (9),

$$\mu_{\rho} = V_1 \left(\frac{\rho_o}{\rho} \right)^2 \exp 2c(\theta - \alpha) (\cos \theta + c \sin \theta)$$

and since $\mu_{\theta} = \mu_{\phi} = 0$, the following strain rates can be found:

$$\begin{aligned} 1) \quad \dot{\epsilon}_{\rho} &= \frac{\delta \mu_{\rho}}{\rho} \\ &= -2V_1 \frac{\rho_o^2}{\rho^3} \exp 2c(\theta - \alpha) (\cos \theta + c \sin \theta) \end{aligned}$$

For simplicity, let

$$\begin{aligned} g &= \exp(c(\theta - \alpha)) \\ g' &= c \exp(c(\theta - \alpha)) \\ g'' &= c^2 \exp(c(\theta - \alpha)) \end{aligned}$$

$$\begin{aligned} \text{Therefore, } \dot{\epsilon}_{\rho} &= -2V_1 \frac{\rho_o^2}{\rho^3} g^2 (\cos \theta + c \sin \theta) \\ &= -2V_1 \frac{\rho_o^2}{\rho^3} (g^2 \cos \theta + c g^2 \sin \theta) \end{aligned}$$

$$2) \quad \dot{\epsilon}_{\theta}$$

Since $\mu_{\theta} = \mu_{\phi} = 0$,

$$\text{therefore, } \dot{\epsilon}_{\theta} = \frac{\mu_{\rho}}{\rho}$$

$$= V_1 \frac{\rho_o^2}{\rho^3} g^2 (\cos\theta + c \sin\theta)$$

$$= V_1 \frac{\rho_o^2}{\rho^3} (g^2 \cos\theta + g^2 c \sin\theta)$$

3) $\dot{\epsilon}_\phi$

$$\mu_\theta = \mu_\phi = 0$$

$$\dot{\epsilon}_\phi = \frac{\mu_\rho}{\rho} = \dot{\epsilon}_\theta$$

$$\dot{\epsilon}_\phi = V_1 \frac{\rho_o^2}{\rho^3} (g^2 \cos\theta + g^2 c \sin\theta)$$

4) $\dot{\gamma}_{\rho\theta}$

$$\mu_\theta = \mu_\phi = 0$$

Therefore, $\dot{\gamma}_{\rho\theta} = \frac{1}{2} \frac{1}{\rho} \frac{\delta \mu_\rho}{\delta \theta}$

$$= \frac{1}{2} V_1 \frac{\rho_o^2}{\rho^3} \frac{\delta \exp(2c(\theta-\alpha))(\cos\theta + c \sin\theta)}{\delta \theta}$$

$$= \frac{1}{2} V_1 \frac{\rho_o^2}{\rho^3} [2c \exp(2c(\theta-\alpha))(\cos\theta + c \sin\theta) +$$

$$\exp(2c(\theta-\alpha))(c \cos\theta - \sin\theta)]$$

$$= \frac{1}{2} V_1 \frac{\rho_o^2}{\rho^3} [(2c \exp(2c(\theta-\alpha)) + c \exp(2c(\theta-\alpha)))\cos\theta$$

$$+ [2c^2 \exp(2c(\theta-\alpha)) - (\exp 2c(\theta-\alpha))\sin\theta]$$

$$\begin{aligned}
 &= \frac{1}{2} V_1 \frac{\rho_o^2}{\rho^3} [3c \exp(2c(\theta - \alpha)) \cos \theta \\
 &\quad + [2c^2 \exp(2c(\theta - \alpha)) - \exp(2c(\theta - \alpha))] \sin \theta] \\
 &= \frac{1}{2} V_1 \frac{\rho_o^2}{\rho^3} [3c g^2 \cos \theta + (2c^2 g^2 - g^2) \sin \theta] \\
 &= \frac{1}{2} V_1 \frac{\rho_o^2}{\rho^3} g^2 [3c \cos \theta + (2c^2 - 1) \sin \theta]
 \end{aligned}$$

$$\begin{aligned}
 5) \quad \dot{\gamma}_{\theta\phi} &= 0 \quad) \quad \text{Since } \mu_\theta = \mu_\phi = 0 \\
 &\quad) \\
 6) \quad \dot{\gamma}_{\phi\rho} &= 0 \quad)
 \end{aligned}$$

A3.2 Derivation of the Equivalent Strain Rate

Substituting equations (17) - (22) into the equivalent strain rate formula gives:

$$\begin{aligned}
 \dot{\epsilon} &= \left(\frac{2}{3} (\dot{\epsilon}_{\rho\rho}^2 + \dot{\epsilon}_{\theta\theta}^2 + \dot{\epsilon}_{\phi\phi}^2 + 2(\dot{\gamma}_{\rho\theta}^2 + \dot{\gamma}_{\theta\phi}^2 + \dot{\gamma}_{\phi\rho}^2)) \right)^{\frac{1}{2}} \\
 \dot{\epsilon} &= V_1 \frac{\rho_o^2}{\rho^3} \left[\frac{2}{3} [6(g^2 \cos \theta + c g^2 \sin \theta)^2 \right. \\
 &\quad \left. + \frac{1}{2} g^4 (3c \cos \theta + (2c^2 - 1) \sin \theta)^2] \right]^{\frac{1}{2}} \\
 &= V_1 \frac{\rho_o^2}{\rho^3} \left[g^4 [4(\cos \theta + c \sin \theta)^2 \right. \\
 &\quad \left. + \frac{1}{3} (3c \cos \theta + (2c^2 - 1) \sin \theta)^2] \right]^{\frac{1}{2}} \\
 &= 2V_1 \frac{\rho_o^2}{\rho^3} \left[g^4 [(\cos \theta + c \sin \theta)^2 \right. \\
 &\quad \left. + \frac{1}{12} (3c \cos \theta + (2c^2 - 1) \sin \theta)^2] \right]^{\frac{1}{2}}
 \end{aligned}$$

$$= 2V_1 \frac{\rho_o^2}{\rho^3} g^2 [(\cos \theta + c \sin \theta)^2 + \frac{1}{12} (3c \cos \theta + (2c^2 - 1) \sin \theta)^2]^{\frac{1}{2}}$$

where g is defined in appendix A3.1.

A3.3 Temperature Rise due to Frictional Work

The mesh employed in the deformation zone is very fine, therefore for a small $d\theta$ between the $J=1$ and $J=2$ line, it can be assumed that the I lines are a surface of a sphere, that is

$$\rho_{(I,1)} = \rho_{(I,2)}$$

$$\begin{aligned} \text{Volume of a sphere} &= \int_V \rho^2 \sin \theta \, d\theta \, d\phi \, d\rho \\ &= \int_{\rho_{(I+1,1)}}^{\rho_{(I,1)}} 2\pi (\cos \theta(J+1) - \cos \theta(J)) \rho^2 \, d\rho \end{aligned}$$

$$\begin{aligned} \text{Therefore, } V_a &= 2\pi (\cos \theta(2) - \cos \theta(1)) \left(\frac{\rho^3}{3}\right)_{\rho_{(I+1,1)}}^{\rho_{(I,1)}} \\ &= \frac{2\pi (\cos \theta(2) - \cos \theta(1))}{3} (\rho_{(I,1)}^3 - \rho_{(I+1,1)}^3) \end{aligned}$$

$$dS = \int_{\rho_{(I+1,1)}}^{\rho_{(I,1)}} 2\pi \rho \sin \alpha \, d\rho$$

$$\text{Therefore, } S = \pi \sin \alpha (\rho_{(I,1)}^2 - \rho_{(I+1,1)}^2)$$

For a particle to move a small radial distance $\Delta\rho$ in a time interval Δt , the velocity is given by:

$$u_\rho = \frac{\Delta\rho}{\Delta t}$$

Substituting the various values into equation (29) gives,

$$\Delta\theta_{(I+1,J)} = \frac{m \sigma \frac{\Delta\rho}{\Delta t} \pi \sin\alpha (\rho_{(I,1)}^2 - \rho_{(I+1,1)}^2) \Delta t}{\sqrt{3} Q \text{ sp d } \frac{2\pi(\cos\theta(2) - \cos\theta(1))(\rho_{(I,1)}^3 - \rho_{(I+1,1)}^3)}{3}}$$

$$\Delta\rho = \rho_{(I,1)} - \rho_{(I+1,1)}$$

Therefore,

$$\Delta\theta_{(I+1,J)} = \frac{3m \sigma \sin\alpha (\rho_{(I,1)} - \rho_{(I+1,1)}) (\rho_{(I,1)}^2 - \rho_{(I+1,1)}^2)}{2\sqrt{3} Q \text{ sp d } [\cos\theta(2) - \cos\theta(1)] (\rho_{(I,1)}^3 - \rho_{(I+1,1)}^3)}$$

$$\text{where } \sigma = \frac{1}{2} (\sigma_{o(I,J)} + \sigma_{(I,J)})$$

A3.4 Derivation of the Velocity Discontinuities Δv_1 and Δv_2 at the Inlet and Outlet Shear Surfaces

Inlet shear surface Γ_1

From figure 2.2a of section 2.2.3.1:

$$\Delta v_1 = \mu_\rho \cos(\beta - \theta) - v_1 \cos\beta$$

At the inlet shear surface, $\mu_\rho = \mu_1$

$$\text{Therefore, } \Delta v_1 = \mu_1 \cos(\beta - \theta) - v_1 \cos\beta$$

Substituting equations (6a) and (8) into the above equation gives:

$$\Delta v_1 = v_1 (\cos\theta + c \sin\theta) \cos(90 - \eta) - v_1 \sin(\eta - \theta)$$

$$= V_1[(\cos \theta + c \sin \theta) \sin(\eta) - \sin(\eta - \theta)]$$

$$= V_1[(\cos \theta + c \sin \theta) \sin(\eta) - (\sin \eta \cos \theta - \cos \eta \sin \theta)]$$

Divide throughout by $\cos(\eta)$, then,

$$\Delta v_1 = V_1[(\cos \theta + c \sin \theta) \tan(\eta) - \tan \eta \cos \theta + \sin \theta] \cos(\eta)$$

$$= V_1[\sin \theta (c \tan(\eta) + 1)] \cos(\eta)$$

Since $\tan(\eta) = c$,

$$\text{therefore, } \Delta v_1 = V_1[\sin \theta (1 + c^2)] \cos(\eta)$$

Outlet shear surface Γ_2

Since Γ_1 and Γ_2 are geometrically similar in shape therefore

$$\Delta v_2 = V_2[\sin \theta (1 + c^2) \cos \eta]$$

The above relationship can be proved as follows:

From figure 2.2b of section 2.2.3.1:

$$\Delta v_2 = \mu_\rho \sin(90 - (\beta - \theta)) - V_2 \cos \beta$$

μ_ρ is now the velocity at a point on the outlet shear surface Γ_2 and can be represented by μ_2 .

From equation (10),

$$\mu_2 = \frac{V_2 \sin \beta}{\cos(90 - (\beta + \theta))}$$

$$\begin{aligned} \text{Therefore, } \Delta v_2 &= \frac{V_2 \sin \beta}{\cos(90 - (\beta - \theta))} \cos(\beta - \theta) - V_2 \cos \beta \\ &= \frac{V_2 \sin \beta}{\sin(\beta - \theta)} \cos(\beta - \theta) - V_2 \cos \beta \end{aligned}$$

The first part of the equation is similar to equation (3) and can be expressed as $V_2 (\cos \theta + c \sin \theta)$

$$\Delta v_2 = V_2 (\cos \theta + c \sin \theta) \cos(\beta - \theta) - V_2 \cos \beta$$

From equations (6) and (6a) it can be shown that,

$$\cos \beta = \sin(\eta - \theta)$$

$$\cos(\beta - \theta) = \sin(\eta)$$

$$\text{Therefore, } \Delta v_2 = V_2 [(\cos \theta + c \sin \theta) \sin(\eta) - \sin(\eta - \theta)].$$

The above equation is similar to that derived for Δv_1 , the only difference is the linear velocity V . Therefore, Δv_2 can be expressed as:

$$\Delta v_2 = V_2 [\sin \theta (1 + c^2)] \cos \eta$$

APPENDIX A4

Theoretical Results

Material: Mild steel
 Area of reduction: 15%
 Die semi-angle: 4.13 degree
 Drawing speed: 20ft. min⁻¹

	Drawing temperature (°C)	Draw Stress (tonf in ⁻²)	Mean flow Stress \bar{Y}_d (tonf in ⁻²)
Constant friction factor $m = 0.0$	20	6.39	28.99
	100	5.47	24.81
	200	5.79	26.24
	300	6.29	28.55
	400	4.53	20.54
	500	3.24	14.68
	600	2.02	9.14
	700	0.86	3.90

	Drawing temperature (°C)	Draw Stress (tonf in ⁻²)	Mean flow Stress \bar{Y}_d (tonf in ⁻²)
Constant friction factor $m = 0.1$	20	10.13	28.92
	100	8.70	24.83
	200	9.20	26.28
	300	9.95	28.37
	400	7.17	20.45
	500	5.13	14.63
	600	3.20	9.10
	700	1.36	3.87

	Drawing temperature (°C)	Draw Stress (tonf in ⁻²)	Mean flow Stress \bar{Y}_d (tonf in ⁻²)
Constant friction factor $m = 0.2$	20	13.89	28.93
	100	11.93	24.85
	200	12.58	26.20
	300	13.59	28.27
	400	9.79	20.38
	500	7.01	14.57
	600	4.37	9.08
	700	1.86	3.85

	Drawing temperature (°C)	Draw Stress (tonf in ⁻²)	Mean flow Stress \bar{Y}_d (tonf in ⁻²)
Constant friction factor $m = 0.3$	20	17.61	28.85
	100	15.12	24.77
	200	15.93	26.12
	300	17.21	28.19
	400	12.41	20.33
	500	8.88	14.54
	600	5.53	9.04
	700	2.35	3.84

Material: Mild steel
 Area of reduction: 18%
 Die semi-angle: 5.2 degree
 Drawing speed: 20 ft. min⁻¹

	Drawing temperature (°C)	Draw Stress (tonf in ⁻²)	Mean flow Stress Y _d (tonf in ⁻²)
Constant friction factor m = 0.0	20	8.20	30.21
	100	7.06	26.01
	200	7.31	26.96
	300	8.21	30.26
	400	5.91	21.78
	500	4.32	15.92
	600	2.78	10.23
	700	1.35	4.97

	Drawing temperature (°C)	Draw Stress (tonf in ⁻²)	Mean flow Stress Y _d (tonf in ⁻²)
Constant friction factor m = 0.1	20	11.97	20.13
	100	10.33	26.02
	200	10.72	27.00
	300	11.96	30.05
	400	8.62	21.68
	500	6.31	15.86
	600	4.06	10.20
	700	1.97	4.94

Constant friction factor m = 0.2	20	15.77	30.15
	100	13.62	26.04
	200	14.08	26.93
	300	15.68	29.96
	400	11.32	21.63
	500	8.28	15.82
	600	5.33	10.15
	700	2.59	4.93

Constant friction factor m = 0.3	20	19.53	30.09
	100	16.86	25.96
	200	17.43	26.86
	300	19.40	29.87
	400	14.00	21.57
	500	10.25	15.76
	600	6.59	10.13
	700	3.20	4.90

Material: Mild steel
 Area of reduction: 22.84%
 Die semi-angle: 7.52 degree
 Drawing speed: 20 ft. min⁻¹

	Drawing temperature (°C)	Draw Stress (tonf in ⁻²)	Mean flow Stress \bar{Y}_d (tonf in ⁻²)
Constant friction factor $m = 0.0$	20	11.65	31.98
	100	10.13	27.81
	200	10.12	27.78
	300	11.73	32.19
	400	8.67	23.80
	500	6.49	17.79
	600	4.23	11.59
	700	2.47	6.74

	Drawing temperature (°C)	Draw Stress (tonf in ⁻²)	Mean flow Stress \bar{Y}_d (tonf in ⁻²)
Constant friction factor $m = 0.1$	20	15.23	31.89
	100	13.28	27.81
	200	13.30	27.84
	300	15.31	32.06
	400	11.33	23.68
	500	8.49	17.74
	600	5.54	11.58
	700	3.22	6.70

	20	18.86	31.91
Constant friction factor $m = 0.2$	100	16.45	27.84
	200	16.42	27.78
	300	18.89	31.96
	400	13.98	23.63
	500	10.47	17.69
	600	6.84	11.56
	700	3.98	6.69

	20	22.44	31.87
Constant friction factor $m = 0.3$	100	19.57	27.78
	200	19.52	27.71
	300	22.45	31.87
	400	16.61	23.56
	500	17.65	12.45
	600	8.14	11.52
	700	4.73	6.67

Material: Mild steel
 Area of reduction: 27%
 Die semi-angle: 6.33 degree
 Drawing speed: 20 ft. min⁻¹

	Drawing temperature (°C)	Draw Stress (tonf in ⁻²)	Mean flow Stress \bar{Y}_d (tonf in ⁻²)
Constant friction factor $m = 0.0$	20	13.19	32.65
	100	11.44	28.30
	200	12.00	29.73
	300	13.03	32.17
	400	9.45	26.69
	500	7.02	17.36
	600	4.63	11.41
	700	2.44	6.03

	Drawing temperature (°C)	Draw Stress (tonf in ⁻²)	Mean flow Stress \bar{Y}_d (tonf in ⁻²)
Constant friction factor $m = 0.1$	20	18.48	32.56
	100	16.09	28.34
	200	16.86	29.73
	300	18.16	31.97
	400	13.22	23.29
	500	9.82	17.26
	600	6.47	11.38
	700	3.41	5.98

	Drawing temperature (°C)	Draw Stress (tonf in ⁻²)	Mean flow Stress \bar{Y}_d (tonf in ⁻²)
Constant friction factor $m = 0.2$	20	23.78	32.50
	100	20.69	28.28
	200	21.66	29.60
	300	21.92	31.84
	400	16.97	23.20
	500	12.60	17.20
	600	8.31	11.35
	700	4.38	5.94

	Drawing temperature (°C)	Draw Stress (tonf in ⁻²)	Mean flow Stress \bar{Y}_d (tonf in ⁻²)
Constant friction factor $m = 0.3$	20	29.00	32.40
	100	25.23	28.18
	200	26.41	29.50
	300	28.41	31.73
	400	20.70	23.12
	500	15.37	17.15
	600	10.14	11.28
	700	5.34	5.93

Material: Mild steel
 Area of reduction: 40%
 Die semi-angle: 9 degree
 Drawing speed: 20 ft. min⁻¹

	Drawing temperature (°C)	Draw Stress (tonf in ⁻²)	Mean flow Stress \bar{Y}_d (tonf in ⁻²)
Constant friction factor $m = 0.0$	20	22.39	35.14
	100	19.72	30.94
	200	20.87	32.76
	300	21.92	34.39
	400	16.27	25.48
	500	12.34	19.34
	600	8.23	12.85
	700	4.98	7.74

	Drawing temperature (°C)	Draw Stress (tonf in ⁻²)	Mean flow Stress \bar{Y}_d (tonf in ⁻²)
Constant friction factor $m = 0.1$	20	28.89	35.09
	100	25.50	30.98
	200	26.61	32.71
	300	28.12	34.11
	400	20.91	25.36
	500	15.24	19.25
	600	10.34	12.82
	700	6.40	7.71

	20	35.29	34.97
Constant friction factor $m = 0.2$	100	31.15	30.86
	200	32.87	32.57
	300	34.32	33.96
	400	29.42	29.11
	500	19.38	19.18
	600	12.94	12.78
	700	7.81	7.69

	20	41.63	34.79
Constant friction factor $m = 0.3$	100	36.73	30.70
	200	38.79	32.45
	300	40.49	33.84
	400	30.10	25.16
	500	22.86	19.07
	600	15.26	12.69
	700	9.21	7.63

Material: Mild steel
 Area of reduction: 45%
 Die semi-angle: 9 degree
 Drawing speed: 20 ft. min⁻¹

	Drawing temperature (°C)	Draw Stress (tonf in ⁻²)	Mean flow Stress \bar{Y}_d (tonf in ⁻²)
Constant friction factor $m = 0.0$	20	25.81	35.63
	100	22.93	31.65
	200	24.85	34.30
	300	24.88	34.34
	400	18.55	25.61
	500	14.11	19.43
	600	9.43	12.98
	700	5.65	7.72

	Drawing temperature (°C)	Draw Stress (tonf in ⁻²)	Mean flow Stress \bar{Y}_d (tonf in ⁻²)
Constant friction factor $m = 0.1$	20	33.51	35.56
	100	29.83	31.66
	200	32.22	34.19
	300	32.11	34.07
	400	23.99	25.41
	500	18.24	19.32
	600	12.21	12.94
	700	7.31	7.69

	Drawing temperature (°C)	Draw Stress (tonf in ⁻²)	Mean flow Stress \bar{Y}_d (tonf in ⁻²)
Constant friction factor $m = 0.2$	20	41.02	35.39
	100	36.55	31.51
	200	39.47	34.02
	300	39.31	33.84
	400	29.38	25.29
	500	22.35	19.24
	600	14.97	12.88
	700	8.95	7.66

	Drawing temperature (°C)	Draw Stress (tonf in ⁻²)	Mean flow Stress \bar{Y}_d (tonf in ⁻²)
Constant friction factor $m = 0.3$	20	48.54	35.23
	100	43.21	31.36
	200	46.68	33.88
	300	46.52	33.72
	400	34.75	25.19
	500	26.43	19.12
	600	17.70	12.77
	700	10.57	7.60

Material: Medium carbon steel
 Area of reduction: 20%
 Die semi-angle: 9 degree
 Drawing speed: 20 ft. min⁻¹

	Drawing temperature (°C)	Draw Stress (tonf in ⁻²)	Mean flow Stress \bar{Y}_d (tonf in ⁻²)
Constant friction factor $m = 0.0$	20	13.91	39.98
	100	11.78	33.85
	200	11.02	31.67
	300	13.68	39.31
	400	10.12	29.04
	500	7.30	20.95
	600	4.61	4.61
	700	2.73	2.73

	Drawing temperature (°C)	Draw Stress (tonf in ⁻²)	Mean flow Stress \bar{Y}_d (tonf in ⁻²)
Constant friction factor $m = 0.1$	20	17.11	39.85
	100	14.39	33.77
	200	13.62	31.73
	300	16.82	39.18
	400	12.44	28.95
	500	8.98	20.91
	600	5.60	13.16
	700	3.32	7.76

Constant friction factor $m = 0.2$	20	20.34	39.81
	100	17.25	33.80
	200	16.20	31.72
	300	19.95	39.06
	400	14.76	28.88
	500	10.66	20.86
	600	6.73	13.09
	700	3.98	7.75

Constant friction factor $m = 0.3$	20	23.56	39.78
	100	20.01	33.78
	200	18.74	31.64
	300	23.06	38.96
	400	17.07	28.81
	500	12.32	20.77
	600	7.78	20.69
	700	4.60	7.74

Material: Medium carbon steel
 Area of reduction: 20%
 Die semi-angle: 9 degree
 Drawing speed: 20 ft. min⁻¹

	Drawing temperature (°C)	Draw Stress (tonf in ⁻²)	Mean flow Stress \bar{Y}_d (tonf in ⁻²)
Constant friction factor $m = 0.4$	20	26.75	39.70
	100	22.71	33.72
	200	21.27	31.59
	300	26.17	38.88
	400	19.36	28.70
	500	13.99	20.74
	600	8.83	13.06
	700	5.22	7.69

	Drawing temperature (°C)	Draw Stress (tonf in ⁻²)	Mean flow Stress \bar{Y}_d (tonf in ⁻²)
Constant friction factor $m = 0.7$	20	36.23	39.48
	100	30.76	33.53
	200	28.79	31.38
	300	35.47	38.68
	400	26.23	28.55
	500	18.95	20.63
	600	11.95	12.96
	700	7.07	7.66

Material: Medium carbon steel
 Area of reduction: 30%
 Die semi-angle: 9 degree
 Drawing speed: 20 ft. min⁻¹

	Drawing temperature (°C)	Draw Stress (tonf in ⁻²)	Mean flow Stress \bar{Y}_d (tonf in ⁻²)
Constant friction factor $m = 0.0$	20	20.38	42.23
	100	17.36	35.96
	200	17.06	35.38
	300	20.09	41.62
	400	14.40	29.83
	500	10.46	21.67
	600	6.61	13.66
	700	3.89	7.99

	Drawing temperature (°C)	Draw Stress (tonf in ⁻²)	Mean flow Stress \bar{Y}_d (tonf in ⁻²)
Constant friction factor $m = 0.1$	20	25.80	42.11
	100	22.04	35.98
	200	21.68	35.39
	300	25.34	41.36
	400	18.19	29.63
	500	13.22	21.53
	600	8.37	13.63
	700	4.91	7.94

	20	31.21	42.03
Constant friction factor $m = 0.2$	100	26.66	35.91
	200	26.19	35.26
	300	30.58	41.18
	400	21.96	29.52
	500	15.97	21.46
	600	10.11	13.59
	700	5.93	7.92

	20	36.55	41.88
Constant friction factor $m = 0.3$	100	31.21	35.77
	200	30.65	35.13
	300	35.82	41.04
	400	25.71	29.42
	500	18.70	21.40
	600	11.85	13.48
	700	6.95	7.90

Material: Medium carbon steel
 Area of reduction: 30%
 Die semi-angle: 9 degree
 Drawing speed: 20 ft. min⁻¹

	Drawing temperature (°C)	Draw Stress (tonf in ⁻²)	Mean flow Stress Y _d (tonf in ⁻²)
Constant friction factor m = 0.4	20	41.85	41.75
	100	35.75	35.66
	200	35.11	35.02
	300	41.04	40.94
	400	29.45	29.34
	500	21.42	21.29
	600	13.56	13.45
	700	7.95	7.86

	Drawing temperature (°C)	Draw Stress (tonf in ⁻²)	Mean flow Stress Y _d (tonf in ⁻²)
Constant friction factor m = 0.7	20	57.82	41.53
	100	49.33	35.39
	200	48.48	34.82
	300	56.79	40.75
	400	40.72	29.17
	500	29.59	21.20
	600	18.71	13.37
	700	10.96	7.81

Material: Medium carbon steel
 Area of reduction: 35%
 Die semi-angle: 9 degree
 Drawing speed: 20 ft. min⁻¹

	Drawing temperature (°C)	Draw Stress (tonf in ⁻²)	Mean flow Stress \bar{Y}_d (tonf in ⁻²)
Constant friction factor $m = 0.0$	20	23.92	42.96
	100	20.52	36.86
	200	20.69	37.15
	300	23.33	41.84
	400	16.72	29.98
	500	12.18	21.85
	600	7.75	13.84
	700	4.51	8.04

	Drawing temperature (°C)	Draw Stress (tonf in ⁻²)	Mean flow Stress \bar{Y}_d (tonf in ⁻²)
Constant friction factor $m = 0.1$	20	30.59	42.86
	100	26.32	36.84
	200	26.50	37.13
	300	29.68	41.54
	400	21.31	29.82
	500	15.54	21.69
	600	9.89	13.80
	700	5.75	7.97

	Drawing temperature (°C)	Draw Stress (tonf in ⁻²)	Mean flow Stress \bar{Y}_d (tonf in ⁻²)
Constant friction factor $m = 0.2$	20	37.16	42.64
	100	31.97	36.69
	200	32.18	36.96
	300	36.02	41.34
	400	25.87	29.63
	500	18.87	21.61
	600	12.01	13.72
	700	6.99	7.95

	Drawing temperature (°C)	Draw Stress (tonf in ⁻²)	Mean flow Stress \bar{Y}_d (tonf in ⁻²)
Constant friction factor $m = 0.3$	20	43.67	42.47
	100	37.57	36.54
	200	37.83	36.82
	300	42.36	41.19
	400	30.41	29.52
	500	22.18	21.54
	600	14.20	13.67
	700	8.21	7.92

red
red

Material: Medium carbon steel
Area of reduction: 35%
Die semi-angle: 9 degree
Drawing speed: 20 ft. min⁻¹

	Drawing temperature (°C)	Draw Stress (tonf in ⁻²)	Mean flow Stress \bar{Y}_d (tonf in ⁻²)
Constant friction factor $m = 0.4$	20	50.18	42.33
	100	43.15	36.40
	200	43.46	36.68
	300	48.72	41.10
	400	34.95	29.45
	500	25.49	21.47
	600	16.22	13.64
	700	9.43	7.87

	Drawing temperature (°C)	Draw Stress (tonf in ⁻²)	Mean flow Stress \bar{Y}_d (tonf in ⁻²)
Constant friction factor $m = 0.7$	20	69.79	42.15
	100	59.97	36.21
	200	60.44	36.49
	300	67.85	40.93
	400	48.65	29.29
	500	35.46	21.35
	600	22.54	13.57
	700	13.07	7.84

Material: Medium carbon steel
 Area of reduction: 40%
 Die semi-angle: 9 degree
 Drawing speed: 20 ft. min⁻¹

	Drawing temperature (°C)	Draw Stress (tonf in ⁻²)	Mean flow Stress \bar{Y}_d (tonf in ⁻²)
Constant friction factor $m = 0.0$	20	27.67	43.42
	100	24.01	37.69
	200	24.79	38.90
	300	26.61	41.69
	400	19.17	30.03
	500	14.01	21.95
	600	8.95	13.96
	700	5.17	8.03

	Drawing temperature (°C)	Draw Stress (tonf in ⁻²)	Mean flow Stress \bar{Y}_d (tonf in ⁻²)
Constant friction factor $m = 0.1$	20	35.64	43.29
	100	31.02	37.68
	200	31.96	38.81
	300	34.08	41.34
	400	24.60	29.84
	500	17.99	21.83
	600	11.50	13.92
	700	6.64	8.00

	20	43.46	43.06
Constant friction factor $m = 0.2$	100	37.84	37.44
	200	38.97	38.61
	300	41.55	41.12
	400	30.00	29.69
	500	21.96	21.68
	600	14.04	13.86
	700	8.10	7.94

	20	51.24	42.86
Constant friction factor $m = 0.3$	100	44.59	37.26
	200	45.94	38.43
	300	49.04	40.98
	400	35.39	29.52
	500	25.89	21.59
	600	16.56	13.82
	700	9.54	7.91

Material: Medium carbon steel
 Area of reduction: 40%
 Die semi-angle: 9 degree
 Drawing speed: 20 ft.min⁻¹

	Drawing temperature (°C)	Draw Stress (tonf in ⁻²)	Mean flow Stress \bar{Y}_d (tonf in ⁻²)
Constant friction factor $m = 0.4$	20	59.06	42.71
	100	51.35	37.14
	200	52.95	38.32
	300	56.57	40.91
	400	40.81	29.46
	500	29.84	21.55
	600	19.07	13.77
	700	10.98	7.85

	Drawing temperature (°C)	Draw Stress (tonf in ⁻²)	Mean flow Stress \bar{Y}_d (tonf in ⁻²)
Constant friction factor $m = 0.7$	20	82.59	42.55
	100	71.76	36.97
	200	74.05	38.17
	300	79.21	40.76
	400	57.08	29.37
	500	41.72	21.43
	600	26.64	13.62
	700	15.32	7.83

Material: Medium carbon steel
 Area of reduction: 45%
 Die semi-angle: 9 degree
 Drawing speed: 20 ft. min⁻¹

	Drawing temperature (°C)	Draw Stress (tonf in ⁻²)	Mean flow Stress \bar{Y}_d (tonf in ⁻²)
Constant friction factor $m = 0.0$	20	31.65	43.67
	100	27.93	38.55
	200	29.40	40.58
	300	29.97	41.36
	400	21.77	29.99
	500	15.97	21.98
	600	10.23	14.04
	700	5.86	8.00

	Drawing temperature (°C)	Draw Stress (tonf in ⁻²)	Mean flow Stress \bar{Y}_d (tonf in ⁻²)
Constant friction factor $m = 0.1$	20	41.02	43.51
	100	36.28	38.48
	200	38.01	40.41
	300	38.60	40.89
	400	28.10	29.77
	500	20.62	21.84
	600	13.23	13.98
	700	7.57	7.97

Constant friction factor $m = 0.2$	20	42.79	43.23
	100	44.38	38.25
	200	46.60	40.17
	300	47.22	40.65
	400	34.38	29.60
	500	25.24	21.73
	600	16.21	13.86
	700	9.27	7.93

Constant friction factor $m = 0.3$	20	59.30	43.05
	100	52.46	38.06
	200	55.11	39.99
	300	55.92	40.54
	400	40.69	29.50
	500	29.86	21.64
	600	19.14	13.81
	700	10.94	7.87

Material: Medium carbon steel
 Area of reduction: 45%
 Die semi-angle: 9 degree
 Drawing speed: 20 ft. min⁻¹

	Drawing temperature (°C)	Draw Stress (tonf in ⁻²)	Mean flow Stress Y _d (tonf in ⁻²)
Constant friction factor m = 0.4	20	68.54	42.95
	100	60.57	37.92
	200	63.68	39.91
	300	64.64	40.41
	400	47.03	29.39
	500	34.48	21.55
	600	22.09	13.77
	700	12.62	7.81

	Drawing temperature (°C)	Draw Stress (tonf in ⁻²)	Mean flow Stress Y _d (tonf in ⁻²)
Constant friction factor m = 0.7	20	96.28	42.77
	100	85.03	37.78
	200	89.46	39.77
	300	90.84	40.24
	400	66.07	29.32
	500	48.41	21.44
	600	31.01	13.74
	700	17.68	7.79

APPENDIX A5

Experimental Results

Material: Mild steel EN2B

Diameter of wire: 0.236 in

Lubricant: Dag 2961

Die material: Chromium carbide

Area of reduction: 15%

Die semi-angle: 4.13 degree

Drawing temperature (°C)	Drawing speed (ft min ⁻¹)	Draw stress (tonf in ⁻²)
20	19.98	4.06
100	20.25	3.41
233	18.36	2.98
300	19.44	3.63
373	19.44	3.71
487	19.44	3.60
500	20.52	3.26
700	20.52	1.81

Area of reduction: 18%

Die semi-angle: 5.2 degree

Drawing temperature (°C)	Drawing speed (ft min ⁻¹)	Draw stress (tonf in ⁻²)
20	20.52	7.19
100	19.44	5.42
200	20.52	5.42
317	19.44	7.11
400	19.44	7.36
480	19.44	6.69
597	20.52	5.08
700	19.17	3.51

Area of reduction: 22.84%

Die semi-angle: 7.52 degree

20	18.90	8.18
100	18.36	7.83
200	19.44	8.82
300	18.90	10.01
400	19.44	10.00
500	20.52	7.95
600	19.98	5.83
700	19.98	3.82

Area of reduction: 27%

Die semi-angle: 6.33 degree

20	19.44	10.00
100	19.44	8.90
200	19.44	8.80
300	19.44	10.72
400	18.90	10.63
500	19.44	9.66
587	19.70	7.59
700	20.25	4.96

Material: Mild steel EN2B

Diameter of wire: 0.236 in

Lubricant: Dag 2961

Die material: Chromium carbide

Area of reduction: 40%

Die semi-angle: 9 degree

Drawing temperature (°C)	Drawing speed (ft min ⁻¹)	Draw stress (tonf in ⁻²)
20	19.44	18.08
100	18.90	16.32
200	19.44	15.67
300	19.17	19.50
387	19.71	17.25
487	20.52	13.92
580	19.71	11.00
700	19.44	7.82

Area of reduction: 45%

Die semi-angle: 9 degree

Drawing temperature (°C)	Drawing speed (ft min ⁻¹)	Draw stress (tonf in ⁻²)
20	19.44	20.34
100	19.44	18.61
193	19.98	18.48
300	19.44	22.40
386	19.17	20.55
500	19.98	16.18
586	20.52	13.82
700	19.98	9.64

Material: Medium carbon steel EN8D

Diameter of wire: 0.236 in

Lubricant: Dag 2961

Die material: 'Syalon'

Die semi-angle: 9 degree

Area of reduction: 20%

Drawing temperature (°C)	Drawing speed (ft min ⁻²)	Draw stress (tonf in ⁻²)
20	19.44	14.75
100	18.90	12.33
200	19.17	10.75
300	18.90	13.01
415	19.17	12.61
500	18.36	10.78
600	18.68	8.62
700	20.52	6.45

Area of reduction: 30%

Drawing temperature (°C)	Drawing speed (ft min ⁻²)	Draw stress (tonf in ⁻²)
20	20.25	21.57
100	20.52	18.52
200	20.52	16.75
300	20.54	18.37
400	19.44	18.15
495	19.98	16.33
600	19.98	12.76
700	20.25	9.69

Area of reduction: 35%

20	18.90	24.49
90	19.44	22.52
200	19.44	20.07
300	19.17	22.07
400	19.44	20.96
500	19.44	19.15
600	19.17	15.70
700	19.44	11.63

Area of reduction: 40%

20	19.98	29.59
100	19.44	25.51
200	19.44	24.66
300	19.44	25.36
400	19.98	24.51
500	20.52	22.53
575	20.52	19.98
700	20.52	13.26

Material: Medium carbon steel EN8D

Diameter of wire: 0.236 in

Lubricant: Dag 2961

Die material: 'Syalon'

Die semi-angle: 9 degree

Area of reduction: 45%

Drawing temper- ature (°C)	Drawing speed (ft min ⁻¹)	Draw stress (tonf in ⁻²)
20	-	-
100	-	-
200	20.52	31.92
300	20.54	33.12
400	19.44	30.80
500	19.98	26.90
600	19.08	22.26
700	21.06	17.56

Material: M2 'high speed' steel

Diameter of wire: 0.2165 in

Lubricant: Dag 2961

Die material: 'Syalon'

Die semi-angle: 9 degree

Area of reduction: 22.68%

Drawing temperature (°C)	Drawing speed (ft min ⁻¹)	Draw stress (tonf in ⁻²)
20	18.90	25.08
100	19.98	21.56
205	19.44	21.16
300	19.44	20.75
410	19.98	18.50
500	19.44	16.75
600	19.98	15.44

Area of reduction: 23.6%

Drawing temperature (°C)	Drawing speed (ft min ⁻¹)	Draw stress (tonf in ⁻²)
20	19.80	31.61
127	19.80	27.49
207	19.80	26.81
307	19.25	26.11
400	18.90	24.39
520	19.80	21.31
607	19.80	19.73
700	19.53	17.49

Area of reduction: 34.5%

20	-	-
103	19.80	34.53
200	19.80	32.67
307	20.40	29.96
400	19.44	28.19
520	19.98	26.79
573	19.98	25.67
700	19.98	22.76

Area of reduction: 40.5%

20	-	-
100	-	-
200	-	-
300	-	-
390	19.44	35.04
480	19.80	32.39
625	20.25	28.62
710	19.80	26.58

APPENDIX A6

Computer Programs

COMPUTER PROGRAM 'DRAW'

C THIS PROGRAM CALCULATES THE MINIMUM DRAW STRESS FOR THE
C DRAWING OF WIRES AT ELEVATED TEMPERATURES FOR MEDIUM CARBON
C STEEL.

C THE READER IS ADVISED TO CONSULT THE NAG ROUTINES ON THE
C 1934S ICL COMPUTERS FOR A BETTER UNDERSTANDING OF THE
C STANDARD ROUTINES USED IN THE PROGRAM

C RR=RADIUS OF ORIGINAL WIRE
C IAR=AREA OF REDUCTION
C V33=OUTLET VELOCITY IN FT. PER MIN
C ALP=DIE SEMI-ANGLE IN DEGREE
C NO=NO. OF ANGULAR DIVISIONS
C NR=NO. OF RADIAL DIVISIONS
C M=CONSTANT FRICTION FACTOR
C NC=NO. OF VALUES OF EXPONENTIAL CONSTANT C
C TT=DRAWING TEMPERATURE

PROGRAM LOH

REAL EQUIV(21,21),CDF(21,21),NT(21,21),IAR
& DF(21,21),DT(21,21),STR(21,21),
& CD(21),CR(21,21),CEQUIV(21,21),CSTRAI(21,21),
& CSIGMA(21,21),CNT(21,21),CDT(21,21)
& R1(21),R2(21),YM(21),DSIG(21,21)
& ST(21),CST(21),CCC(50),CCST(21)
REAL JM,M,INDEX,INTRGT,INTP1,INDEX1,INDEX2
PARAMETER(PIE=3.1415826535)
COMMON/CB1/STRAIN(21,21),SIGMA(21,21)
COMMON/CB2/R(21,21)
COMMON/CB3/F(21)

C INPUT THE DATA

READ*,RR
READ*,IAR
READ*,V33
READ*,ALP
READ*,NO
READ*,NR
READ*,M
READ*,NC

C READ THE EXPONENTIAL CONSTANT C

DO 65 KJ=1,NC,1
READ*,CCC(KJ)
PRINT*,CCC(KJ)
65 CONTINUE
901 READ*,TT
IF(TT.GE.1000.0)GOTO 902
ALPHA=(PIE*ALP)/180.0
A=ALPHA
R1(1)=RR
R2(1)=R1(1)*(SQRT(1.0-IAR*0.01))

C V1=INS PER SEC

C V11=FT PER MIN

C V3=INS PER SEC

V11=((R2(1)/RR)**2)*V33
V1=V11*0.2
V3=V33*0.2

C FIND THE MEAN STRAIN-RATE EQUIVM

EQUIVM=V3*TAN(A)*((1-IAR*0.01)+SQRT(1-IAR*0.01))
& /R2(1)
PRINT*,MEAN STRAIN-RATE BY ATKINS FORMULA',EQUIVM
PRINT*,

C SET THE POWER TO MAXIMUM VALUE FOR COMPARISON

WORK=1.0E60

T=TT

R1(1)=RR

RO=R1(1)/SIN(A)

C COMPUTING THE STRAIN, STRAIN RATE, TEMPERATURE AND STRESS

DO 700 K=1,NC,1

C=CCC(K)

F(2)=A-(A*1.0/NO*1.0)

```

C COMPUTING THE JTH LINE
DO 500 J=1,NO+1,1
  JJ=J-1
  F(J)=A-(A*JJ*0.1/(NO*0.1))
  D=F(J)
  R1(J)=R0*EXP(C*(D-A))*SIN(D)
  R2(J)=R1(J)*(SQRT((100-IAR)/100.0))
  R(1,J)=R0*EXP(C*(D-A))

```

```

C PARAMETERS AT INLET SHEAR SURFACE
EQUIV(1,J)=0.0
STRAIN(1,J)=0.0
NT(1,J)=TT
DT(1,J)=0.0
DF(1,J)=0.0
OSIG(1,J)=0.0
SIGMA(1,J)=0.0

```

```

C COMPUTING THE ITH LINE
DO 80 I=2,NR+1,1
  IF(J.EQ.(NO+1))THEN
    R(1,NO+1)=R0*EXP(C*(D-A))
    R(NR+1,NO+1)=R(1,NO+1)*SQRT(1.0-IAR*0.01)
    R(I,NO+1)=(R(1,NO+1)-R(NR+1,NO+1))*(NR+1.0+1.0-I+1.0)/(NR+1.0)
    + (R(NR+1,NO+1))
  8 GOTO 81
  ENDF
  R(I,J)=(((R1(J)-R2(J))/SIN(D))*(NR+1.0+1.0-I)/(NR+1.0))
    + (R2(J)/SIN(D))
  8 E=(COS(D)+C*SIN(D))*2+
    ((3.0*C*COS(D)+(2.0*C*C-1.0)*SIN(D))*2)
    /12.0
  EQUIV(I,J)=2.0*V1*(R0**2)*EXP(2.0*C*(D-A))*SQRT(E)
    / (R(I,J)**3)
  STRAIN(I,J)=2.0*LOG(R(1,J)/R(I,J))*
    (SQRT(E)/(COS(D)+C*SIN(D)))
  STR(I,J)=STRAIN(I,J)-STRAIN(I-1,J)

```

```

C FINDING THE FLOW STRESS
CALL TMK1(TT,0.0,EQUIV(I,J),B1,INDEX1,TKM2)
IF(TMK2.LT.500.0)THEN
  ADD=((500.0-TMK2)*0.06)+114.0
ELSE
  ADD=((725.0-TMK2)*0.0628)+112.0
ENDIF
OSIG(I,J)=B1*(STRAIN(I,J)**INDEX1)*ADD/100.0
IF((B1.LE.0.0).OR.(INDEX1.LE.0.0))GOTO 902

```

```

C JM= CONVERSION FACTOR BETWEEN MECHANICAL AND THERMAL ENERGIES
C CM= SPECIFIC HEAT OF WIRE
C RM=DENSITY OF WIRE
C CALCULATING THE TEMPERATURE RISE AND
C ESTABLISHING THE NEW FLOW STRESS
CM=0.1124
JM=9336.0
RM=0.2840344
TEMP=0.5*(OSIG(I,J)+OSIG(I-1,J))*STR(I,J)/(JM * CM * RM)
DT(I,J)=TEMP*0.55556
IF(J.EQ.1)GOTO 310

```

C TEMPERATURE RISE DF IN DEGREES CENTRIGRADE DUE TO

C FRICTIONAL WORK

C IF NO FRICTIONAL WORK

```

  DF(I,J)=0.0
  GOTO 320
310 VA=(R(I-1,J)-R(I,J))*
  8 (R(I-1,J)**2.0-R(I,J)**2.0)/(R(I-1,J)**3.0-R(I,J)**3.0)
  TEMPF=3.0*JM*0.5*(OSIG(I,J)+OSIG(I-1,J))*SIN(X)*VA/(2.0*JM*CM*
  8 RM*1.732*(COS(F(2))-COS(F(1))))
  IF(TEMPF.LT.0.0)THEN
    PRINT*,*TEMPF IS -VE*
    GOTO 902
  ENDF
  DF(I,J)=TEMPF*0.55556

```

C THE NEW TEMPERATURE TAKING INTO ACCOUNT TEMPERATURE RISE

320 NT(I,J)=DT(I,J)+DF(I,J)+T

TTT=DT(I,J)+DF(I,J)

C FINDING THE NEW STRESS

```

CALL TMK1(T,TTT,EQUIV(I,J),B,INDEX,TKM3)
IF(TMK3.LT.500.0)THEN
  ADD1=((500.0-TMK3)*0.06)+114.0
ELSE
  ADD1=((725.0-TMK3)*0.0628)+112.0
ENDIF
SIGMA(I,J)=B*(STRAIN(I,J)**INDEX)*ADD1/100.0

```

```

C SET T(L) TO THE NEW TEMPERATURE FOR THE NEXT I-LINE
  T=NT(I,J)
30  CONTINUE
  T=TT
  ST(J)=0.5773502*(1.0+C*C)*TAN(F(J))/
    & (1+C*TAN(F(J)))
500  CONTINUE

C CALCULATING THE VARIOUS POWER
C DEFORMATION POWER
C FIND THE MEAN FLOW STRESS
  CALL INTPD(NO,NR,YD,YF,YS)
  HD=INTRGT(0.0,A,C,A)
  IF(HD.LE.0.0)THEN
    PRINT*,'HD -VE',HD
    GOTO 902
  ENDIF

C CHANGE TO FT. LB PER SEC
  PD=4.0*PIE*V1*YD*RO*RO*LOG(R1(1)/R2(1))*HD/12.0

C CALCULATING THE SHEAR POWER
  H=INTP1(0.0,A,C,A)
  IF(H.LE.0.0)GOTO 902
  P1=1.1547*PIE*YD*V1*(RO**2.0)*H/12.0
  P2=P1

C FRICTIONAL POWER
  PF=(1.154*PIE*M*YD*V1*RO*RO*LOG(R1(1)/R2(1))*COS(A)
    & *SIN(A))/12.0

C TOTAL POWER IN FT LB PER SEC
  PT=(P1+P2+PD+PF)

C COMPARING THE POWER AND RETAINING THE PARAMETERS
  IF(PT.LT.WORK)THEN
    CM=M
    CC=C
    CYF=YF/2240.0
    CYD=YD/2240.0
    CPD=PD
    CP1=P1
    CP2=P2
    CPF=PF
    CPT=PT
    CH=H
    CHD=HD
    DO 300 JJ=1,NR+1,1
    DO 200 II=1,NO+1,1
      CD(JJ)=F(JJ)
      CR(II,JJ)=R(II,JJ)
      CEQUIV(II,JJ)=EQUIV(II,JJ)
      CSTRAI(II,JJ)=STRAIN(II,JJ)
      CSIGMA(II,JJ)=SIGMA(II,JJ)/2240.0
      CNT(II,JJ)=NT(II,JJ)
      CDF(II,JJ)=DF(II,JJ)
      CDT(II,JJ)=DT(II,JJ)
200  CONTINUE
      CST(JJ)=ST(JJ)
      CCST(JJ)=CST(JJ)+CSTRAI(NO+1,JJ)
300  CONTINUE
    ENDIF
    CYS=CSIGMA(NO+1,NR+1)

C SET TOTAL POWER FOR COMPARISON
  WORK=CPT
700  CONTINUE

C FIND THE MINIMUM DRAW STRESS IN TONF PER SQ IN
  STRESS=(CPT*12.0)/(PIE*R2(1)*R2(1)*V3*2240.0)

C PRINT THE RESULTS
  PRINT*,'MATERIAL:MEDIUM CARBON STEEL'
  PRINT*,'DRAWING TEMPERATURE IN DEGREES CENTRIGRADE',TT
  PRINT*,'AREA OF REDUCTION',IAR,'PERCENT'
  PRINT*,'DIE SEMI-ANGLE IN DEGREES',ALP
  PRINT*,'ORIGINAL RADIUS OF WIRE IN INS.',R1(1)
  PRINT*,'FINAL RADIUS OF WIRE IN INS',R2(1)
  PRINT*,'SPEED OF DRAWING IN FT. PER MIN',V33
  PRINT*,'CONSTANT FRICTION FACTOR M',M
  PRINT*,'EXPONENTIAL CONSTANT C',CC
  PRINT*,'POWER OF DEFORMATION PD IN FT LB PER SEC.',CPD
  PRINT*,'POWER OF FRICTION IN FT LB PER SEC',CPF
  PRINT*,'POWER OF SHEARING AT INLET IN FT LB PER SEC',CP1
  PRINT*,'POWER OF SHEARING AT OUTLET IN FT LB PER SEC',CP2
  PRINT*,'TOTAL POWER OF DRAWING FT LB PER SEC',CPT
  PRINT*,'MEAN YIELD STRESS CYD IN TONF PER SQ. IN',CYD
  PRINT*,'MEAN YIELD STRESS AT INLET IN TONF PER SQ. IN',CYD
  PRINT*,'MEAN YIELD STRESS AT OUTLET TONF PER SQ. IN',CYD
  PRINT*,'MEAN YIELD STRESS AT CONICAL SURFACE TONF PER SQ. IN',CYF
  PRINT*,'MEAN YIELD STRESS AT CONICAL SURFACE TONF PER SQ. IN',STRESS

```

```

C   WRITING THE VARIABLES FOR CONTOUR PLOTTINGS
      DO 400 J1=1,NR+1,2
      DO 600 I1=1,NO+1,2
      PRINT*,C2(J1),C2(I1,J1),CSTRAI(I1,J1),CST(J1),CCST(J1),
      * CEQUIV(I1,J1),CNT(I1,J1),CSIGMA(I1,J1)
600   CONTINUE
400   CONTINUE
      PRINT*
      GOTO 901
902   STOP
      END

C   INTEGRATION FOR SHEAR POWER
      REAL FUNCTION INTP1(XLOW,XHIGH,C2,A2)
C   INTEGRATION DO1AGF
      COMMON/C36/A,C
      PARAMETER(MAXDIV=64,EPS=1.0E-8,ACC=0.0)
      INTEGER IFAIL,NOFUN
      REAL A,B, ERROR,ANS,FUN
      EXTERNAL FUN4
      A=A2
      C=C2
      IFAIL=1
      CALL DO1AGF(XLOW,XHIGH,FUN4,MAXDIV,EPS,ACC,ANS,ERROR,NOFUN,IFAIL)
      IF(IFAIL.GT.0)THEN
        PRINT*, 'FAILED IN DO1AGF'
        STOP
      ELSE
        INTP1=ANS
      ENDIF
      RETURN
      END
      REAL FUNCTION FUN4(D)
      COMMON/C36/A,C
      FUN4=(SIN(D)*SIN(D)*(1+C*C)*EXP(2.0*C*(D-A)))
      RETURN
      END

C   INTEGRATION DO1AGF

C   INTEGRATION FOR DEFORMATION POWER
      REAL FUNCTION INTRGT(XLOW,XHIGH,C2,A2)
      REAL Y(92)
      COMMON/C36/A,C
      PARAMETER(MAXDIV=64,EPS=1.0E-4,ACC=0.0)
      INTEGER IFAIL,NOFUN
      REAL A,B, ERROR,ANS,FUN
      REAL A,B,C,D,E,F
      ALL=0.0
      AREA=0.0
      A=A2
      C=C2
      DX=A*1.0/90.0
      DO 80 I=1,91,1
        D=A*(I-1)*1.0/90.0
        B=(COS(D)+C*SIN(D))**2
        E=(3.0*C*COS(D)+(2.0*C*C-1.0))**2
        F=SIN(D)*EXP(2.0*C*(D-A))
        Y(I)=F*(SQRT(3+E/12.0))
        IF(I.EQ.1)GOTO 90
        ALL=ABS(0.5*DX*(Y(I)+Y(I-1)))
      GOTO 75
90   ALL=0.0
75   AREA=AREA+ALL
80   CONTINUE
      INTRGT=AREA
      RETURN
      END

C
C
C   INTEGRATION F
C   FINDING THE YIELD STRESS FOR FRICTIONAL POWER
C   FINDING THE MEAN YIELD YD STRESS FOR DEFORMATION WORK
      SUBROUTINE INTPD(NO,NR,YD,YF,YS)
      COMMON/C31/STRAIN(21,21),SIGMA(21,21)
      COMMON/C32/R(21,21)
      COMMON/C33/F(21)
      REAL X(50),Y(50),YY(30),XX(30),YM(30)
      INTEGER IFLAG,SA,SB,ICOUNT
C   INTEGRATION USING MILLER'S METHOD
      DO 90 J=1,NO+1,1
      DO 50 I=1,NR+1,1
        X(I)=R(NR+2-I,J)
        Y(I)=SIGMA(NR+2-I,J)

```



```

CALL DO1GAF(X,Y,NR+1,Z,ERROR,IFLAG)
IF(Z.LE.0.0)PRINT*, 'Z IS -VE IN INTPD'
YM(J)=Z/(R(1,J)-R(NR+1,J))
IF(YM(J).LE.0.0)PRINT*, 'YM IS -VE IN INTPD'
IF(IFLAG)90,90,21
21 IF(IFLAG.EQ.1)PRINT*, 'FAILS IN INTPD AS DATA IS LESS THAN 4'
IF(IFLAG.EQ.2)PRINT*, 'FAILS IN INTPD AS DATA NOT INCREASING'
IF(IFLAG.EQ.3)PRINT*, 'FAILS IN INTPD AS POINTS NOT DISTINCT'
STOP
90 CONTINUE
YF=YM(1)
YS=YM(21)
AREA=0.0
DO 70 I=NR,1,-1
DX=SIN(F(I))*R(NR+1,I)-R(NR+1,I+1)*SIN(F(I+1))
IF(DX.LE.0.0)PRINT*, 'DX -VE IN INTPD'
A=0.5*DX*(YM(I)+YM(I+1))
AREA=AREA+A
70 CONTINUE
YD=AREA/(R(NR+1,1)*SIN(F(1))-R(NR+1,NO+1)*SIN(F(NO+1)))
IF(YD.LE.0.0)PRINT*, 'YD IS -VE IN INTPD'
RETURN
END

```

```

C FINDING THE B AND N VALUES
C THIS SUBROUTINE EXPRESS THE VALUES OF B IN
C LBF PER SQ.IN

```

```

SUBROUTINE TMK1(T,TDF,E,B,N,TMK)
REAL NX*MAX,NX*MIN,NX,N,NT0,NT1,NT2,K
K=0.08
SO=2.0
CONV=2240.0
TMK=(T+TDF+273.0)*(1-K*LOG(E/SO))
C FINDING THE VALUES OF B
IF(TMK.LE.200.0)THEN
B=((200.0-TMK)*0.095+57.0)*CONV
N=0.08
GOTO 30
ENDIF
IF(TMK.GE.775.0)THEN
B=(16.0-((TMK-775.0)/50.0)*4.0)*CONV
IF(B.LE.0.0)THEN
B=2.5*CONV
ENDIF
N=0.12
GOTO 30
ENDIF
C POLYNOMIAL OF DEGREE 1
IF (TMK.LE.350.0)THEN
B=((200.0-TMK)*0.095+57.0)*CONV
GOTO 10
ENDIF

```

```

C
C POLYNOMIAL OF DEGREE 2
IF (TMK.LE.425.0)THEN
A0=88.3742
A1=1.3943
A2=2.189334
A3=0.0
A4=0.0
A5=0.0
XMAX=440.0
XMIN=325.0
GOTO 5
ENDIF

```

```

C
C POLYNOMIAL OF DEGREE 3
IF (TMK.LE.525.0)THEN
A0=94.0
A1=-0.666
A2=-2.642357
A3=-0.03333
A4=0.0
A5=0.0
XMAX=525.0
XMIN=425.0
GOTO 5
ENDIF

```

```

C      POLYNOMIAL OF DEGREE 3
      IF (TMK.LE.775.0)THEN
        A0=55.95
        A1=-13.33451
        A2=0.8341
        A3=-0.727
        A4 = 0.0
        A5 = 0.0
        XMAX = 775.0
        XMIN = 525.0
        GOTO 5
      ENDIF

C      FINDING THE VALUE OF B
C      5
      X = (2.0*TMK-XMAX-XMIN)/(XMAX-XMIN)
      T0 = 1.0
      T1 = X
      T2 = 2.0* X * X-1.0
      T3 = 4.0*(X**3)-3.0*X
      T4 = 8.0*(X**4)-8.0*(X**2)+1.0
      T5 = 16.0*(X**5)-20.0*(X**3)+5.0*X
      B = (0.5*A0*T0 + A1*T1 + A2*T2 + A3*T3 + A4*T4 + A5*T5)*CONV
      IF(B.LE.0.0)THEN
        PRINT*, 'VALUE OF B IS NEGATIVE AND EQUALS TO ',B
      ENDIF

C      FINDING THE N VALUES
C      POLYNOMIAL OF DEGREE 2
C      10
      IF (TMK.LE.275.0)THEN
        A0=0.3069
        A1=0.05325
        A2=-0.015468
        NXMAX = 275.0
        NXMIN = 200.0
        GOTO 15
      ENDIF

C      POLYNOMIAL OF DEGREE 2
C      IF (TMK.LE.400.0)THEN
        A0=0.38417
        A1=0.00197326
        A2=-0.00007459
        NXMAX=400.0
        NXMIN=275.0
        GOTO 15
      ENDIF

C      POLYNOMIAL OF DEGREE 2
      IF (TMK.LE.525.0)THEN
        A0=0.37431
        A1=-0.033
        A2=-0.023906
        NXMAX = 525.0
        NXMIN = 400.0
        GOTO 15
      ENDIF
      IF (TMK.GE.525.0)THEN
        N=0.12
        GOTO 30
      ENDIF
      NX=(2.0*TMK-NXMAX-NXMIN)/(NXMAX-NXMIN)
      NTO=1.0
      NT1=NX
      NT2=2.0*NX*NX-1.0
      N=0.5*A0*NTO + A1*NT1 + A2*NT2
      IF (N.LE.0.0)THEN
        PRINT*, 'STRAIN-HARDENING INDEX LESS THAN 0.0',N,'AT'
        PRINT*, 'TMK=',TMK,'TEMP',T,'STRAINRATE',E,'TEMP RISE',TDF
      ENDIF
      30
      RETURN
      END

```

SUB-PROGRAM 'CONSTANT'

```

C THIS PROGRAM PLOTS THE STRESS -TMK CURVES FOR VARIOUS
C VALUES OF STRAIN AND CONSTANT K
C THE READER IS ADVISED TO CONSULT THE GINOGRAPH ROUTINE ON
C THE 1904S ICL COMPUTERS
C K=CONSTANT IN THE VELOCITY-MODIFIED TEMPERATURE FORMULA
C NCURVE=NO. OF GRAPHS
C NSETS=NO. OF CURVES PER GRAPH
C NPTS=NO. OF POINTS PER CURVE
C SRATE=STANDARD STRAIN RATE
C
  PROGRAM LOH
  REAL X(10,20),Y(10,20),TMK(10,20),K,XVAL(20),YVAL(20)
  8      Z(10,20),U(10,20),V(10,20),DF(10,20)
  INTEGER NPTS(10)

  READ*,NCURVE
  READ*,NSETS
  READ*,SRATE
  CALL OPEN
  XDIST=(NCURVE+3)*250.0
  CALL DEVPAF(XDIST,350.0,0)
  CALL CHASIZ(1)
  CALL CHASIZ(2.5,2.5)
  CALL SHIFT2(20.0,20.0)
  CALL MOVTO2(0.0,0.0)

C INPUT ACTUAL DATA*TEMP.,STRESS,STRAIN RATE,B,N
  DO 55 I=1,NSETS,1
    READ*,NPTS(I)
    DO 60 J=1,NPTS(I),1
      READ*,X(I,J),Y(I,J),Z(I,J),U(I,J),V(I,J)
60    CONTINUE
55    CONTINUE

210  READ*,K
      PRINT*,'K=',K,'STD. RATE',SRATE
      IF (K.GE.10000.0)GOTO 115

C FINDING THE MAXIMUM AND MINIMUM X-Y VALUES
      XHIGH=-10000000.0
      YHIGH=-10000000.0
      XLOW=100000000.0
      YLOW=1000000000.0
      PRINT*
      PRINT*,' TEMP.          STRESS          STRAIN-RATE          TMK'

C CALCULATION OF TEMPERATURE RISE AND INCORPORATING INTO TMK
      DO 75 I=1,NSETS,1
        DO 80 J=1,NPTS(I),1
          DT=1450.0*(U(I,J)/(V(I,J)+1.0))*(0.5*(1+V(I,J)))/
          8      (9336.0*0.2840344*(420.0+0.504*X(I,J))+0.000239)
          DF(I,J)=DT*0.55556
          TMK(I,J)=(X(I,J)+DF(I,J)+273.0)*(1-K*(ALOG(Z(I,J)/SRATE)))

C FIND MAX TMK I.E. MAX X
          IF (TMK(I,J).GT.XHIGH)THEN
            XHIGH=TMK(I,J)
          ENDIF
          IF (TMK(I,J).LE.XLOW)THEN
            XLOW=TMK(I,J)
          ENDIF

C FIND MAX Y
          IF (Y(I,J).GT.YHIGH)THEN
            YHIGH=Y(I,J)
          ENDIF
          IF (Y(I,J).LT.YLOW)THEN
            YLOW=Y(I,J)
          ENDIF
          PRINT*,X(I,J),Y(I,J),Z(I,J),U(I,J),V(I,J),DF(I,J),TMK(I,J)
30    CONTINUE
75    CONTINUE
      PRINT*,'XLOW',XLOW,'XHIGH',XHIGH,'YLOW',YLOW,'YHIGH',YHIGH
      PRINT*

```

```
GRAPH PLOTTING
C SCALING THE GRAPH
C CALL AXIPDS(1,0.0,0.0,200.0,1)
CALL AXIPDS(1,0.0,0.0,300.0,2)
CALL AXISCA(3,10,XLOW,XHIGH,1)
CALL AXISCA(3,10,YLOW,YHIGH,2)
CALL AXIDRA(-1,1,1)
CALL AXIDRA(1,-1,2)

C DRAW THE GRAPH
C DO 65 II=1,NSETS,1
DO 70 JJ=1,NPTS(II),1
XVAL(JJ)=FMK(II,JJ)
YVAL(JJ)=Y(II,JJ)
70 CONTINUE
ISYM=II
CALL GRASYM(XVAL,YVAL,NPTS(II),ISYM,0)
65 CONTINUE
CALL SHIFT2(250.0,0.0)
CALL MOVT02(0.0,0.0)
GOTO 210
115 CALL DEPEND
STOP
END
```

SUB-PROGRAM 'CURVE'

```

C THIS PROGRAM FINDS THE BEST CURVE TO A SET OF POINTS.
C THE STANDARD ROUTINE USED IS EO2ADF ON THE 1904S ICL
C COMPUTERS.
C THE READER IS ADVISED TO CONSULT THAT ROUTINE

C M=NO. OF DATA
C K=DEGREE OF FREEDOM
C T=TEMPERATURE

      PROGRAM L3H
      INTEGER R,R2
      REAL X(100),Y(100),W(200),A(50,50),S(50),WORK1(3,10),
&      BX(10),EX(50),WORK2(2,8)
      NROWS=50

20  READ*,M
      IF(M.GE.10000)GOTO 30
C   SET THE MAXIMUM DEGREE AS 7
      IF(M.GE.3)THEN
        K=7
        GOTO 12
      ENDIF
      K=M-1
C   KPLUS1 MUST NOT BE GREATER THAN M
12  KPLUS1=K+1

C   READ THE INPUT VALUES
      DO 60 R=1,M
C   X VALUES MUST BE IN ASCENDING ORDER
      READ*,X(R),EX(R)
      W(R)=1.0
      Y(R)=EX(R)
60  CONTINUE

C   EXECUTING THE NAG ROUTINE
      IFAIL=1
      CALL EO2ADF(M,KPLUS1,NROWS,X,Y,W,WORK1,WORK2,A,S,IFAIL)
C   IF PROGRAM FAILS-----
      IF(IFAIL.NE.0)GOTO 300

C   PRINT THE RESULTS
      DO 160 IPLUS1=1,KPLUS1
        I=IPLUS1-1
        PRINT*, 'DEGREE=',I
        PRINT*, 'COEFFICIENTS ='
        PRINT*,(JPLUS1,A(IPLUS1,JPLUS1),JPLUS1=1,IPLUS1)
        PRINT*, 'RESIDUAL',S(IPLUS1)

C   COMPUTING THE COEFFICIENTS OF THE POLYNOMIALS
      DO 100 JJ=2,M
        XMIN=X(1)
        XMAX=X(M)
        DO 80 J=1,5
          BX(1)=X(JJ-1)
          BX(5)=X(JJ)
          DI=(BX(5)-BX(1))*(J-1)/4.0
          DX=X(JJ-1)+DI
          XX=((DX-XMIN)-(XMAX-DX))/(XMAX-XMIN)
          T0=1.0
          T1=XX
          T2=2.0*(XX**2)-1
          T3=4.0*(XX**3)-3.0*XX
          T4=8.0*(XX**4)-8.0*(XX**2)+1.0
          T5=16.0*(XX**5)-20.0*(XX**3)+5.0*XX
          T6=32.0*(XX**6)-48.0*(XX**4)+18.0*(XX**2)-1.0
          T7=64.0*(XX**7)-112.0*(XX**5)+56.0*(XX**3)-7.0*XX
          T8=128.0*(XX**8)-256.0*(XX**6)+160.0*(XX**4)
          -32.0*(XX**2)+1

```

```

      IF(I.EQ.0) THEN
      Y1=0.5*A(I+1,1)*T0
      ENDIF
      IF(I.EQ.1) THEN
      Y2=0.5*A(I+1,1)*T0+A(I+1,2)*T1
      ENDIF
      IF(I.EQ.2) THEN
      Y3=0.5*A(I+1,1)*T0 + A(I+1,2)*T1+A(I+1,3)*T2
      ENDIF
      IF(I.EQ.3) THEN
      Y4=0.5*A(I+1,1)*T0 + A(I+1,2)*T1 + A(I+1,3)*T2+A(I+1,4)*T3
      ENDIF
      IF(I.EQ.4) THEN
      Y5=0.5*A(I+1,1)*T0+A(I+1,2)*T1+A(I+1,3)*T2+A(I+1,4)*T3
      &      +A(I+1,5)*T4
      ENDIF
      IF(I.EQ.5) THEN
      Y6=0.5*A(I+1,1)*T0+A(I+1,2)*T1+A(I+1,3)*T2+A(I+1,4)*T3
      &      +A(I+1,5)*T4+A(I+1,6)*T5
      ENDIF
      IF(I.EQ.6) THEN
      Y7=0.5*A(I+1,1)*T0+A(I+1,2)*T1+A(I+1,3)*T2+A(I+1,4)*T3
      &      +A(I+1,5)*T4+A(I+1,6)*T5+A(I+1,7)*T6
      ENDIF
      IF(I.EQ.7) THEN
      Y8=0.5*A(I+1,1)*T0+A(I+1,2)*T1+A(I+1,3)*T2+A(I+1,4)*T3
      &      +A(I+1,5)*T4+A(I+1,6)*T5+A(I+1,7)*T6+A(I+1,8)*T7
      ENDIF
      IF(I.EQ.0) YY=Y1
      IF(I.EQ.1) YY=Y2
      IF(I.EQ.2) YY=Y3
      IF(I.EQ.3) YY=Y4
      IF(I.EQ.4) YY=Y5
      IF(I.EQ.5) YY=Y6
      IF(I.EQ.6) YY=Y7
      IF(I.EQ.7) YY=Y8
      IF(DX.EQ.X(JJ-1)) THEN
      EY=YY
C   PRINTING THE ACTUAL AND CALCULATED VALUES
      PRINT*,DX,' ',YY,' ',Y(JJ-1),' ',EY,' ',EX(JJ-1)
      ELSE
      PRINT*,DX,' ',YY
      ENDIF
30    CONTINUE
100    CONTINUE
160    CONTINUE
      GOTO 20

C   PROGRAMS FAIL DUE TO.....
300    GOTO(320,340,360,380,400),IFAIL
320    PRINT*, 'NON POSITIVE WT'
      GOTO 20
340    PRINT*, 'VALUES OF INDEPENDENT VALUES NOT INCREASING'
      GOTO 20
360    PRINT*, 'VALUES OF INDEPENDENT VARAIBLES ALL EQUAL'
      GOTO 20
380    PRINT*, 'TOO FEW DISTINCT VALUES OF INDEPENDENT VALUE'
      GOTO 20
400    PRINT*, 'NROWS FAILS TO EXCEED MAX. DEGREE'
      GOTO 20
30    STOP
      END

```

SUB-PROGRAM 'CONTOUR'

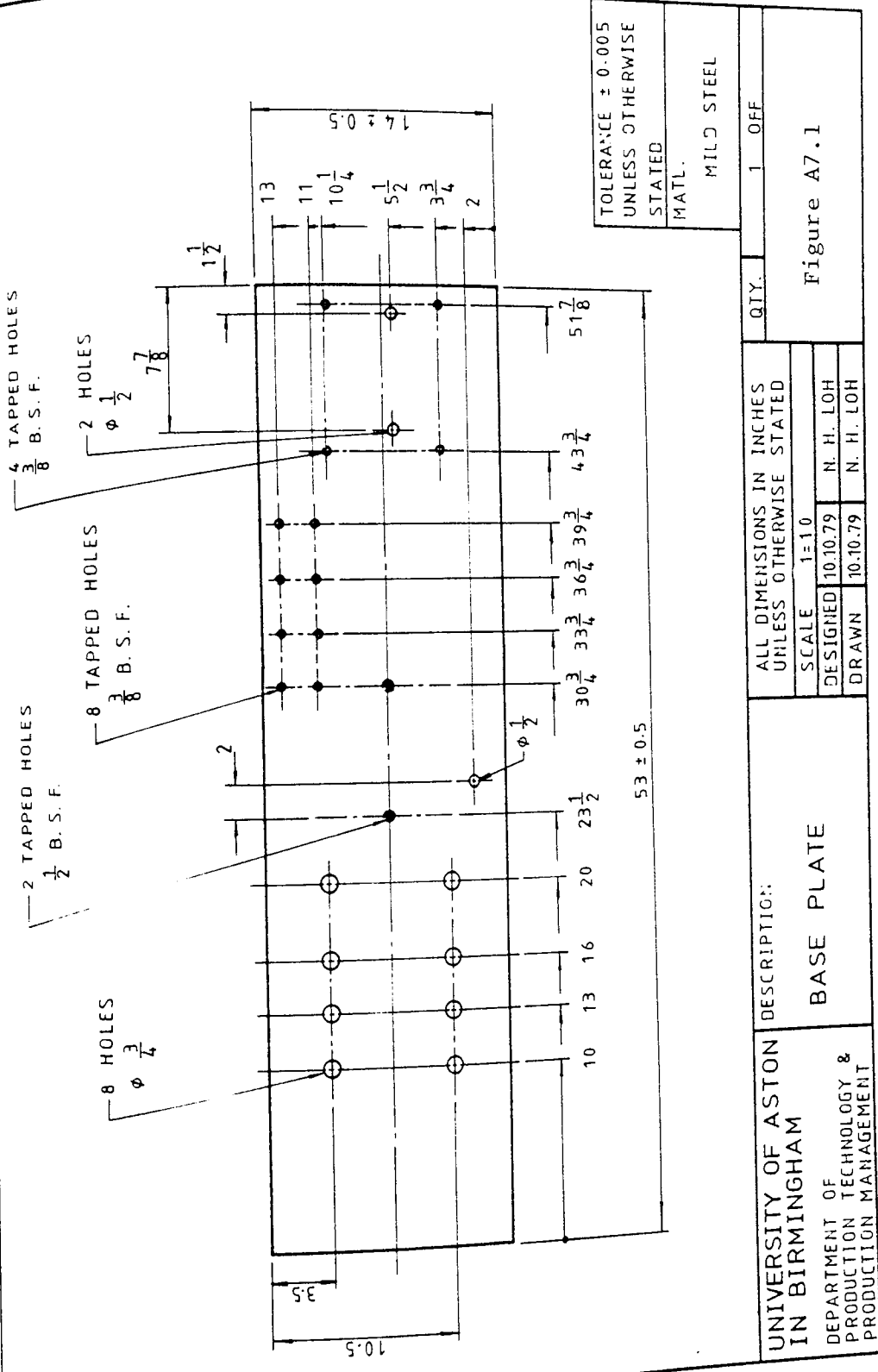
```

C CONTOUR PLOTTINGS FOR STRAIN, STRAIN RATE
C TEMPERATURE AND STRESS DISTRIBUTIONS IN THE
C DEFORMATION ZONE
C
C THE READER IS ADVISED TO CONSULT THE GINOSURF
C ROUTINE ON THE ICL 1904S COMPUTER FOR A
C BETTER UNDERSTANDING OF THIS PROGRAM.
C
C NUMBER=NO. OF CONTOUR LEVELS
C NP=NO. OF DATA POINTS
C Z1=CONTOUR VALUES
C
C
C PROGRAM LOH
C REAL X(250),Y(250),Z(250),W(4300),AZ(40,40),
C & Z1(10),L,CC(10),XX(250),YY(250),ZZ(250)
C & A(250),B(250)
C CALL OPEN
C CALL CHASIZ(1)
C CALL CHASIZ(2.5,2.5)
C NUMX=40
C NUMY=40
C ISM=1
C
C INPUT DATA
C READ*,NUMBER
C DO 12 II=1,NUMBER
C READ*,Z1(II)
12 CONTINUE
C READ*,NP
C
C SET THE VALUES OF X AND Y FOR ESTABLISHING
C THE MINIMUM AND MAXIMUM VALUES OF X AND Y
C XLOW=10000000000.0
C XHIGH=-10000000000.0
C YLOW=10000000000.0
C YHIGH=-10000000000.0
C
C READ THE X,Y,STRAIN,STRAIN RATE,TEMPERATURE
C AND STRESS VALUES
C DO 100 I=1,NP,1
C READ*,XX(I),YY(I),Z(I),ZZ(I)
C READ*,A(I),B(I)
C X(I)=YY(I)*COS(XX(I))
C Y(I)=YY(I)*SIN(XX(I))
C
C COMPARE THE X AND Y VALUES TO FIND THE MINIMUM
C AND MAXIMUM VALUES OF X AND Y
C SO AS TO SET THE X AND Y SCALE
C IF (X(I).LT.XLOW)THEN
C XLOW=X(I)
C ENDIF
C IF (X(I).GE.XHIGH)THEN
C XHIGH=X(I)
C ENDIF
C IF (Y(I).LT.YLOW)THEN
C YLOW=Y(I)
C ENDIF
C IF (Y(I).GE.YHIGH)THEN
C YHIGH=Y(I)
C ENDIF
100 CONTINUE
C
C THE CONTOUR PLOTTINGS
C NW=2*NUMX*NUMY + 4*NP
C CALL CIRPTS(50)
C CALL RANGRD(NP,X,Y,Z,NUMX,XLOW,XHIGH,NUMY,YLOW,YHIGH,AZ,NW,W)
C CALL WINDOZ(30.0,190.0,20.0,140.0)
C CALL SETSCA(0.01,0.01,1)
C CALL DRACON (NUMX,XLOW,XHIGH,NUMY,YLOW,YHIGH,AZ,0,ISM,NW,W)
C DO 65 I=1,NUMBER
C CALL ADDCON(Z1(I),ISM,NW,W)
55 CONTINUE
C CALL DEVENO

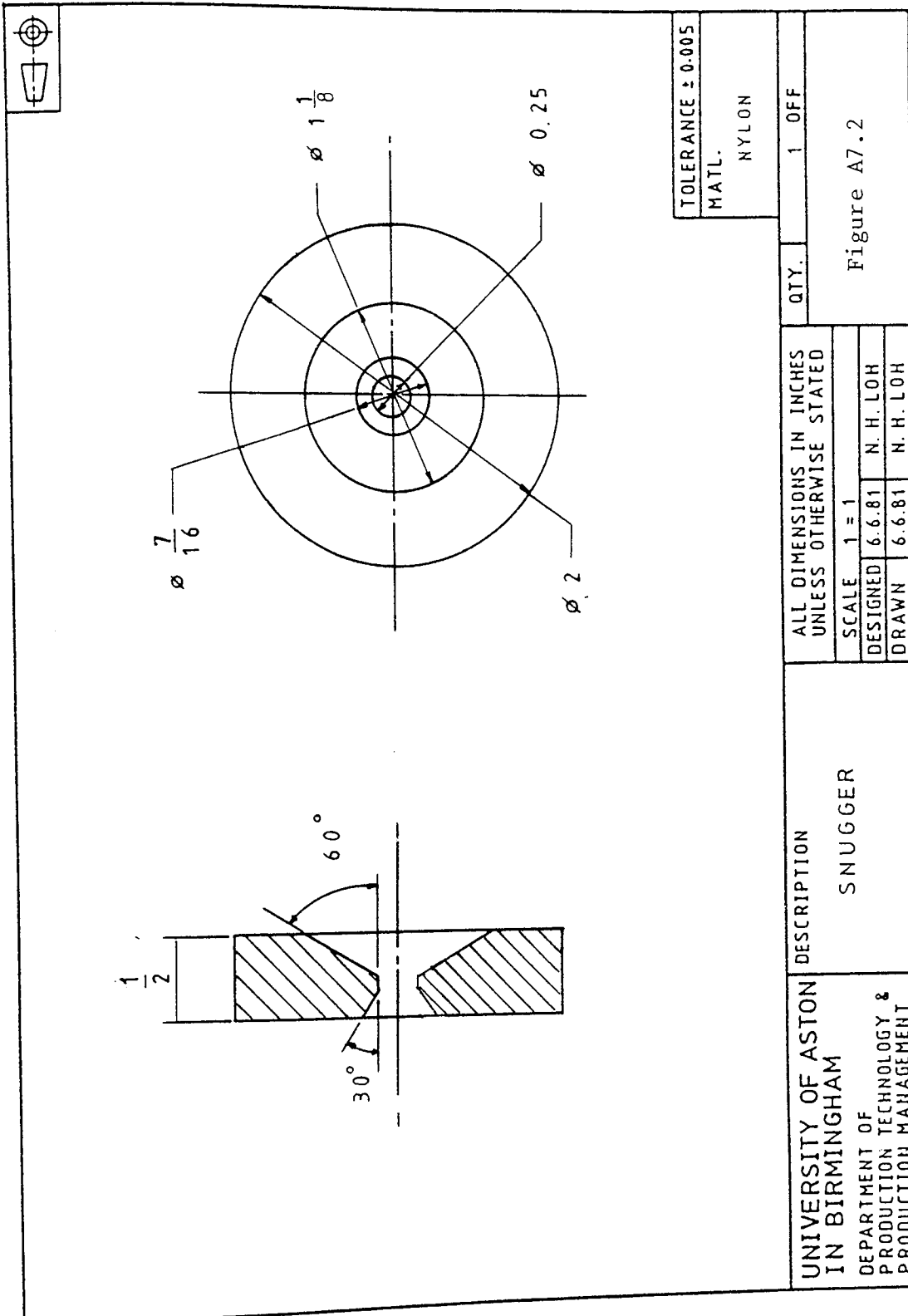
```

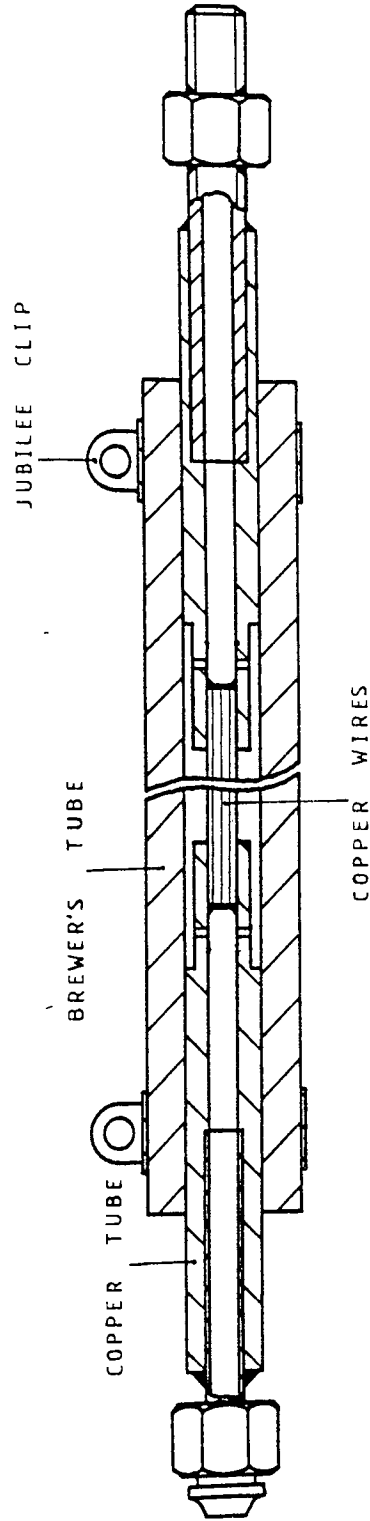
APPENDIX A7

Mechanical Drawings

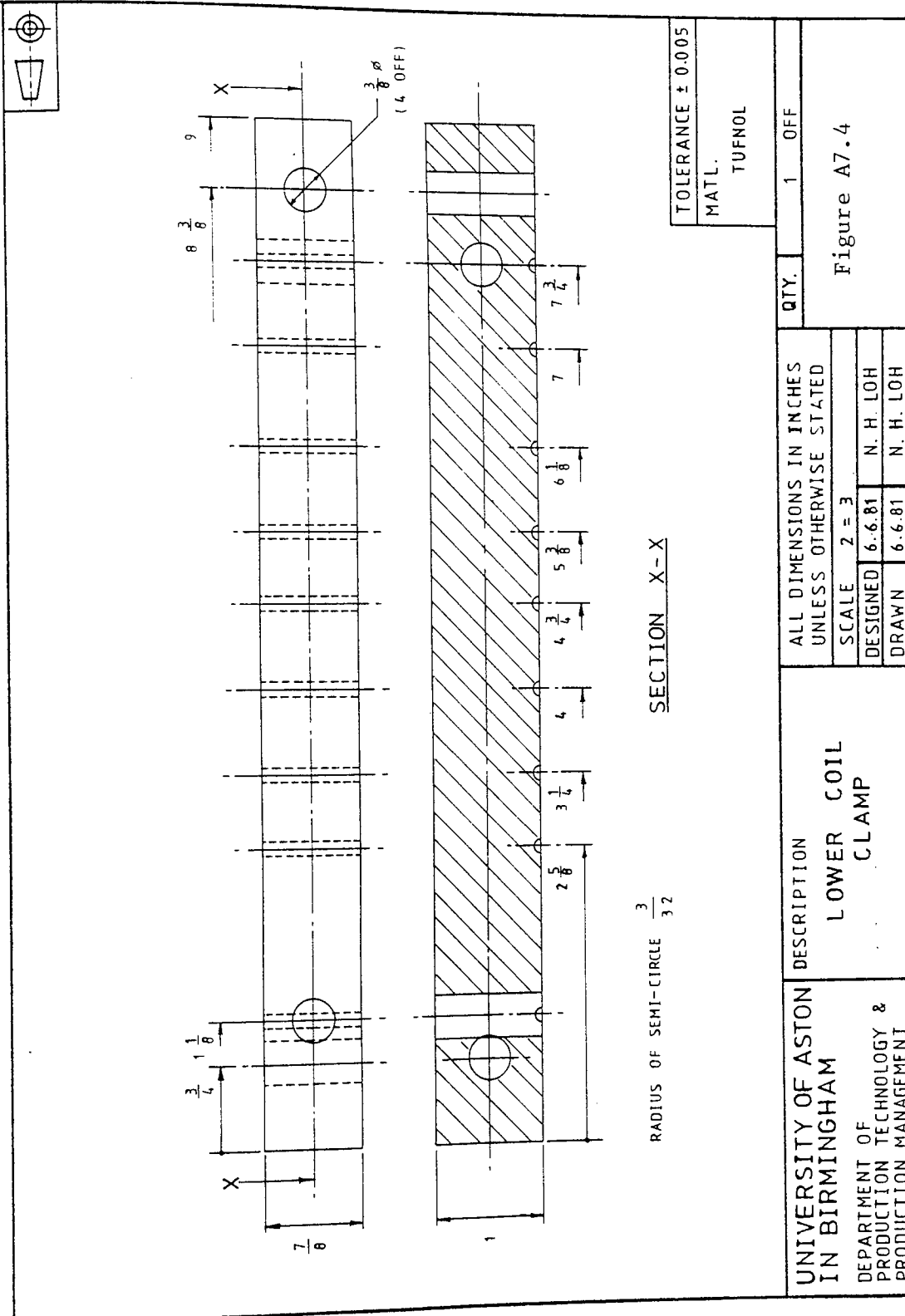


UNIVERSITY OF ASTON IN BIRMINGHAM	DESCRIPTION: BASE PLATE	ALL DIMENSIONS IN INCHES UNLESS OTHERWISE STATED		QTY.	1	OFF
		SCALE 1=10				
		DESIGNED	10.10.79			
		DRAWN	10.10.79			
		N. H. LOH				
DEPARTMENT OF PRODUCTION TECHNOLOGY & PRODUCTION MANAGEMENT	N. H. LOH		Figure A7.1			





UNIVERSITY OF ASTON IN BIRMINGHAM DEPARTMENT OF PRODUCTION TECHNOLOGY & PRODUCTION MANAGEMENT	DESCRIPTION FLEXIBLE EXTENSION	ALL DIMENSIONS IN INCHES UNLESS OTHERWISE STATED		QTY	2	OFF
		SCALE NOT TO SCALE		Figure A7.3		
		DESIGNED	25.9.79			
		DRAWN	25.9.79			



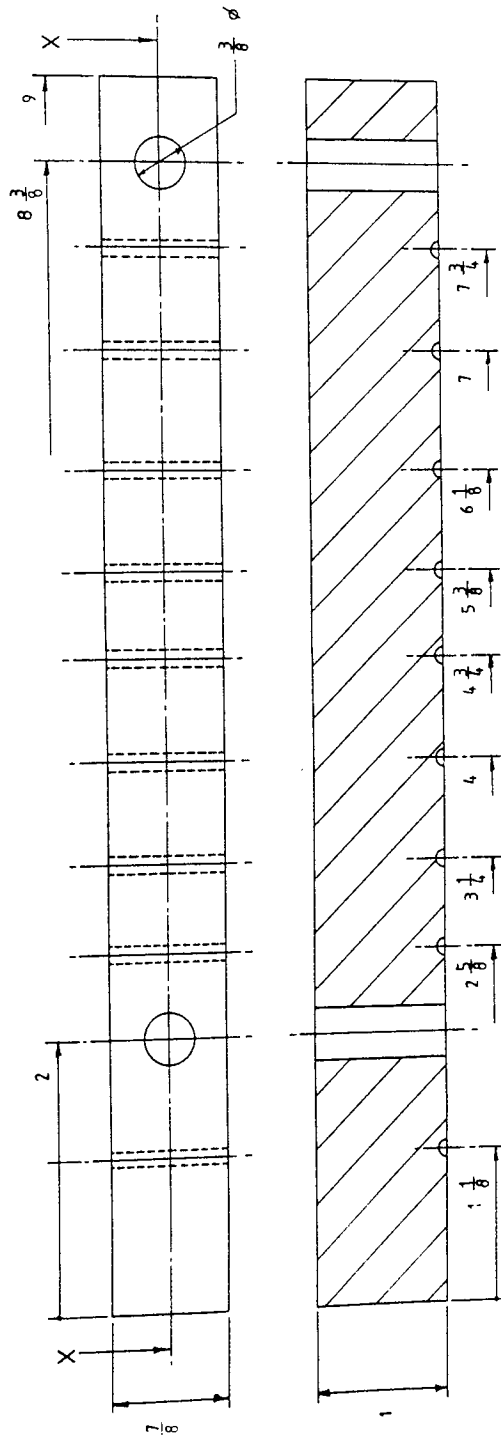
SECTION X-X

RADIUS OF SEMI-CIRCLE $\frac{3}{32}$

32

UNIVERSITY OF ASTON IN BIRMINGHAM	DEPARTMENT OF PRODUCTION TECHNOLOGY & PRODUCTION MANAGEMENT	DESCRIPTION LOWER COIL CLAMP	ALL DIMENSIONS IN INCHES UNLESS OTHERWISE STATED		QTY.	1	OFF
			SCALE 2 = 3				
			DESIGNED	6.6.81			
			DRAWN	6.6.81			
			N. H. LOH				
		N. H. LOH					
			Figure A7.4				

TOLERANCE ± 0.005
MATL.
TUFNOL

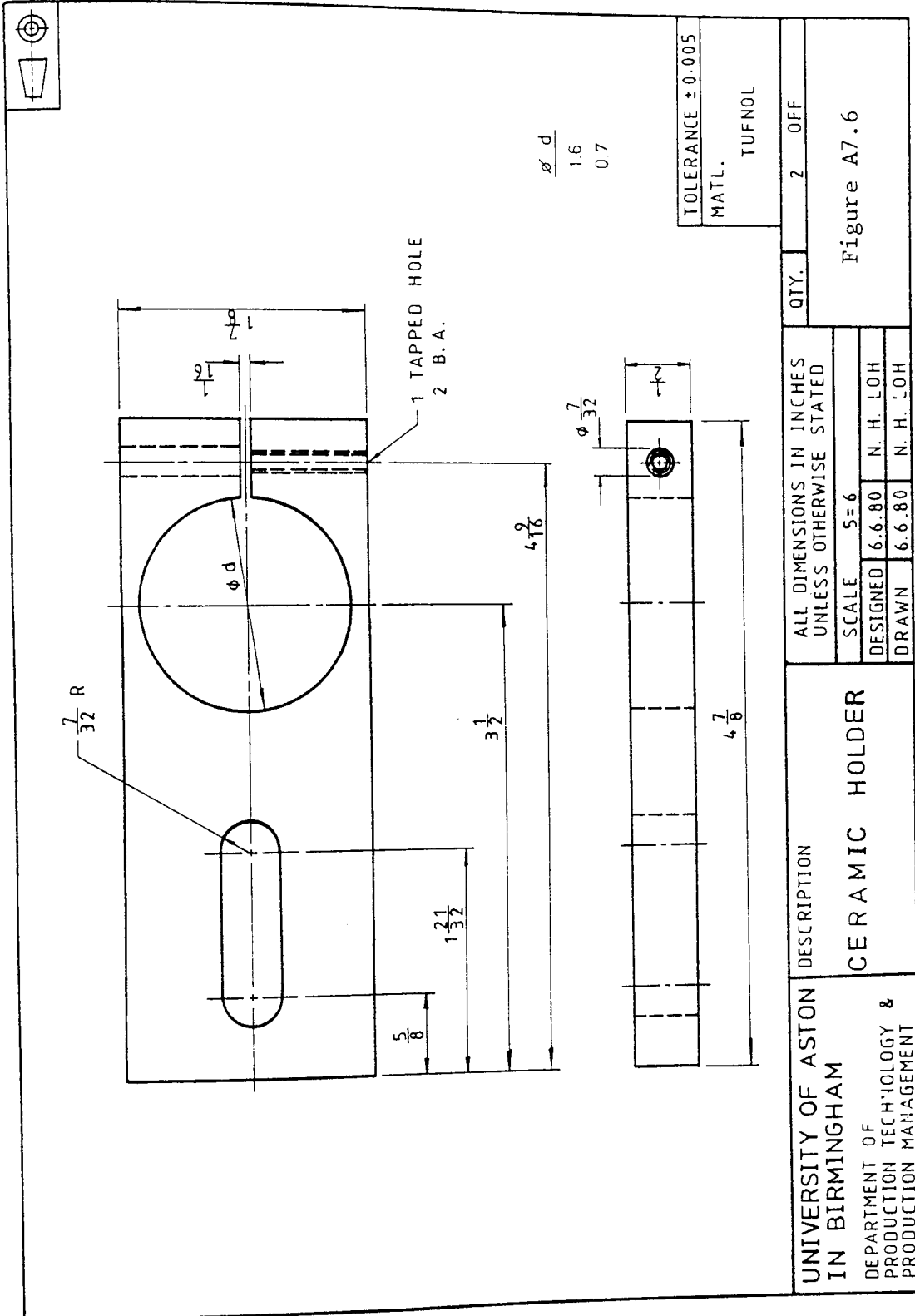


RADIUS OF SEMI-CIRCLE $\frac{3}{32}$

SECTION X-X

TOLERANCE \pm 0.005
MATL.
TUFNOL

UNIVERSITY OF ASTON IN BIRMINGHAM	DEPARTMENT OF PRODUCTION TECHNOLOGY & PRODUCTION MANAGEMENT	DESCRIPTION UPPER COIL CLAMP	ALL DIMENSIONS IN INCHES UNLESS OTHERWISE STATED		QTY.	1	OFF	
			SCALE 2 = 3					
			DESIGNED	6.6.81				N. H. LOH
			DRAWN	6.6.81				N. H. LOH
			Figure A7.5					



UNIVERSITY OF ASTON
IN BIRMINGHAM

DESCRIPTION

CERAMIC HOLDER

ALL DIMENSIONS IN INCHES
UNLESS OTHERWISE STATED

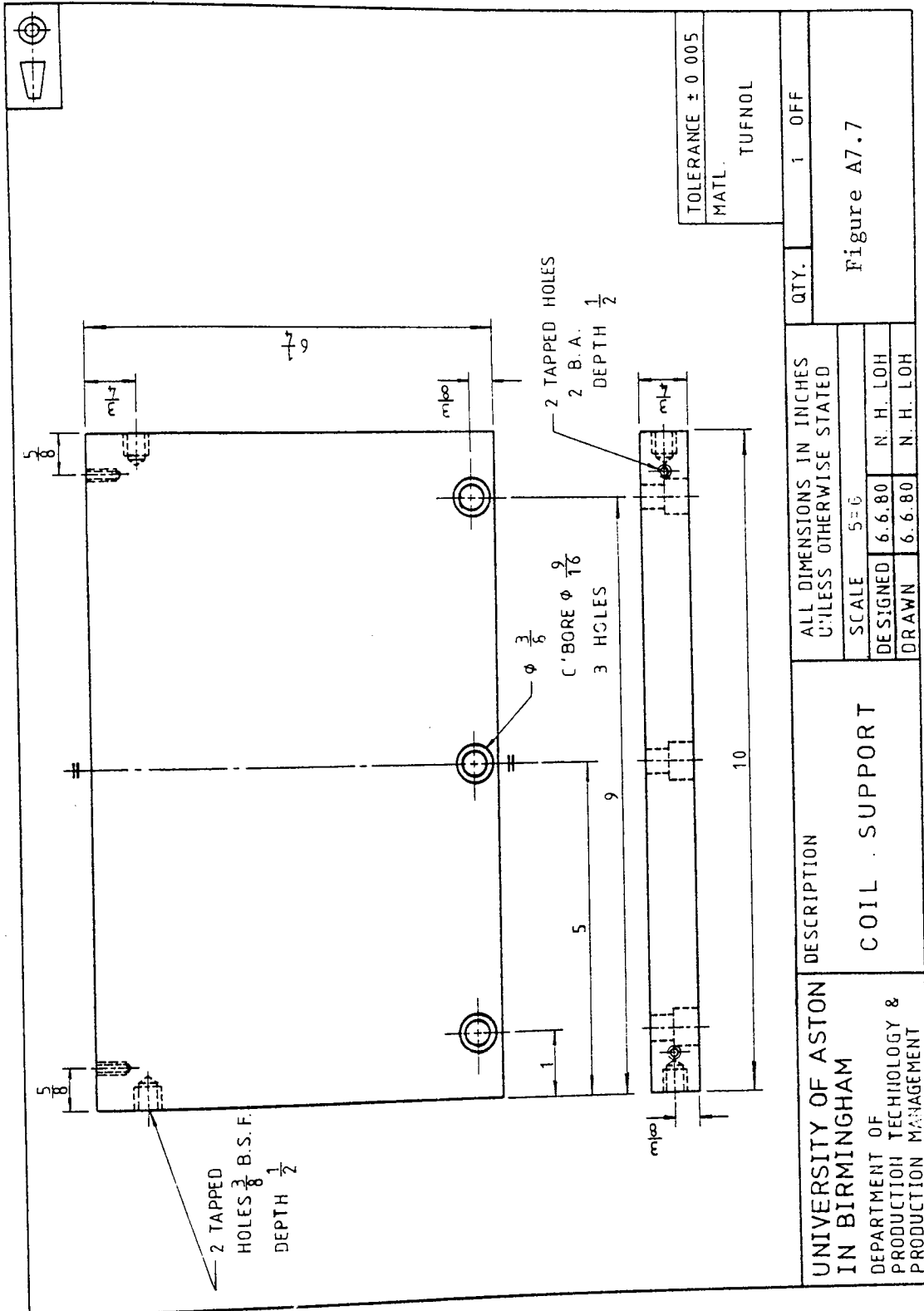
SCALE 5=6

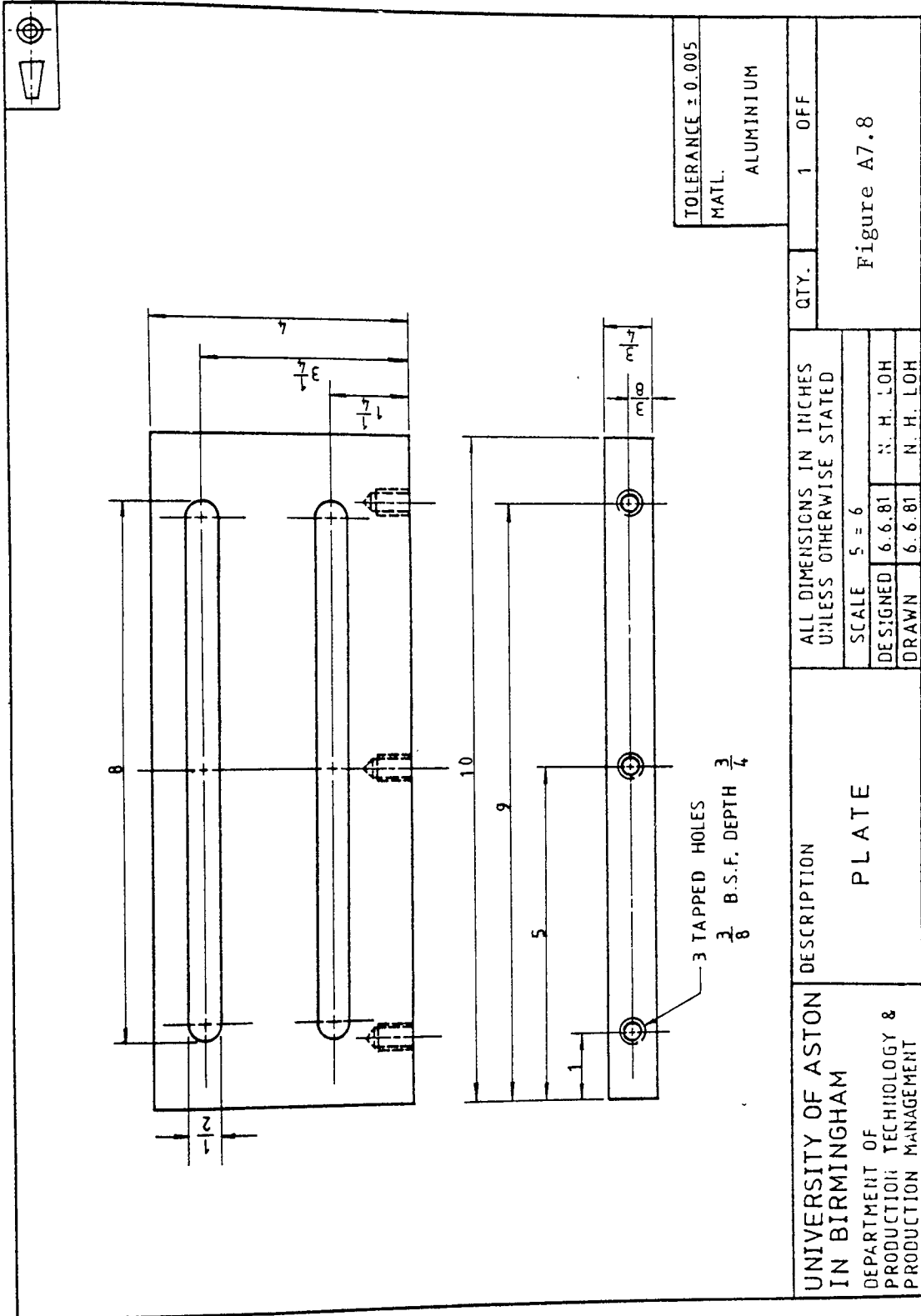
DESIGNED 6.6.80 N. H. LOH

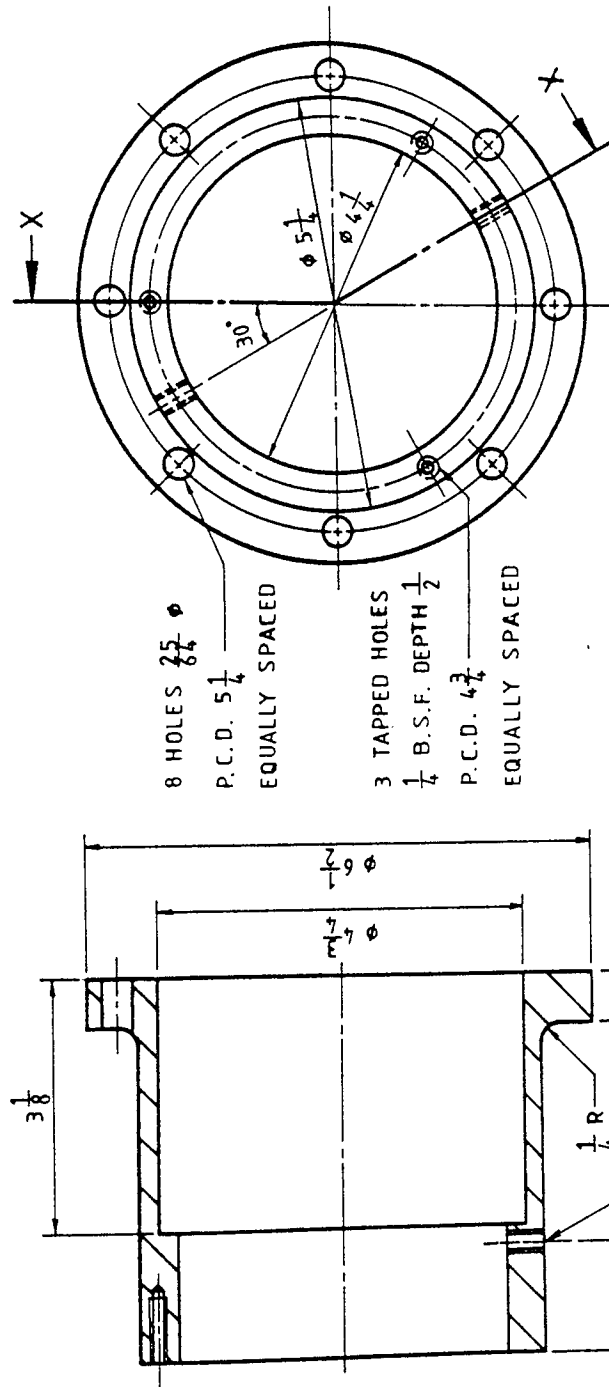
DRAWN 6.6.80 N. H. LOH

QTY.

2 OFF

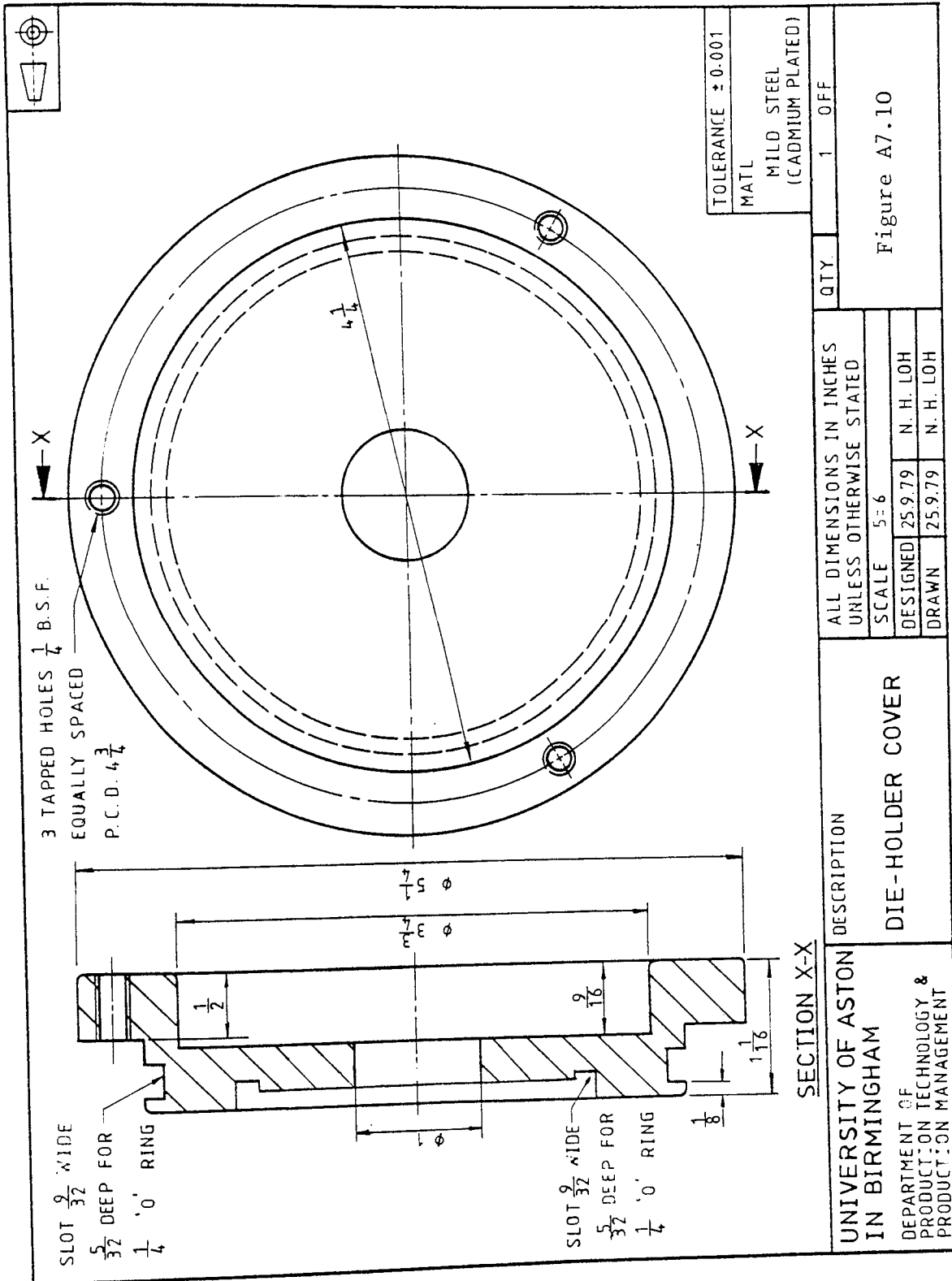


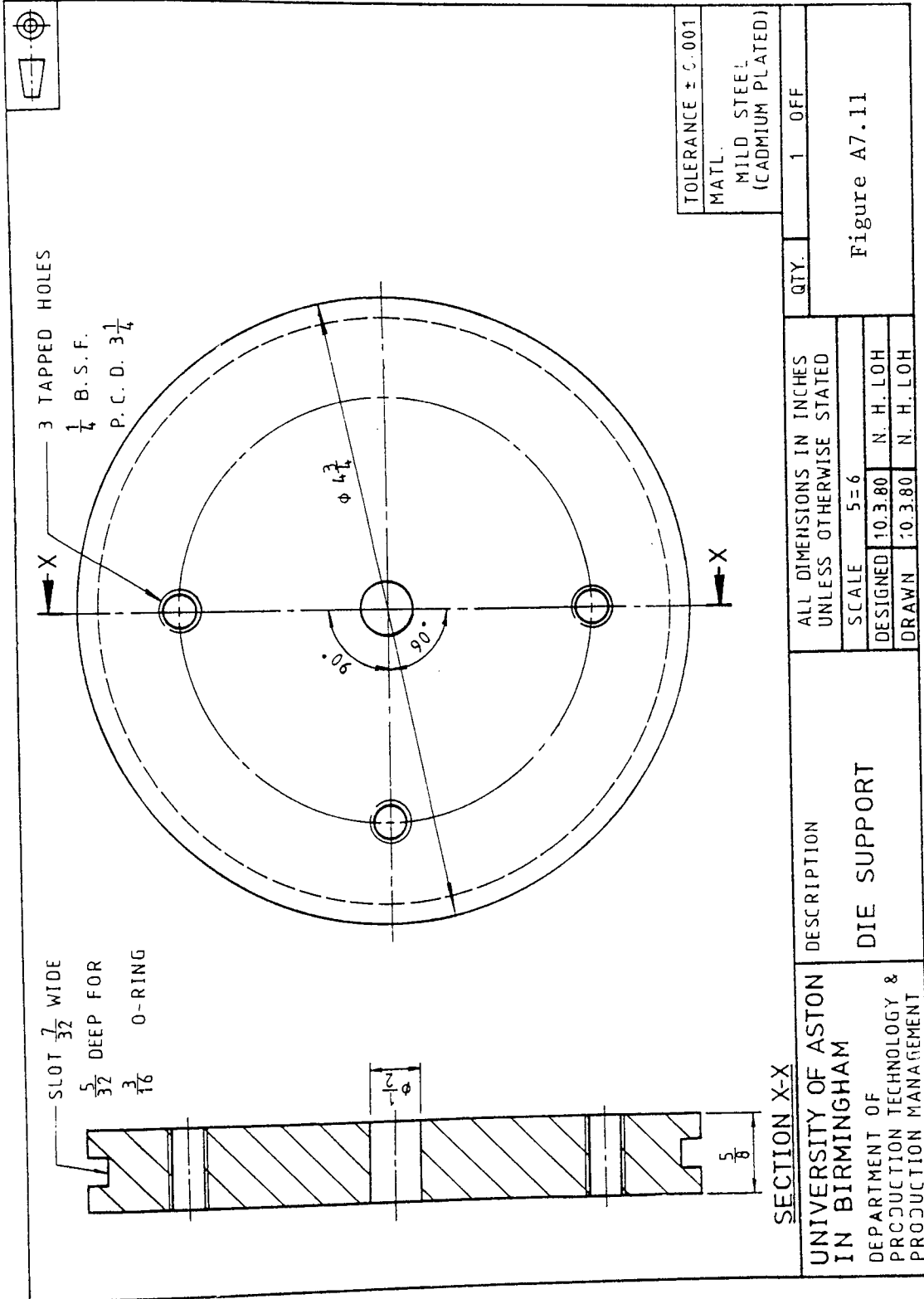




TOLERANCE ± 0.001
MATL.
MILD STEEL
(CADMIUM PLATED)

UNIVERSITY OF ASTON IN BIRMINGHAM	DESCRIPTION DIE - HOLDER	ALL DIMENSIONS IN INCHES UNLESS OTHERWISE STATED		QTY.	1	OFF	Figure A7.9
		SCALE NOT TO SCALE					
		DESIGNED	7.10.79				
		N. H. LOH					
		DRAWN	7.10.79				
N. H. LOH							





SECTION X-X

UNIVERSITY OF ASTON
 IN BIRMINGHAM
 DEPARTMENT OF
 PRODUCTION TECHNOLOGY &
 PRODUCTION MANAGEMENT

DESCRIPTION

DIE SUPPORT

ALL DIMENSIONS IN INCHES
 UNLESS OTHERWISE STATED

SCALE 5=6

DESIGNED 10.3.80 N. H. LOH

DRAWN 10.3.80 N. H. LOH

QTY.

1

OFF

Figure A7.11

APPENDIX A8

List of References

APPENDIX A8

REFERENCES

1. Sansome, D H 'Metal forming processes'
Dept of Prod Tech & Mgt,
Univ of Aston in Birmingham
2. Sansome, D H 'People, Pence and Plasticity'
Inaugural Lecture,
Univ of Aston in Birmingham, 1975
3. Loh, N H
Sansome, D H 'A review of the warm drawing of
wire'
Fine Wires International Conference,
30 - 31 Oct 1980, Aachen, West
Germany
4. Anon 'Elevated temperature drawing gives
steel unique properties'
Iron and Steel Engineer, 1957, 34,
191
5. Francis, E L 'Studies of the wire-drawing process'
Part III - Lubrication'
Carnegie Scholarship Memoirs,
Iron and Steel Institute, 1932,
1 - 34
6. Sachs, G Z Ang Math Mech, 1927, I, 235 - 236
7. Siebel, E 'Der derzeitigestand der Erkemtnisser
uber die mechanischen Vorgange bein
Drahtsichen'
Stahl und Eisen, 1947, 66 - 67, 171
8. Korber, F
Eichinger, A Die Grundlagen der bildamen
Verformung, Mitt KW Inst
Eisenforsachung, 1940, 22, 57
9. Davis, E A
Dokos, S J 'Theory of wire drawing'
J Appl Mech,
1944, 66, A193 - A210
10. MacLellan, G D S 'A critical survey of wire drawing
theory'
J Iron and Steel Inst,
1948, 158, 347 - 356
11. Avitzur, B 'Analysis of wire drawing and
extrusion through conical dies of
small cone angle'
Trans ASME, J Eng Ind,
1963, 85, 89 - 96

12. Kobayashi, S 'Upper bound solutions of axisymmetric forming problems - II'
Trans ASME, J Eng Ind,
1964, 86, 326 - 332
13. Thomsen, E G 'Mechanics of plastic deformation
in metal processing'
The MacMillan Company, 1965
14. Alder, J F 'The effect of strain rate and
Phillips, V A temperature on the resistance
of aluminium, copper, and steel
to compression'
J Inst Metals,
1954 - 55, 83, 80 - 86
15. Cook, P M 'True stress-strain curves for
steel in compression at high
temperatures and strain rates,
for application to the calculation
of load and torque in hot rolling'
Proceedings of conference on
properties of materials at high
rates of strain. 1957, 86 - 97
16. Doraivelu, S M 'Development of a tool set-up for
Gopinathan, V studying the influence of
temperature on compressive flow
strength under dynamic conditions'
Proc 18th Int MTDR Conf,
1977, 37 - 42
17. Suzuki, 'Report of the Institute of
et al industrial science'
University of Tokyo, 1968, 18,
No 117
18. Manjoine, M J 'Influence of rate of strain and
temperature on yield stresses
of mild steel'
J Appl Mech, 1944, A211 - A218
19. Ford, H 'Advanced mechanics of materials.
Alexander, J M Part IV'
Longmans, 1963, 578
20. Mamalis, A G 'A current state review of the
et al warm-working of metals'
Proc 18th Int MTDR Conf, 1977,
173 - 180
21. Hodierne, F A 'A torsion test for use in metal-
working studies'

- J Inst Metals,
1962 - 1963, 91, 267 - 273
22. Rao, K P
Doraivelu, S M 'Flow curves and deformation of materials at different temperatures and strain rates' Journal of Mechanical Working Technology, 1982, 63 - 88
23. Grothe, M PhD Dissertation, Berlin, 1969
24. Doraivelu, S M PhD Thesis, IIT, Madras, India, 1979
25. Samanta, S 'Effect of strain rate on compressive strength of tool steel' Deformation under hot working conditions, 1966, 122 - 130
26. Zener, C
Holloman, J H 'Effect of strain rate upon plastic flow of steel' J Appl Phys, 1944, 15, 22 - 32
27. Jonas, J J Acta Met, 1969, 17, 397 - 405
28. Sellars, C M
McG Tegart, W J Mem Sci Rev Met, 1966, 63, 731 - 746
29. MacGregor, C W
Fisher, J C 'Tension tests at constant true strain rates' J Appl Mech, 1945, A217 - A227
30. MacGregor, C W
Fisher, J C 'A velocity-modified temperature for the plastic flow of metals' J Appl Mech, 1946, A11 - A16
31. Inoue, K J of Iron and Steel Inst of Japan, 1955, 41, 593 - 601
32. Nakayama, K 'Studies on the mechanism of metal cutting' Bulletin of the faculty of Engineering. Yokohama National Univ, 1959, 8, 1 - 25
33. Oyane, M
et al 'The behaviour of some steels under dynamic compression' The 10th Japan Congress on testing materials, 1967, 72

- 34. Oxley, P L B
'Allowing for strain rate effects
in the analysis of metal working
processes'
Conference series no 21, The Inst
of Physics, 1974, 359 - 381
- 35. Ranger, A E
'An electrical analogue for
estimating die temperatures
during wire drawing'
J Iron and Steel Inst, 1958,
383
- 36. Siebel, E
Kobitsch, R
'Die Erwärmung des Zie-hgutes
beim Drahtziehen'
Mitt Kaiser Wilh Institute,
1941, 23, Nr 410
- 37. Bishop, J F W
'An approximate method for
determining the temperatures
reached in steady motion
problems of plane plastic
strain'
Journal of Mech and Applied Math,
1956, 9, Pt 2, 237 - 246
- 38. Tay, A O
et al
'A numerical method for calculating
temperature distributions in
metal working processes'
Int J Mech Sci, 1980, 22, 41 - 57
- 39. Alexander, J M
'A slip-line field for the hot-
rolling process'
Proc Inst Mech Engrs, 1955
169, 1021 - 1028
- 40. Johnson, W
Kudo, H
'The use of upper-bound solutions
for the determination of
temperature distributions in
fast hot rolling and axis-symmetric
extrusion processes'
Int J Mech Sci, 1960, 1, 175 - 191
- 41. Altan, T
'Heat generation and temperature in
wire and rod drawing'
Wire Journal, 1970, 3, 54 - 59
- 42. Altan, T
Kobayashi, S
'A numerical method for estimating
the temperature distributions in
extrusion through conical dies'
Trans ASME, J Eng Ind, 1968, 90,
107 - 118

43. Asada, Y
et al 'Analysis of temperature distribution
in wire and tube drawing processes
by the finite element method'
J Japan Soc Tech Plasticity, 1981,
22, 488 - 494
44. Kobatake, K
et al 'An analysis of temperature
distribution in continuous die-
less drawing'
Proc 18th Int MTDR Conf, 1977,
253 - 258
45. Nishihara, M
et al 'Hot hydrostatic extrusion of non-
ferrous metals'
Proc 18th Int MTDR Conf, 1977,
91 - 96
46. Avitzur, B 'Metal forming : the application
of limit analysis'
Marcel Dekker, 1980
47. MacLellan, G D S 'Some friction effects in wire-
drawing'
J Inst Metals, 1952 - 53, 81,
1 - 13, 713 - 714
48. Yang, C T 'On the mechanics of wire drawing'
Trans ASME, J Eng Ind, 1961, 83,
523 - 530
49. Major, H 'Studies in cold drawing. Pt 3'
Trans ASME, 1956, 78, 19
50. Moore, G G
Wallace, J F 'A method for investigating the
coefficient of friction in tube
sinking through conical dies'
J Mech Eng Sci,
1965, 7, No 3, 279 - 282
51. Greenwood, H
Thompson, F C 'An investigation of rod drawing
with die rotation'
Nature, 1931, 128, 152
52. Linicus, W
Sachs, G Mitt Dt Mater Anst 'Spanlose
Formung der Metalle'
1931, 16, 38 - 67
53. Rothman, D
Sansome, D H 'An investigation of rod-drawing
with die-rotation'
Proc 10th Int MTDR Conf,
1969, 179 - 192
54. Hofsten, V &
Linstrand, E Jernkontovets Ann,
1958, No 3, 128 - 164

55. Evans, E
Avitzur, B
'Measurement of friction in drawing and rolling'
Trans ASME, J Eng Ind, 1968,
90, 72 - 91
56. Prager, W &
Hodge, P G
'Theory of perfectly plastic solids'
Chapman & Hall Ltd, London, 1951
57. Drucker, D C
J Appl Mech, 1954, 21, 71
58. Avitzur, B
'Metal Forming'
McGraw Hill, 1968
59. Avitzur, B
et al
'Limit analysis of flow through conical converging dies'
Journal of the Franklin Institute,
1975, 299, 339 - 358
60. Osakada, K
Niimi, Y
'A study on radial flow field for extrusion through conical dies'
Int J Mech Sci, 1975, 17, 241 - 254
61. Semenovna, N
et al
'Method of warm drawing of metal workpieces'
British patent 1234111
62. Sachs, G
et al
'Drawing thin-walled tubing with a moving mandrel through a single stationary die'
J Appl Mech, 1944, A199 - A210
63. Ekelund, S
'The analysis of factors influencing rolling pressure and power consumption in the hot rolling of steel'
Steel, 1933, 93, Nos 8 - 14
64. Orowan, E
'The calculation of roll pressure in hot and cold flat rolling'
Proc Inst Mech Engrs, 1943,
150, 140 - 167
65. Sims, R B
'Calculation of roll force and torque in hot rolling mills'
Proc Inst Mech Engrs, 1954, 168,
191 - 200
66. Orowan, E
British Iron and Steel Research
Association Report No MW/F/22/50
1950

67. Cook, P M
McCrum, A W 'Calculation of load and torque in hot flat rolling'
The British Iron and Steel Association, 1958
68. Hirst, S
Ursell, D H 'Proceedings of the Conference on Technology of Engineering Manufacture', London
(Inst Mech Eng), 1958
69. Johnson, W BISRA Report MW/E/55/54
70. Farag, M M &
Sellars, C M 'Flow stress in hot extrusion of commercial - purity aluminium'
J Inst Metals, 1973, 101, 137 - 145
71. Kudo, H 'Some analytical and experimental studies of axi-symmetric cold forging and extrusion-I'
Int J Mech Sci, 1960, 2, 102 - 127
72. Childs, T H 'Metal flow in the hot extrusion of mild steel'
Metals Technology, 1974, 305 - 309
73. Winsper, C E 'An investigation of the mechanics of wire drawing with the superposition of an oscillatory drawing stress'
PhD, 1966, Univ of Aston
74. Dawson, G R 'A study of the application of low frequency oscillations to multi-tool drawing'
PhD, 1972, Univ of Aston
75. Wistreich, J G 'Investigation of the mechanics of wire drawing'
Proc Inst Mech Engrs, 1955, 169, 654
76. Fuchs, D G 'Industrial tests on hot drawing of high strength steels'
Stahl und Eisen, 1977, 97 154 - 158
77. Schroder, G 'On the cold and hot drawing of the titanium alloy Ti Al 6V4'
Wire, 1980, 184 - 187
78. Basily, B B 'The mechanics of section drawing'
PhD Thesis, 1976, Univ of Aston

79. Sellars, C M
McG Tegart, W J 'Hot workability'
Int Met Reviews, 1972, 17, 1 - 24
80. Hastings, W F
et al 'Predicting a material's machining
characteristics using flow stress
properties obtained from high-
speed compression tests'
Proc Inst Mech Engrs, 1974, 188,
245 - 252
81. Campbell, J D Philosophical Magazine, 1970, 21, 63
82. Thomason, P F
et al 'The effect of temperature and strain
rate on the cold and warm working
characteristics of alloy steels'
Proc 14th Int MTDR Conf, 1973,
791 - 798
83. Samanta, S 'Resistance to dynamic compression
of low carbon steel and alloy steels
at elevated temperatures and at
high strain-rates'
Int J Mech Sci, 1968, 10, 613 - 636
84. Atkins, A G 'Consequences of high strain rates
in cold working'
J Inst Metals, 1969, 97, 829 - 898
85. Thomason, P F 'An investigation into the effects
of pre-heat temperature on
ductility in a warm heading process'
Proc Instn Mech Engrs, 1969 - 70,
184, 885 - 895
86. Glen, J 'Effect of alloying elements on the
high temperature tensile strength
of normalized low carbon steel'
Journal of Iron and Steel Inst,
1957, 186, 21
87. Osakada, K 'Mechanical properties of mild steel
after cold and warm high-speed
forging'
Proc 13th Int MTDR Conf, 1972,
357 - 362
88. Dean, T A
Sturgess, C 'Stress-strain characteristics of
various steels over a wide range
of strain-rates and temperatures'
Proc Instn Mech Engrs, 1973, 187,
523 - 533

89. Eleiche, A S

'A literature survey of the combined effects of strain rate and elevated temperature on the mechanical properties of metals'

Brown Univ. AFML-TR-72-1308, 1972